

University of Trento
University of Bergamo
University of Brescia
University of Padova
University of Trieste
University of Udine
University IUAV of Venezia

Md. Shahin Reza

**SEISMIC SAFETY EVALUATION OF INDUSTRIAL
PIPING SYSTEMS AND COMPONENTS UNDER
SERVICEABILITY AND ULTIMATE LIMIT STATE
CONDITIONS**

Tutor: Prof. Oreste S. Bursi

April, 2013

UNIVERSITY OF TRENTO

Ph. D. in Engineering of Civil and Mechanical Structural Systems

Cycle: XXV

Head of the Doctoral School: Prof. Davide Bigoni

Final Examination: 29 / 04 / 2013

Board of Examiners

Prof. Egidio Rizzi (Università di Bergamo)

Prof. Spyros Karamanos (University of Thessaly)

Prof. Dennis Kochmann (California Institute of Technology)

Prof. Giovanna Concu (Università degli studi di Cagliari)

SUMMARY

Although industrial piping systems and their components have been found highly vulnerable under earthquake events, there exists an inadequacy of proper seismic analysis and design rules for these structures. Current seismic design Standards and Codes are found to be over-conservative and some components, e.g., elbows, bolted flange joints and Tee joints, do not have detailed design guidelines that take into account earthquake loading. Thus, a clear need for the development of improved seismic design rules for such systems is evident. In this respect, numerical and experimental studies on piping systems and their components subjected to earthquake loading could be useful. As a result, valuable information, such as seismic capacities and demands under different limit states, could be utilized for the amendment of relevant design Codes and Standards.

This thesis undertook a numerical and experimental investigation on a typical industrial piping system and some of its components in order to assess their seismic performance. In particular, the following issues have been pursued: (i) design of two non-standard Bolted Flange Joints (BFJs) suitable for seismic applications; (ii) experimental testing of the designed BFJs under monotonic and cyclic loading in order to check their leakage, bending and axial capacities; (iii) finite element analysis of a piping system containing several critical components under seismic loading; (iv) implementation of a pseudo-dynamic and real time testing schemes to test the piping system under seismic loading; and (v) pseudo-dynamic and real time tests on the piping system under several levels of earthquake loading corresponding to both serviceability and ultimate limit states.

The above-mentioned activities were attained in this thesis. In particular, two different non-standard BFJs, comparatively thinner than the Standard ones, were designed, and their performance was examined through a number of monotonic and cyclic tests. Experimental results exhibited a favourable performance of the BFJs under bending and axial loading and moderate internal pressure; a good capacity in terms of strength, ductility, energy dissipation and leakage was observed. Performance of a typical full-scale industrial piping system containing several critical components, such as elbows, a bolted flange joint and a Tee joint, under realistic seismic loading was investigated through extensive numerical and experimental activities. The techniques of pseudo-dynamic and real time testing with dynamic substructuring –hybrid testing- were adopted to carry out experimental activities on the piping system under several limit state earthquake loading

suggested by performance-based earthquake Standards. Implementations of hybrid tests were challenging mainly because the piping system was endowed with distributed masses and subjected to distributed earthquake forces, for which these experimental techniques have been considered inadequate so far. A number of mode synthesis techniques, namely the Craig-Bampton and SEREP methods, were discussed and their effectiveness was analysed for the realisation of these tests. A characterization of the actuators to be used in the experimental tests was performed based on a transfer function. Relevant hybrid tests were successfully executed and they displayed a favourable performance of the piping system and its components; they remained below yield limits without any leakage even for the collapse limit state.

ACKNOWLEDGEMENTS

First and foremost, I express my deepest thanks and gratitude to my supervisor Prof. Oreste S. Bursi, whose invaluable guidance, encouragement and support helped me in all the time of research and writing of this thesis. I do owe my full appreciation.

My sincere thanks to the University of Trento for granting me the Ph.D. fellowship to commence this thesis and to carry out the necessary research work.

I want to thank the European research project INDUSE (Grant No: RFSR-CT-2009-00022) to offer an opportunity to perform analysis and experimental tests on a piping system and its components.

My many colleagues provided me with a stimulating and fun environment in which I learnt and grew. I am especially thankful to Prof. Fabrizio Paolacci, Dr. Alessio Bonelli, Dr. Anil Kumar, Eng. Giuseppe Abbiati, Eng. Md. Rashedul Hasan, Eng. Alessia Ussia, Eng. Gabriele Zanon, Dr. Marco Molinari, Dr. Tiziano Sartori, Dr. Nicola Tondini, Dr. Zhen Wang, Dr. Ja Chuanguo, Eng. Zhu Mei, Eng. Claudio Zamboni and Eng. Nicola Piccardoni.

Finally, my special and heartfelt thanks to my parents, my family and my wife for their endless love and support.

PUBLICATIONS

As a result of the work conducted in this thesis, the following publications have been produced:

Journal Publications:

Paolacci F., Reza M. S., Bursi O. S., 2013. Evaluation and Design of Refinery Piping Systems in Earthquake-Prone Areas. *Journal of Pressure Vessel Technology*. (under review).

Reza M. S., Bursi O. S., Paolacci F., 2013. Performance of Seismically Enhanced Bolted Flange Joints for Industrial Piping Systems. *International Journal of Pressure Vessels and Piping*. (under preparation).

Reza M. S., Abbiati G., Paolacci F., Bursi O. S., 2013. Seismic Performance Evaluation of a Full-Scale Industrial Piping System for Serviceability and Ultimate Limit States. *International Journal of Pressure Vessels and Piping*. (under preparation).

Conferences:

Paolacci F., Reza M. S., Bursi O. S., 2011. Seismic Analysis and Component Design of Refinery Piping Systems. III ECCOMAS Thematic Conference on Computational Methods in Structural Dynamics and Earthquake Engineering, Corfu, Greece, 26-28 May 2011.

Bursi O. S., Reza M. S., Paolacci F., Kumar A., 2012. Seismic Performance of Bolted flange Joints in Piping Systems for Oil and Gas Industries. 15th World Conference on Earthquake Engineering, Lisbon, Portugal, 24-28 September 2012.

Paolacci F., Reza M. S., Bursi O. S., Gresnigt N., Kumar A., 2013. Main Issues on the Seismic Design of Industrial Piping Systems and Components. Proceedings of the ASME 2013 Pressure Vessels & Piping Division Conference, PVP 2013, July 14-18, 2013, Paris, France. (in print).

Reza M. S., Bursi O. S., Abbiati G., Bonelli A., 2013. Pseudo-Dynamic Heterogeneous Testing with Dynamic Substructuring of a Piping System under Earthquake Loading. Proceedings of the ASME 2013 Pressure Vessels & Piping Division Conference, PVP 2013, July 14-18, 2013, Paris, France. (in print).

CONTENTS

1 INTRODUCTION	1
1.1 Seismic risks in industrial piping systems and components	1
1.2 Objectives of the thesis	5
1.3 Organization of the thesis	5
2 DESIGN, ANALYSIS AND TESTING OF PIPING SYSTEMS AND COMPONENTS	9
2.1 Introduction	9
2.2 Piping systems and components	9
2.3 Piping systems: seismic design, analysis and testing	11
2.3.1 Codes and Standards	12
2.3.2 Main issues in seismic design and analysis	13
2.3.3 Previous experimental tests	26
2.4 Pipe Elbows: seismic design, analysis and testing	29
2.5 Bolted Flange Joints: design, analysis and testing	33
2.5.1 Bolted flange joint	33
2.5.2 Design Codes and Standards	38
2.5.3 Component Standards	41
2.5.4 Design methods	44
2.5.5 Previous experimental tests	49
2.6 Pseudo-dynamic and real time tests with dynamic substructuring	54
2.7 Conclusions	63
3 DESIGN AND ANALYSIS OF NON-STANDARD BOLTED FLANGE JOINTS	65
3.1 Introduction	65

3.2	Design of BFJs using Standards	65
3.3	Design of non-standards BFJs	66
3.3.1	Motivation	66
3.3.2	Design procedure	67
3.4	Design resistances of non-standard BFJs	76
3.4.1	Axial resistance	77
3.4.2	Bending resistance	78
3.5	Design checks of non-standard bolted flange joints	80
3.6	Conclusions	81
4	EXPERIMENTAL TESTS ON BOLTED FLANGE JOINTS	83
4.1	Introduction	83
4.2	Test program	83
4.3	Material testing	84
4.4	Tightening of bolts at assembly	87
4.5	Test specimens and experimental set-up	88
4.6	Instrumentation and definition of joint rotations and displacements	92
4.7	Loading protocols	99
4.8	Main observations and results from experimental tests	102
4.8.1	Results of bending tests	102
4.8.2	Results of axial tests	108
4.9	Performance evaluation of designed BFJs	114
4.9.1	Comparison between experimental results and allowable design loads	114
4.9.2	Comparison between seismic demands and capacity	119
4.10	Conclusions	121
5	CHARACTERIZATION OF ACTUATORS FOR PSEUDO-DYNAMIC AND REAL TIME TESTS	123
5.1	Introduction	123
5.2	Hardware and software for hybrid tests	123
5.3	Estimation of a transfer function of the actuator and control system	125
5.4	Performance of MOOG actuators coupled to the piping system	130

5.5	Conclusions	133
6	NUMERICAL IMPLEMENTATIONS OF PSEUDO-DYNAMIC AND REAL TIME TESTING WITH DYNAMIC SUBSTRUCTURING ON A PIPING SYSTEM UNDER SEISMIC LOADING	135
6.1	Introduction	135
6.2	Objectives of the hybrid tests	136
6.3	The piping system under investigation	136
6.4	FE modelling and modal analysis of the piping system	139
6.5	Analyses of the piping system under seismic loading	147
6.5.1	Selection of input seismic loading	147
6.5.2	Analyses of the piping system with selected seismic loading	151
6.6	Substructuring of the piping system	153
6.7	Equations of motion for hybrid tests	159
6.8	Time integration and delay compensation for hybrid tests	163
6.8.1	The LSRT2 integration algorithm	163
6.8.2	Delay compensation method for the RTDS	165
6.9	Model reduction of the Physical Substructure	167
6.9.1	Effectiveness of different reduction techniques	174
6.10	Modification of the piping system model for the RTDS	177
6.11	Hardware-Software architecture for hybrid tests	178
6.12	Conclusions	179
7	EXPERIMENTAL TESTS ON THE PIPING SYSTEM: PSEUDO-DYNAMIC AND REAL TIME TESTS	181
7.1	Introduction	181
7.2	Test program	181
7.3	Test Specimen and experimental set-up	183
7.4	Instrumentation and measurements	186
7.5	Identification tests on the PS	192
7.6	Main observations and results from experimental tests	197
7.6.1	Results of PDDS	198
7.6.2	Results of RTDS	203

7.7	Conclusions	208
8	SUMMARY, CONCLUSIONS AND FUTURE PERSPECTIVES	211
8.1	Summary	211
8.2	Conclusions	213
8.3	Future perspectives	216

LIST OF FIGURES

1.1	An industrial piping network.	1
1.2	Some components of a piping system.	2
1.3	Some typical failures of piping systems and components during past earthquakes: (a) petroleum complex conflagration (1964 Niigata Earthquake, Japan); (b) damage of tank and piping system (1999 Kocaeli Earthquake, Turkey); (c) deformation of piping and pipe racks (1995 Kobe Earthquake, Japan); (d) breakage of a bolted flange joint (1995 Kobe Earthquake, Japan).	3
2.1	Typical piping systems.	10
2.2	Some components of a piping system: (a) a weld-neck flange; (b) an elbow; (c) a Tee joint; (d) a reducer.	10
2.3	(a) Pipe ways; (b) pipe racks.	11
2.4	Effect of q factor on the selection of S	15
2.5	Damping ratio according to ASME Code case 411-1.	17
2.6	A typical Response Spectrum.	20
2.7	An earthquake acceleration time history.	22
2.8	Failure of a piping system under shaking table test carried out by DeGrassi et. al. (2008).	27
2.9	Crack in a Tee joint under shaking table test carried out by Nakamura et al. (2011).	28
2.10	Parts of an elbow.	29
2.11	Elbow parameters.	30
2.12	Failure of elbow in the flank found from shaking table tests performed by (a) (DeGrassi et. al., 2008); (b) (Otani et al., 2011).	32

2.13 A bolted flange joints and its components.	33
2.14 Some common types of flange.	34
2.15 Flange faces.	36
2.16 Placement of a gasket between two flanges.	36
2.17 Some metallic and non-metallic gaskets: (a) a corrugated metal gas- ket; (b) a metallic spiral wound gasket; (c) a non-metallic fibre rein- forced gasket; (d) a non-metallic rubber gasket.	37
2.18 Axial forces balance in a BFJ used in the Taylor Forge calculation. . .	45
2.19 Loads considered in EN 1591 mechanical model.	47
2.20 Experimental test performed on an ANSI joint under internal pressure, bending and tensile load (Nash and Abid, 2000).	50
2.21 Schematic of the test set-up carried out by (Semke et al., 2006). . . .	52
2.22 Experimental set-up for leakage test under internal pressure and ex- ternal bending moment carried out by (Horiuchi et al., 2011).	53
2.23 Measurements of inertia and damping forces in pseudo-dynamic and real time tests.	60
2.24 Basic concept of hybrid tests with an integration scheme.	61
2.25 Test rig and piping arrangement for pseudo-dynamic tests by Melo et al. (2001).	62
2.26 Schematic of a PDDS and an RTDS on a piping system under seismic loading.	63
3.1 The selected Standard flange.	70
3.2 The selected spiral wound gasket.	71
3.3 Failure modes according to Eurocode 1993-1-8 (2005).	73
3.4 Thickness vs. failure modes according to Eurocode 1993-1-8 (2005): (a) with safety factors; (b) without safety factors.	74
3.5 (a) Designed non-standard BFJs and dimensions; (b) spiral wound gasket; (c) stud bolt.	75
3.6 Schematic of flange opening and bolt elongation under bending mo- ment (simplified and approximated).	79
4.1 Stress-strain curve of pipe material.	85

4.2	(a) Pipe material coupon; (b) an MTS extensometer attached to pipe coupon; (c) METROCOM machine.	86
4.3	(a) Flange material coupon; (b) GALDABINI machine.	86
4.4	(a) The torque-wrench; (b) bolt tightening sequence according to ASME PCC-1 (2010).	88
4.5	(a) Design 01 and (b) design 02 BFJ.	89
4.6	a) Bending test specimen, BS1; b) axial test specimen, AS1; c) a spiral wound gasket; d) a stud bolt.	90
4.7	Load application points in (a) bending tests; (b) axial tests.	91
4.8	Experimental set-up for (a) bending tests; (b) axial tests.	91
4.9	Actual experimental set-up for (a) bending tests; (b) axial tests.	92
4.10	Placements of strain gauges in the pipe.	93
4.11	(a) An AEP transducer; (b) an inclinometer; (c) a Gefran transducer; (d) a wire transducer.	94
4.12	Instrumentation for bending tests (dimensions are in mm; not drawn to scale).	95
4.13	Instrumentation for axial tests (dimensions are in mm; not drawn to scale).	95
4.14	Some instruments mounted in a bending test.	96
4.15	Some instruments mounted in an axial test.	96
4.16	Definition of pipe and flange rotations in bending.	97
4.17	Displacements of flanges under axial loading.	98
4.18	ECCS loading protocol: (a) definition of e_y ; (b) ECCS cyclic loading.	99
4.19	Cyclic loading protocol for (a) BSCL18; (b) BSCL27 according to ECCS45.100	
4.20	Cyclic loading protocol for (a) ASCL18; (b) ASCL27-1; (c) ASCL27-2.	101
4.21	Load-displacement curve of test BSML18.	103
4.22	Moment-rotation curve of test BSML27.	103
4.23	Moment-rotation curve of test BSCL18.	104
4.24	Moment-rotation curve of test BSCL27.	104
4.25	Envelop of cyclic and monotonic moment-rotation curves under bending loading.	105

4.26 Failure in the pipe of: (a) a Design 01 BFJ (test BSCL18); (b) a Design 02 BFJ (test BSCL27).	105
4.27 Moment-strain (strain gauge- S6) diagram of (a) BSML18; (b) BSML27; (c) BSCL18; (d) BSCL27.	106
4.28 Bi-linear and tri-linear approximation of a non-linear response after Bursi et al. (2002).	107
4.29 Ductile behaviour of (a) Design 01 (BSCL18); (b) Design 02 (BSCL27) BFJ.	108
4.30 Load - flange-displacement curve of test ASML18.	109
4.31 Load - flange-displacement curve of test ASCL18.	110
4.32 Load - flange-displacement curve of test ASCL27-1.	110
4.33 Load - flange-displacement curve of test ASCL27-2.	110
4.34 Envelops of cyclic and monotonic load-displacement curves under axial loading.	111
4.35 Test specimen, AS2 after test ASCL18.	111
4.36 Stress-strain (strain gauge- S5) diagram of (a) ASML18; (b) ASCL18; (c) ASCL27-1; (d) ASCL27-2.	112
4.37 Ductile behaviour of (a) Design 01 and (b) Design 02 BFJ under axial loading.	114
4.38 Comparison between experimental and Coded moments.	118
4.39 Comparison between experimental and Coded loads.	119
4.40 The piping system considered in the Case Study.	120
5.1 Hardware for hybrid tests.	125
5.2 Controller configuration for a MOOG actuator.	126
5.3 Simplified representation of the TF of the transfer system.	126
5.4 A MOOG actuator attached with masses.	127
5.5 A sine chirp signal used for the estimation of actuator TF.	128
5.6 Bode diagram.	129
5.7 Step response.	129
5.8 Experimental set-up for the hybrid tests.	131
5.9 Response of (a) MOOG 1 and (b) MOOG 2 actuator under an applied displacement history.	131

5.10	Double amplitude, X.	132
5.11	Frequency vs. displacements of MOOG actuators.	132
6.1	A 3D sketch of the reference piping system on a support structure (dimensions are in mm).	137
6.2	Specifications and dimensions of the piping system after DeGrassi et al. (2008).	138
6.3	Boundary conditions present in the piping system (u = displacement; θ = rotation).	138
6.4	Geometry of the equivalent straight elbow element.	140
6.5	FE analysis on 8" elbow elements after Varelis et al. (2011): (a) force-displacement curve under axial loading; (b) force-displacement curve under shear loading; (c) moment-rotation curve under bending loading (Red- Closing; Blue- Opening).	142
6.6	Displacement, rotation, force and moment in the EB Beam.	143
6.7	Comparison of elastic stiffness of 6" and 8" elbows.	144
6.8	FE model of the piping system.	145
6.9	(a) Mode #1 and (b) Mode #2 of the piping system model.	146
6.10	Support structure of the piping system: (a) 3D FE model; (b) dimensions and lateral views.	148
6.11	Support structure and filtered earthquake with relevant spectrum generated at point (1).	150
6.12	Actions of the piping system under reference earthquake loading without damping: (a) bending moment; (b) shear.	152
6.13	Bending moments close to zero in the piping system.	154
6.14	PS, NS and relevant coupling nodes.	155
6.15	Dimensions, coupling forces and actuator positions in the PS.	155
6.16	Displacement time histories (in x) and relevant Fourier spectra of (a) Coupling Node #1; (b) Coupling Node #2; (Blue CM; Red RM).	158
6.17	(a) Displacement (in x) and (b) rotation (along z) time histories and relevant Fourier spectra of Node #5 (Blue CM; Red RM).	159
6.18	The two substructures of the piping system and forces acting on them.	160
6.19	Schematics of the delay overprediction scheme.	166

6.20	FE model of the piping system developed in ANSYS.	176
6.21	Displacement histories and relevant Fourier spectra of Coupling Node #2: (a) and (b) are relevant to the CB reduction; (b) and (d) are relevant to SEREP2 reduction.	176
6.22	Added masses in the NS.	177
6.23	Displacement histories and relevant Fourier spectra of (a) Coupling Node #1 and (b) Coupling Node #2 (Blue- Reduced Model; Black- Reference Model).	178
6.24	Hardware-Software configuration for the hybrid tests.	179
7.1	Specifications and components of the test specimen.	183
7.2	Schematic of the experimental set-up for the hybrid tests.	184
7.3	Actual test set-up for the hybrid tests.	184
7.4	Some components of the test specimen: (a) Elbow #1; (b) Tee joint; (c) bolted flange joint.	185
7.5	(a) Support #1; (b) Support #2.	185
7.6	(a) A ball bearing; (b) a roller bearing.	186
7.7	A 1000 kg mass attached to the pipe.	186
7.8	Locations of strain gauges.	187
7.9	Positions of strain gauges in (a) Elbow #1 and (b) straight pipe.	188
7.10	Positions of strain gauges in Elbow #2.	188
7.11	Positions of strain gauges in Elbow #3.	188
7.12	Strain gauges mounted in (a) Elbow #2; (b) straight pipe.	189
7.13	Locations of displacement transducers.	189
7.14	Displacement transducers: (a) Gefran 500 mm, G2; (b) AEP, T2.	190
7.15	Measurement of rotations of the Tee joint.	190
7.16	Measurement of rotations of Elbow #2.	191
7.17	Positions of accelerometers in the test specimen.	193
7.18	Points of hammer impacts.	194
7.19	(a) Accelerometer, A4x; (b) hammer.	195
7.20	IDT3: (a) Stabilization diagram for frequency estimation; (b) Cluster diagram for damping estimation.	196
7.21	Estimation of damping using long signal acquired during IDT4.	197

7.22 Strain histories in the flank of Elbow #2 at: (a) SLVT; (b) SLCT.	198
7.23 End node rotation histories and relevant Fourier spectra for Elbow #1 at: (a) SLVT; (b) SLCT.	199
7.24 Moment-Rotation curve relevant to Elbow #1 obtained from an FE anal- ysis.	199
7.25 Rotation histories and relevant Fourier spectra of the Tee joint at: (a) SLVT; (b) SLCT.	200
7.26 Strain histories in the 6" branch pipe of the Tee joint at: (a) SLVT; (b) SLCT.	200
7.27 Displacement histories and relevant Fourier spectra of Coupling Node #1 at: (a) SLVT; (b) SLCT.	201
7.28 Acceleration histories and relevant Fourier spectra of Coupling Node #1 at: (a) SLVT; (b) SLCT.	201
7.29 Displacement histories and relevant Fourier spectra of Coupling Node #2 at (a) SLVT; (b) SLCT (Red- Experimental; Blue- Numerical).	203
7.30 Displacement histories and relevant Fourier spectra of (a) Coupling Node #1; (b) Coupling Node #2 at RT1.	204
7.31 Velocity histories and relevant Fourier spectra of (a) Coupling Node #1; (b) Coupling Node #2 at RT1.	204
7.32 Acceleration histories and relevant Fourier spectra of (a) Coupling Node #1; (b) Coupling Node #2 at RT1.	205
7.33 Displacement histories and relevant Fourier spectra of (a) Coupling Node #1; (b) Coupling Node #2 at RT2.	205
7.34 Velocity histories and relevant Fourier spectra of (a) Coupling Node #1; (b) Coupling Node #2 at RT2.	206
7.35 Acceleration histories and relevant Fourier spectra of (a) Coupling Node #1; (b) Coupling Node #2 at RT2.	206
7.36 Experimental delay compensation.	207
7.37 Displacement histories and relevant Fourier spectra of (a) Coupling Node #1; (b) Coupling Node #2 at RT1 (Red- Experimental; Blue- Nu- merical).	208

7.38 Displacement histories and relevant Fourier spectra of (a) Coupling Node #1; (b) Coupling Node #2 at RT2 (Red- Experimental; Blue- Numerical). 208

LIST OF TABLES

3.1	Design conditions	68
3.2	Dimensions of connecting pipes	68
3.3	Materials of different components of the BFJ	69
3.4	Nominal yield and ultimate strength of different components of the BFJ	69
3.5	Gasket properties (Source: EN 1092-1:2007)	69
3.6	Dimensions of the Standard flange	70
3.7	Dimensions of the spiral wound gasket	72
3.8	Dimensions of bolts	72
3.9	Failure mechanisms associated with the three failure modes	73
3.10	Dimensions of designed non-standard BFJs.	76
3.11	Bolt lengths for non-standard BFJs	76
3.12	Failure modes of non-standard BFJs	77
3.13	Resistances of non-standard BFJs in axial loading	77
3.14	Yield and Ultimate load of the pipe in axial loading	78
3.15	Plastic moment of the pipe	78
3.16	Plastic moment of non-standard BFJs	80
3.17	Load ratios of the designed BFJs according to EN 1591	81
4.1	Test program on non-standard bolted flange joints	84
4.2	Mechanical properties of pipe and flange material (average values) . .	85
4.3	Tightening torques applied per bolt of non-standard BFJs	88
4.4	Lengths of test specimens	89
4.5	Strain gauges used in experimental tests	93
4.6	Instruments used in experimental tests	94
4.7	Maximum moments and leakage moments obtained during bending tests	102

4.8	Observations of different components of test specimens in bending tests	106
4.9	Yield moments and rotations of designed flange joints during bending tests	108
4.10	Leakage and maximum loads reached during axial tests	109
4.11	Observations of different components of test specimens in axial tests	112
4.12	Yield moments and yield displacements of non-standard BFJs under axial loading	113
4.13	Allowable moments and loads in straight pipes	115
4.14	Design yield moments in straight pipes suggested by Standards . . .	116
4.15	Comparison between experimental and allowable design moments . .	117
4.16	Comparison between experimental and allowable design loads	117
4.17	Comparison between experimental moments and yield moments by Standards	117
4.18	Comparison between experimental, plastic and buckling moments . .	118
4.19	Maximum bending moment and tension in the pipes from the Case Study	121
4.20	Maximum bending moment and axial force	121
5.1	Identified parameters of the actuator TF using the ARX algorithm . . .	128
5.2	Original gains of the controller	130
5.3	Tuned gains of the controller	130
5.4	Estimation of total delay of MOOG actuators	130
6.1	Characteristics of the piping system	139
6.2	Mechanical properties of the pipe material	139
6.3	Geometry of the original elbow elements (dimensions are in mm) . . .	140
6.4	Modified properties of elbow elements considered in the piping system model	144
6.5	First 20 eigenfrequencies and participation masses of the piping system model	146
6.6	Some design parameters of the support structure	149
6.7	PGA corresponding to different limit states	150
6.8	Maximum moment and stresses in the piping system under reference seismic loading	151

6.9	Maximum values of bending moment in coupling nodes	155
6.10	First 20 eigenfrequencies and participation masses of the PS	156
6.11	MAC Matrix between eigenvectors of the RM and CM	158
6.12	e_{RMS} between time history responses of the RM and CM	159
6.13	e_{RMS} for different reduction methods	175
6.14	Added masses in the nodes of the NS model	177
6.15	1st ten eigenfrequencies of the modified FE model of the piping system	178
7.1	Experimental test program on the piping system	182
7.2	No of strain gauges and displacement transducers used during hybrid tests	187
7.3	Types and number of displacement transducers	190
7.4	Identification tests carried out on the physical substructure	193
7.5	Positions and directions of accelerometers used in the identification tests	194
7.6	Points of hammer impact and relevant excited modes	195
7.7	Summary of results of identification tests	196
7.8	Maximum responses of the piping system and components from PDDS	202

CHAPTER 1

INTRODUCTION

1.1 Seismic risks in industrial piping systems and components

In industries like chemical/petrochemical plants, refineries, electric power stations and nuclear facilities, piping systems play a vital role by transferring raw and refined materials from one place to another connecting all the components involved in the transformation process, e.g., tanks, distillations columns and furnaces. Often hundreds of miles of pipes are installed for the transportation of petroleum products, natural gas, corrosive and hazardous chemicals in different operating conditions. Depending on the nature of working fluids, piping systems are designed to work over a wide range of temperature and pressure. A typical industrial piping network is shown in Figure 1.1.

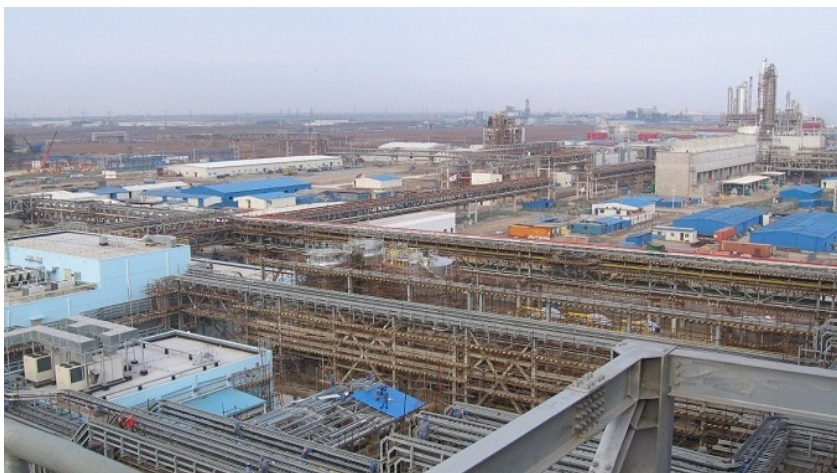


Figure 1.1: An industrial piping network.

Piping systems typically found in a petrochemical plants or refinery complex contain various components and support structures and operate in a broad range of working environments. Most of the piping, within the plants and off-site, for long and medium distance transportation, is metallic. In specific cases, the use of materials like cast iron, ceramics, glass and concrete is required mainly for reasons of corrosion resistance. Some common components usually used in piping systems include straight pipes, bolted flange joints, elbows, Tee Joints, various types of valves, pressure vessels, tanks, strainers and reducers as illustrated in Figure 1.2.

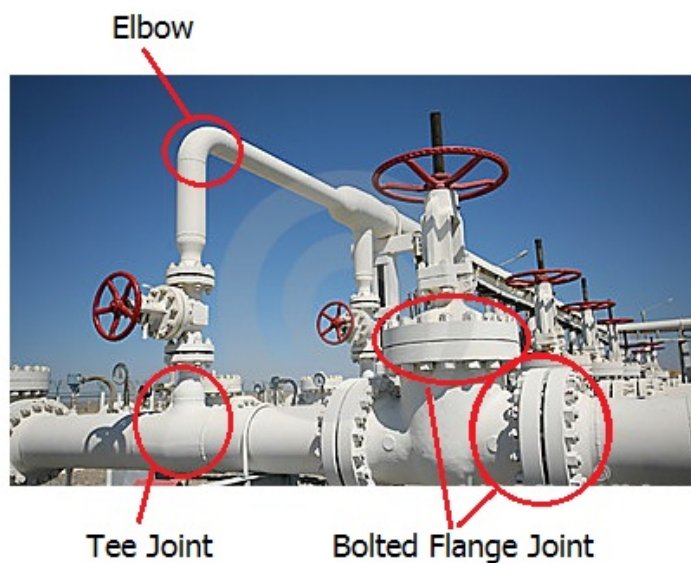


Figure 1.2: Some components of a piping system.

All the components of a piping system contribute to the overall transportation process and a single failure/damage in pipes or any component may cause disruption of the whole operation. Hence, a correct functioning of a piping system including all of its components under designed operating conditions is an essential requirement. Nevertheless, failure of piping systems and components under seismic events is a common picture.

Recent seismic events showed a quite high vulnerability of piping systems, where damage ranges from the simple failure of joints to the failure of supporting structures (Eshghi and Razzaghi, 2003; Suzuki, 2006; Sezen and Whittaker, 2006; Giannini

and Paolacci, 2006; Global Risk Miyamoto, 2007; Krausmann et al., 2010). A list of earthquake damages in pipelines occurred in the past century has been reported by Zare and Wilkson (2010). Consequences of such damages can be characterized by several degrees of severity, depending on the material delivered by pipes. For dangerous liquids or gases, even a simple failure of a joint may cause release of inflammable or toxic substances and can trigger a significant accidental chain, with severe consequences both for the environment and human lives. Damages may also result in plant shut-down with obvious economic consequences and threaten the post earthquake continuity of power/water supply lifelines. Some typical failures during past seismic events are presented in Figure 1.3.

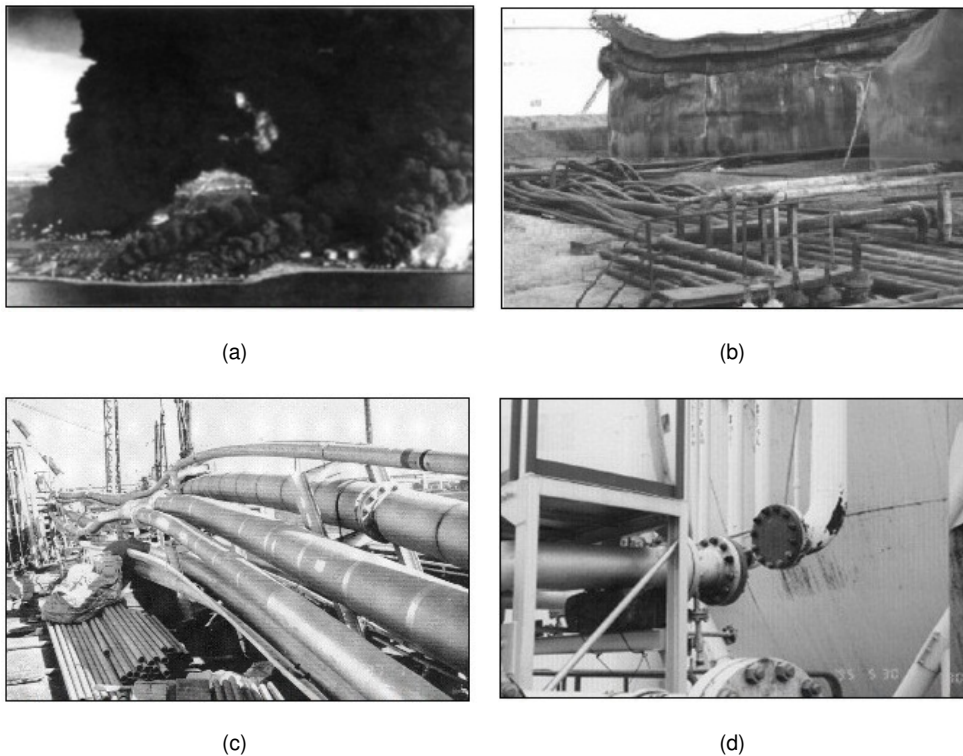


Figure 1.3: Some typical failures of piping systems and components during past earthquakes: (a) petroleum complex conflagration (1964 Niigata Earthquake, Japan); (b) damage of tank and piping system (1999 Kocaeli Earthquake, Turkey); (c) deformation of piping and pipe racks (1995 Kobe Earthquake, Japan); (d) breakage of a bolted flange joint (1995 Kobe Earthquake, Japan).

Failure in the piping system during an earthquake mainly occurs in components having complex geometrical shapes or sections, e.g., flexible curved segments such as elbows, welded joints such as a bolted flange joint or a Tee joint (Yahiaoui et al., 2000; Suzuki and Abe, 2005; Varelis et al., 2012; Karamanos et al., 2013) as depicted in Figure 1.3. This is primarily due to the stress intensification phenomena caused by geometrical irregularities present in those components (Otani et al., 2011).

Safeguarding the structural integrity of piping systems against earthquakes is a key issue toward increased safety and unhindered operation of an industrial facility. Structural behaviour, and in particular seismic design of a piping system and its components, is quite different than steel buildings and has several peculiarities, requiring a combined civil and mechanical engineering expertise. The special features stem from their shape and geometry, the high internal pressure and temperature, the enclosed liquid effects, and the presence of damages and defects that reduce their load-carrying capacity and resistance.

Unfortunately, a few contributions are available in literature that clarify seismic requirements that piping systems and components should comply with. Current American and European Standards do not contain enough rules and details for a proper seismic analysis and design of a piping system. For example, Eurocode 8 (EN 1998-4), which was developed for the design of silos, tanks and pipelines for earthquake resistance, contains no effective guidance for the seismic design of industrial piping systems. Moreover, studies, e.g., Touboul et al. (1999, 2006); Otani et al. (2011), showed that available Standards for piping systems design under seismic loading are over-conservative and modifications have been proposed to relax oversizing. In addition, some critical components, e.g., elbows, bolted flange joints and Tee joints, do not have detailed design guidelines that take into account seismic loading. Additionally, there exists limited experimental data on this subject (Touboul et al., 1999, 2006; Semke et al., 2006; Yahiaoui et al., 2002), especially in the presence of internal pressure. Some works in this area are currently going on under a European project INDUSE (INDUSE, 2009). Nevertheless, there are no specific design guidelines in relevant specifications and this fact necessitates numerical and experimental works in this area.

1.2 Objectives of the thesis

As discussed in the preceding section, piping systems and components are highly vulnerable to earthquake events while there exists an inadequacy of proper design rules of these structures under seismic loading. Current seismic design Codes have been proved to be over-conservatives and some components do not have any Codes for their seismic design. The present situation clearly shows a need for the development of an improved seismic design guideline for piping systems and components. In order to fulfil this requirement, numerical and experimental activities on a piping system and its components subjected to earthquake loading can be useful. Valuable information, e.g., seismic capacities and performances of a piping system and its components and seismic demands on them in different limit states, can be obtained through these studies which could be utilized for the amendments of current Standards and Codes for the seismic design of such structures.

To this end, this thesis undertook some numerical and experimental activities in order to assess the seismic performance of an industrial piping system and some of its components, e.g., bolted flange joints, Tee joints and elbows. In particular, the following activities are carried out in this dissertation: i) design of two non-standard bolted flange joints suitable for seismic applications; ii) experimental testing on the designed bolted flange joints in order to investigate their leakage, bending and axial capacities; iii) finite element analysis of a typical full-scale industrial piping system containing elbows, a Tee joint and bolted flange joint subjected to seismic loading; iv) development of pseudo-dynamic and real time testing schemes in order to test the piping system under different earthquake loading levels and v) investigation of performance of a piping system and its components through pseudo-dynamic and real time tests under different levels of earthquakes corresponding to both serviceability and ultimate limit states.

1.3 Organization of the thesis

This thesis presents the research performed mainly by the author and his co-workers on the seismic safety assessment of a piping system and some of its com-

ponents. The research was sponsored by INDUSE, a funded project of the European Commission to the University of Trento (INDUSE, 2009). The research is presented through the following chapters.

Chapter 2 provides a state of the art on the design, analysis and testing of piping systems and its components, i.e., pipe elbows and bolted flange joints, under seismic loading. Main issues on seismic design and analysis of piping systems and components are discussed and past experimental tests on such structures are summarised. Since there exist no seismic design and analysis rules for bolted flange joints, design and analysis methods and past experimental tests on such joints under regular loading are presented. Moreover, an overview and state of the art of the pseudo-dynamic and real time testing techniques is also offered in this chapter.

Design of two non-standard bolted flange joints based on a structural Eurocode is shown in Chapter 3. Analyses of the designed joints in terms of their axial and bending resistance are performed. Moreover, a design check of these non-standard joints is also carried out according to a relevant Eurocode.

An experimental test campaign on the designed non-standard bolted flange joints is presented in Chapter 4. Experimental set-up, instrumentation and test program are described. A number of bending and axial experimental tests were carried out in order to investigate the capacity of the designed joints. A detail analysis on the experimental results is offered and a comparison between test results and Coded design loads is performed. Moreover, a comparison between the capacity and seismic demands on these joints coming from a Case Study on a piping system is presented and discussed.

Chapter 5 presents a characterization of MOOG hydraulic actuators to be used for the pseudo-dynamic and real time tests on a piping system. Performance of the actuators and identification of a transfer function are discussed.

In Chapter 6, implementations of pseudo-dynamic and real time tests with dynamic substructuring on a typical industrial piping system at full-scale under seismic loading are demonstrated. Selection procedure of appropriate seismic loading and finite element analyses of the piping system under those seismic loading are presented. Substructuring of the piping system and minimization of error due to this substructuring

are discussed. Since the piping system contains distributed masses and is subjected to distributed earthquake loading, a reduction of the experimental substructure and the earthquake forces on it are performed using a number of mode synthesis techniques. Effectiveness of the reduction techniques and validation of test algorithms are discussed. Moreover, a hardware-software architecture to be used in the experiments are presented.

A detail description of the pseudo-dynamic and real time tests carried out on the piping system under several levels of earthquake loading corresponding to serviceability and ultimate limit states is offered in Chapter 7. Experimental program, test set-up and instrumentation are shown. Experimental results are presented and analysed in detail. Finally, performance of the piping system and its components under limit state earthquake events are discussed and commented.

The findings are summarised in Chapter 8, where the main results of the research are underlined together with future perspectives.

CHAPTER 2

DESIGN, ANALYSIS AND TESTING OF PIPING SYSTEMS AND COMPONENTS

2.1 Introduction

This chapter provides a state of the art and technical background on the design, analysis and testing of piping systems and some of their components, mainly under seismic loading. In particular, main issues of seismic design and analysis of piping systems and pipe elbows are discussed. Previous experimental tests carried out to investigate seismic performance of piping systems and their critical components, such as elbows and Tee joints, are also presented. Because, no seismic design and analysis rules for bolted flange joints -used in piping systems- are available, design and analysis methods and experimental tests on such joints under regular loading are described. Moreover, an overview and state of the art of pseudo-dynamic and real time testing techniques are also offered.

2.2 Piping systems and components

A piping system (Nayyar, 2007) is a network of pipes, fittings and valves mainly used to carry or transfer fluids from one place to another. It is one of the most important parts of many industries, especially of energy industries that deal with transferring and exploring oil and gas. They are also the most preferred means of transportation and distribution of oil and natural gas worldwide. The most common components of a piping system are pipes, fittings and valves.

Pipes are long cylinders used to carry or transfer fluids.

Pipe Fittings are used to connect lengths of pipes to construct a long piping system; commonly used fittings are flanges, elbows, Tee joints, reducers and expansion bellows.

Valves are used to stop, divert or control fluid flow. Common valve types are gate valves, globe valves, butterfly valves, ball valves, control valves; the selection is based on intended function and application.

In addition, a number of devices like strainers, traps, expansion loops are necessary for keeping the fluid clean and in good condition, and to accommodate expansion/contraction due to temperature variations. Typical piping systems and some components are shown in Figure 2.1 and Figure 2.2.

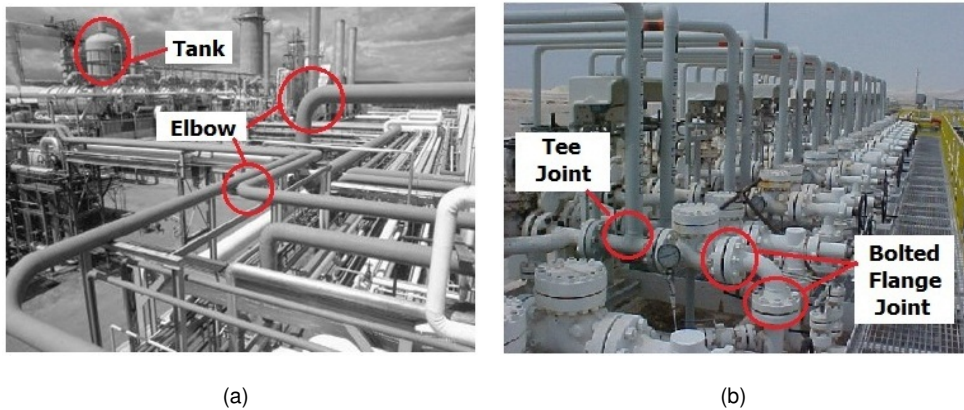


Figure 2.1: Typical piping systems.

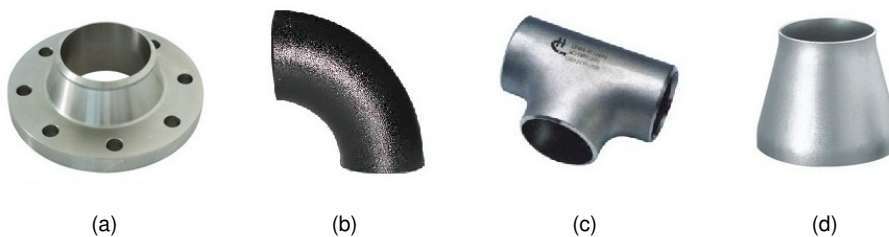


Figure 2.2: Some components of a piping system: (a) a weld-neck flange; (b) an elbow; (c) a Tee joint; (d) a reducer.

Piping systems may consist of a variety of materials including mild steel, stainless steel, aluminium, brass, copper, glass or plastic. Usually, pipe fittings and valves are made of the same material as the pipe. The material selection as well as pipe sizing depends upon parameters like nature of fluid, pressure, temperature and flow rate.

A pipe-way, shown in Figure 2.3(a), is the space allocated for routing several parallel adjacent pipelines within process plants. A pipe rack, presented in Figure 2.3(b), is the structure employed for supporting the pipelines and carrying electrical and instrument trays. The pipe rack is usually made of steel or concrete frames, on top of which the pipeline rests. Pipe racks are necessary for arranging the process and service pipelines throughout the plant, and they are used in secondary ways; principally to provide a protected location for auxiliary equipment, pumps, utility stations, manifolds, and fire-fighting and first-aid stations. Lighting and other fixtures can be fitted to the pipe rack columns.



(a)

(b)

Figure 2.3: (a) Pipe ways; (b) pipe racks.

2.3 Piping systems: seismic design, analysis and testing

In this Section, design and analysis of piping systems mainly under seismic loading are discussed. In addition, performance of piping systems under earthquake loading in previous experimental tests are also presented and commented.

2.3.1 Codes and Standards

Nowadays, both European and American Codes are available for the design of piping systems under seismic events. The major American and European Codes containing indications on dynamic analysis of and seismic design of pipes and pipelines are listed below.

American Codes and Standards:

- (i) ASCE (1984)
- (ii) ASME B31.3 (2006)
- (iii) ASME B31.1 (2001).
- (iv) ASME N 411-1 (1986)
- (v) ASME Section III Division 1 (2002)
- (vi) FEMA 450 (2003)

European Codes and Standards:

- (i) EN 1998-4 (2006)
- (ii) EN 13480-3 (2002)

American experience on piping system is very rich, especially in terms of design standardization and seismic design calculation, and the long list of Standards and Codes available it is a clear demonstration of it. The main standard is represented by ASME B31.3 (2006), but many other contributions and guidelines are also available, e.g., ASCE (1984); American Lifeline Alliance (2002).

The main European contributions is chiefly represented by EN 13480-3 (2002), dedicated to metallic piping systems. EN 1998-4 (2006) has been the first attempt of Structural Eurocodes to introduce novel seismic design concepts for industrial structures. This European Code has provisions for the seismic design of both above-ground and buried pipelines, but lacks adequacy in this respect (Paolacci et al., 2011).

The seismic analysis of a piping system involves several basic steps that allow defining the proper seismic action, the suitable numerical model and analysis method

and the verification format to be used. European, e.g., EN 13480-3 (2002), and American, e.g., ASME B31.3 (2006), Codes and Standards for piping systems differ for several of these aspects.

It is necessary to stress that the American Standard does not contain explicit indications on the seismic analysis of piping systems, but rather refers to the American Standard for seismic analysis of structure (ASCE7-05, 2005), which includes all the required prescriptions. On the contrary the European Standard, EN 13480-3 (2002) contains an entire Annex (Annex A) dedicated to the dynamic and seismic analysis of piping systems, but does not contain explicit quantification of the seismic action. At this end the Eurocode 8 part 1 (EN 1998-1, 2005) should be used.

2.3.2 Main issues in seismic design and analysis

The seismic design of a piping system entails several issues such as correct definition of the seismic actions and use of an appropriate design method. In this Subsection, main issues considered during seismic design and analysis of piping systems are collected.

2.3.2.1 Design loading conditions

Loads on a piping system can be classified into three categories: (i) sustained load; (ii) occasional load, and (iii) expansion load (ASME B31.1, 2001). While designing a piping system, all these loads should be considered.

Sustained loads are expected to be present throughout normal plant operation. Typical sustained loads are pressure and weight loads during normal operating conditions.

Occasional loads are present at infrequent intervals during plant operation. Examples of occasional loads are earthquake, wind, and fluid transients such as water hammer and relief valve discharge.

Expansion loads are those loads due to displacements of piping. Examples in-

clude thermal expansion, seismic anchor movements, thermal anchor movements, and building settlement.

The seismic load falls into the category of Occasional loads. Seismic loads on a piping system can be considered according to suggestions provided in Codes and Standards. For example, FEMA 450 (2003) at point 6.1 states:

"...Where the individual weight of supported components and non-building structures with periods greater than 0.06 seconds exceeds 25 percent of the total seismic weight, W , the structure shall be designed considering interaction effects between the structure and the supported components..."

Moreover, the same Standard indicates at point 14.4:

"...If a non-building structure is supported above the base by another structure and the weight of the non-building structure is not more than 25 percent of the seismic weight, W , the design seismic forces for the supported non-building structure shall be determined in accordance with the requirements of Chapter 6 (as a building structure)..."

Similar indications are given in ASCE7 (Azizpour and Hosseisni, 2009).

2.3.2.2 Response modification factor or behaviour factor

The response modification factor, R factor (in American Codes), or behaviour factor, q factor (in Eurocodes), is a strength reduction factor which accounts for ductility, overstrength, redundancy, and damping of a structural system (Cardone et al., 2008). It provides an indication of how well a structure can be expected to provide energy absorption in the inelastic range. The q factor can be defined as the ratio of the elastic strength demand imposed on a single Degree of Freedom (DoF) system to the inelastic strength demand for a given ductility ratio. Selection of appropriate behaviour factor is an important part of seismic design.

The q factor plays an important role in the selection of an appropriate design earthquake loading from an Elastic Response Spectra (ERS). An ERS is a plot of period of a structure, T , vs. earthquake acceleration, S , from where an appropriate S can be chosen for a structure relevant to its fundamental period, T_S . An ERS can be modi-

fied by a q factor, as illustrated in Figure 2.4, in order to consider a reduced S . For example, in Figure 2.4, ERS1 is reduced to ERS2 by a factor, q . Hence, the design acceleration is reduced to S_2 from S_1 , where,

$$S_2 = \frac{S_1}{q} \quad (2.1)$$

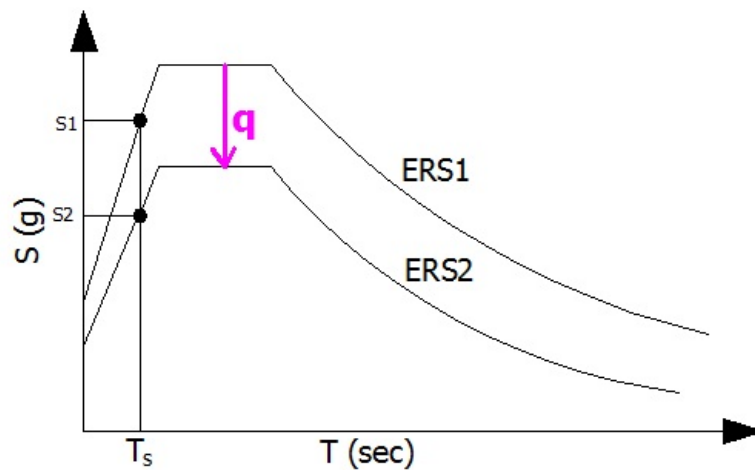


Figure 2.4: Effect of q factor on the selection of S .

Regarding selection of the q factor, EN 1998-4 (2006) at point 5.5 provides the following suggestions:

” ...

(i) *The dissipative capacity of an above-ground pipeline, if any, is restricted to its supporting structure, since it is both difficult and inconvenient to develop energy dissipation in the supported pipes, except for welded steel pipes. On the other hand, shapes and material used for the supports vary widely, which makes it infeasible to establish values for the behaviour factors with general applicability.*

(ii) *For the supporting structures of non-seismically-isolated pipelines, appropriate values of q may be taken from EN 1998-1 and EN 1998-2, on the basis of the specific layout, material and level of detailing.*

(iii) *Welded steel pipelines exhibit significant deformation and dissipation capacity, provided that their thickness is sufficient. For non-seismically-isolated pipelines which have a radius over thickness ratio (r/t) of less than 50, the behaviour factor, q , to be*

used for the verification of the pipes may be taken as equal to 3,0. If the r/t ratio is less than 100, q may be taken as equal to 2,0. Otherwise, the value of q for the design of the pipeline may not be taken greater than 1,5. In case of flange pipes, the dissipation capability is devolved to the supporting structure (in the typical design way).
..."

The American Code, *FEMA 450* suggests to use the values of the response factor indicated in the Table 4.3.1 of this Code. In particular for steel moment resisting frames $q = 4$ and for concentrically braced frame is $q = 4$. This is the case of dynamic uncoupled behaviour between pipes and pipe rack. In case were the coupling cannot be neglected, FEMA 450 at point 14.1.5 says:

"...for supported non-building structures that have rigid component dynamic characteristics, the Rfactor for the supporting structural system shall be used for the combined system. For supported non-building structures that have flexible component dynamic characteristics, the R factor for the combined system shall not be greater than 3. The supported non-building structure, and its supports and attachments, shall be designed for the forces determined from the analysis of the combined system..."

2.3.2.3 Importance factor

The importance factor is essentially an extra safety adjustment used to increase the calculated load on a structure based on its occupancy and/or function (IBC, 2000). An importance factors greater than 1.0 has the effect of reducing the q factor, which reduces inelastic behaviour, which in turn reduces the potential for damage. Selection of an importance factors is a vital part of seismic design of a system. Both American and European Codes has the suggestions regarding the choice of this factor. For example, FEMA450 (2003), at point 14.2.1, suggests importance factors for no-building structures dividing them into two main groups: function and hazard. Whereas, EN 1998-4 (2006) lists the importance factor as function of the class of the structure.

2.3.2.4 Damping

Damping is a crucial factor in the design and analysis of any structure including piping systems under seismic loading. In ASME Code Case N-411 (ASME N-411-1, 1986), damping values for response spectrum analysis of Classes 1, 2, and 3 piping are given as shown in Figure 2.5. They are independent of the pipe size.

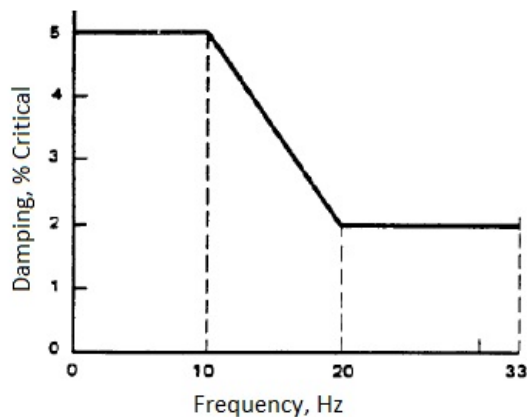


Figure 2.5: Damping ratio according to ASME Code case 411-1.

The same law is provided by EN 13480-3 (2002).

2.3.2.5 Limit states of pipes and pipelines

For the limit state design of structures under seismic loading, it is important to satisfy different limit state criteria as defined in Codes. A limit state is a condition of a structure beyond which it no longer fulfils the relevant design criteria. Different definitions of limit states for pipelines are provided both in American and European Codes.

FEMA 450 (2003), in Appendix 6, provides some precise indications on the requirements for the seismic qualification of pipes. Different performance criteria, according to this Standard are defined as follows:

- i) *Leak Tightness: The condition of a piping system characterized by containment*

of contents, or maintenance of a vacuum, with no discernible leakage.

ii) Operability: The condition of a piping system characterized by leak tightness as well as continued delivery, shutoff or throttle of pipe contents flow by means of unimpaired operation of equipment and components such as pumps, compressors and valves.

iii) Position Retention: The condition of a piping system characterized by the absence of collapse or fall of any part of the system.

In addition, EN 1998-4 (2006), at point 5.2, and EN 1993-4-3 (2006), at point 2.5 and 2.6, defines several serviceability, damage and ultimate limit states for piping systems. In particular, EN 1998-4 (2006) at point 5.2 defines the following limit states for pipelines:

Damage limitation state

1) Pipeline systems shall be constructed in such a way as to be able to maintain their supplying capability as a global servicing system, after the seismic action relevant to the 'minimum operating level' (see 2.1.3), even with considerable local damage.

2) A global deformation of the piping not greater than 1.5 times its yield deformation is acceptable, provided that there is no risk of buckling and the loads applied to active equipment, such as valves, pumps, etc., are within its operating range.

Ultimate limit state

1) The main safety hazard directly associated with the pipeline rupture during a seismic event is explosion and fire, particularly with regard to gas pipelines. The remoteness of the location and the exposure of the population to the impact of rupture shall be taken into account in establishing the level of the seismic action relevant to the ultimate limit state.

2) For pipeline systems in environmentally sensitive areas, the damage to the environment due to pipeline ruptures shall also be taken into account in the definition of the acceptable risk.

2.3.2.6 Seismic actions and analysis methods

Both European and American Standards assume as necessary the following two types of analysis for pipes: (a) movements due to inertia effects; and (b) differential movement of the supports (within supporting structure or between adjacent supporting structures).

The first type of analysis is essentially related to the effects of the absolute acceleration on the pipe mass. The second one is due to the relative movements between two supports, within the supporting structure or belonging to adjacent structures. Often the relevant effects are due to the displacement effect rather than acceleration effects (Paolacci et al., 2011).

Generally, piping seismic analysis is performed through one of the following three methods.

- (i) Equivalent lateral force method Analysis
- (ii) Modal response spectrum analysis and
- (iii) Time-history analysis.

Equivalent lateral force method analysis

The concept employed in equivalent lateral force method is to place static loads on a structure with magnitudes and direction that closely approximate the effects of dynamic loading caused by earthquakes. It is basically a static analysis procedure. The effective earthquake loads are calculated in terms of a base shear which is dependent on the properties of a structure, e.g., mass (effective seismic weight), imposed ground acceleration, dynamic characteristics, ductility and the importance of the structure. The base shear is then applied to the structure as an equivalent lateral load vertically distributed to the various elevations using Code prescribed equations given in Codes. The equivalent lateral force method is described in Eurocode, EN 1998-1 (2005) at point 4.3.3.2. A similar prescription is provided in FEMA 450.

Modal response spectrum analysis

Modal response spectrum analysis is perhaps the most common method used in design to evaluate the maximum structural response due to the seismic action (Costa, 2003). This is a linear approximate method based on modal analysis and on a response spectrum definition. This method measures the contribution from each natural mode of vibration to indicate the likely maximum seismic response of an essentially elastic structure. The seismic response spectra, which is used to carry out this analysis, is a plot of acceleration or velocity or displacement vs. frequency or period, see Figure 2.6. A response spectra is the main representation of a seismic action and usually are defined by the seismic Codes in terms of hazard conditions of the site, the level of dissipation capability of the supporting structure and pipes (response or behaviour factor), the right level of damping to be employed, and the level of structure reliability to impose, identified by the importance factor.

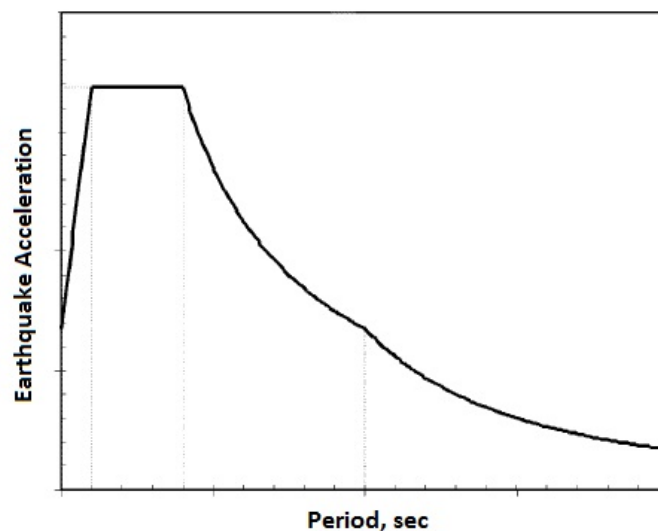


Figure 2.6: A typical Response Spectrum.

The modal response spectrum analysis provides insight into dynamic behaviour by measuring pseudo-spectral acceleration, velocity, or displacement as a function of structural period for a given time history and level of damping. This analysis method is useful for design decision-making because it relates structural type-selection to

dynamic performance. Structures of shorter period experience greater acceleration, whereas those of longer period experience greater displacement. Structural performance objectives should be taken into account during preliminary design and response-spectrum analysis.

This analysis method is described in European Code EN1998-1 at point 4.3.3.3.2. The indications of FEMA 450 are similar to the European Code prescriptions.

Time history analysis

The time history analysis is a step-by-step procedure where the loading and the response history are evaluated at successive time increments. During each step the response is evaluated from the initial conditions existing at the beginning of the step (typically, displacements and velocities) and the loading history in the interval. In addition to linear behaviour, this method also allows to investigate the non-linear behaviour of a structure by changing the structural properties, e.g., stiffness, from one step to the next. The time history method is one of the most effective for the solution of non-linear response, among the many methods available. A dynamic equation of motion, such as Equation (2.2), of the structure under consideration is used to carry out a time history analysis under seismic loading.

$$\mathbf{M}\ddot{\mathbf{u}} + \mathbf{C}\dot{\mathbf{u}} + \mathbf{K}\mathbf{u} = -\mathbf{M}\mathbf{I}\ddot{u}_g \quad (2.2)$$

where \mathbf{M} , \mathbf{C} , \mathbf{K} are mass, damping and stiffness matrices, respectively of the structure; \mathbf{I} is a vector containing 1 and 0 that projects earthquake forces to the desired DoFs of the model; $\ddot{\mathbf{u}}$, $\dot{\mathbf{u}}$ and \mathbf{u} are acceleration, velocity and displacement vectors, respectively; \ddot{u}_g is the ground acceleration coming from an earthquake.

The time history input consists in one or a series of seismic motions (displacement, velocity or accelerations) as a function of time, that last for the full extent of ground shaking, as illustrated in Figure 2.7. The maximum ground acceleration reached during the earthquake is called the peak ground acceleration. The seismic time history ground motion is established for each of three directions, typically east-west, north-south and vertical up-down.

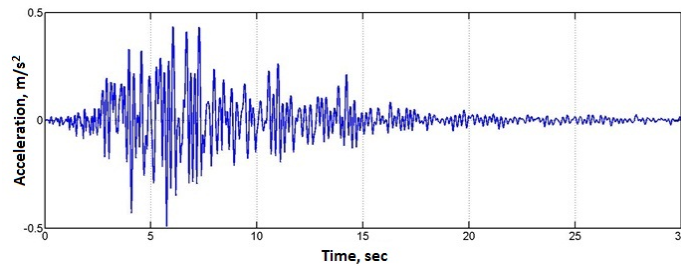


Figure 2.7: An earthquake acceleration time history.

A time history seismic input is rarely used for the design of piping systems; often it is used to generate facility specific response spectra analyses, or as a research tool, to study in detail the behaviour of a component or system as a function of time (Paolacci et al., 2011). Nowadays, the scientific community has widely accepted the use of natural records to re-produce a real input, for several reasons. For many engineering application, the purpose of selection and scaling of real earthquake is to fit the Code design spectrum considering the seismological and geological parameters of the specific site. To comply with the seismic codes set of accelerograms, regardless its type, should basically match the following criteria (EN1998-1 at point 3.2.3.1.2)

- *minimum of 3 accelerograms should be used;*
- *the mean of the zero period spectral response acceleration values (calculated from the individual time histories) should not be smaller than the value of the $a_g \times S$ for the site in question (S is the soil factor, a_g is design ground acceleration);*
- *in the range of periods between $0.2T_1$ and $2T_1$, where T_1 is the fundamental period of the structure in the direction where the accelerogram will be applied, no value of the mean 5% damping elastic spectrum, calculated from all time histories, should be $< 90\%$ of the corresponding value of the 5% damping elastic response spectrum.*

To help engineers in selecting a proper set of records, some tools have been proposed in the literature. The most recent is REXEL proposed by Iervolino et al. (2007). Sometimes (rarely) artificial or synthetic accelerograms are used to carry out a time history analysis. Time-history analysis is described in EN1998-1 at point 3.2.3 and similar methods are suggested by FEMA 450.

2.3.2.7 Modelling of piping systems

The piping system is usually modelled as a series of masses connected by massless springs having the properties of the piping. The mathematical model should include the effects of piping geometry changes, elbow flexibilities, concentrated weights, changes in piping cross sections, and any other parameters affecting the stiffness matrix of the model. Valves can be modelled as lumped masses at valve body and operator, with appropriate section properties for valve body and valve topworks. Rigid supports, snubbers, springs, and equipment nozzles should be modelled with appropriate spring rates in particular DoFs. Piping distributed weight should include pipe weight, insulation weight, and entrained fluid weight. Moreover, stress intensity factors, i , should be used to take into account the stress concentration effect induced by geometrical irregularities present in different components, e.g., elbows, Tee joints, branch connections. The factor, i , can be calculated according to European or American Standards (e.g., EN13480 or ASME B31.3).

2.3.2.8 Seismic qualification

The seismic qualification of piping system can be evaluated through experimental testing, e.g., shaking table tests or analytically, e.g., stress analysis.

Seismic qualification by testing

The most direct method to seismically qualify an active component that must perform a function during or after an earthquake is through shake table testing (American Lifeline Alliance, 2002; Kumar et al., 2010). In a shaking table test, the structure to be tested is placed on a shake table which is capable of exciting the whole structure with an earthquake ground motion. Essentially in the shaking table technique, the three basic dynamic forces namely, inertial, elastic and damping forces are induced in the tested structure. Such a pure experimental seismic response evaluation of structures necessitates the use of sophisticated and expensive dynamic actuators and control systems. Moreover, tests generally must be conducted on a reduced scale model

due to limitations on the size and payload capacity of the shaking-table, as well as for economical reasons (Carrion and Spencer, 2006).

A seismic test must be well planned and entrusted to a test facility experienced in applying seismic testing and test Standards. e.g., ICBO AC156, IEEE-344, IEEE-382 (American Lifeline Alliance, 2002).

Seismic qualification by stress analysis

One of the fundamental steps for the qualification of a pipe system is the fulfilment of some limits of the pipe stress or strain, for a given working condition. For a seismic action, usually the following two working conditions are considered (Paolacci et al., 2011).

(i) Operating condition or design basis earthquake condition (OBE)

OBE refers to a earthquake which, considering the regional, local geology and seismology, could be reasonably expected to affect the site during the operating life of the plant. It is the earthquake during which the operating conditions of the plant can be still assured.

(ii) Safe shutdown earthquake condition (SSE)

SSE corresponds to the maximum ground motion for which some critical components of the plant must be designed to remain functional.

In order to evaluate the safety level stress-based or strain-based approach can be used. The first approach intends to evaluate the maximum stress in the pipes and the calculation is usually based on elastic analysis of the structure.

While stress based approach for pipelines is acceptable for a material with a well defined yield point and with a well defined yield ductility and strength, this design criteria becomes invalid when the stress in pipelines exceeds the limit under some displacement control loads, such as earthquakes and landslides (Liu et al., 2009). In this case, strain based approach provides the design rule where the strain in the pipeline is allowed to exceed the specified yield strain provided that the safe operation can be ensured under displacement load. This method allows selected extensions to the stress-based design possibilities to take advantage of steel's well-known ability to

deform plastically, but remain a stable structure. Codes and Standards are available for the strain based design approach, see Liu et al. (2009) for reference. With the strain-based approach maximum strain in the pipes is calculated and compared with specified strain-limits related to limit states usually identified with buckling or ovalization of the pipes. Unfortunately, this approach needs the calculation of seismic response in the non-linear range. This is one of the reasons why the stress approach is used more (Paolacci et al., 2011).

Only EN13480-3 contains explicit indications for calculating the pipe stresses limits, considering both the above conditions (OBE and SSE), whereas ASME B31.3 indicates only occasional load conditions that can be identified as OBE condition. For the verification of the pipes against earthquake, the allowable stress approach is usually adopted.

The response to seismic and other loads, e.g., sustained, thermal, pressure, have to be combined. European and American Code prescribe similar combinations. In this respect the seismic load prescribed by the seismic Codes(EN1998-1, ASCE 07) can be considered as an exceptional seismic action. Under this condition, usually Load and Resistance Factor design (LRFD) approach is adopted. If the allowable stress approach is used, the seismic action has to be reduced, as usual, of a certain safety factor, typically 1.4 (see ASCE-07). ASME B31.3 does not provide an explicit equation for calculating the longitudinal stress, whereas EN13480-3 provides at point 12.3.3 the formula to evaluate the longitudinal stresses due to sustained, occasional and exceptional loads, e.g. the earthquake. A similar formula is given in ASME B31.1. The equation is expressed as follows:

$$\sigma = \frac{p_c d_o}{4e_n} + \frac{0.75iM_A}{Z} + \frac{0.75iM_B}{Z} \leq k f_h \quad (2.3)$$

where, i = stress intensity factor; M_A = moment from sustain mechanical loads; M_B = moment from occasional loads (in our case, an earthquake); p_c = internal pressure; d_o = pipe outer diameter; e_n = pipe wall thickness; f_h = allowable stress as expressed in these Codes; Z = section modulus; $k = 1.2$ and 1.33 according to EN 13480-3 and ASME 31.3, respectively for a design basis earthquake.

ASME Section III (2002) provides the following equation stress equation:

$$B_1 \frac{P_D D}{2t} + B_2 \frac{M_E}{Z} \leq 3S_m \quad (2.4)$$

where,

B_1 = primary stress index from Table NC-3673.2(b)-1 of ASME Section III (2002)

P_D = system pressure during the earthquake

B_2' = primary stress index from Table NC-3673.2(b)-1 of ASME Section III (2002)

M_E = amplitude of resultant inertial seismic and weight moment

S_m = allowable stress according to ASME Section III (2002)

There are several other stress formulas provided by Codes, e.g., RCCM (2000), RCC-MR (2002), which can also be used to perform stress analyses of piping systems under seismic loading.

2.3.3 Previous experimental tests

A significant number of experimental tests have been carried out by several researchers in order to investigate performances of piping systems under seismic loading, e.g., Slagis (1997); Suzuki et al. (2003); DeGrassi et al. (2003); Namita et al. (2003); Nakamura et al. (2004); Suzuki and Abe (2005); Martinez (2007); DeGrassi et al. (2008); Otani et al. (2011). These experiments were mainly conducted through shaking table tests. It was found from these experiments that piping systems exhibit satisfactory seismic behaviour and seismic motion is not severe enough to significantly damage piping systems unless large differential motions of anchorage are imposed. Experimental results confirmed that present design criteria for piping are over-conservative and modifications have been proposed to relax this aspect (Touboul et al., 2006; Otani et al., 2011).

Several experimental tests have been carried out on piping systems since 1990s to verify the ultimate strength against earthquake. In USA, *Piping and Fitting Dynamic Reliability Program* is a well known successful research program carried out by EPRI (1994). In Japan, NUPEC undertook experimental campaign on piping system under research programs, *Seismic Proving Test of Ultimate Piping Strength* (Suzuki et al., 2003; Suzuki and Abe, 2005) and *Seismic Proving Test of Eroded Piping* (Namita et al., 2003). These experiments showed that most of the failures by seismic excitation were low cycle fatigue, except for only a few case of collapse failure. It is described as

the seismic load is dynamic reversing load and the inertia force acts in the opposite direction to the deformation direction, then it is caused low cycle fatigue for most of the failures with dynamic reversing load.

DeGrassi et. al. (2008) conducted several shaking table tests under the program, *Seismic Analysis of Large-Scale Piping Systems*. The authors performed experiments on a large scale piping system containing 8" pipes, several elbows and a Tee joint. Several levels of earthquake loading were used during these tests. Experimental tests demonstrated the strain ratcheting behaviour of the pipes. A very high level of earthquake compare to that suggested by Codes was required to cause failure to the piping system. Failure initiated in one of the elbows of the piping system. All pipe failures observed in this test program were characterized as through-wall cracks that occurred as a result of fatigue ratcheting.

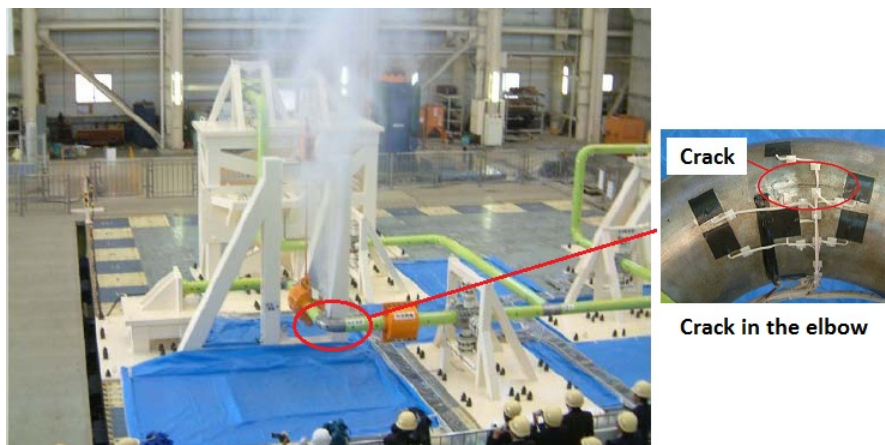


Figure 2.8: Failure of a piping system under shaking table test carried out by DeGrassi et. al. (2008).

Nakamura et al. (2004, 2010a) investigated safety margins of piping systems subjected to seismic loading and the failure behaviour of pipe components such as straight pipes and elbows. Recently, tri-axial shake table tests on sound and degraded piping systems were performed by Nakamura et al. (2010b). An interesting finding was that the failure mode changed depending on the presence of wall thinning. Test results showed that the dominant frequency and the maximum response

acceleration reduced due to the existence of wall thinning.

Touboul carried out significant experimental work on piping systems and components (Blay et al., 1997; Touboul et al., 1999). Their experimental results showed that present design criteria are very conservative and piping systems and components (with or without defects) can withstand a high level of earthquake loading without being damaged. In 2006, Touboul proposed enhanced seismic criteria for piping based on experimental tests and extensive analysis (Touboul et al., 2006). Some modifications of Code based formulas for seismic analysis were proposed by the authors in order to relax the over-conservatism present in the available design Codes.

A number of shaking table tests on piping systems and components have recently been reported, e.g., Shibutani (2011); Otani et al. (2011); Nakamura et al. (2011). Otani et al. (2011) analysed performance of a piping system with elbow elements and evaluated the seismic design margin of the system. Test results were compared with the primary stress and usage factor based on the design Code. The authors found that the usage factors based on design Code were excessive. They suggested that this excessive margin can be reduced by considering the response reduction effect by plastic deformation and the reasonable equivalent cycles.

Nakamura et al. (2011) carried out an investigation on the seismic safety capacity of aged piping system by shaking table test. From the experiment, the seismic margin of the piping system with wall thinning was found about five times the design level compared with the primary stress limitation based on the model without wall thinning. The failure mode of the test models was the crack penetration at a Tee, no unstable failure, such as excessive progressive deformation occurred.

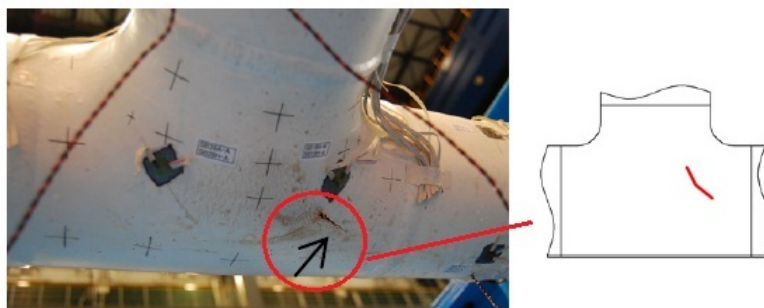


Figure 2.9: Crack in a Tee joint under shaking table test carried out by Nakamura et al. (2011).

The above experimental tests confirmed a favourable seismic performance of piping systems and components. Failures mainly occurred in the critical elements of the piping systems, but under high levels of earthquake. It has been confirmed that present seismic design rules are highly conservative for piping systems and modifications have been suggested to relax this over-conservatism.

2.4 Pipe Elbows: seismic design, analysis and testing

An elbows is a very important and common component of a piping system which can be found almost in all piping systems. It is a pipe fitting installed between two lengths of pipe or tubing to allow a change of direction. The ends of an elbow can be connected with pipes by several means such as butt welding and threaded connections. Important parts of an elbow include elbow radius, crown, flank, extrados and intrados as illustrated in Figure 2.10.

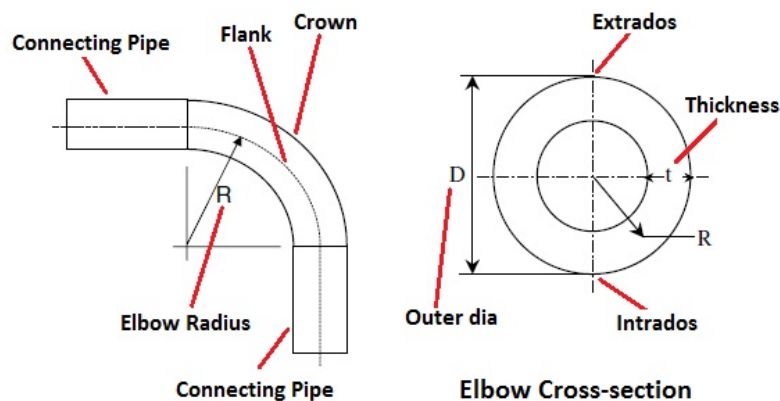


Figure 2.10: Parts of an elbow.

Elbows are very flexible and due to their geometric irregularity, stresses are intensified in these components (Nayyar, 2007). During an earthquake event, in addition to other service loads, they are subjected to strong repeated cyclic structural loading that may lead to failure due to cyclic accumulation of plastic strain or collapse. Furthermore, due to their flexibility, significant non-linearities occur and the elbow cross-section shape distorts as cyclic loading takes place resulting at an oval or flat-

ten shape at the end of the loading sequence (Varelis et al., 2011).

Both American and European Codes for piping system design, e.g., ASME B31.1 (2001); ASME B31.3 (2006); ASME B31.8 (2003); EN 13480-3 (2002), contains design and analysis guidelines for elbow elements. Since the stress distribution of an elbow is essentially complicated, the simplified and convenient method to calculate the stress is provided by design Code based on previous researches (Otani et al., 2011). These Codes provide equations to calculate parameters for elbow design and analysis, e.g., thickness, flexibility factor and stress intensity factor (see for example, EN13480-3, points 6.2, 8.3 and Annexes B, E and H).

The flexibility factor, k_B and stress intensity factor, i are two important parameters for stress analysis of piping system under seismic loading. Annex H of EN13480-3 gives the following equations to calculate these factors.

$$k_B = \frac{1.65}{h} \quad (2.5)$$

$$i = \frac{0.9}{h^{2/3}} \quad (2.6)$$

h is called the flexibility characteristic which is defined as:

$$h = \frac{4Re_n}{d_m^2} \quad (2.7)$$

where, R = elbow radius; e_n = elbow thickness; and d_m = mean diameter of the elbow. These terms are illustrated in Figure 2.11.

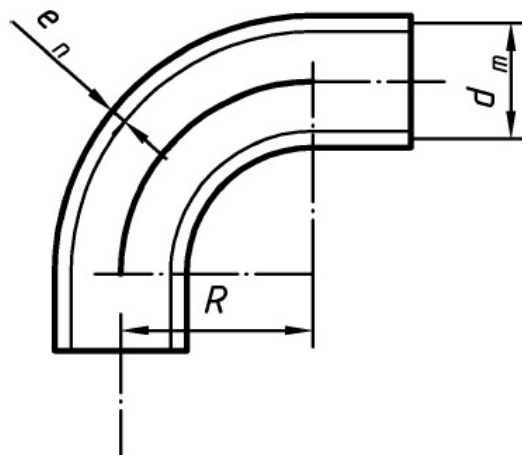


Figure 2.11: Elbow parameters.

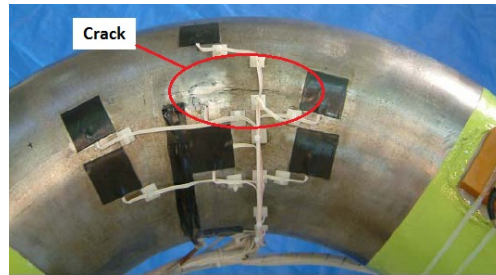
While carrying out stress analysis of piping system, the stress intensity factor is used in the equations to take into account the flexibility characteristics of an elbow. For example, in the stress equation (Equation 4.13, showed again below), i is calculated using above equations.

$$\sigma = \frac{p_c d_o}{4e_n} + \frac{0.75iM_A}{Z} + \frac{0.75iM_B}{Z} \leq k f_h$$

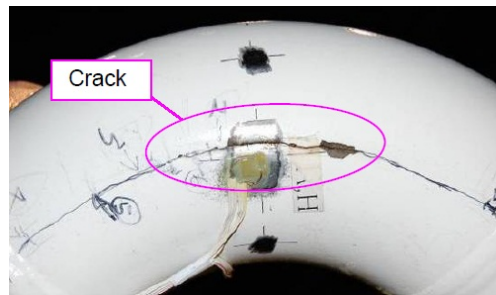
Note that, in case of straight pipes, the term, $0.75i$ has the value of unity. Whereas, for an elbow the value of i is usually greater than one. Hence, the stress level on the left hand side of this equation becomes greater due to applied moments in case of an elbow. This indicates that, under seismic loading, a higher level of stress generates in the elbow compare to straight pipes.

A significant amount of numerical work has been devoted on the analysis of elbow elements since the beginning of 20th century, e.g., Rodabaugh and George (1957); Suzuki and Nasu (1989); Mourad and Younan (2001); Chattopadhyay et al. (2006); Varelis et al. (2011, 2012); Karamanos et al. (2013). However, most of these works were dedicated to analyse the performance of elbows under monotonic and cyclic loading. These analyses proved that elbow elements show favourable performance, e.g., good energy dissipation capacity, favourable non-linear behaviour, under monotonic and cyclic loading.

A number of experimental tests were also conducted on the elbow component under seismic loading, e.g., DeGrassi et. al. (2003); Martinez (2007); DeGrassi et. al. (2008); Shibutani (2011); Otani et al. (2011). These experiments were mainly carried out by means of shaking table tests on piping systems. Results from these experimental tests showed that typical failure of an elbow generally occurs in the flank on the elbow, see Figure 2.12. It was found that longitudinal cracks initiated on the inner surface of the flank and progressed through to the outer surface. The cracks were caused by local bending at the flank.



(a)



(b)

Figure 2.12: Failure of elbow in the flank found from shaking table tests performed by (a) (DeGrassi et. al., 2008); (b) (Otani et al., 2011).

Shibutani (2011) conducted failure analysis of piping system with and without thinned elbows through shaking table tests. In the case of the sound piping system, the elbow under investigation failed under in-plane bending. The accumulated equivalent strain increased at the flank of the elbow where the crack initiated. The fatigue crack was found to be induced by in-plane cyclic bending. Whereas for the degraded piping system, failure occurred under out-of-plane bending.

All experimental results have shown that available design Codes are quite conservative for elbows and failure loads are far higher than those described by the design criteria. It has been confirmed that the seismic design margin is extremely conservative for this component (Otani et al., 2011).

2.5 Bolted Flange Joints: design, analysis and testing

2.5.1 Bolted flange joint

One of the most essential and complex components present nearly in all piping systems is the Bolted Flange Joint (BFJ). Such a joint consists of two matching metallic disks called flanges which are usually welded or screwed into piping systems. The flanges are bolted together having a gasket in between them in order to achieve a strong seal. Thus a BFJ connects pipes, valves, pumps and other equipment to form a piping system. A flange joint consists of four main parts: (i) flange; (ii) connecting pipe; (iii) bolt and (iv) gasket as shown in Figure 2.13.



(a)



(b)

Figure 2.13: A bolted flange joints and its components.

The main component of a bolted flange joint is the flange. Flanges are classified into different types depending on the way in which the flange is attached to a pipe. Different types of flanges are described in American and European Codes, e. g., ASME B16.5 (2009) and EN 1092-1 (2007), respectively. EN 1092-1 classifies flanges into 14 different types. Some of the common flange types are described below and pre-

sented in Figure 2.14.

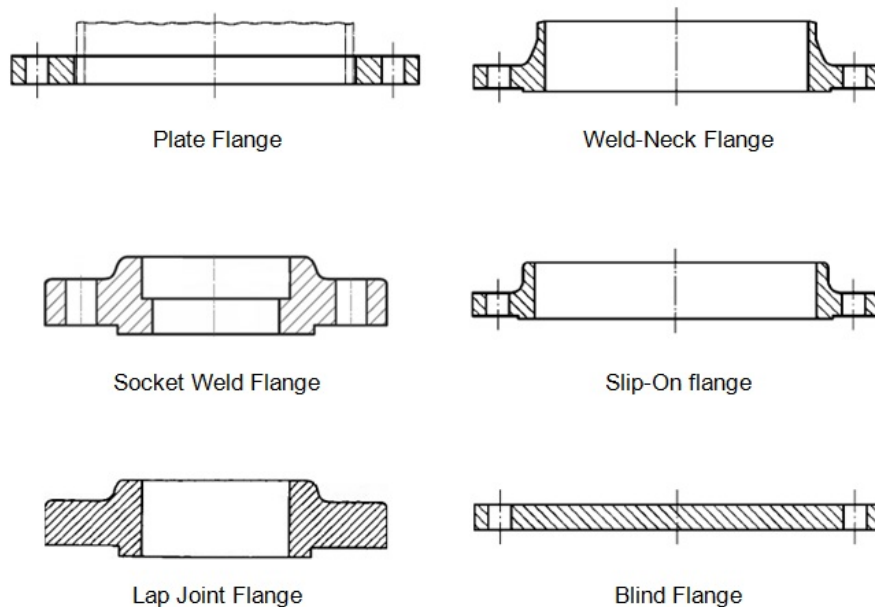


Figure 2.14: Some common types of flange.

(i) *Plate flange:*

This is the simplest type of flange and classified as Type 01 flange in EN 1092-1. A plate flange is a flat, circular disk that is normally fillet welded onto the end of a pipe. This type of flange is typically used in fuel and water pipelines.

(ii) *Weld neck flange:*

The weld neck flange is the most commonly used type of flange including in petrochemical facilities. It is butt-welded to the pipe. This flanges are typically used on arduous duties such as high pressures and/or hazardous fluids. EN 1092-1 classifies this flange as Type 11 flange.

(iii) *Socket weld flange:*

Socket weld flanges may used on high pressure, hazardous duties but are limited to a Nominal Pipe Size (NPS) of 11/2 inches. The pipe is fillet welded to the hub of

the socket weld flange. The use of this flanges in petrochemical facilities is limited and not preferable.

(iv) *Slip-On flange:*

In this flange, the pipe is double-welded both to the hub and the bore of the flange. This type of flange is typically used on low pressure, low hazard services such as fire water, cooling water, etc. Like socket weld flange, the use of this flanges in petrochemical facilities is limited and not preferable. This flange is the Type 12 flange according to EN 1092-1.

(v) *Lap joint flange:*

This flange is classified as Type 33 flange in EN 1092-1. It comprises of a hub or stub end welded to the pipe and a backing flange or capped flange which is used to bolt the joint together. This type of flange joint is typically found on Cunifer and other high alloy pipework. This type of flange is not commonly used in petrochemical facilities.

(vi) *Blind flange:*

This flange is used to blank off pipelines, valves and pumps, it can also be used as an inspection cover. It is sometimes referred to as a blanking flange. This is classified as Type 05 flange in EN 1092-1.

Flanges are also given certain classifications in the Codes depending on the operating conditions such as PN designated, (see, for example, EN1092-1, 2007) and class-designated, (see, for example, EN1759-1, 2004), under which they are designed to use.

An important aspect of a flange is the flange face. A flange face determines the flange-gasket-flange contact type. EN 1092-1 classifies flange faces into 8 categories among which two commonly used flange faces in a refinery plant are the flat face and raised face ones, see Figure 2.15.

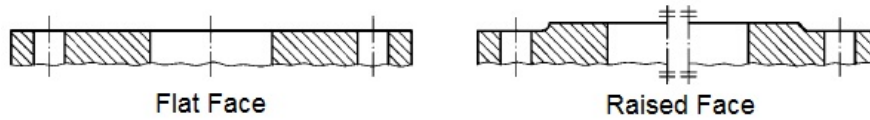


Figure 2.15: Flange faces.

Another important part of a flange joint is the gasket which is placed between two flanges in order to prevent leakage, see Figure 2.16. Since a gasket is always in contact with the media in which it is working, it requires resistance against the media and temperature within the range of the given application. Some essential requirements of a gasket include good compressibility, face adaptability, good recovery, strength, limited relaxation, chemical resistance and temperature resistance.

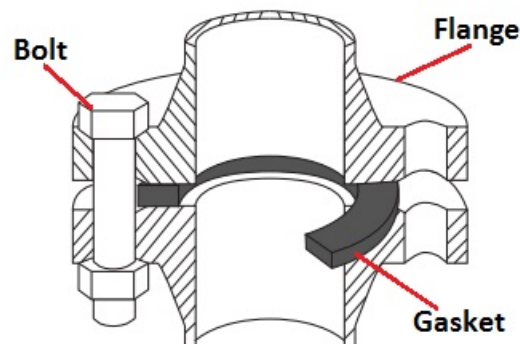


Figure 2.16: Placement of a gasket between two flanges.

Gaskets can be classified into two main categories: (i) Metallic and semi-metallic gasket and (ii) non-metallic gasket.

Metallic or semi-metallic gaskets consist of metal or a combination of metal parts and non-metal parts. These gaskets are suitable for medium and high pressure applications. Metallic gaskets require a much higher quality of the sealing surface compared to non-metallic gaskets. Some examples of these types of gasket are corrugated metal gaskets, metal jacketed gaskets, ring joints and spiral wound gaskets, see Fig-

ure 2.17.

Non-metallic materials are used in low to medium pressure applications usually up to nominal pressures of 40 or 63 bars on the raised face and up to 200 bars in tongue grooved flanges (a flange has a tongue which is inserted into a groove of the mating flange). Some of the non-metallic gaskets are fibre reinforced gaskets, graphite gaskets, PTFE gaskets and rubber gaskets, see Figure 2.17.

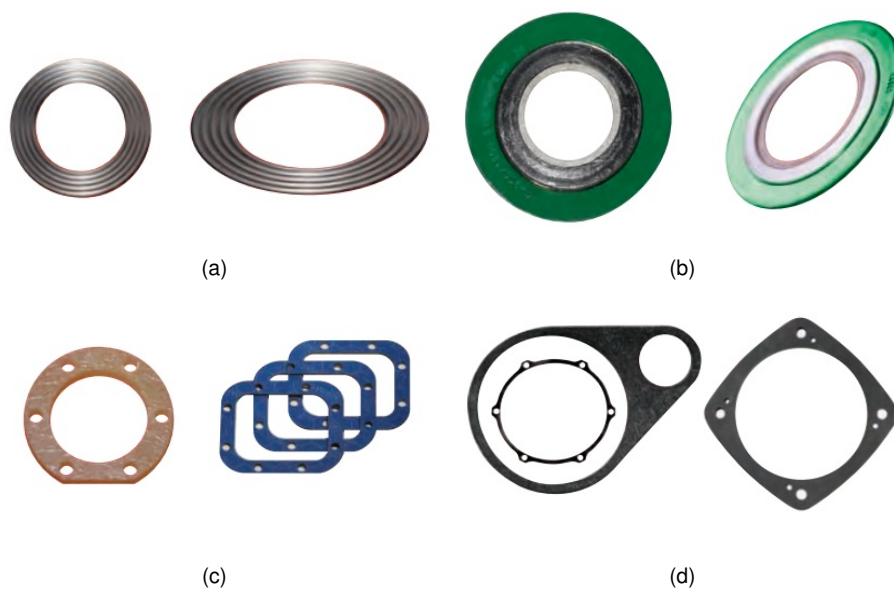


Figure 2.17: Some metallic and non-metallic gaskets: (a) a corrugated metal gasket; (b) a metallic spiral wound gasket; (c) a non-metallic fibre reinforced gasket; (d) a non-metallic rubber gasket.

A flange joint is considered to function correctly if it is tight, and its integrity is guaranteed for the entire period of operation. Tightness means that the joint remains within its tightness class under all states of operation, i.e. the leak rates (emissions) are limited. Integrity is achieved by limiting the stresses in the component (safety against failure). Both the demanded tightness class and the stress limitations are input values for the analysis of the joint; they determine the efforts that are necessary to prove function.

2.5.2 Design Codes and Standards

The successful design and operation of a bolted flange joint in service are determined by several factors- namely, the interaction between the bolting, flange, and gasket, as well as important non-linear variables such as friction and gasket properties (William, 2006). Nowadays, both American and European Codes and Standards are available for the design of bolted flange joints. These Standards and Codes provide a method for sizing the flange and bolts to be structurally adequate for the specified design conditions. In the following, major American and European Codes used by the industry to address the design of flange joints are presented.

2.5.2.1 American Codes and Standards

The following American Codes provide design guidelines for BFJs.

- i) ASME Section VIII Division 1 (2007)
- ii) ASME Section VIII Division 2 (2007)
- iii) ASME Section VIII Division 3 (2010)
- iv) ASME Section I (2010)
- v) ASME Section III (2007)
- vi) ASME B31.3 (2006)
- vii) ASME B31.1 (2001)
- viii) ASME B31.8 (2003)
- ix) ASME B31.4 (2002)

The design rules provided in *ASME Section VIII Division 1 (2007)* allow the use of flanges in accordance with Standards ASME B16.5 (2009); ASME B16.42 (1998) and ASME B16.47 (2006), which provide dimensions of flanges and their components at various pressure-temperature ratings. This Code also provide design rules for the design of special flanges. Design of flange joints is addressed in Appendix 2, Y, S; paragraphs UG-44, U-3, UG-11(a)(2), UG-22 and UG-34.

ASME Section VIII Division 2 (2007), in part 4 and 5, gives the provision to design

BFJs considering all operating conditions and utilizing the applicable allowable stress values. External forces and moments are also included in the design basis.

In *ASME Section VIII Division 3 (2010)*, flange connections are generally of a special design.

The design rules provided in *ASME Section I (2010)* allows the use of flanges in accordance with the Standards; however, no rules are provided for non-standard flanges. Design guidelines are included in Appendix A and paragraph PG-31, PG-59.1.1.2, PG-42.1, PG-42.4.4, PG-42.4.5, PG-42.4.7 and PG-42.4.8.

Section III of ASME Code (ASME Section III, 2007) contains provisions for BFJ design by the use of referenced Standards and provisions for design-by-analysis and design-by-formula approaches similar to those of Section VIII. Main paragraphs in this standard containing design rules for BFJs are NB-3132, NB-3200, NB-3222, NB-3227.4, NB-3230, NB-3647, NB-3658, NC-3658.2 and NC-3658.3.

ASME B31.3 (2006) has design rules that accept both Standard and non-standard flanges. These rules are addressed in paragraph 302.2.1, 304.7.2, F312, 301.3.2, 302.2.4, 306.4, Chapter IX and Appendix L.

In *ASME B31.1 (2001)*, similar to ASME B31.3, listed Standards are accepted and design rules are provided for non-standard flanges. Important paragraphs containing BFJ design rules are 104.5 and 108.5. Table 112 of this standard provides flange bolting, facing, and gasket requirements.

ASME B31.8 (2003) has provisions for the designing of flange joints using Standards ASME B16.5. In this standard, a formula is provided to estimate the external moment that produces leakage in a BFJ.

ASME B31.4 (2002) allows the design of BFJ in accordance with the listed Standards in Table 426.1. Paragraph 40.4.5 contains design rules for BFJs.

2.5.2.2 European Codes and Standards

The following two European Standards are mainly used for the design of bolted flange joints:

i) *EN 13445-3 (2002)*

ii) *EN 1591 (EN 1591-1, 2009; EN 1591-2, 2009)*

EN 13445-3 is based on the ASME procedure which is incorporated in chapter 11 of this Code. However, this Standard provides more or less a dimensioning guideline only applicable for a formal stress analysis. It is not possible to perform a tightness analysis on this base. Appendix G of this Standard incorporates the comparatively new flange calculation rules provided in European Standard EN 1591-1 (2009).

EN 1591 is a comparatively new European Standard which, unlike most conventional flange design methods, e.g., ASME VIII, provides design rules that ensure leak tightness of a BFJ. This Standard is based on an old German standard, TGL 32903/13 that has been used in the design of BFJs without any leakage problems since the 1980s (Zerres and Guerout, 2004). It has two parts: (i) EN 1591-1 (2009)-dedicated to the calculation method and (ii) EN 1591-2 (2009)- contains gasket parameters.

The ASME rules for the design of bolted flange joints are based on the Taylor-Forge method (Waters et al., 1937) and PVRC alternative rules (Mikitka, 2002). Calculations with the Taylor Forge enable checking the admissibility of the BFJ for the calculation conditions. The alternatives rules proposed by PVRC are more complete than the Taylor Forge method since they consider external forces and bending moments in the calculation, as well as the scatter of the tightening device. However, the deformations of the BFJ components during operation are not taken into account. As a consequence, the remaining gasket surface pressure cannot be determined. Therefore, the leak-rate, which depends on the remaining gasket surface pressure at the considered calculation condition, cannot be determined.

On the other hand, the new European Standard, EN 1591-1 is based on a mechanical model which includes the deformations of all the components of a BFJ; the internal forces can be determined for all the load conditions. The admissibility of an initial bolts tightening is checked based on both leak-tightness and strength criteria, combined with the consideration of the scattering due to the tightening device. This

standard, therefore, ensures both the mechanical integrity and leak-tightness criteria of a flange joint under designed operating conditions.

In the above-mentioned Codes and Standards, main loads acting on a BFJ considered are internal pressures, external forces, external bending moments and thermal loads. Design rules ensure joint integrity and leak-tightness of a BFJ in operating conditions. However, none of the design rules takes into account seismic loading for the design of a BFJ.

2.5.3 Component Standards

There are several Standards that provide dimensions of different parts of a BFJ. These Standards are helpful while designing a BFJ using Standard flanges. As there are several types of flange joints in industrial plants the standardization of designs makes sense, especially in terms of cost reduction. Standardized modelling of material behaviour and the use of standardized calculation procedures reduce the complexity of the analysis.

2.5.3.1 Flange Standards

The major American and European Standards for flanges are listed below.

American Standards:

- i) *ASME B16.5 (2009)*
- ii) *ANSI/ASME B16.1 (2005)*
- iii) *ANSI/ASME B16.24 (2006)*
- iv) *ANSI/ASME B16.34 (2009)*
- v) *ASME B16.42 (1998)*
- vi) *ASME B16.47 (2006)*
- vii) *ANSI/ASME B16.48 (2009)*

European Standards:

- i) *EN 1092-1 (2007)*

- ii) *EN 1092-2 (1997)*
- iii) *EN 1092-3 (2003)*
- iv) *EN 1092-4 (2004)*
- v) *EN 1759-1 (2004)*
- vi) *EN 1759-2 (2002)*
- vii) *EN 1759-3 (2003)*
- viii) *EN 1759-4 (2004)*

2.5.3.2 Gasket Standards

American Standards

The ASME Pressure Vessel and Piping Codes do not provide specific guidance on how to select the correct gasket for a specific application; doing so is the responsibility of the user. The flange Standards, such as ASME B16.5 and B16.47, are based on certain gasket types and dimensions as specified in the standard. Some gasket-design issues (William, 2006) are: (i) gasket type and characteristics- density, flexibility, creep, suitability for the process and temperature, and so forth; (ii) gasket properties for design-PVRC gasket constants and ASTM Standard tests; (iii) reference to a dimensional standard, such as ASME B16.21, is recommended; (iv) ring joint gasket materials shall conform to ASME B16.20. Materials for other gaskets shall be in accordance with ASME B16.5 ANNEX C. Following are some major American gasket Standards:

- i) *ANSI/ASME B16.20 (2007)*
- ii) *ANSI/ASME B16.21 (2005)*

European Standards

European Standards distinguish gasket Standards into two categories: (i) Standards for PN designated flanges and (ii) Standards for Class designated flanges.

Standards for PN designated flanges

- i) *EN 1514-1 (1998)*
- ii) *EN 1514-2 (2005)*

- iii) EN 1514-3 (1998)
- iv) EN 1514-4 (1998)
- v) EN 1514-5 (1998)
- vi) EN 1514-6 (2004)
- vii) EN 1514-7 (2005)

Standards for Class designated flanges

- i) EN 12560-1 (2001)
- ii) EN 12560-2 (2001)
- iii) EN 12560-3 (2001)
- iv) EN 12560-4 (2001)
- v) EN 12560-5 (2001)
- vi) EN 12560-6 (2003)
- vii) EN 12560-7 (2004)

2.5.3.3 Bolt and Nut Standards

There are Standards for bolts and nuts developed by ASME which can be used in order to select suitable bolts for a flange joint. Following are some American Standards for bolts and nuts:

- i) ASME B18.2.1 (2010)
- ii) ASME B18.2.2 (2010)
- iii) ASME B18.2.5M (2009)

Some European Standards are developed solely for selecting bolts and nuts for flange joints. Commonly used European Standards for bolts and nuts to be used in a BFJ are listed below:

- i) EN 1515-1 (2002)
- ii) EN 1515-2 (2004)
- iii) EN 1515-3 (2005)

The Standards mentioned above can be used to find appropriate dimensions and materials of different components at given operating conditions while designing a BFJ.

2.5.4 Design methods

A historical summary and bibliography on the methodology used to design bolted flange joints can be found in Blach and Bazergui (1981). The first calculation method dedicated to BFJ design was developed in the 1930s by the Taylor Forge Company (Waters et al., 1937) which was quickly introduced in the ASME Boiler and Pressure Vessel Code in the 1940s, and later in other national Codes such as BS 5500 in UK or CODAP in France (Zerres and Guerout, 2004). Although the Taylor-Forge method ensured joint integrity of a BFJ in designed operating conditions, it did not have a design rule for leak tightness. In order to overcome this limitation, the alternatives design rules, which were more complete than the Taylor Forge method, were proposed by PVRC (Mikitka, 2002). However, these alternative rules still could not fully ensure leak-tightness of a BFJ (Zerres and Guerout, 2004). The new European Standard, EN 1591 (EN 1591-1, 2009; EN 1591-2, 2009) was developed for the design of BFJs ensuring the leak-tightness criteria and admissibility of the joints in all load conditions.

The basic design methodology of a BFJ can be understood by the Taylor-Forge method. The Taylor Forge method, which is based on a mechanical calculation of the joint, verifies the admissibility of a BFJ for given calculation conditions. The calculation is based on an axial forces balance as follows,

$$F_B = F_G + F_P \quad (2.8)$$

where, F_B , F_G and F_P are the bolt load, gasket reaction and axial force due to internal pressure, respectively, as illustrated in Figure 2.18.

The admissibility of the BFJ is verified for all the calculation conditions considering integrity criteria. The following conditions must be satisfied,

$$\left. \begin{array}{l} P_G > Y \\ P_G > m \times P \end{array} \right\} \begin{array}{l} \text{at assembly} \\ \text{at other calculaton conditions} \end{array} \quad (2.9)$$

where, P_G is the gasket surface pressure; Y is a gasket seating pressure as defined

in the ASME Codes; P is the internal pressure; and m is a multiplication factor. P_G must be ensured by applying a certain tightening force to the bolts.

The Taylor Forge method is also based on a fundamental assumption by considering that the gasket surface pressure at all calculation conditions is the required one, i.e., Y or $m \times P$.

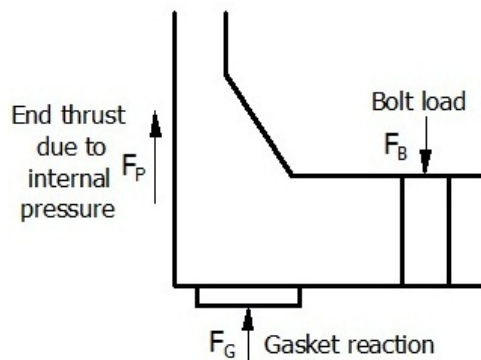


Figure 2.18: Axial forces balance in a BFJ used in the Taylor Forge calculation.

Bolts forces are calculated in order to maintain the required compressive stress, i.e., Y and $m \times P$, on the gasket at all the calculation conditions. Then, the total required cross-sectional area of bolts is determined and compared to the actual cross-sectional area of bolts. The admissibility of the flanges is checked by calculating the most critical stresses, which are the longitudinal stress in hub, the radial stress in flange and the tangential stress in flange.

Using the Taylor-Forge method, mechanical integrity of the BFJ can be checked but the evolution of the internal forces cannot be known. It means that for a given initial bolts tightening, it is not possible to determine the remaining bolt load and gasket reaction for the subsequent calculation conditions. Moreover, the gasket parameters, m and Y do not consider the leak-rate of the flange joint and, therefore, the leak-tightness of the BFJ cannot be checked according to this method.

In order to overcome the above-mentioned limitation of the Taylor-Forge method, the PVRC alternative rules (Mikitka, 2002) was developed in the 1980s. These rules defined some new gasket constants, based on experimental tests, that characterized

the leak-tightness behaviour of gaskets (Payne, 2002). With these new gasket parameters, three tightness classes, corresponding to three given leak-rates, were defined. A minimum required tightness, T_{pmin} , is determined with respect to a chosen tightness class. To maintain, T_{pmin} , after considering the effect of internal pressure, external forces, bending moments and scattering due to the tightening device, a required gasket surface pressure, P_{Greq} is determined using the newly defined gasket factors. In order to maintain P_{Greq} , a required bolt load is determined for each calculation condition. A minimum required cross-sectional area of bolts is then calculated. The most critical stresses and the rigidity of the flanges are then evaluated. Thus, the integrity of a BFJ is verified for all the calculation conditions.

Unlike the Taylor-Forge method, the alternative rules also consider external forces and bending moments and a possible scattering due to the tightening device in the design of the BFJs. Nevertheless, this method is still based on the axial forces balance. It does not consider the deformations of the BFJ components such as the gasket compression, the bolts elongation and the flanges rotations, neither differential axial thermal expansion between the bolts and the flanges. It means that the fundamental calculation assumption of the Taylor Forge method is still used. Moreover, evolution of internal forces, e.g., bolts load and reaction on the gasket, for a given initial bolts tightening cannot be determined. Hence, the leak-rate, which depends on the remaining gasket surface pressure at the considered calculation condition, cannot be determined.

The newly developed European Standard, EN 1591 (EN 1591-1, 2009; EN 1591-2, 2009) provides a better knowledge of the behaviour of a flange joint at different operating conditions. Based on both leak-tightness and strength criteria, EN 1591 enables a better tightening recommendation and an improvement of the leak-tightness in view of the respect of new requirements concerning fugitive emissions limitation. It is recognized as being the only methods that specifically addresses flange leakage in a rigorous way (Mair, 2011).

The aim of the calculation method described in EN 1591-1 is to analyse the behaviour of a BFJ for given load conditions and to check the admissibility of the joint at all load conditions for a given initial bolts tightening. The calculation method is based

on an axially symmetrical mechanical model, taking into account the whole flanges-bolts-gasket system behaviour (Zerres and Guerout, 2004). Loads and some other important parameters treated by EN 1591-1 mechanical model to carry out calculations are listed below and illustrated in Figure 2.19:

- i) fluid pressure;
- ii) mechanical strength values of flanges, bolts and gaskets;
- iii) gasket compression factors;
- iv) nominal bolt load;
- v) possible scatter due to bolting-up procedure;
- vi) changes in gasket force due to deformation of all components of the joint;
- vii) influence of connected shell or pipe;
- viii) effect of external axial forces and bending moments;
- ix) differential axial thermal expansion between the flanges and the bolts.

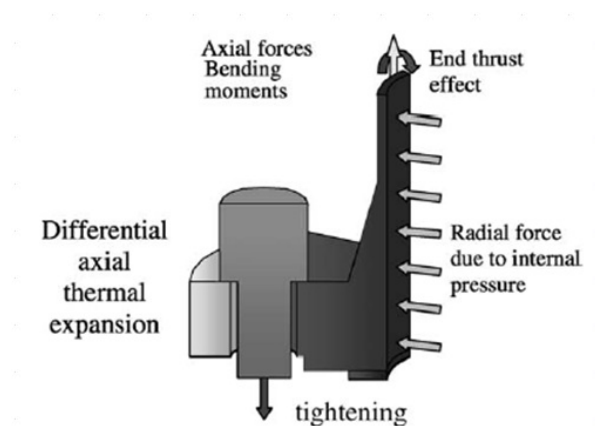


Figure 2.19: Loads considered in EN 1591 mechanical model.

The first step in EN1591 calculation is to determine the required initial bolts tightening to maintain a sufficient gasket surface pressure at all load conditions. The gasket seating criterion in assembly condition and leak tightness criterion with internal pressure must be fulfilled.

Seating criterion is defined as,

$$P_G > Q_{min}; \text{ at assembly} \quad (2.10)$$

where, P_G and Q_{min} are the gasket surface pressure and minimum gasket pressure, respectively, at assembly. This leads to the determination of the minimum required force, F_{Gmin} , to be applied at assembly in order to ensure a proper seating of the gasket.

The leak-tightness criterion is expressed as,

$$P_G > Q_l; \text{ at other operating conditions} \quad (2.11)$$

where, Q_l is the required gasket surface pressure to maintain a chosen leak rate for a given temperature, pressure and maximum surface pressure applied on the gasket. Required values of gasket properties for different leak rates are provided in EN 1591-2 (2009).

In order to maintain required Q_l at all operating conditions, the required force at assembly, F_{G0req} , is determined through a compliance equation. The compliance equation takes into account axial fluid pressure, external axial force, external bending moment and thermal effect to calculate a gasket force, $F_{G\Delta}$, in different operating conditions. Thus, the required force, F_{G0req} , to be applied on the gasket at assembly in order to satisfy both seating and leak-tightness criteria is obtained as,

$$F_{G0req} = \max\{F_{Gmin}; F_{G\Delta}\} \quad (2.12)$$

Once the required assembly load is found, the next step is to calculate load ratios of the flange, bolt and gasket to check the mechanical integrity of the BFJ at all load conditions where the load ratio is defined as the ratio between applied load and allowable load.

The load ratio of the gasket enables to limit the compression of the sealing component. The gasket surface pressure must remain lower than the maximum allowable gasket pressure, Q_{max} . Load ratio of the bolt provides a limitation of the traction as well as a limitation of the torsion when bolt tightening is performed using a torque. The flange load ratio limits the rotation of the flange ring cross-sections. All load ratios in an operating condition must have a value less than or equal to unity for all load conditions to ensure the mechanical integrity of a BFJ.

The required assembly gasket force, F_{G0req} , is provided through a tightening torque

applied to each bolts of the BFJs during the assembly. Necessary guidelines to calculate this tightening torque are also provided in EN 1591-1.

2.5.5 Previous experimental tests

Although significant studies were carried out on the numerical analysis of bolted flange joints, e.g., Abid and Nash (2003); Tenma et al. (2011); Nagata et al. (2011); Abid et al. (2011a), only a few experimental works on such joints have been reported so far, e.g., Guizzo (1998); Nash and Abid (2000); Semke et al. (2006). These numerical and experimental analyses mainly investigated the sealing capacity of flange joints under internal pressure and external loads. Some experimental works on bolted flange joints are currently being undertaken by an European Project, INDUSE INDUSE (2009).

Guizzo carried out a number of experimental tests on bolted flange joints consist of Class 150 and Class 300 flanges (Guizzo, 1998). The work was an attempt to verify whether the new gasket constants theory, developed by the PVRC to help in the design of bolted flanges, can be used to predict the actual field behaviour of a bolted joint using a non-metallic gasket in conjunction with standard Class 150 and Class 300 flanges. Leakage measurements were made under various fluid pressures and temperatures. Results were compared with the expected values used to determine the gasket assembly loads according to the new gasket constants concepts. In order to have a direct comparison, the same fluid used to determine the gasket constants (Nitrogen) was also used in the experimental work. In order to compare the leakage obtained in an actual bolted joint with the leakage rate (Tightness Class) used to determine the torque to be applied on the gasket during assembly, using the new gasket constants concept, Guizzo ran a series of experiments using a non-asbestos compressed sheet gasket in conjunction with standard commercial flanges. A total of fifteen tests were made, with six different gaskets, using Class 150 cells; and a total of 21 tests were made, using nine gasket samples, in the Class 300 cells. All tested samples were cut from the same gasket material.

The main findings of the experimental tests were: (i) the leak rate obtained in ac-

tual bolted joint connections was significantly lower than the predicted in the torque calculation procedure; (ii) with time and temperature the gasket material modified its internal structure and even though the gasket load was reduced due to the creep effect, the actual leak rate still remained much lower than the predicted one. Based on the test results, the author concluded that the new gasket constants concepts and calculation procedure should not be used neither for leakage prediction nor for performance analysis type of calculations and it should only be used for flange design purposes.

A considerable amount of work, both numerical and experimental, on bolted flange joints has been carried out by Abid and Nash, e.g., Nash and Abid (1998, 2000); Abid and Nash (2003); Abid et al. (2011b). In order to assess the effects of external loading on flanges, Abid and Nash conducted some experimental tests (Nash and Abid, 2000) on a number of number of flange joints including ANSI joints and compact VCF joints. A combined load test rig, see Figure 2.20, was used to test the joints for a variety of load combinations. A total of 7 load combinations including bending moment, internal pressure and tensile load were used during the experiments.

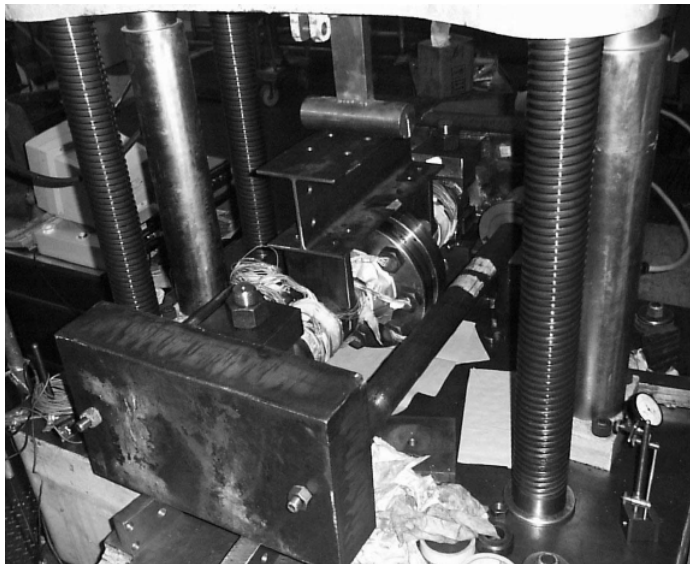


Figure 2.20: Experimental test performed on an ANSI joint under internal pressure, bending and tensile load (Nash and Abid, 2000).

Experimental results showed that the joints under investigation can safely withstand high level of axial and bending loads along with high internal pressure. No leakage was observed for both ANSI and VCF joints. However, a comparison of the overall results showed that the VCF joint is more effective. This phenomenon was already proved through stress analysis by Power (1997) and Nash and Abid (1998). In addition, the authors indicated that, due to low weight, easy handling, low risk, less maintenance and smaller physical size, the VCF had the advantage over the ANSI flange joint.

Abid and Nash undertook another experimental campaign in 2006 (Abid and Nash, 2006) where they studied a gasketed flange joint during assembly, highlighting the importance of proper bolt tightening sequences, bolt pre-loading, bolting and bolt tightening methodology, number of passes to make a joint, gasket quality, gasket physical condition, gasket location and use of different gaskets in the joint, as all these factors can provide joint relaxation. It was concluded from the experimental results that even using same bolts, same set-up, same technician, same lubricant, calibrated torque wrench, controlled bolt tightening methods or environment, the behaviour of joint relaxation for a gasketed flange joint can not be avoided. It varies even for the same joint tightened each time and also for different joints used. The authors commented that joint relaxation behaviour in gasketed joint results in dynamic mode, providing fatigue mechanism in the joint, and is the main cause for its failure.

Semke et al. (2006) conducted an important experimental work in 2006 on some bolted flange joints. In that work they investigated the effect of a bolted joint on the dynamic response of a pipe on various spans is investigated. The problem was analysed both experimentally and numerically by use of computer modelling. In the experimental set-up, the bolted flange joint was placed in the middle of a pipe which rested on on two supports as illustrated in Figure 2.21. Tests were carried out on 2 inch and 4 inch pipes with Schedule 40. The flanges tested were of Class 300 RFWN 2 inch and Class 300 RFWN 4 inch.

Experimental results showed that the varying mid-span of the piping system had a non-linear effect on the corresponding natural frequencies. This was also found from the numerical FE model which they developed. An important findings was that

the use or lack of a gasket was found to have insignificant impact on the frequency response of the piping system tested and modelled. The authors also developed a much simpler beam element models with the flange/gasket introduced as a lumped mass and carried out numerical analysis. It was found that this model predicted well both natural frequencies and mode shapes of the piping system. This was a far more computationally efficient method of analysis, saving both time and expense.

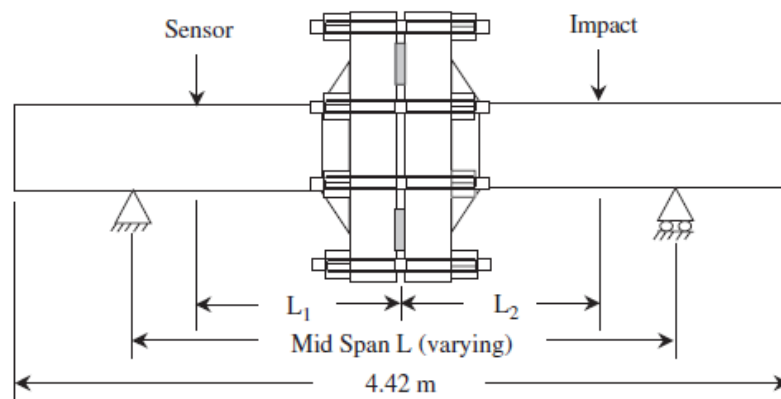


Figure 2.21: Schematic of the test set-up carried out by (Semke et al., 2006).

A recent experimental test was carried out by Abid et al. (2011b) which investigated the performance of a bolted flange joints under combined pressure and thermal loading. The authors carried out Helium leak testing with a combined pressure and temperature load was carried out in accordance with ASME Section V (2001). The experimental set-up was designed to study the sealing behaviour of flange joint at the design/working pressure. For the tests, an internal pressure of 14 MPa and a temperature of 100°C using helium as a fluid inside pipe for ANSI 4 inch, Class 900 bolted flange joint. During the tests, no helium leak occurred from the BFJ and the gasket suffered no damage. A good performance of the flange joint was therefore observed.

In order to examine the effect of loading on the sealing performance of bolted flange joints, Horiuchi et al. (2011) conducted a number of experimental tests on some BFJs. The study also aimed at establishing a design method for the a flange joint subjected to bending moment and internal pressure. Effect of loading on the sealing perfor-

mance due to different loading history was examined and pipe length in each usage condition was determined for two loading histories using tensile strength of hub side and allowable leak rate of sippy bubble method to establish a design method of flange subjected to bending moment. A weld neck type pipe flange connections with Class 600 flanges with nominal diameter is 3 inches was used for the tests, see Figure 2.22. Experimental result showed that average contact gasket stress for different loading history changed due to non-linearity and hysteresis of non-asbestos gasket.



Figure 2.22: Experimental set-up for leakage test under internal pressure and external bending moment carried out by (Horiuchi et al., 2011).

Tenma et al. (2011) undertook a test program on bolted flange joints to investigate the sealing performance of a BFJ with ring joint gasket subjected to internal pressure. Finite element analysis was also carried out to compare with experimental results. The authors examined the effects of tightening methods and gasket types on the sealing performance. The following main results of this study were concluded.

(i) Sealing performance of bolted flange joints depended on tightening methods. When the tightening method was the starlike tightening, it was found that the leak

rate became small because the uneven clamping -which occurred due to the clockwise tightening- was prevented.

(ii) The type of gaskets also determined the sealing performance a BFJ. It was found that the leak rate measured with ring joint gasket reduced significantly compared with the leak rate measured with the spiral wound gasket.

(iii) It was found that the the sealing performance improved significantly when the gasket and flange groove fitted completely.

An insignificant amount of experimental work exists in literature dedicated to the performance evaluations of bolted flange joints. These experimental works mainly analysed the sealing performance of such joints. No experiment tests of BFJs with cyclic loading are reported yet and performance investigations of these joints under seismic loading are still to be carried out.

2.6 Pseudo-dynamic and real time tests with dynamic substructuring

Pseudo-dynamic (Mahin and Shing, 1985; Takanashi and Nakashima, 1987; Bursi and Shing, 1996; Bonelli and Bursi, 2004) and real time testing (Wagg et al., 2008; Shing, 2008; Bursi et al., 2008, 2011) are novel hybrid techniques for dynamic testing of structures/systems. In recent years, these testing techniques have gained significant popularity due to their applicability in testing several types of non-linear structures/systems producing comparatively more realistic responses of structures under dynamic loading. Unlike conventional slower tests such as slow cyclic and quasi-static tests, a pseudo-dynamic or real time test takes into account the inertia and damping effect of a structure thus providing better response of the structure under dynamic loading, e.g., seismic loading. By the use of actuators, computers, finite element software and controllers, these tests can potentially reproduce a shaking table test.

During a pseudo-dynamic or real time test with dynamic substructuring, a heterogeneous model of the emulated system is created by combining a Physical Substructure (PS) with a Numerical Substructure (NS) that describes the remainder of the system. Usually, the PS is the most critical part of a structure which is difficult to be well repli-

cated by numerical models and is physically loaded dynamically through powerful actuators. Whereas the rest of the structure is numerically modelled and solved via real-time software. The dynamic response of the whole structure is obtained by solving these two structure simultaneously. However, while performing a pseudo-dynamic or real time test with dynamic substructuring, dynamics of both substructures must be accurately reproduced, as well as their mutual interactions (Shing, 2008).

Pseudo-Dynamic tests with Dynamic Substructuring (PDDS)

The concept of pseudo-dynamic test was originated in 1975 by Takanashi (Takanashi, 1975). Since then, many researchers, e.g., Takanashi and Nakashima (1987); Mahin et al. (1989); Shing et al. (1996); Bursi and Shing (1996); Bonelli and Bursi (2004); Bursi et al. (2011) developed the concept and verified the suitability of this method. The basic concept of pseudo-dynamic test is that the dynamic response is computed using the experimental result in each time step. During the analysis process, a computer calculates the structural response, e.g., displacement in a time step. Inertial and damping forces, required during the analysis process, for the solution of the equations of motion are modelled analytically. The computer, after calculating structural displacement at a specific time step, electronically provides this result to the actuator system. In the experimental process, actuator control system imposes the calculated displacement and then measures and returns the restoring force, $R(t)$, to the computer. Using the measured data, the computer calculates the response in the next time step. With this feedback procedure, the dynamic response of the structure can be obtained.

Since, damage is intrinsically a local phenomenon of a structure, often testing of the entire structural system is not required. At this point, the substructuring technique plays a vital role allowing experimental testing to be carried out only on the parts of the structure of interest, e.g., the part where damage is expected and which is difficult to be replicated well by numerical models, while the rest of the structure is modelled numerically. Through the interaction of the physical and numerical substructures during the test, the dynamic response of the entire system is obtained. The substructuring technique was first implemented for pseudo-dynamic testing by

Dermitzakis and Mahin (1985), and subsequently has been widely used.

The substructuring technique leads to the full scale testing of a structure allowing the experimental model to be only on the critical part of the structure. Unlike conventional cyclic testing, demands on the critical parts of a structure is represented more realistically by substructuring. Tests on substructures usually reduce the number and interaction of DoFs controlled at the laboratory. They are thus potentially able to run fast, close to or even at real time (Pegon, 2008). In particular, the following main advantages are offered by the dynamic substructuring technique (Klerk et al., 2008): i) it allows evaluating dynamic behaviour of structures that are too large or complex to be analysed as a whole; ii) local dynamic behaviour of the PS can be recognized more easily than when the entire system is analysed; iii) it gives the possibility of combining modelled parts (discretized or analytical) and experimentally identifying components; iv) it allows sharing and combining substructures from different project groups.

While coupling two or more substructures, two conditions must always be satisfied (Klerk et al., 2008): i) compatibility condition (compatibility of the substructures' displacements at the interface nodes) and ii) equilibrium condition (force equilibrium on the substructures' interface DoFs). However, during an experimental dynamic substructuring, one has to overcome some difficulties in order to avoid an erroneous analysis. All of these difficulties originate from the inability to accurately measure all the subsystem's properties. In particular, the difficulties are encountered due to errors originated from several factors, e.g., modal truncation, improper measurements and applications of rotations and torques in the PS (Duarte and Ewins, 1995; Gialamas et al., 1996; Liu and Ewins, 1999), unable to manage proper continuity at the coupling nodes, time delay and experimental errors. Details on these errors can be found in Klerk et al. (2008).

In a pseudo-dynamic test, displacements are imposed to the physical substructure on an extended time-scale which typically ranges from 50 to 1000 times the actual earthquake duration. This time modification allows for the use of larger actuators without high hydraulic flow requirements, careful observation of the response of the structure during the test, and the ability to pause and resume the experiment. Because the actuators can generate larger forces, structures can be tested readily at

large- or full-scale. However, the pseudo-dynamic testing technique also presents some disadvantages. Because the number of actuators that can be attached to a structure is limited, the method is practical only for structures in which the physical substructure have concentrated masses or can be modelled with a few lumped masses; usually, the number of required actuators is equal to the number of DoFs associated with lumped masses. Additionally, the use of an extended time scale renders this method inapplicable when the restoring forces are rate dependent (Carrion and Spencer, 2007).

In order to overcome some limitations of the pseudo-dynamic testing method and to expand its field of application, the *continuous pseudo-dynamic method* was developed. Unlike the conventional pseudo-dynamic tests -which are carried out using a quasi-static loading- a continuous PDDS is performed in a continuous manner (Magonette, 2001), even with a time scale identical to the earthquake (Nakashima et al., 1992). Thus, the dynamic loading allows components with velocity-dependent characteristics to be physically tested, which include most of the dissipative devices for structural vibration control (Nakashima, 2001). The continuous movement of the actuators is commonly achieved by using a response prediction-correction method to generate continuous command signals between each time step.

Another type of pseudo-dynamic testing is the *distributed pseudo-dynamic testing* which uses the internet to link geographically distributed facilities, expanding considerably the type and size of structural systems that can be tested (Pan et al., 2005). Because the time required for network communication is relatively large, response prediction-correction methods are required to generate the actuator command signals at continuous or fast-rate tests (Schellenberg et al., 2005).

Real time Tests with Dynamic Substructuring (RTDS)

Real time testing (Nakashima et al., 1992; Horiuchi et al., 1996; Nakashima and Masaoka, 1999; Horiuchi et al., 1999; Darby et al., 2001; Shing et al., 2004; Wagg et al., 2008; Shing, 2008; Bursi et al., 2008, 2011) is a variation of the pseudo-dynamic testing method in which the imposed displacements and response analysis are executed in a common time scale, i.e., real time, thus allowing testing of systems with

rate-dependent components. Real time hybrid testing makes it possible to test the large category of structural components associated with vibration control including passive, semi-active, and active control devices, e.g., base isolation and dampers, which are typically non-linear and rate-dependent.

The implementation of a RTDS is challenging because it is necessary to perform all of the calculations, apply the displacements, and measure and feedback the forces within a single time step (typically less than 10 msec). Because the test is conducted in real time, the dynamics of the testing system and specimen become important. For example, when hydraulic actuators are used to apply forces to the test specimen, a time lag exists between when the displacement is commanded and when the actuator actually reaches the commanded position. There are also some inevitable time delays associated with the numerical calculations and the communication between the computer and data acquisition systems. The computing time can become large, especially for complex models, e.g., a model having numerous DoFs, or numerical substructures with non-linear response. Because of these time delays and lags, the force measured and fed back from the experiment does not correspond to the desired position (it is measured before the actuator has reached its target position). The effect of this error is to introduce additional energy into the system, which unless properly compensated, will typically cause the experiment to become unstable (Horiuchi et al., 1996). Nevertheless, Several techniques have been proposed and are available in literature to compensate this delay (Horiuchi et al., 1999; Darby et al., 1999a; Horiuchi and Konno , 2001; Carrion and Spencer, 2006; Chen C. and Ricles J. M., 2008). One must overcome the problem of delay through an appropriate compensation technique in order to successfully carry out an RTDS.

As we see from the above discussion, the main difference between the pseudo-dynamic and real time tests is the rate of execution of an experiment, i.e., a PDDS is carried out at a rate slower than the time scale of an earthquake while an RTDS is performed in the actual time scale of the earthquake. To better demonstrate, a time scale factor, λ can be used as the ratio between the experimental time scale and the actual earthquake time scale, i.e.,

$$\lambda = \frac{\Delta t_s}{\Delta t_{algorithm}} = \frac{N_s \Delta t_s}{\Delta T} \quad (2.13)$$

where, Δt_s is the sampling time of the controller; $\Delta t_{algorithm}$ is the algorithmic time step; ΔT is the time step of an original earthquake accelerogram; N_s is an integer number of division of ΔT . $\lambda = 1$, indicates that the test is executed in real time. If $\lambda > 1$, it is usually called a fast continuous pseudo-dynamic testing (Taucer, 2004).

In order to carry out a PDDS or an RTDS, first, a system of dynamic equations of motion of a structure is developed, often in the form of second-order ordinary differential equations as,

$$\mathbf{M}\ddot{\mathbf{u}}(t) + \mathbf{C}\dot{\mathbf{u}}(t) + \mathbf{R}(t) = \mathbf{F}(t) \quad (2.14)$$

where, \mathbf{M} and \mathbf{C} are the structural mass and damping matrices, respectively; $\ddot{\mathbf{u}}(t)$ and $\dot{\mathbf{u}}(t)$ are the time-dependent acceleration and velocity vectors, respectively; $\mathbf{R}(t)$ is the vector of nodal restoring forces, and $\mathbf{F}(t)$ is the external load vector. In particular, for a linear elastic system $\mathbf{R}(t) = \mathbf{K}\mathbf{u}(t)$ where \mathbf{K} denotes the stiffness matrix of the structure and $\mathbf{u}(t)$ is the displacement vector. The initial values of $\mathbf{u}(t)$, $\dot{\mathbf{u}}(t)$ and $\ddot{\mathbf{u}}(t)$ along with the appropriate boundary condition complete the problem statement.

In case of earthquake loading, the system of equations of motion reads,

$$\mathbf{M}\ddot{\mathbf{u}}(t) + \mathbf{C}\dot{\mathbf{u}}(t) + \mathbf{R}(t) = -\mathbf{M}\mathbf{I}a_g(t) \quad (2.15)$$

in which, $a_g(t)$ is the ground earthquake acceleration and \mathbf{I} is a vector containing 1 and 0 that projects earthquake forces to the desired DoFs of the model.

An important distinction between pseudo-dynamic and real time test is that, in case of a PDDS, the inertia and damping forces are numerically modelled in the computer, whereas, for a real time test, these forces are experimentally measured as illustrated in a simplified manner in Figure 2.23.

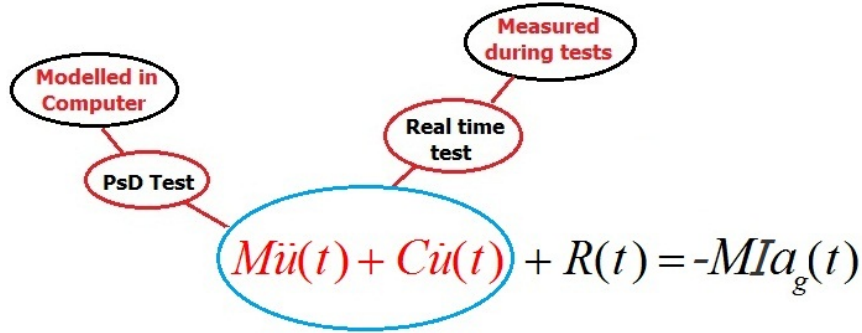


Figure 2.23: Measurements of inertia and damping forces in pseudo-dynamic and real time tests.

Equation (2.15) refers to the equations of motion of the entire structure which includes contributions from both the PS and the NS. Since, the PS is constructed in the laboratory, its contribution is measured as a coupling force during an experiment while the NS is numerically modelled and solved in a computer. Equation (2.15) can be rewritten as,

$$M^N \ddot{u}^N(t) + C^N \dot{u}^N(t) + K^N u^N(t) = F^P(t) + F^N(t) - (M^P \ddot{u}^P(t) + C^P \dot{u}^P(t) + K^P u^P(t)) \quad (2.16)$$

where, subscript P and N corresponds to the PS and the NS, respectively. Note that, in case of an RTDS, the coupling force from the PS, i.e., $(M^P \ddot{u}^P(t) + C^P \dot{u}^P(t) + K^P u^P(t))$ is experimentally measured. In case of a PDDS, only the restoring force of the PS, i.e., $K^P u^P(t)$ is experimentally measured, while the inertia, and damping forces, $C^P \dot{u}^P(t)$ and $M^P \ddot{u}^P(t)$, respectively, are numerically modelled.

To carry out a PDDS or an RTDS, an appropriate integration scheme has to be employed to solve (2.16) in every time step and to generate a displacement command in order to load the PS. Direct numerical time integration algorithms such as such as the time integration schemes based on the finite difference (FD) are widely used for the solution of (2.16). In the time integration schemes, Equation (2.16) is enforced at time $t = t_{n+1}$ leaving u_{n+1}^N , \dot{u}_{n+1}^N and \ddot{u}_{n+1}^N to be the unknowns. The time discrete equation can be solved together with two finite difference formulas, which express the relationships between u_{n+1}^N , \dot{u}_{n+1}^N and \ddot{u}_{n+1}^N . Thus, one advances the solution from time t_n to t_{n+1} by Δt , the time step. In every time step, the PS is loaded by

means of a transfer system, e.g., an actuator, to load the PS with the displacement command, $\mathbf{u}^N(t)$ and the resulting restoring force from the transfer system is fed back to the numerical model in order to advance to the next time step. The procedure is successively repeated to retrieve a time discrete response of the structures. The basic idea of a hybrid test with an integration scheme is presented in Figure 2.24.

The integration scheme to be used must be robust and stable in the presence of numerical and experimental feedback errors (Shing and Mahin, 1987, 1990). Several time stepping algorithms including central difference, Wilson- θ and Newmark- β algorithms, have been proposed for hybrid tests, e.g., Bursi and Shing (1996); Combescure and Pegon (1997); Chang (1997); Buonopane S. (1997); Bonelli and Bursi (2004); Bursi et al. (2008). An unconditionally stable implicit algorithm is an attractive feature for hybrid tests while dealing with large number of DoFs and high-frequency modes in the numerical substructure. Different methods of applying implicit integration schemes have been proposed for hybrid testing, e.g., Shing et al. (2004); Wu et al. (2006b, 2007); Bursi et al. (2008).

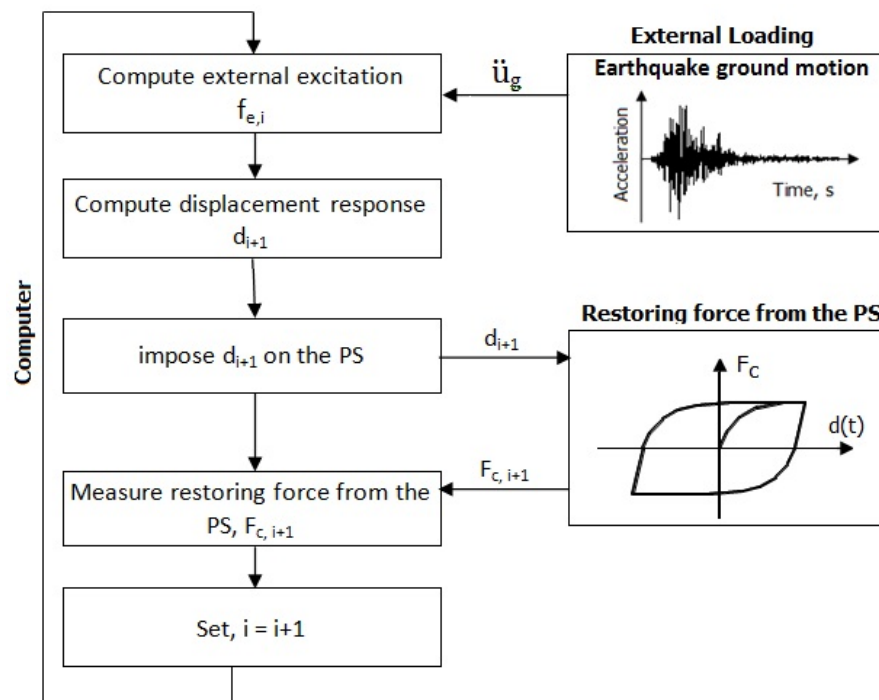


Figure 2.24: Basic concept of hybrid tests with an integration scheme.

Pseudo-dynamic and real time testing with dynamic substructuring have been successfully used in testing several systems including civil structures (Molina et al., 1998; Nakashima and Masaoka, 1999; Darby et al., 1999b; Pegon and Pinto, 2000; Darby et al., 2001; Blakeborough et al., 2001; Pinto and Pegon, 2004; Wu et al., 2006a). During the past years, several limitations of these experimental techniques have been overcome and significant researches are currently being undertaken in this area.

In 2001, Melo et al. (2001) took an attempt to use the techniques of PDDS in order to carry out dynamic analysis of a piping system. They used a simple piping system containing an elbow mounted in a rigid test rig to carry out the experimental test as depicted in Figure 2.25. However, the external force was considered as only a ramp which was applied in-plane. The authors found some discrepancy between experimental and numerical results for displacements and rotations in different points of the piping and suggested some modifications of the test rig in order to overcome this limitation.

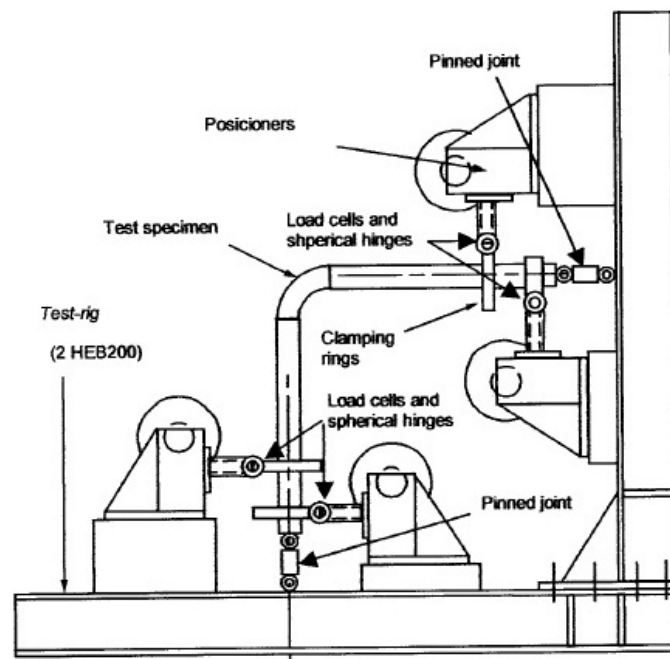


Figure 2.25: Test rig and piping arrangement for pseudo-dynamic tests by Melo et al. (2001).

The aforementioned idea of hybrid tests can potentially be employed to test piping systems under seismic loading, as illustrated in Figure 2.26. However, as discussed previously, so far these techniques have been considered applicable only for structures characterized by concentrated masses. It will be, therefore, challenging to carry out such experiments on a piping system, which is endowed with distributed masses and subjected to distributed earthquake forces. However, implementations of the PDDS and RTDS techniques and relevant experimental tests on a piping system under seismic loading will be presented in Chapter 6 and Chapter 7, respectively.

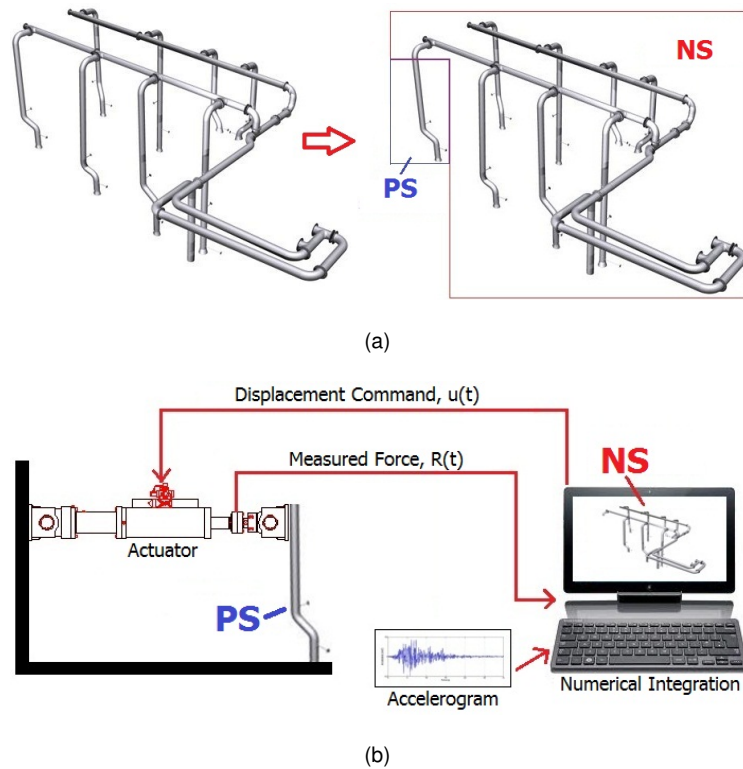


Figure 2.26: Schematic of a PDDS and an RTDS on a piping system under seismic loading.

2.7 Conclusions

A state of the art on the design, analysis and testing of piping systems and some of its critical components under seismic loading (piping systems and pipe elbows) and under regular loading (bolted flange joints) has been presented in this chapter. An

overview and state of the art of the pseudo-dynamic and real time testing was also offered.

A lack of proper seismic design rules for piping systems and components, especially in Europe, is evident. In addition, there exists a need for proper seismic design guidelines for BFJs. Experimental results has proved that current seismic design Standards are over-conservative for piping systems components and modifications have been proposed to relax this over-conservatism. The novel testing techniques, PDDS and RTDS, were found to be challenging for seismic testing of piping systems.

CHAPTER 3

DESIGN AND ANALYSIS OF NON-STANDARD BOLTED FLANGE JOINTS

3.1 Introduction

This chapter deals with the design of two non-standard Bolted Flange Joints (BFJs) suitable for seismic applications. Usually, Standard BFJs are thicker and highly stiff which makes them unsuitable for energy dissipation, at joint locations of a piping system, during seismic events. In this respect, to endow a BFJ with an energy dissipation capability, the non-standard flanges were designed to be more ductile and thinner, compared to the Standard ones, based on Eurocode EN 1993-1-8 (2005). Analysis of the designed joints in terms of their axial and bending resistance were performed. Moreover, the mechanical integrity and leak-tightness performance of the non-standard BFJs were checked through a calculation performed according to European Standard EN 1591-1 (2009).

3.2 Design of BFJs using Standards

As discussed in Chapter 2, a BFJ consists of four main components, i.e., flange, pipe, bolt and gasket. In order to design a flange joints using the Standards, a designer has to select these components using relevant Standards discussed in Chapter 2. First, dimensions of a selected type of flange are chosen based on the dimensions of connecting pipes and operating conditions, e.g., pressure and temperature, from tabulated values given in Standards, e.g., ASME B16.5 (2009); EN 1092-1 (2007).

Number of bolts and their dimensions are also suggested in these Standards. Suitable bolts and nuts can also be taken from relevant Standards, e.g., ASME B18.2.1 (2010); EN 1515-1 (2002); EN 1515-2 (2004); EN 1515-3 (2005). A gasket matching with the dimensions of the flange and suitable to be used under the working environment can be chosen from a gasket Standards, e.g., EN 1514-2 (2005); EN 12560-2 (2001). Materials of different components are chosen to be suitable for use under design operating conditions. A calculation, which is recommended, should then be performed to check the admissibility of the flange joint according to one of the calculation methods mentioned in Chapter 2, e.g., ASME alternative rules (Mikitka, 2002); European Standards (EN 13445-3, 2002; EN 1591-1, 2009). The procedure discussed above is iterative; a user has to go back to the selection of the parts and start again with a modified design till the admissibility of the flange joint is satisfied.

Once the admissibility of a bolted flange joint is confirmed through calculations, one has to use appropriate tightening devices to tight the bolts in order to assemble the components of the BFJ to form a joint. The tightening force can be found through the calculation method used to design the joint, e.g., EN 1591-1; other Standards, e.g., ASME PCC-1 (2010) can also be used.

Calculations according to ASME rules, e.g., Mikitka (2002) are widely used for design of flange joints. However, the new European Standard, EN 1591, is also gaining popularity to perform these calculations. Both the ASME Standards and EN 1591 apply only to flanges with the gasket floating between the flange plates. Nevertheless, none of these design methods takes into account seismic loading in order to design a flange joint to be used under an earthquake.

3.3 Design of non-standards BFJs

3.3.1 Motivation

As mentioned earlier, currently, available Codes and Standards for the design of bolted flange joints, e.g., EN 1591-1 (2009), ASME Section VIII Division 1 (2007), mainly ensure joint integrity and leak tightness under operating conditions but these

Standards do not have design rules that take into account seismic loading. The suggested thicknesses of Standard flanges are high which makes these joints stiff and unsuitable for seismic applications. In contrary, a thinner and ductile flange is expected to dissipate some energy during an earthquake and help to avoid a brittle failure of such joint. Experimental results by Nash and Abid (2000) showed that flanges with lower weights have advantages over the flanges with higher weights. Moreover, studies made by Touboul et al. (1999, 2006) and Huang et al. (2007) has demonstrated that seismic demands are not very high in piping systems and a very high level of seismic input is required to introduce damage to the components of piping systems. Hence, under a regular earthquake, even a thinner BFJ could perform equally well. Furthermore, the use of thinner joints may also save significant amount of steel and costs provided that these joints exhibit favourable performance under seismic events. Motivated by this fact, we designed two non-standard BFJs which were comparatively thinner than Standard joints in order to assess their capacity and performance under bending and axial loading.

3.3.2 Design procedure

The non-standard BFJs were designed by reducing the thickness of a Standard flange chosen from Standard EN 1092-1 (2007) while retaining its other original dimensions. In order to design a BFJ using Standard flanges, a designer has to select required dimensions of flanges from tabulated values given in Standards based on the dimensions of connecting pipes and operating conditions.

3.3.2.1 Selection of initial dimensions and component materials

As mentioned previously, the research activity presented herein was part of the European research project INDUSE (INDUSE, 2009), that involved several partner institutions each responsible for specific research tasks. In order to have the possibility to compare analysis and experimental results, the consortium agreed to use similar materials, dimensions and operating conditions to carry out the research work. As a

result, an operating condition typically used for the design of BFJs in petrochemical industries, as reported in Table 3.1, was considered for the design of non-standard BFJs. An 8" (DN 200), schedule 40 pipe size was selected for connecting pipes with dimensions presented in Table 3.2.

Table 3.1: Design conditions

Design conditions	
Temperature	-4/290 C
Pressure	4 MPa

Table 3.2: Dimensions of connecting pipes

Dimensions of connecting pipe	
Pipe size	DN 200, SCH 40
Outer diameter, d_o	219.08 mm
Thickness, t	8.18 mm
Inner diameter, d_i	202.72 mm

With regard to component materials, Grade P355N and P355NH materials were selected for connecting pipes and flanges, respectively, while the bolts were of grade 8.8, as reported in Table 3.3. Grade P355N and P355NH possessed good mechanical properties, e.g., good toughness, strengths and corrosion resistance. The bolt material, i.e, Grade 8.8, possessed high tensile strength and was suitable to be applied in combination with the flange material. A spiral wound gasket of material X2CrNiMo was selected as it could be tailored to suit a wide variety of operating conditions. It was suitable to seal fluids having high pressure and temperatures. The selected component materials are commonly used in petrochemical industries. Nominal values of some material properties of different components are reported in Table 3.4 and Table 3.5.

Table 3.3: Materials of different components of the BFJ

Component	Material
Pipe	P355N
Flange	P355NH
Bolt	Grade 8.8
Nut	Grade 8
Gasket	X2CrNiMo

Table 3.4: Nominal yield and ultimate strength of different components of the BFJ

Item	Yield Strength, f_y	Ultimate Strength, f_u
	MPa	MPa
Pipe	355	490
Flange	355	490
Bolt	640	800

Table 3.5: Gasket properties (Source: EN 1092-1:2007)

Symbol	Description	Value
Q_{min}	Minimum seating stress	50 MPa
Q_{max}	Maximum seating stress	300 MPa
E_0	Gasket modulus	10000 MPa
K_1	Gasket factor	20
C_1	Gasket factor	0
g_c	Gasket factor	0.9
m	Gasket factor	1.6

Based on the operating conditions and dimensions of connecting pipe reported in Table 3.1 and Table 3.2, respectively, a PN 40, Type 1 Standard flange was selected from EN 1092-1 (2007). It was a plate type flange -shown in Figure 2.14 of Chapter 2- and was potentially suitable for seismic applications. Moreover, it had an allow-

able pressure of 4 MPa which was suitable for the design conditions. The selected Standard flange and its dimensions are presented in Figure 3.1 and Table 3.6.

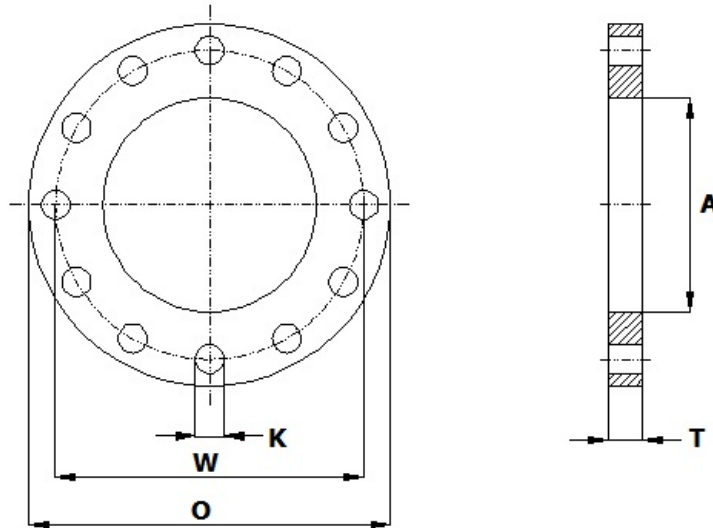


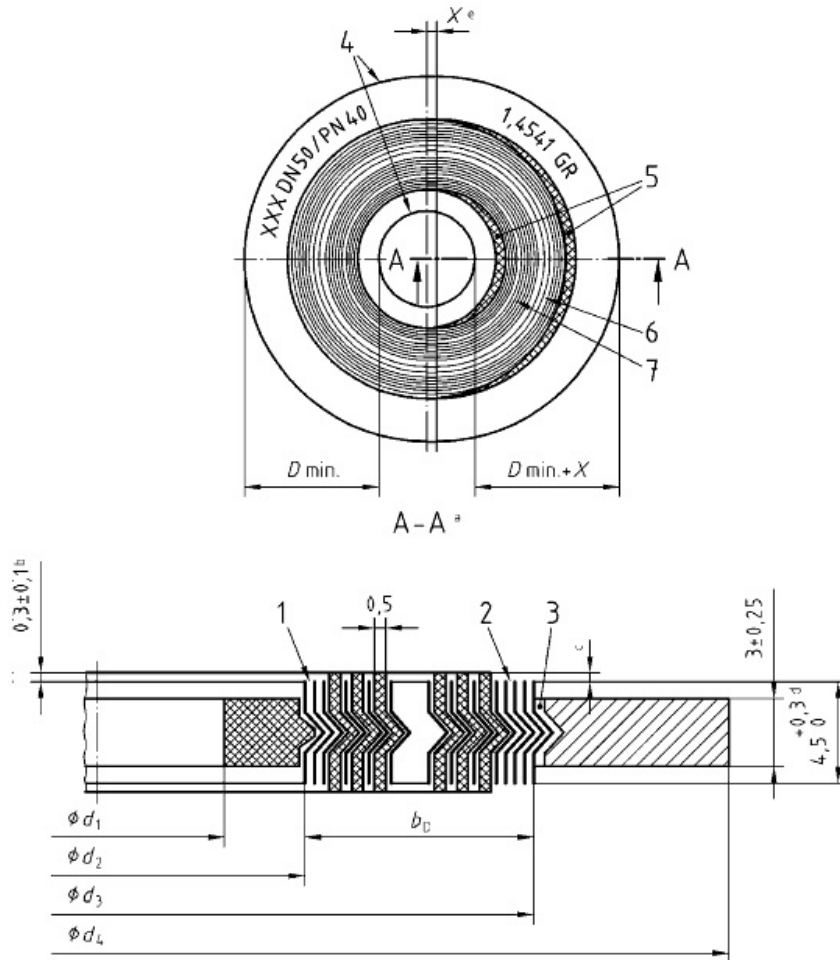
Figure 3.1: The selected Standard flange.

Table 3.6: Dimensions of the Standard flange

Symbol	Description	Dimension, mm
-	Pipe size	DN 200
O	Outer diameter of the flange	375.00
W	Bolt circle diameter	320.00
K	Bolt hole diameter	30.00
T	Thickness of the flange	36
A	Bore diameter	221.5
-	No of Bolts	12
-	Bolt Size	M 27 x 3.00

A total of 12 bolts of size M27 with dimensions reported in Table 3.8 were suggested for the Standard flange. A spiral wound gasket compatible with dimensions of the flange and connecting pipe was selected according to EN 1514-2 (2005). The gasket

and its dimensions are presented in Figure 3.7 and Table 3.7.



- 1 2 to 3 empty wraps
- 2 3 to 5 empty wraps
- 3 Central groove $\pm 0,1$ mm
- 4 Sharp edges removed
- 5 Minimum of four welding points for each
- 6 Metal thickness $0,2$ mm $\pm 0,02$ mm
- 7 Thickness as appropriate to filler type
Graphite Ash content < 2 %, PTFE filler to contain no re-cycled material and may be either sintered or non-sintered.

Figure 3.2: The selected spiral wound gasket.

Table 3.7: Dimensions of the spiral wound gasket

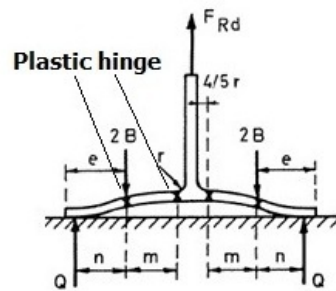
Symbol	Description	Dimension
-	DN	200
-	PN	40
ϕd_1	Inner diameter of the inner ring ring	216
b_I	Width of the inner ring	6
ϕd_2	Inner diameter of the sealing element	228
b_D	Width of the sealing element	10
ϕd_3	Inner diameter of the guide ring	248
ϕd_4	Outer diameter of the guide ring	290

Table 3.8: Dimensions of bolts

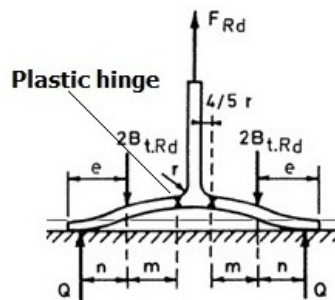
Dimensions of bolts	
Bolt size	M27
Outer diameter	27 mm
Pitch	3.0 mm
Stress area	459.0 mm

3.3.2.2 Reduction of flange thickness

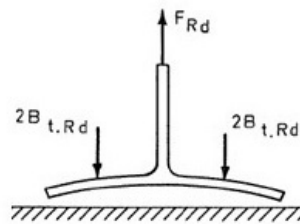
Once dimensions and materials of different components of the BFJ were chosen, we used Eurocode EN 1993-1-8 (2005) in order to select two reduced thicknesses for the joint. Eurocode 1993-1-8 provides rules for choosing appropriate dimensions of a joint according to three failure modes under tensile loading as shown in Figure 3.3. As can be seen from Figure 3.3, Mode #1 and Mode #2 failures are associated with comparatively thinner flanges and strong bolts. These modes are capable of dissipating energy through the formation of plastic hinges. On the other hand, Mode #3 is a purely rigid failure due to the existence of thick plate and weak bolts; see Table 3.9 for reference. We were interested in the first two failure modes which are ductile and suitable for energy dissipation during an earthquake.



Mode 1 Failure
Thin plate and strong bolts



Mode 2 Failure
Intermediate plate and bolts



Mode 3 Failure
Thick plate and weak bolts

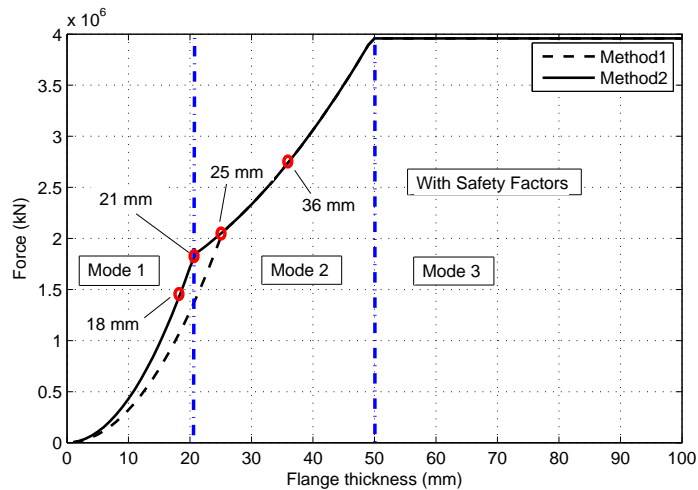
Figure 3.3: Failure modes according to Eurocode 1993-1-8 (2005).

Table 3.9: Failure mechanisms associated with the three failure modes

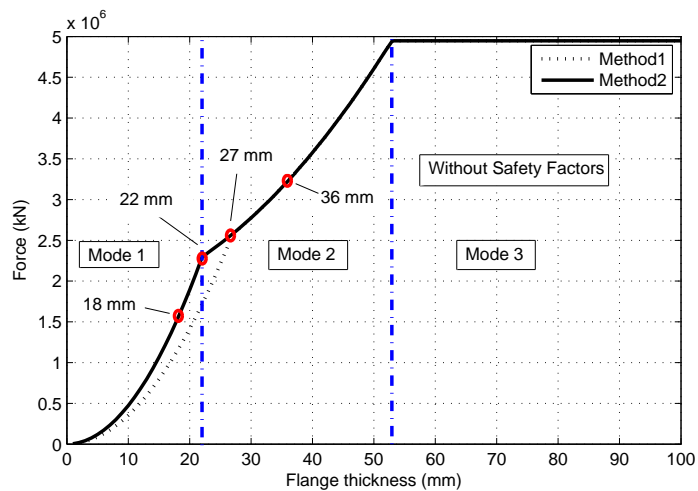
Failure Mode	Failure Mechanism
Mode 1	Complete yielding of the flange
Mode 2	Bolt failure with yielding of the flange
Mode 3	Bolt failure

The formulas provided in Eurocode 1993-1-8 use dimensions of a BFJ in order to calculate failure forces in different failure modes. Varying the thickness, a "thickness vs. failure force" curve in different failure modes for the selected flange was devel-

oped as shown in Figure 3.4. Calculations were performed both with and without considering safety factors.



(a)



(b)

Figure 3.4: Thickness vs. failure modes according to Eurocode 1993-1-8 (2005): (a) with safety factors; (b) without safety factors.

EN 1993-1-8 prescribes two methods to calculate the failure force for Mode #1 failure both of which were considered in the calculations as can be noted from Figure

3.4. In order to fail in Mode #1 and Mode #2, two different thicknesses, 18 mm (Design 01) and 27 mm (Design 02), respectively, were selected for the two non-standard BFJs. One may observe that according to both methods, thicknesses 18 mm and 27 mm were in Mode #1 and Mode #2 failure regions, respectively. Note that the original thickness of the Standard flange was 36 mm. The designed non-standard BFJs and relevant dimensions are shown in Figure 3.5 and Table 3.10. Required bolt lengths were calculated according to an industrial guideline (Ferdinando and Lopez, 2001) and are reported in Table 3.11. The flanges were connected to the pipe by a fillet welding.

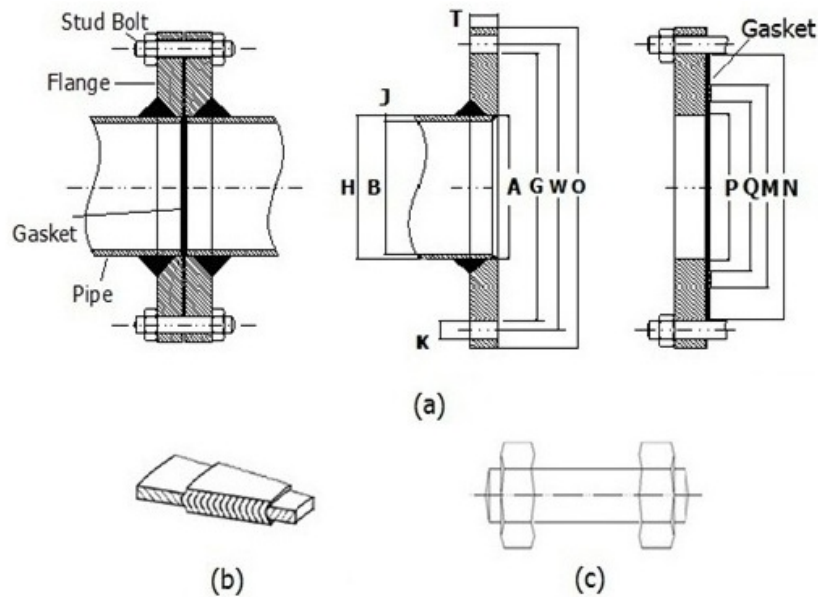


Figure 3.5: (a) Designed non-standard BFJs and dimensions; (b) spiral wound gasket; (c) stud bolt.

Table 3.10: Dimensions of designed non-standard BFJs.

Symbol	Description	Dimension, mm
O	Outer diameter of the flange,	375.00
W	Bolt circle diameter	320.00
K	Bolt hole diameter	30.00
G	W-K	290.00
T	Thickness of the flange	18 (Design 01)
T	Thickness of the flange	27 (Design 02)
J	Thickness of the pipe	8.18
A	Bore diameter	221.50
B	Inner diameter of the pipe	202.74
H	Outer diameter of the pipe	219.08
P	Inner diameter of the gasket, P	216.00
Q	Diameter of inner gasket contact point, Q 228.00	
M	Diameter of outer gasket contact point, M	248.00
N	Outer diameter of the gasket, N	290.00
-	No of Bolts	12
-	Stud Bolt Size	M 27 x 3.00

Table 3.11: Bolt lengths for non-standard BFJs

Non-standard joint	Stud bolt size	Stud bolt length
Design 01	M27 x 3.0	115 mm
Design 02	M27 x 3.0	134 mm

3.4 Design resistances of non-standard BFJs

We designed two non-standard BFJs potentially suitable for seismic applications. These joints consisted of several components, i.e., flange, pipe, gasket, stud bolts and nuts. Since we performed bending and axial experimental tests on these joints, their bending and axial resistance were estimated in order to determine the level of loading to be applied during the tests and to plan relevant experimental set-ups.

3.4.1 Axial resistance

Axial capacities of designed BFJs were evaluated in Section 3.3.2 while selecting appropriate thicknesses of the joints. Relevant failure modes and axial resistances of non-standard joints are reported in Table 3.12 and Table 3.13, respectively. One may see that very high forces, i.e., about 1520 kN for Design 01 and 2580 kN for Design 02 -according to method 2 without considering safety factors- were required to cause a failure to the joints. In this calculations, safety factors for bolts and flanges were taken as 1.25 and 1.1, respectively.

Table 3.12: Failure modes of non-standard BFJs

Failure modes of non-standard bolted flange joints		
Non-standard BFJ	Pipe Size	Failure Mode
Design 01	DN 200 (NPS 8), SCH 40	Mode 1
Design 02	DN 200 (NPS 8), SCH 40	Mode 2

Table 3.13: Resistances of non-standard BFJs in axial loading

	Failure force of Design 01 BFJ	
	without safety factors	with safety factors
Method 1	1145.8 kN	1041.6 kN
Method 2	1519.7 kN	1381.6 kN

	Failure force of Design 02 BFJ	
	without safety factors	with safety factors
	2579.3 kN	2154.4 kN

One of the components of the BFJs was the pipe to which flanges were connected through welding. Hence, it was also important to estimate its resistance. In order to find the yield and ultimate load corresponding to the yield and ultimate strengths of the

pipe, we used the nominal material properties and dimensions of the pipe reported in Table 3.4 and Table 3.2, respectively. The yield, F_y , and ultimate, F_u , loads of the pipe subjected to axial loading were calculated according to the following relationships,

$$F_y = f_y A_p \quad (3.1)$$

$$F_u = f_u A_p \quad (3.2)$$

where, f_y , f_u and A_p are yield strength, ultimate strength and cross-sectional area of the pipe. Relevant values are presented in Table 3.14. One can see that a high level of axial load was required to cause yielding and failure to the pipe.

Table 3.14: Yield and Ultimate load of the pipe in axial loading

Yield load, F_y	1924.01 kN
Ultimate load, F_u	2655.68 kN

3.4.2 Bending resistance

Regarding the bending capacity of the pipe, we calculated the a plastic moment, $M_{p,P}$, due to an applied bending loading using the following relationship,

$$M_{p,P} = f_y Z_p \quad (3.3)$$

where, f_y is the yield strength of the pipe and Z_p is plastic section modulus defined as,

$$Z_p = \frac{d_o^3 - d_i^3}{6} \quad (3.4)$$

where d_o and d_i are the outer and inner diameter of a pipe. The values of $M_{p,P}$ are presented in Table 3.15.

Table 3.15: Plastic moment of the pipe

Plastic moment of pipe, $M_{p,P}$	
without safety factor	with safety factor (1.1)
129.2 kNm	117.5 kNm

An estimation of the plastic moment of the flange joint, $M_{p,FI}$, was also made. Given the involvement of several components and owing to its complex geometry, it was difficult to estimate the plastic moment of a BFJ. Moreover, there was no method available for such purpose. Hence, we followed a simplified method to calculate the $M_{p,FI}$; in particular, it was assumed that the flanges were rigid and during bending they opened rigidly causing elongations of the bolts as schematically depicted in Figure 3.6. This assumption entailed an upper bound of the $M_{p,FI}$, which was later utilized for the experimental set-up design. It was also considered that the end bolt reached a maximum elongation of 12% of its original length as suggested by Bursi and Jaspart (1997). Elongations of remaining bolts were assumed to vary linearly with respect to distances from the end bolt. The total moment required to cause bolt elongations were then considered as $M_{p,FI}$. The estimated values of $M_{p,FI}$ calculated both with and without safety factors are reported in Table 3.16. A safety factor of 1.25 and 1.1 was taken for the ultimate strength and yield strength of a bolt, respectively. It can be noted that same values of plastic moments were obtained for both the flanges. This was because bolt elements controlled the joint capacity.

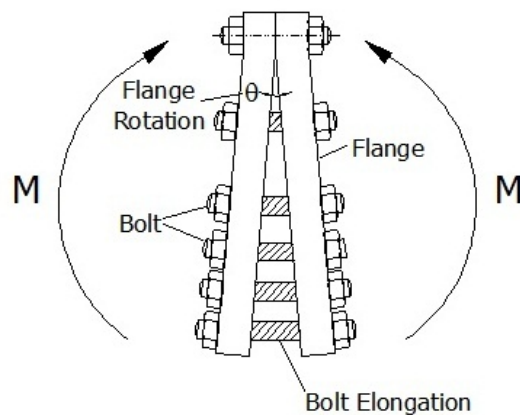


Figure 3.6: Schematic of flange opening and bolt elongation under bending moment (simplified and approximated).

Table 3.16: Plastic moment of non-standard BFJs

BFJ	Plastic moment of BFJs, $M_{p,FI}$	
	Without safety factors	With safety factors
Design 01	743.5 kNm	594.8 kNm
Design 02	743.5 kNm	594.8 kNm

One may note from Table 3.13 - Table 3.16 that, compared to the pipe, resistance of the flange joint was much higher in bending, whereas, it was similar or lower in case of axial loading.

3.5 Design checks of non-standard bolted flange joints

A design check on non-standard BFJs according to EN1591(EN 1591-1, 2009; EN 1591-2, 2009) was performed in order to check their mechanical integrity and leak-tightness performance. EN 1591 is a comparatively new Standard and provides design rules that satisfy both leak-tightness and strength criteria of a bolted flange joint. This method is recognized as being the only methods that specifically addresses flange leakage in a rigorous way (Mair, 2011) whereas conventional calculation method, e.g., Taylor Forge method (Waters et al., 1937), do not ensure leak tightness of a flange joint. This calculation method has also been incorporated into Appendix G of the European Pressure Vessel Standard EN 13445-3 (2002). The calculation method according to this Standard was discussed in Section 2.5.4 of Chapter 2.

A MATLAB code was developed according to EN 1591-1 to perform the design check. Required gasket properties for a leak rate of 0.1 mg/sm (milligram per second per meter of circumference length) were chosen from EN 1591-2 and the maximum design operating condition, i.e., pressure: 4 MPa and temperature: 290°C was considered for the calculations. In order to check whether the mechanical integrity of the designed BFJs was ensured, we calculated load ratios of its different components as reported in Table 3.17. Load ratios were defined in Section 2.5.4 of Chapter 2; all

load ratios have to be less than 1 to satisfy a mechanical integrity of the joint. One may note from Table 3.17 that bolt and gasket load ratios were within the safe limit, i.e., less than unity. However, load ratio of the flange exceeded the value of unity which meant that, under the design conditions, flanges were overloaded. Therefore, the mechanical integrity of the designed BFJs was not ensured at the selected leak rate and operating conditions according to this Standard.

Table 3.17: Load ratios of the designed BFJs according to EN 1591

BFJ	Load Ratio		
	Gasket Load Ratio	Bolt Load Ratio	Flange Load Ratio
Design 01	0.112	0.483	2.752
Design 02	0.088	0.420	1.549

3.6 Conclusions

In this chapter, design of two non-standard BFJs -potentially suitable for seismic applications- based on Eurocode EN 1993-1-8 (2005) was described. It was found that both the non-standard joints possessed high bending and axial capacities. The estimated bending resistances of the joints were found to be significantly higher than that of the pipe while their axial resistances were similar or lower compared to the pipe. According to a calculation based on EN 1591, the joint integrity of non-standard BFJs, for a chosen leak-rate of 0.1 mg/sm, was not ensured under design operating conditions. However, the experimental program, presented in Chapter 4, will provide realistic leakage and ultimate capacities of the designed joints.

CHAPTER 4

EXPERIMENTAL TESTS ON BOLTED FLANGE JOINTS

4.1 Introduction

In order to investigate the capacity of non-standard BFJs designed in Chapter 3, under bending and axial loading, a number of experimental tests were conducted both with cyclic and monotonic loading. The experimental test campaign is described in this chapter. Test program, experimental set-up and instrumentation for measurements of rotations and displacements are shown. A detail analysis is performed on the experimental results and a comparison between test results and allowable design loads are performed. Finally, the capacity of non-standard BFJs and relevant seismic demands obtained from a realistic Case Study on a piping system are also compared and discussed.

4.2 Test program

In order to assess capacities and performances, e.g., leakage behaviour, ductility, strength and failure modes, of the designed non-standard bolted flange joints under monotonic and cyclic loading, we performed a series of axial and bending tests on the designed BFJs. A total of eight tests including four bending and four axial tests were carried out in room temperature and with a moderate internal pressure of 1.5 MPa which was half of a regular operating pressure of a petrochemical industry. The test program is reported in Table 4.1.

Table 4.1: Test program on non-standard bolted flange joints

No.	Test type	Test name	Loading type	Internal pressure	Specimen
1	Bending	BSML18	Monotonic	1.5 MPa	BS1
2	Bending	BSML27	Monotonic	1.5 MPa	BS2
3	Bending	BSCL18	Cyclic	1.5 MPa	BS3
4	Bending	BSCL27	Cyclic	1.5 MPa	BS4
5	Axial	ASML18	Monotonic	1.5 MPa	AS1
6	Axial	ASCL18	Cyclic	1.5 MPa	AS2
7	Axial	ASCL27-1	Cyclic	1.5 MPa	AS3
8	Axial	ASCL27-2	Cyclic	1.5 MPa	AS4

The monotonic tests were mainly performed to find yield displacements of the joints in bending and axial loading. These values were then used to construct ECCS45 loading protocols (ECCS45, 1986) for the cyclic tests. On the other hand, cyclic tests were carried out to investigate strength, ductility, degradation and energy dissipation of the joints.

4.3 Material testing

To characterize some mechanical properties of flange and pipe materials, a number of tensile tests were performed on coupons of flange and pipe materials. Four tensile tests on pipe material coupons and two tensile tests on flange material coupons were conducted. A METROCOM machine was used for the tensile tests of pipe coupons. An MTS extensometer was attached with the pipe coupon to measure the extensions as shown in Figure 4.2. Small flange coupons were extracted from a flange and tested by means of a GALDABINI machine shown in Figure 4.3. Average values of some material properties obtained from these tests are reported in Table 4.2, while a stress-strain curve, of the pipe material is presented in Figure 4.1.

It can be noted from Table 4.2 that actual mechanical properties, i.e., yield strength, f_y and ultimate strength, f_u , of the pipe material were found to be above their nominal values, i.e., $f_y = 355$ MPa, $f_u = 490$ MPa. However, we found that the yield strength of

flange material were below the nominal value, i.e., 355 MPa. It can also be found that strengths of the flange material were lower than those of the pipe material. Both pipe and flange materials reached good level of elongation before failure which confirmed a good ductile behaviour of these materials.

Table 4.2: Mechanical properties of pipe and flange material (average values)

Material	Yield Strength, f_y	Ultimate Strength, f_u	Maximum Elongation, ϵ
Pipe	426 MPa	582 MPa	19%
Flange	325 MPa	508 MPa	20%

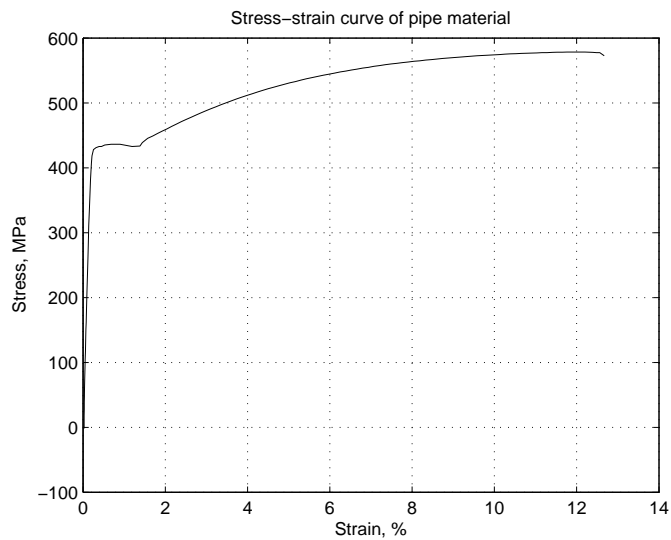


Figure 4.1: Stress-strain curve of pipe material.

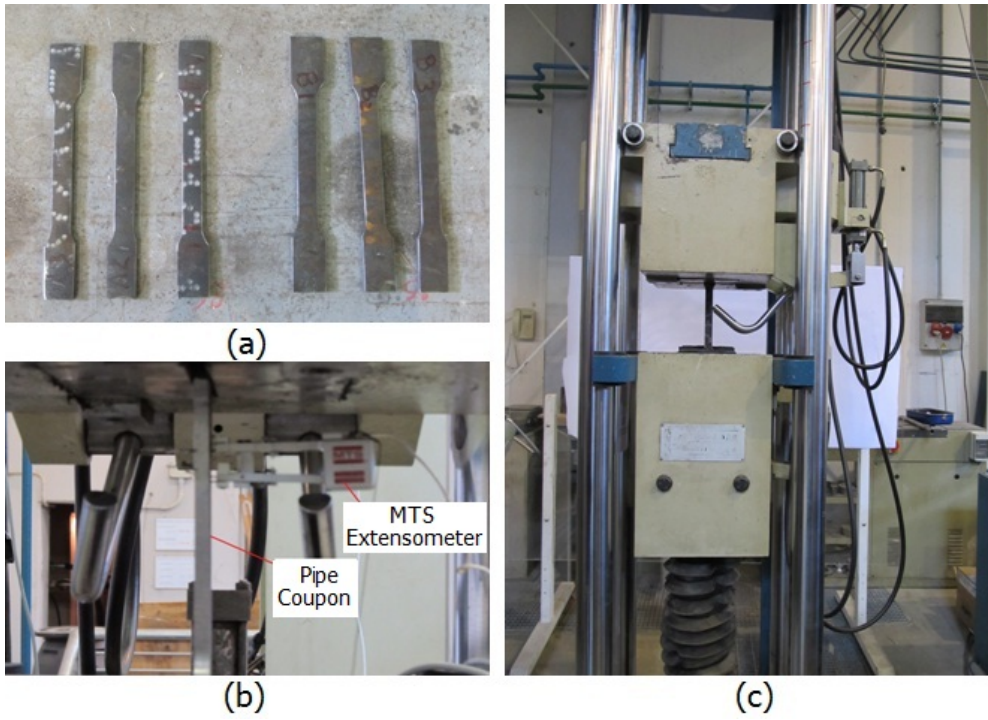


Figure 4.2: (a) Pipe material coupon; (b) an MTS extensometer attached to pipe coupon; (c) METROCOM machine.

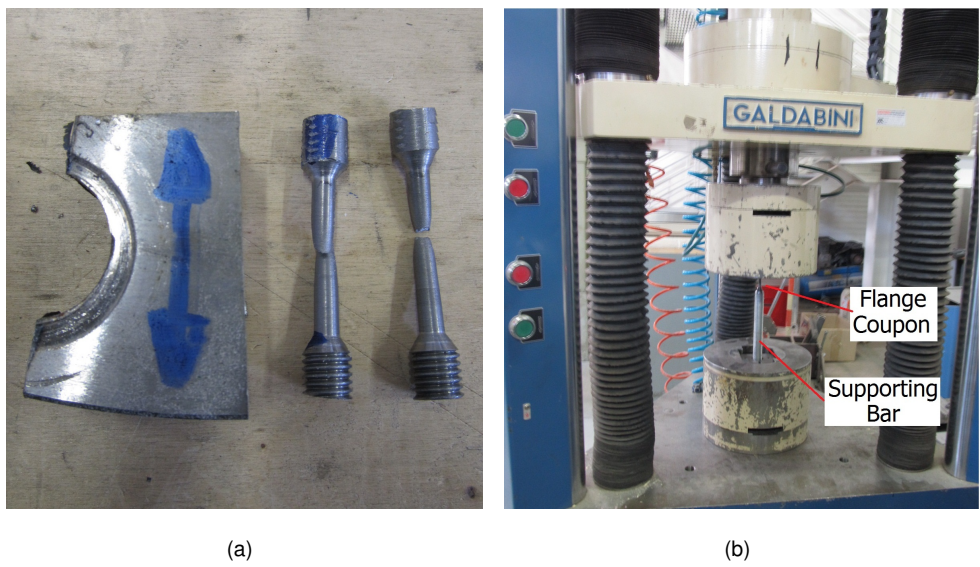


Figure 4.3: (a) Flange material coupon; (b) GALDABINI machine.

4.4 Tightening of bolts at assembly

The tightening torques to be applied during the assembly of non-standard BFJs were calculated according to Appendix O of ASME PCC-1 (2010). This Standard provides guidance for the determination of an appropriate assembly bolt stress and torque with due consideration for joint integrity. The detailed procedures are intended for flange joints for which controlled assembly methods are to be used. There are provisions for both a simple approach and for a joint component approach; the latter was used for the calculation of tightening torque. The minimum and maximum allowable gasket stresses were 68.9 MPa and 300 MPa, respectively, as provided by the gasket manufacturer.

In order to perform calculations according to ASME PCC-1, first some limit values, e.g., minimum and maximum permissible bolt stress, minimum and maximum assembly gasket stress, are defined. Some of these limit values are selected by the end user and some are provided by the manufacturer. Once the limits are defined, the target bolt stress, $\sigma_{b\text{sel}}$ at assembly was calculated using the following relationship,

$$\sigma_{b\text{sel}} = \sigma_{gT} \frac{A_g}{n_b A_b} \quad (4.1)$$

where, σ_{gT} is the target gasket stress, A_g is the gasket area, n_b is the number of bolts and A_b is the bolt resistance area.

Some checks were then done in order to ensure that, with this level of applied bolt stress, stress levels in different components of the flange joints, e.g., gasket and flange, were within their allowable stress limits. Moreover, it was also to be ensured that the gasket operating stress was maintained for all working conditions. The target bolt stress was then converted into a target torque, τ_b using the following formula,

$$\tau_b = \sigma_{b\text{sel}} k A_b \phi_b \quad (4.2)$$

where, ϕ_b is the bolt diameter and k is a nut factor defined in ASME PCC-1.

The calculated values of tightening torques to be applied in each bolt at assembly of the two non-standard BFJs and relevant bolt stresses during assembly are collected in Table 4.3. It can be noted that applied stress level in a bolt of Design 01 flange joint reached 62.5% of its yield stress whereas a bolt of Design 02 joint reached 70%

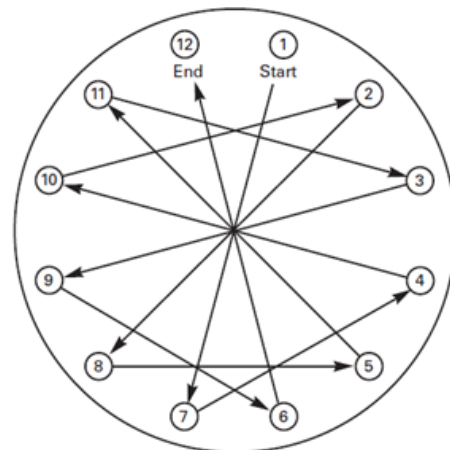
of its yield stress. These values were within the suggested limits of the Standard ASME PCC-1, i.e., 40%-60% of bolt yield stress. A torque wrench, shown in Figure 4.4(a), was used to apply required torques to the bolts according to the bolt tightening sequence suggested by the Standard as illustrated in Figure 4.4(b).

Table 4.3: Tightening torques applied per bolt of non-standard BFJs

Non-standard joint	Tightening torque	Bolt stress	% of yield stress applied per bolt
Design 01	991.66 Nm	400 MPa	62.50%
Design 02	1110.65 Nm	448 MPa	70%



(a)



Bolt Tightening Sequence (Round 1 through Round 3) 1-7-4-10 → 2-8-5-11 → 3-9-6-12

(b)

Figure 4.4: (a) The torque-wrench; (b) bolt tightening sequence according to ASME PCC-1 (2010).

4.5 Test specimens and experimental set-up

Two different types of specimens were tested in bending and axial tests. Test specimens were constructed by joining two flanges connected to two pipe segments through bolted connections. Flanges were connected to the pipes through fillet welds

and the joint was placed in the middle position of a specimen. Design 01 and design 02 joints are presented in Figure 4.5.

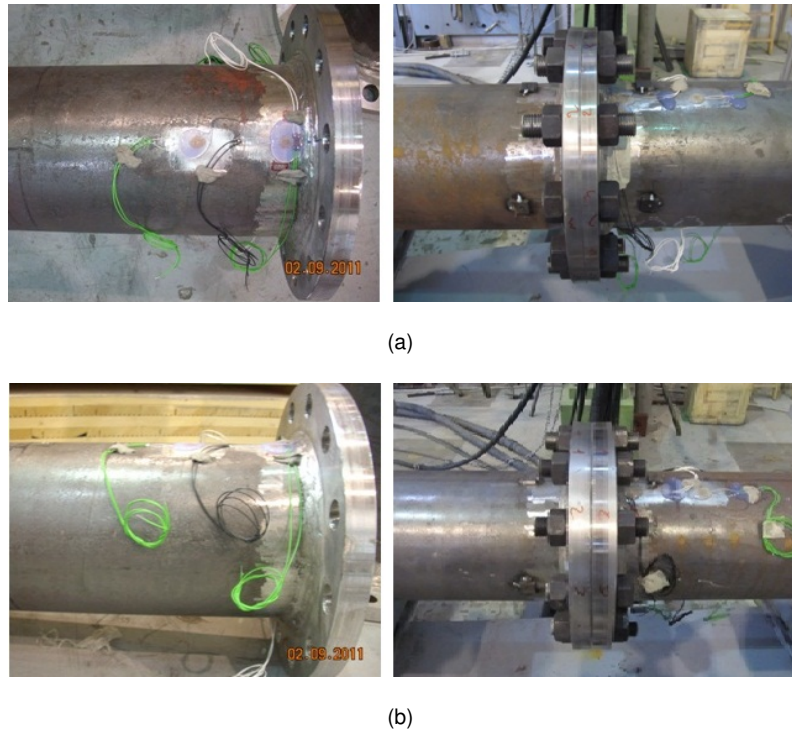


Figure 4.5: (a) Design 01 and (b) design 02 BFJ.

For an axial test specimen, stiffeners were used in its two ends which were welded to 30 cm thick plates. This was done to avoid failures in the end welded connections. Lengths of the bending and axial test specimens are reported in Table 4.4 while the test specimens and their components are shown in Figure 4.6.

Table 4.4: Lengths of test specimens

Test Specimens		Length
Bending specimen	BS1, BS2, BS3, BS4	3100 mm
Axial specimen	AS1, AS2, AS3, AS4	2050 mm

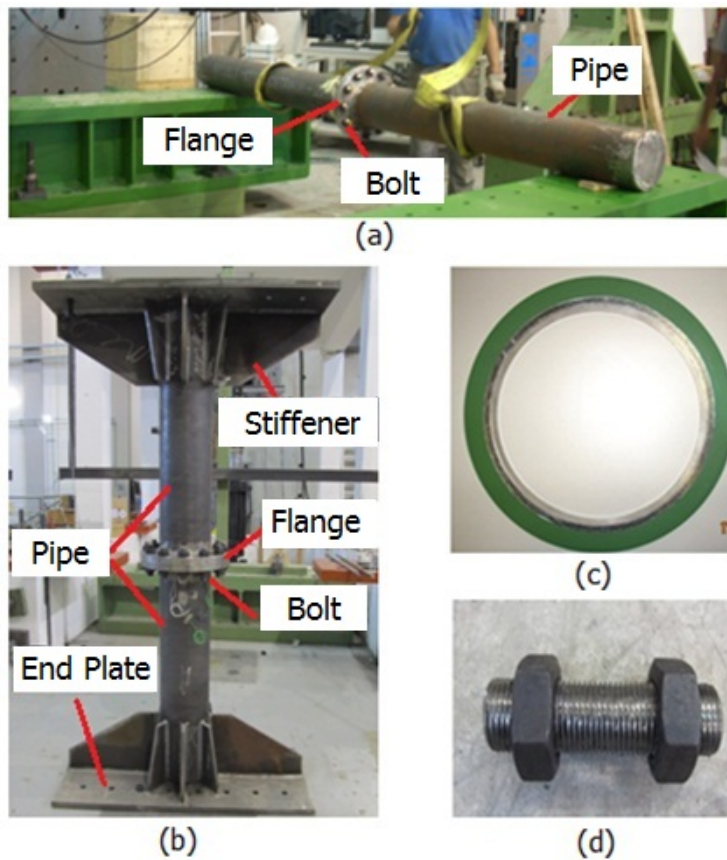


Figure 4.6: a) Bending test specimen, BS1; b) axial test specimen, AS1; c) a spiral wound gasket; d) a stud bolt.

A four point bending test configuration was adopted for the experimental set-up of bending tests. The two ends of pipes were provided with hinge connections and loads were applied in two points of the pipe through a 1000 kN MOOG actuator, see Figure 4.7(a). We used one 1000 kN actuator because the force required to produce a plastic moment in the pipe was below 1000 kN as reported in Table 3.15.

On the other hand, since the bolted flange joint and pipe showed much higher resistant to axial loads as can be seen from Table 3.13, where even to reach the yield stress of the pipe, an axial load above 1000 kN was required. Therefore, we used two 1000 kN MOOG actuators in parallel to apply axial loading to the vertically placed test specimens during axial tests as depicted in Figure 4.7(b). The ends of axial test

specimens were fixed with two strong iron supports. Sketches of experimental set-ups for bending and axial tests are presented in Figure 4.8, while the actual set-ups are shown in Figure 4.9.

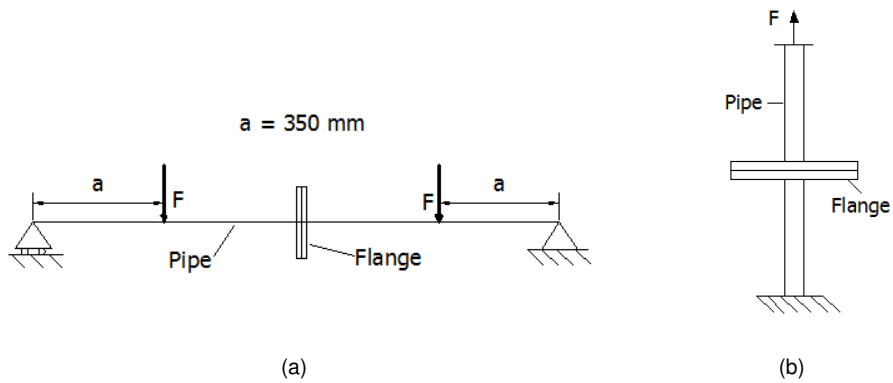


Figure 4.7: Load application points in (a) bending tests; (b) axial tests.

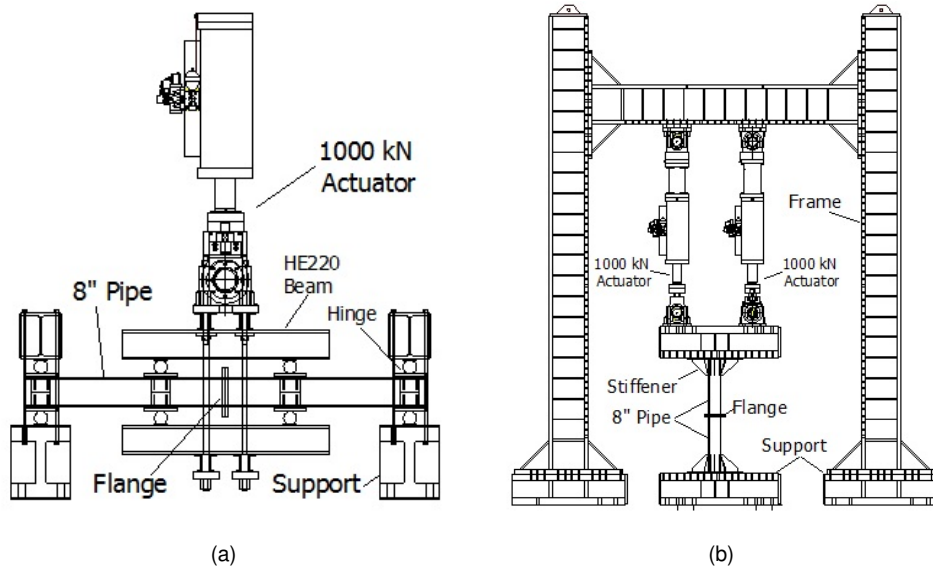


Figure 4.8: Experimental set-up for (a) bending tests; (b) axial tests.

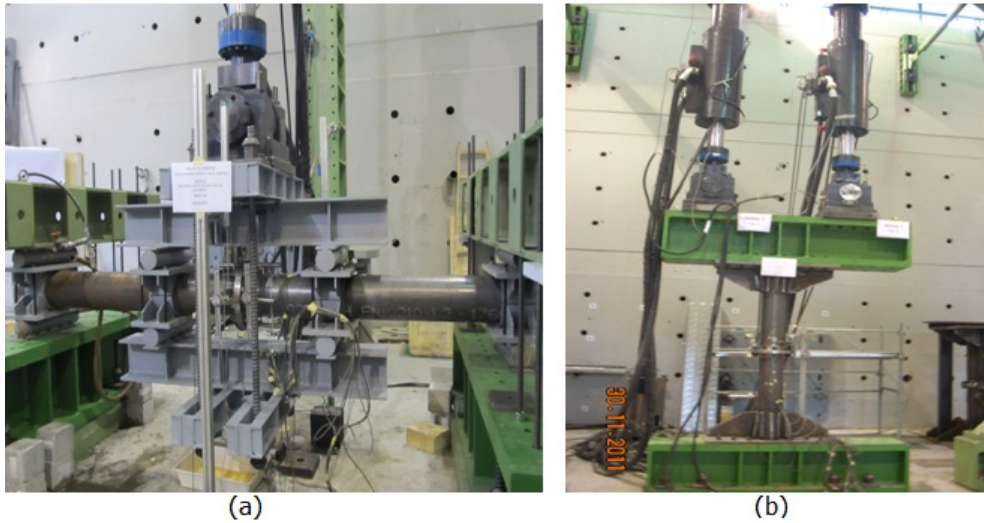


Figure 4.9: Actual experimental set-up for (a) bending tests; (b) axial tests.

4.6 Instrumentation and definition of joint rotations and displacements

Instrumentation

Eight strain gauges were mounted in each test specimen as shown in Figure 4.10 in order to measure strain levels in the pipe wall. Six of the strain gauges were placed in longitudinal direction of the pipe while two were placed in circumferential directions as reported in Table 4.5. In order to have an estimation of stresses generated near welded sections, strain gauges, S1, S2, S3, S4, S7 and S8 were placed according to the recommendations for the assessment of structural hot spot given by Hobbacher (2008) and Zhao et al. (2001). Strain gauges S5 and S6 were placed at a distance equal to half of the diameter of the pipe from the joint as the plastic deformation of the pipe spread across this region.

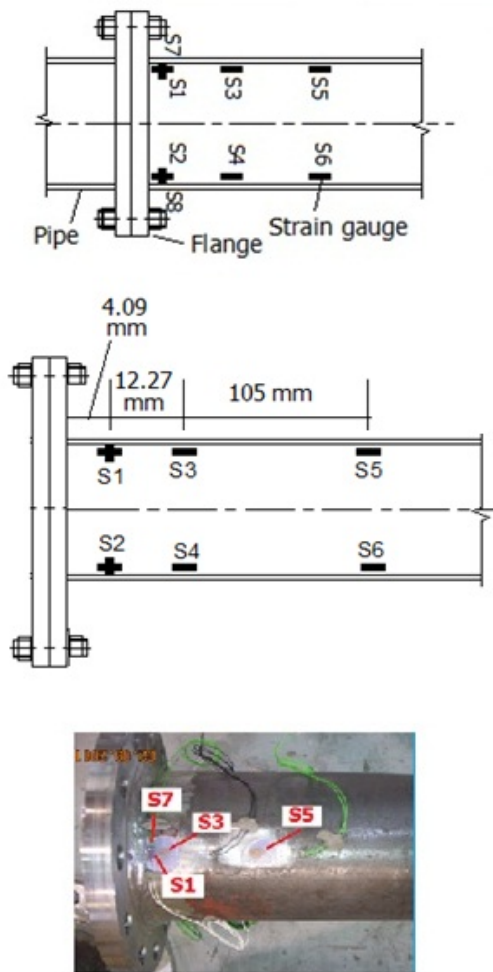


Figure 4.10: Placements of strain gauges in the pipe.

Table 4.5: Strain gauges used in experimental tests

Strain Gauge	Direction
S1, S2, S3, S4, S5, S6	Longitudinal
S7, S8	Circumferential

In order to measure rotations and displacements of the BFJs during experimental tests, we used twelve displacement transducers and two inclinometers in bending tests and eight displacement transducers in axial tests as presented in Table 4.6 and

Figure 4.11. Instrumentation schemes for bending and axial tests are presented in Figure 4.12 and Figure 4.13, respectively. Some instruments mounted in a bending and axial specimen are shown in Figure 4.14 and Figure 4.15, respectively. Test specimens were filled with water with a moderate pressure of 1.5 MPa.

Table 4.6: Instruments used in experimental tests

Instrument type	No Instruments used in bending tests	No Instruments used in axial tests
Displacement Transducers, AEP 50	8	8
Displacement Transducers, Gefran	2	0
Displacement Transducers, Wire	2	0
Inclinometers	2	0



(a)



(b)



(c)



(d)

Figure 4.11: (a) An AEP transducer; (b) an inclinometer; (c) a Gefran transducer; (d) a wire transducer.

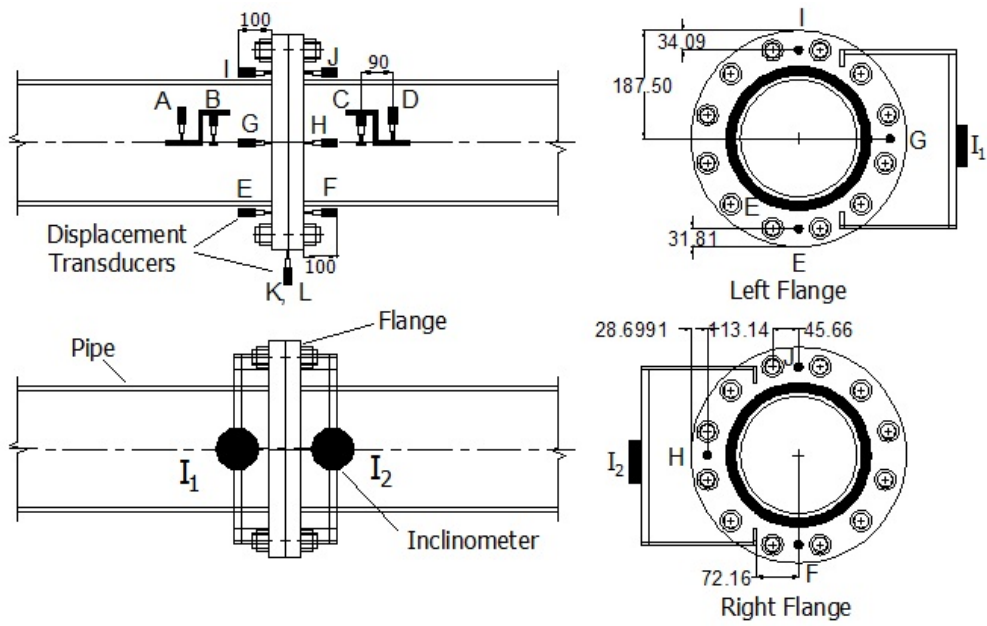


Figure 4.12: Instrumentation for bending tests (dimensions are in mm; not drawn to scale).

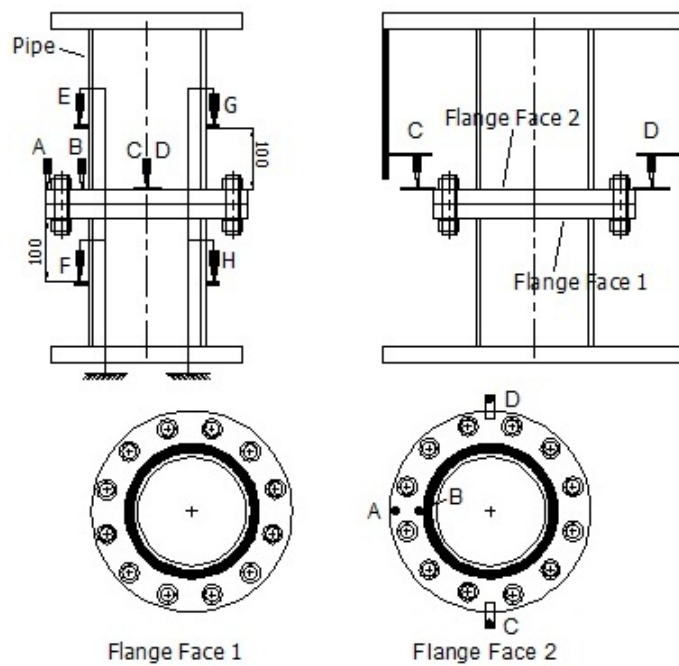


Figure 4.13: Instrumentation for axial tests (dimensions are in mm; not drawn to scale).



Figure 4.14: Some instruments mounted in a bending test.

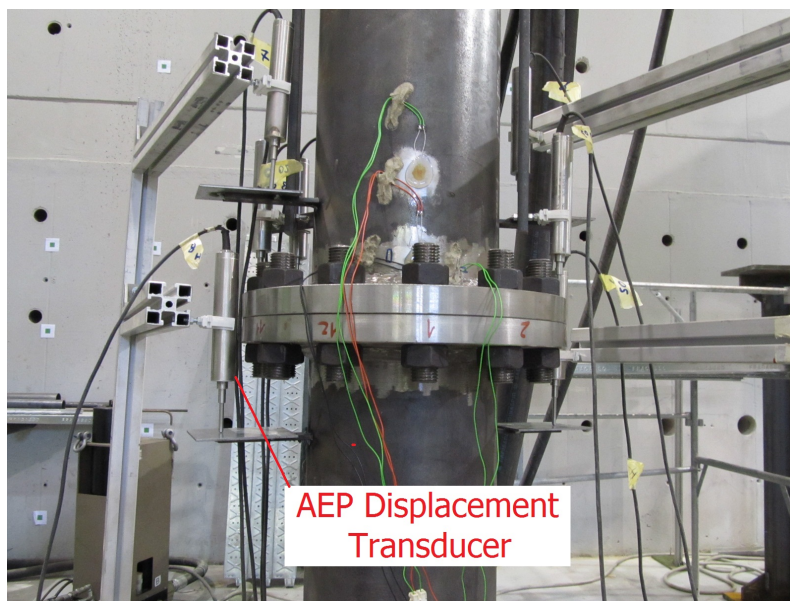


Figure 4.15: Some instruments mounted in an axial test.

Definition of joint rotations during bending tests

Rotations of a BFJ under bending loading was defined considering contributions of both of the pipe and flange rotations. Total rotation of the joint, ϕ_{tot} was calculated

through the following relationship,

$$\phi_{tot} = \phi_f + \phi_p \quad (4.3)$$

where, ϕ_f and ϕ_p are the rotations of the flange and pipe, respectively, defined as,

$$\phi_f = \phi_{I1} + \phi_{I2} \quad (4.4)$$

$$\phi_p = \phi_1 + \phi_2 \quad (4.5)$$

in which, ϕ_{I1} and ϕ_{I2} are rotations of Inclinator I1 and I2; ϕ_1 and ϕ_2 are rotations of the two segments of pipe as illustrated in Figure 4.16 .

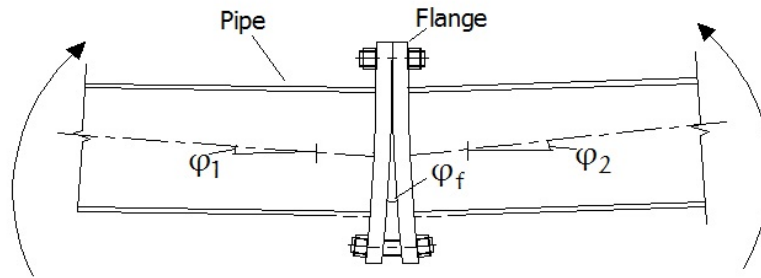


Figure 4.16: Definition of pipe and flange rotations in bending.

ϕ_1 and ϕ_2 are defined as,

$$\phi_1 = (\Delta_I - \Delta_E)/L_{EI} \quad (4.6)$$

$$\phi_2 = (\Delta_J - \Delta_F)/L_{FJ} \quad (4.7)$$

where, Δ_I , Δ_E , Δ_J and Δ_F are displacements of transducer I, E, J and F, respectively; L_{EI} is the length between displacement transducers E and I; L_{FJ} is the length between displacement transducers F and J shown in Figure 4.12. It can be noted from Figure 4.12 that transducers E, F, I, J were mounted on the pipe each at a distance of 100 mm from the flange in order to avoid a possible plastic zone near the welding.

Definition of joint displacements during axial tests

Eight displacement transducers were used in the axial tests to measure displacements of different points of axial test specimens as depicted in Figure 4.13. Total displacement, δ_{tot} of the joint was measured considering the displacements of both of the flanges. Displacements of the flanges were measured in two opposite sides of the pipe axis, see Figure 4.17, and an average value of these displacements was taken as the total displacement of the BFJ.

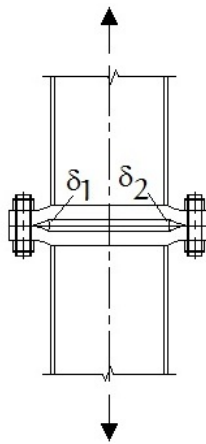


Figure 4.17: Displacements of flanges under axial loading.

$$\delta_{tot} = (\delta_1 + \delta_2)/2 \quad (4.8)$$

in which, δ_1 , and δ_2 are displacements of flanges in two opposite sides of the pipe axis measured by transducers E, F, G and H, see Figure 4.13.

$$\delta_1 = (\lambda_E + \lambda_F)/2 \quad (4.9)$$

$$\delta_2 = (\lambda_G + \lambda_H)/2 \quad (4.10)$$

where, λ_E , λ_F , λ_G and λ_H are displacements of transducer E, F, G and H, respectively.

4.7 Loading protocols

As mentioned earlier, experimental tests on the designed joints were carried out both under monotonic and cyclic loading. Cyclic loading procedures for the experiments were constructed according to the ECCS45 loading protocols (ECCS45, 1986). The ECCS45 loading procedure is based on the evaluation of a yielding displacement, e_y caused by a force, F_y corresponding to the conventional yield stress in the tested component. The conventional yield stress may be defined by the intersection of the initial stiffness and a tangent stiffness as shown in Figure 4.18. e_y is determined for the tension and compression parts separately from a monotonic test in case of the complete procedure. The cyclic test is designed as a displacement-controlled one with the increase of the amplitude of subsequent cycles of $e_y/4$, $e_y/2$, $3e_y/4$, e_y , $2e_y$, $(2+2n)e_y$, for $n = 1, 2, 3, \dots$. The ECCS45 cyclic loading procedure is presented in Figure 4.18.

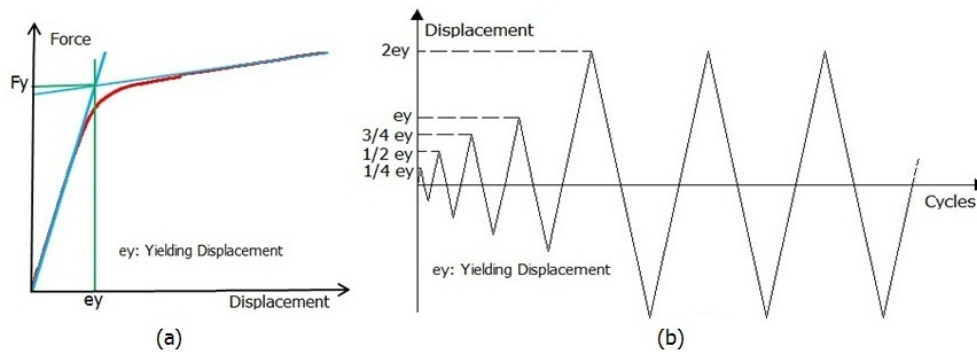


Figure 4.18: ECCS loading protocol: (a) definition of e_y ; (b) ECCS cyclic loading.

For both cyclic bending and cyclic axial tests, we constructed loading protocols according to the ECCS45 protocols. It was found during the first cyclic bending test that, already with the displacement of $4e_y$, we had failure in the specimen. Hence, for the remaining cyclic tests, we chose to perform 3 cycles of e_y in order to observe a better cyclic effect at this level. The yield displacements were calculated from monotonic tests. In case of axial tests, we applied loading only in positive cycles, i.e., tensile loading. This is because test specimens like the ones used, under compression load, are highly stiff and there are dangers of buckling and damages. Moreover, we were

mainly interested to observe the opening and closing behaviour of the BFJs for which the use of only tensile loading was appropriate.

However, it was found that the capacity of the two actuators was limited to a displacement of $2e_y$ of an axial test specimen. Hence, once the limit displacement, $2e_y$, was reached, we continued cycling with that displacement to observe low cycle fatigue behaviour of the BFJ. Loading procedures for cyclic bending and axial tests are illustrated in Figure 4.19 and Figure 4.20, respectively.

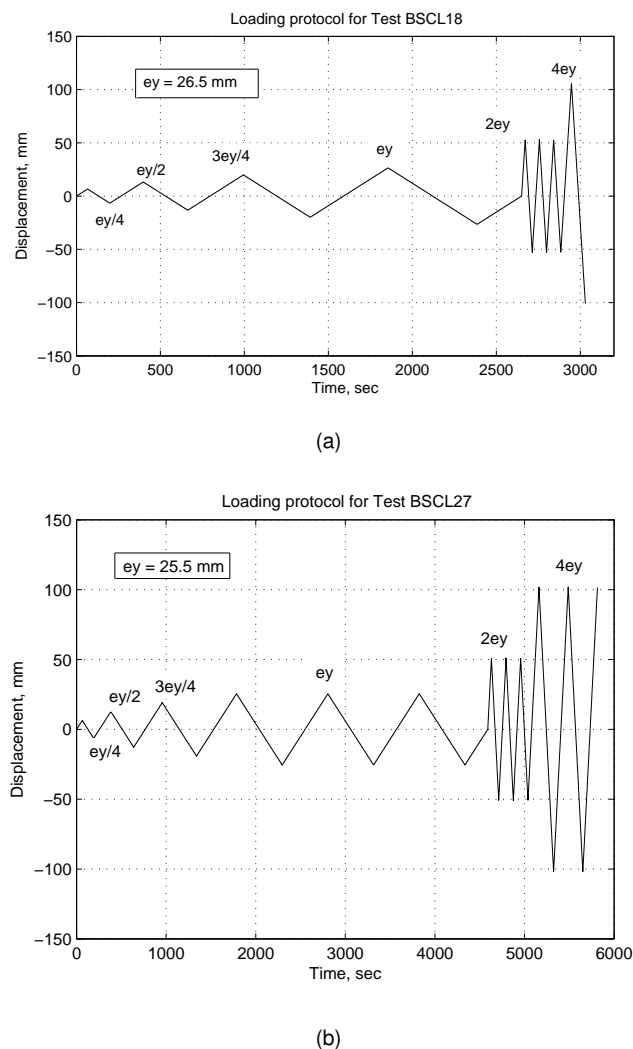
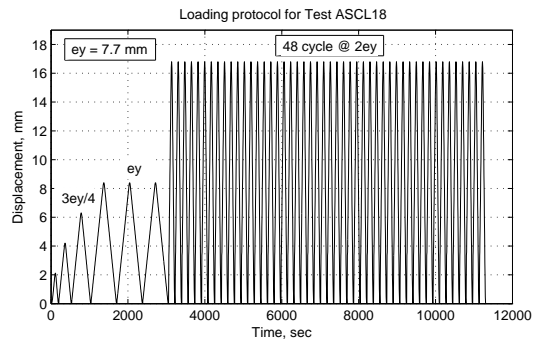
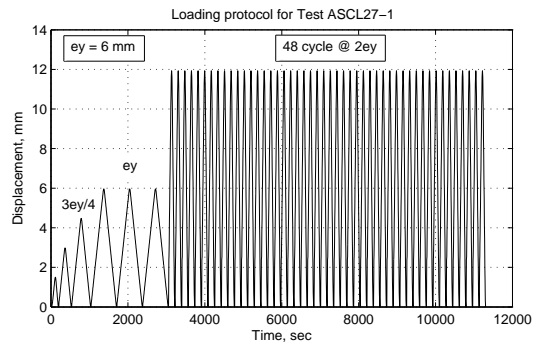


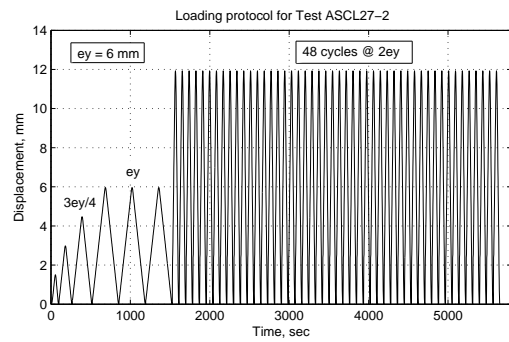
Figure 4.19: Cyclic loading protocol for (a) BSCL18; (b) BSCL27 according to ECCS45.



(a)



(b)



(c)

Figure 4.20: Cyclic loading protocol for (a) ASCL18; (b) ASCL27-1; (c) ASCL27-2.

The monotonic tests were carried out at a slower rate, e.g., maximum test speed was 0.2 mm/sec for a displacement up to ey ; maximum speed beyond this displacement was 2.5 mm/sec in order to expedite the tests.

4.8 Main observations and results from experimental tests

All experimental tests were performed in displacement control using an MTS FT60 controller and 1000 kN MOOG actuators. Data were acquired at a frequency of 2Hz using both the MTS FT60 controller and Spider8 data acquisition systems. The actuators were controlled by means of internal LVDTs. Rotations and displacements of the flange joints were measured by external instruments attached to the test specimens.

4.8.1 Results of bending tests

A total of four bending tests were carried out as planned in the experimental program. Two of the tests were performed under monotonic loading while the other two were performed under cyclic loading. The non-standard BFJs exhibited favourable performance both under monotonic and cyclic bending loading. Both the joints exhibited good energy dissipation capacity and none of the flange joints failed during the tests. High levels of leakage moments were achieved. Maximum moments and leakage moments achieved during bending tests are reported in Table 4.7.

Table 4.7: Maximum moments and leakage moments obtained during bending tests

Bending test	Leakage moment	Maximum moment	Failure Cycle
BSML18	99 kNm	196 kNm	-
BSML27	106 kNm	203 kNm	-
BSC18	80.24 kNm	190 kNm	8
BSC27	90.93 kNm	201 kNm	11

Load-displacement and moment-rotation diagrams of monotonic and cyclic bending tests are presented in Figure 4.21, Figure 4.22, Figure 4.23 and Figure 4.24. One can see that both the joints showed favourable ductile behaviour and high energy dissipation capacity. Almost no degradation of the flange joints was noticed. However, it can be noted that cyclic behaviour of design 02 joint under bending loading,

as presented in Figure 4.24, was not perfectly symmetric. In fact, during this test, It was found that while the actuator was pushing the specimen, some bolts elongated beyond their yield limit and assumed a plastic deformation under tension. Hence, those bolts showed less resistance and flanges had a higher rotation under comparatively lower load. On the other hand, when the specimen was being pulled, a higher load was required to bring those elongated bolts to their original length. As a result, the joint showed a comparatively stiffer behaviour during pulling and the above phenomenon was observed.

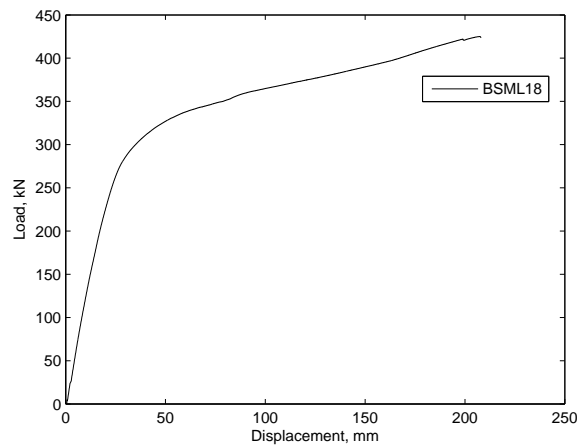


Figure 4.21: Load-displacement curve of test BSML18.

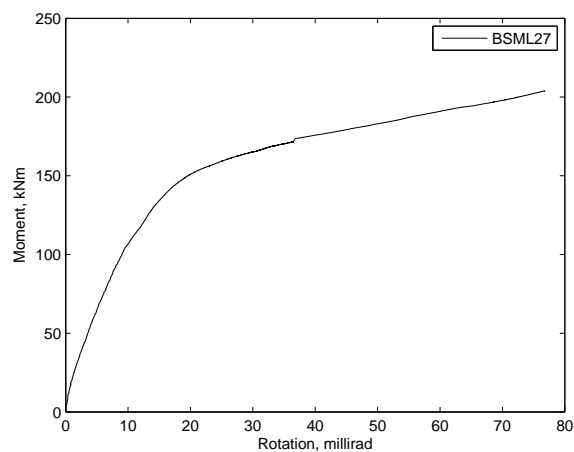


Figure 4.22: Moment-rotation curve of test BSML27.

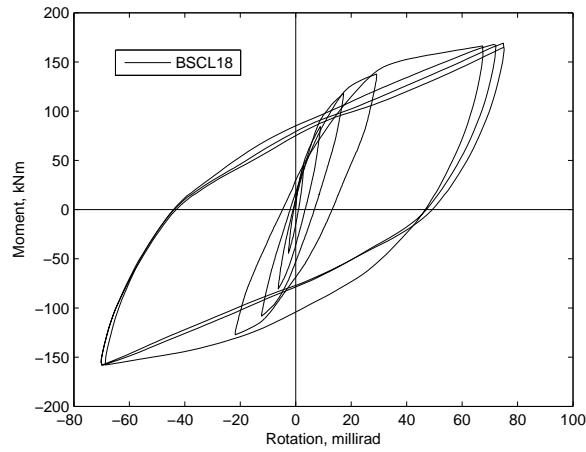


Figure 4.23: Moment-rotation curve of test BSCL18.

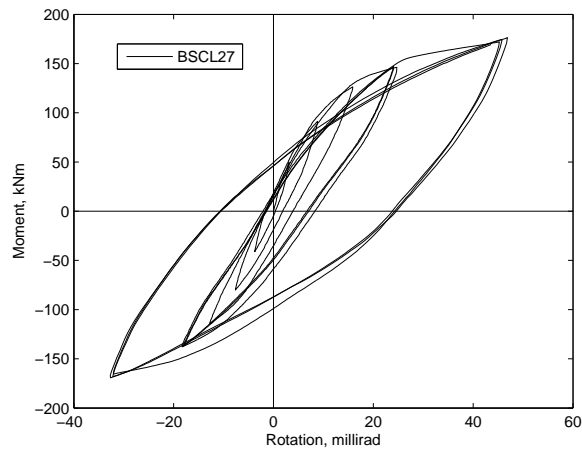


Figure 4.24: Moment-rotation curve of test BSCL27.

Regarding the stiffness, as expected, Design 02 BFJ - which is the thicker one - presented stiffer behaviour than Design 01 joints as illustrated in Figure 4.25. Envelops of moment-rotation curves from monotonic and cyclic bending tests are collected together in Figure 4.25 and one can clearly see the comparatively stiffer behaviour of Design 02 joint.

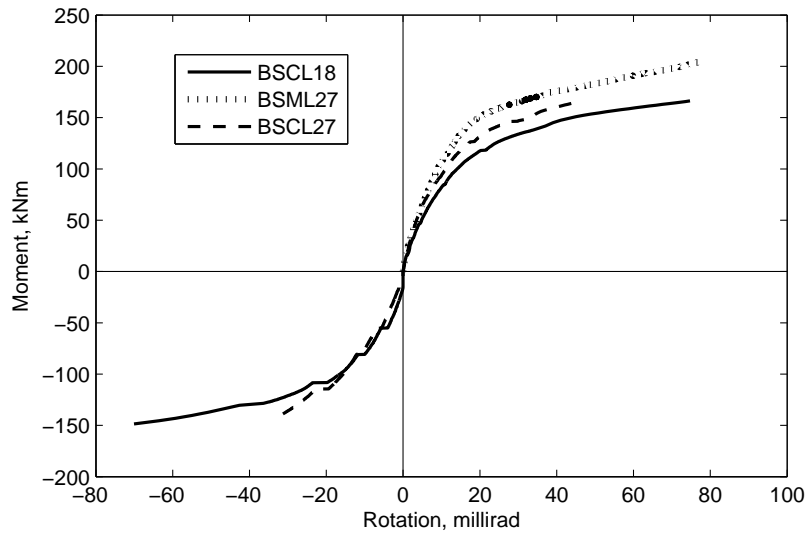


Figure 4.25: Envelop of cyclic and monotonic moment-rotation curves under bending loading.

During bending tests, buckling/cracking failures occurred in the pipe in low cycles (see Table 4.7 for numbers of Failure cycles) near the welding region of the BFJs as shown in Figure 4.26. Bending was observed in bolts, while pipe wall exceeded its yield strain limit as can be observed from Figure 4.27. The average yield strain of pipe wall was about $2053 \mu\text{m}/\text{m}$ obtained from relevant material testing. A list of observations of different components after relevant bending tests is collected in Table 4.8.

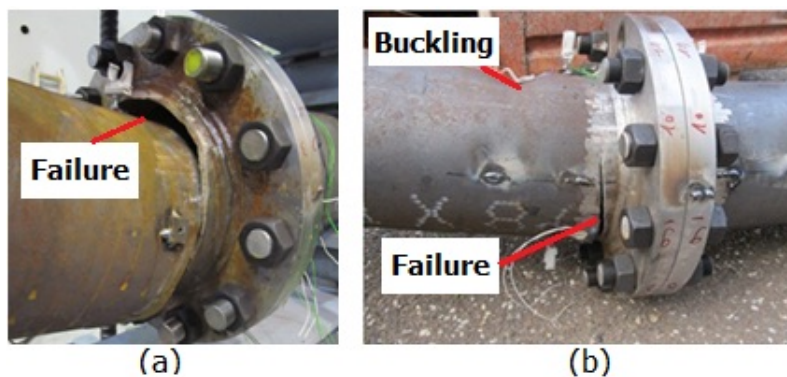
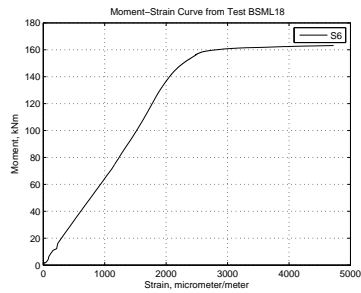
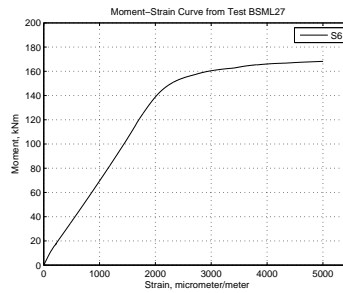


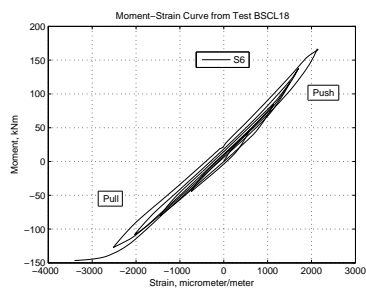
Figure 4.26: Failure in the pipe of: (a) a Design 01 BFJ (test BSCL18); (b) a Design 02 BFJ (test BSCL27).



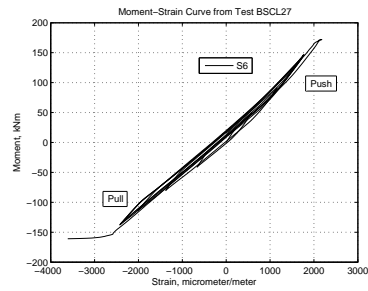
(a)



(b)



(c)



(d)

Figure 4.27: Moment-strain (strain gauge- S6) diagram of (a) BSML18; (b) BSML27; (c) BSCL18; (d) BSCL27.

Table 4.8: Observations of different components of test specimens in bending tests

Test	Pipe	Flange	Gasket	Bolts	Welding
BSML18	Buckling near the joint	Small deformation	Plastic deformation	bending	No deformation
BSML27	Buckling near the joint	small deformation	Plastic deformation	bending	No deformation
BSCL18	Buckling/cracking near the joint	Small deformation	Plastic deformation	bending	No deformation
BSCL27	Buckling/cracking near the joint	small deformation	Plastic deformation	bending	No deformation

In order to visualise the ductile behaviour of the flange joint under bending loading, we defined the ductility of a joint, μ_ϕ , as,

$$\mu_\phi = \frac{\phi_{tot}}{\phi_y} \quad (4.11)$$

where, ϕ_{tot} and ϕ_y are total and yield rotations of the BFJ.

The positive and negative yield rotations, i.e., ϕ_y^+ and ϕ_y^- , respectively, and yield moments, i.e., M_y^+ and M_y^- , respectively, were calculated using bi-linear and tri-linear approximations of moment-rotation curves according to Bursi et al. (2002) as illustrated in Figure 4.28. These values are reported in Table 4.9.

Cyclic behaviour of a Design 01 and a Design 02 joint in terms of ductility under bending loading are presented in Figure 4.29; a favourable ductile behaviour of both the joints can be noted. Moreover, one may notice that a Design 01 joint showed a better ductile performance compared to a Design 02 joint.

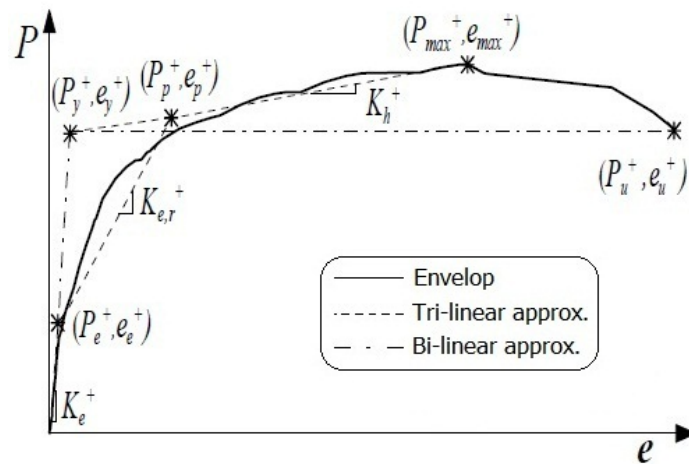


Figure 4.28: Bi-linear and tri-linear approximation of a non-linear response after Bursi et al. (2002).

Table 4.9: Yield moments and rotations of designed flange joints during bending tests

Test	Flange Joint	Loading type	ϕ_y^+ millirad	M_y^+ kNm	ϕ_y^- millirad	M_y^- kNm
BSML27	Design 02	Monotonic	10.8	151	-	-
BSCL18	Design 01	Cyclic	13.3	120.88	-12.59	-111.95
BSCL27	Design 02	Cyclic	11.18	131.96	-13.26	-134.07

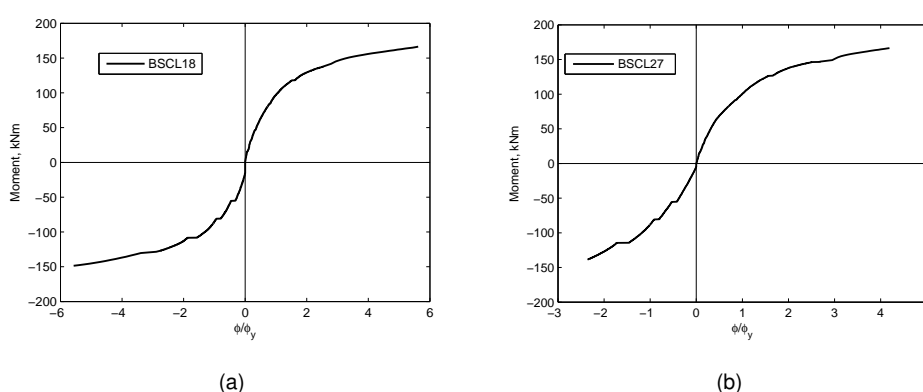


Figure 4.29: Ductile behaviour of (a) Design 01 (BSCL18); (b) Design 02 (BSCL27) BFJ.

4.8.2 Results of axial tests

As planned in the test program, four axial tests were carried out under monotonic and cyclic loading. One of the tests was performed under monotonic loading while the other three were carried out under cyclic loading. Like in bending tests, the BFJs also showed favourable performance under axial loading. High level of leakage loads were achieved during all axial tests as reported in Table 4.10. The joints underwent small displacements while cycling with high level of axial loads. A good energy dissipation capacity was observed and almost no degradation of the joints were found. Load-displacement curves of monotonic and cyclic axial tests are presented in Figure 4.30 - Figure 4.33.

As discussed earlier, axial loads were applied only in tension. However, it can be noted from Figure 4.31, Figure 4.32 and Figure 4.33 that about 600 kN and 250 kN of

compressive loads were applied during the cyclic testing of Design 01 and Design 02 joints to bring them back to their neutral positions, i.e., zero displacement. One may be curious to notice that a lower level of force was required to bring Design 02 joints to their neutral positions compared to Design 01 joint. We note that, at the level of $2e_y$, displacements of a Design 01 joint were higher than that of a Design 02 joint. In fact, in the ECCS45 loading protocols of axial tests, the value of e_y used for a Design 02 joint, i.e., 6 mm, was less than the that used for a Design 01 joint, i.e., 7.2 mm. Therefore, components, e.g., flanges and bolts, of a Design 01 joint had a higher level of deformation than a Design 02 joint. Hence, a higher level of compressive load was required to bring this joint to its neutral position. Again we report that the above load-displacement curves of axial tests show displacements of flanges and not that of the actuators. Hence, while the actuators reached their neutral positions, flanges still had some residual displacements.

Table 4.10: Leakage and maximum loads reached during axial tests

Axial Test	Leakage Loads	Maximum loads reached during tests
ASML18	1170 kN	1980 kN
ASCL18	1243 kN	1865 kN
ASCL27-1	1812 kN	1812 kN
ASCL27-2	1894 kN	1894 kN

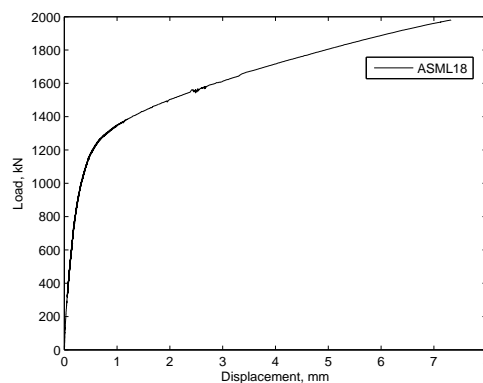


Figure 4.30: Load - flange-displacement curve of test ASML18.

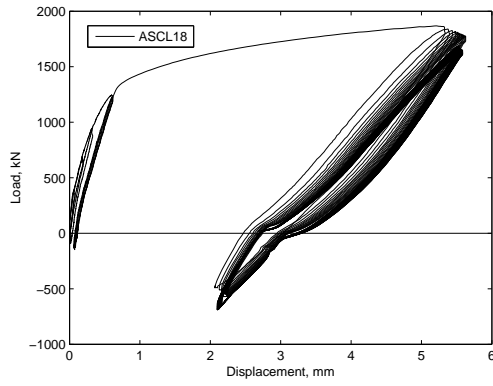


Figure 4.31: Load - flange-displacement curve of test ASCL18.

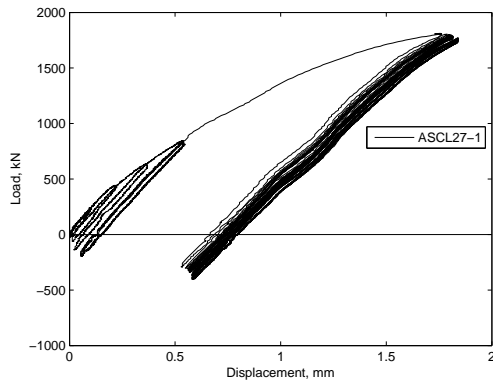


Figure 4.32: Load - flange-displacement curve of test ASCL27-1.

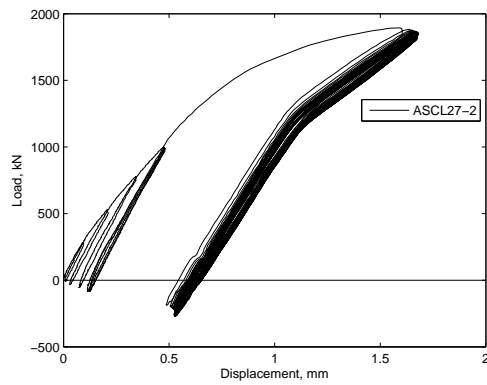


Figure 4.33: Load - flange-displacement curve of test ASCL27-2.

As observed during bending tests, Design 02 joints showed comparatively stiffer behaviour as can be noted from Figure 4.34 in which envelopes of load-displacement curves from monotonic and cyclic axial tests are collected together.

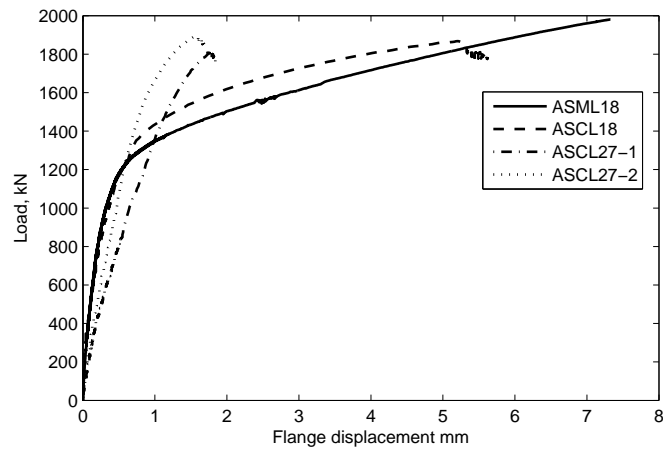
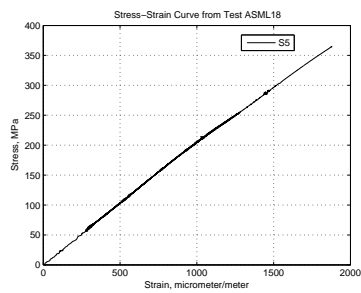


Figure 4.34: Envelopes of cyclic and monotonic load-displacement curves under axial loading.

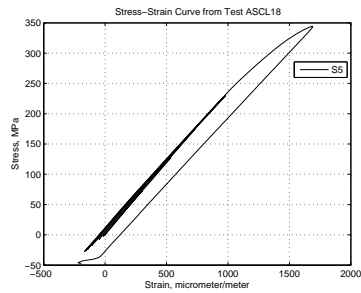
No failure occurred in the pipe or joint during axial tests. A test specimen after an axial test is presented in Figure 4.35. Small bending was observed in bolts. Strain levels in the pipe remained below yielding limit as can be noted from Figure 4.36. A list of observations of different components of axial test specimens after relevant tests is reported in Table 4.11.



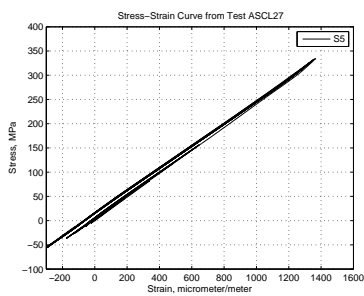
Figure 4.35: Test specimen, AS2 after test ASCL18.



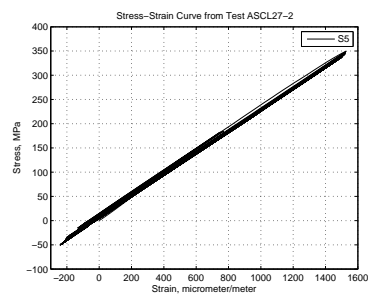
(a)



(b)



(c)



(d)

Figure 4.36: Stress-strain (strain gauge- S5) diagram of (a) ASML18; (b) ASCL18; (c) ASCL27-1; (d) ASCL27-2.

Table 4.11: Observations of different components of test specimens in axial tests

Test	Pipe	Flange	Gasket	Bolts	Welding
ASML18	No deformation	small deformation	Small deformation	small bending	No deformation
ASCL18	No deformation	small deformation	Small deformation	small bending	No deformation
ASCL27-1	No deformation	small deformation	Small deformation	small bending	No deformation
ASCL27-2	No deformation	small deformation	Small deformation	small bending	No deformation

In order to facilitate a better observation on the ductility of non-standard joints, we defined ductility of a joint, μ_{δ} , as,

$$\mu_{\delta} = \frac{\delta_{tot}}{\delta_y} \quad (4.12)$$

where, δ_{tot} and δ_y are total and yield displacements of flanges, respectively.

The yield displacements, δ_y and loads, F_y were calculated using bi-linear and tri-linear approximations of the load-displacement curves according to Bursi et al. (2002) as shown in Figure 4.28; relevant values are reported in Table 4.12. It can be noted from Table 4.12 that both the joints showed high resistance in axial loading. Small levels of yield displacement with high level of yield loading were achieved by the BFJs. However, as mentioned earlier, we note that the maximum loading of the actuators was limited to 2000 kN and, at this level of load, a Design 02 joint seemed to have a maximum displacement in its elastic region as can be noted from Figure 4.34. Different values of yield loads and displacements of a Design 02 joint might be found in case a test was carried out with a higher level of axial loading.

Cyclic behaviour of a Design 01 and a Design 02 joint in terms of ductility under axial loading are presented in Figure 4.37. For a Design 02 joint, a maximum value of μ_{δ} can be observed to be about 1 for the reason previously discussed. However, a favourable ductile performance is noticed for a Design 01 joint.

Table 4.12: Yield moments and yield displacements of non-standard BFJs under axial loading

Test	Flanged Joint	Loading type	δ_y^+ , mm	F_y^+ , kN
ASML18	Design 01	Monotonic	0.48	1400
ASCL18	Design 01	Cyclic	0.50	1385
ASCL27-1	Design 02	Cyclic	1.76	1812
ASCL27-2	Design 02	Cyclic	1.59	1867

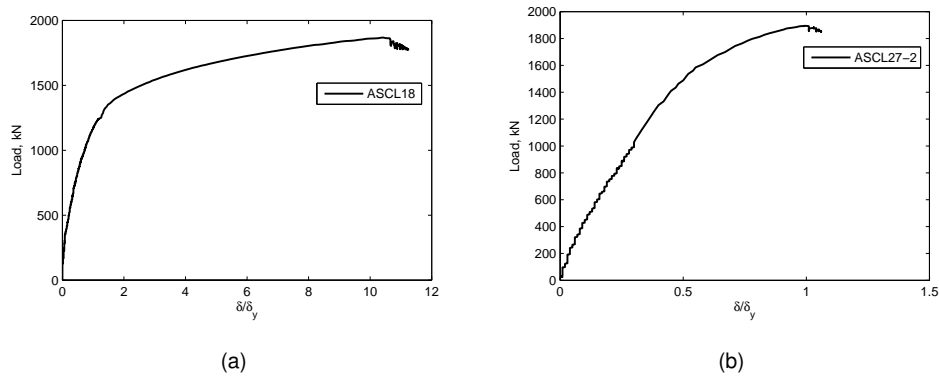


Figure 4.37: Ductile behaviour of (a) Design 01 and (b) Design 02 BFJ under axial loading.

4.9 Performance evaluation of designed BFJs

The experimental campaign on the designed non-standard BFJs demonstrated good performance of the joints under bending and axial loading. We performed a comparison between test results, i.e., leakage load and allowable load, and allowable design load suggested by Codes and Standards. Moreover, a comparison between seismic demand and capacity of the joints through a Case Study on a typical industrial piping system were also performed.

4.9.1 Comparison between experimental results and allowable design loads

A comparison of experimental results with allowable design loads for a BFJ was deemed necessary to appreciate the performance of non-standard joints. Nevertheless, a lack of appropriate Standards exists in this respect. Calculation methods of EN 1591-1 might be used to obtain a maximum applicable external load, but, as discussed in Chapter 3, such Standard already disapproved the design of non-standard BFJs for a specific leak-rate and design operating conditions. Hence, as an alternative, test results were compared with allowable design loads for a pipe under seismic loading. These comparisons were rational, because BFJs are part of a pipeline and they also experience the load that act upon their connecting pipes. Moreover, in our experiments, applied moments were considered to be the same for both the pipe and

joint.

Several European and American standards, e.g., EN 13480-3 (2002); ASME B31.1 (2001); ASME B31.3 (2006), provide formulas for the calculations of allowable design loads in pipes under seismic events. ASME B31.1 and EN 13480-3 provide similar design formula expressed as follows,

$$\sigma = \frac{p_c d_o}{4e_n} + \frac{0.75iM_A}{Z} + \frac{0.75iM_B}{Z} \leq kf_h \quad (4.13)$$

where, i is the stress intensity factor; M_A is a moment from sustain mechanical loads; M_B is a moment from occasional loads; Z is the section modulus; p_c is the internal pressure; d_o is the pipe outer diameter; e_n is the pipe wall thickness; and f_h is the allowable stress defined in these Standards. For a design basis earthquake, the value of k is 1.2 and 1.33 according to EN 13480-3 and ASME B31.3, respectively.

Allowable moments and loads calculated for the straight pipes used in the test specimens considering a design basis earthquake are reported in Table 4.13.

Table 4.13: Allowable moments and loads in straight pipes

Standard	Allowable Moment, M_a	Allowable load, F_a
EN 13480-3, 2002	51.23 kNm	885.20 kN
ASME B31.1 & B31.3	57.08 kNm	885.20 kN

The allowable stress, f_h in (4.13), is defined in EN 13480-3 as follows,

$$f_h = \min(f_y/1.5; f_u/3; f_{cr}); \quad (4.14)$$

in which, f_y and f_u are the yield and ultimate strength, respectively; f_{cr} design stress in the creep range.

In order to compare experimental results with yield moment suggested by Standards, instead of using f_h on the right hand side of (4.13), we used the value of f_y of the pipe. Thus, the yield design moments were calculated using the following formulas,

$$\sigma = \frac{p_c d_o}{4e_n} + \frac{0.75iM_A}{Z} + \frac{0.75iM_B}{Z} \leq kf_y \quad (4.15)$$

The yield moments calculated for the straight pipes using (4.15) are reported in Table 4.14. In this calculation, nominal values of yield strength of the pipe material was used.

Table 4.14: Design yield moments in straight pipes suggested by Standards

Design Standard	Yield Moment, M_y
EN 13480, 2002	114.6 kNm
ASME B31.1 & B31.3	127.31 kNm

In addition, a plastic moment of the pipe was calculated using the following relationship,

$$M_p = f_y Z_p \quad (4.16)$$

where, Z_p is the plastic section modulus of the pipe; relevant value of M_p was 155.07 kNm.

A calculation was also performed according to the newly developed strain-based design approach (CSA-Z662, 2007) to calculate a buckling moment of the pipe using the following formula,

$$\varepsilon_c^{crit} = 0.5 \frac{t}{D} - 0.0025 + 3000 \left(\frac{(P_i - P_e)D}{2tE_s} \right)^2 \quad (4.17)$$

where, ε_c^{crit} is the ultimate compressive strain capacity of the pipe wall; P_i is the internal pressure; P_e is the external pressure; t is the pipe wall thickness; D is the pipe outer diameter; and E_s is the modulus of elasticity.

The stress corresponding to the ultimate compressive strain, σ^{crit} , was taken from the material testing data reported in Table 4.2. The buckling moment, M_b was then calculated as,

$$M_b = \sigma^{crit} Z \quad (4.18)$$

where, Z is the elastic section modulus of the pipe; relevant value of M_b was found to be 134.99 kNm.

To perform a comparison between experimental and Coded loads, minimum values of leakage and yield loads obtained during bending and axial tests were compared

with the allowable and yield design loads and with the plastic and buckling moments, as reported in Table 4.15 - Table 4.18. One can see that allowable moments and forces in the pipe were considerably lower than experimental leakage and yield loads. Hence, the proposed non-standard joints could be safely used in a pipeline designed according to available Standards.

Table 4.15: Comparison between experimental and allowable design moments

Experimental moment		Allowable moment by Standard	
Minimum leakage moment	Minimum yield moment	EN 13480-3 (2002)	ASME B31.1 & B31.3
80.24 kNm	111.95 kNm	51.23 kNm	57.08 kNm

Table 4.16: Comparison between experimental and allowable design loads

Experimental load		Allowable load by Standards	
Minimum leakage load	Minimum yield load	EN 13480-3 (2002)	ASME B31.1 & B31.3
1170 kN	1385 kN	885.20 kN	885.20 kN

Table 4.17: Comparison between experimental moments and yield moments by Standards

Experimental moment		Yield moment by Standards	
Minimum leakage moment	Minimum yield moment	EN 13480-3 (2002)	ASME B31.1 & B31.3
80.24 kNm	110.95 kNm	114.6 kNm	127.31 kNm

Table 4.18: Comparison between experimental, plastic and buckling moments

Experimental moment		Plastic/Buckling moments	
Minimum leakage moment	Minimum yield moment	M_p	M_b
			CSA-Z662-07
80.24 kNm	110.95 kNm	155.07 kNm	134.99 kNm

The comparison between experimental and Coded moments and forces are graphically illustrated in Figure 4.38 and Figure 4.39, in which different levels of Coded and experimental moments and forces are indicated in the envelopes of cyclic and monotonic bending and axial experimental curves. It can be clearly noted from these figures that leakage loads were well above the allowable design loads and maximum seismic demands (which will be discussed in the following Subsection). Moreover, one may also observe that buckling and plastic moments were below the maximum moments achieved during bending tests.

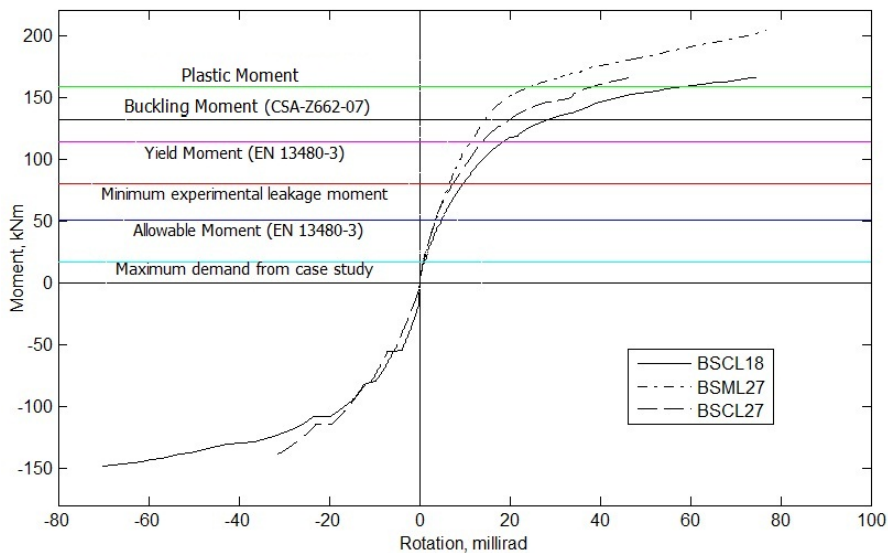


Figure 4.38: Comparison between experimental and Coded moments.

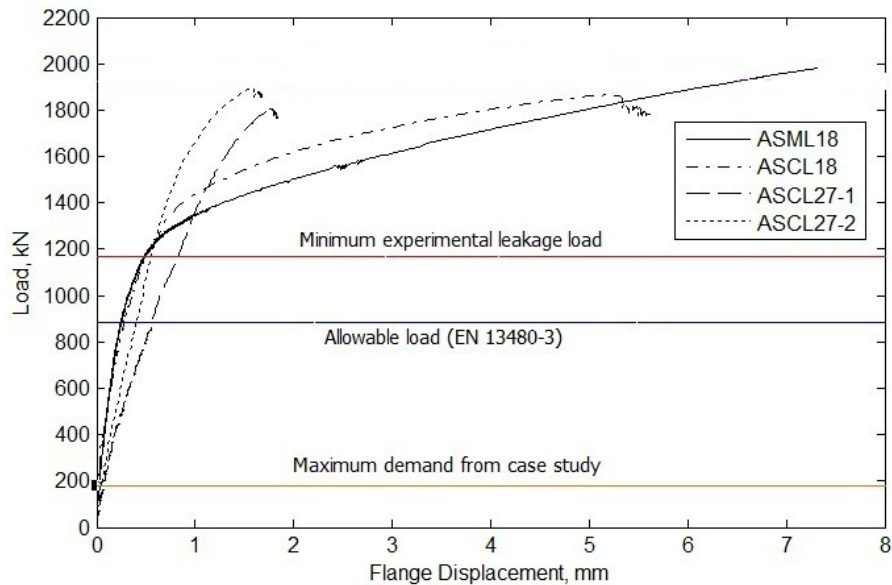


Figure 4.39: Comparison between experimental and Coded loads.

4.9.2 Comparison between seismic demands and capacity

In order to assess seismic performance of non-standard BFJs, it was required to compare the capacity of the joints with the demand coming from an earthquake. In this view, we used results of a Case Study carried out on a typical piping system within the European project INDUSE (INDUSE, 2009). Details of the Case Study is available in literature (Paolacci et al., 2011).

The piping system considered in the Case Study belonged to a refinery. The support steel structure was composed of seven transverse moment resisting frames placed every 6 m, realized with commercial HEA/B steel profiles. In the longitudinal direction it behaved like a truss structure, which was reinforced with 6 braces. Horizontal bracings were also installed to avoid excessive relative displacements between the pipe supports. The piping system presented a typical piping layout with pipes having different diameters. To simplify the analysis, only the structural contribution of 8" pipes was considered. The remaining pipes were considered only as weight. This was helpful for our comparison for it contained the same pipe size as used in the BFJs. Several flanged elbows were present within the pipe-rack and at both ends of

the piping system. The model of the piping systems is illustrated in Figure 4.40. In-elastic fibre beam elements were used for the frames, whereas linear truss elements were used for the vertical and horizontal bracing. The pipe was modelled using linear beam element for the straight parts of pipe and by using shell elements to better simulate the behaviour of the elbows.

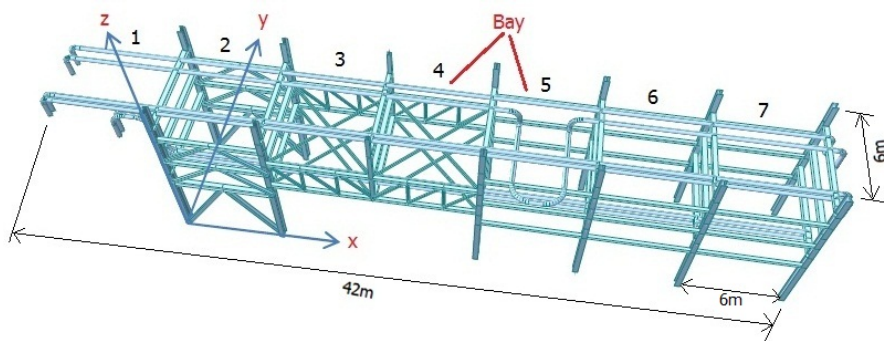


Figure 4.40: The piping system considered in the Case Study.

A dynamic analysis was performed using a set of 7 accelerograms compatible with the EC8 spectrum for Soil B and selected according to a Magnitude range 6-7, a distance from the epicentre <30 km, and a PGA in the range 0.25-0.35 g. These parameters are referred to the Operating Basis Earthquake (OBE) condition, for which operating conditions of the plant can be still assured after a seismic event (Paolacci et al., 2011). A behaviour factor, $q=4$ was used for the analysis.

Results of the analysis in terms of moments along local axes y , M_y and z , M_z of the pipe are reported in Table 4.19. The resultant moment M_R of the single moments, M_y and M_z , calculated according to the EN13480-3 and ASME B31.3 are also reported. The maximum moment was found near the left edge of the rack (bay 2), even if similar values were also obtained within bay 6 and 7. In addition, the maximum stress level of the pipe in the same points was also calculated according to the rules suggested in EN13480-3.

Table 4.19: Maximum bending moment and tension in the pipes from the Case Study

Moment	Bay						
	1	2	3	4	5	6	7
My (kNm)	1.56	6.91	5.98	4.94	5.04	3.47	2.5
Mz (kNm)	13.72	15.3	14.15	7.01	8.75	15.84	15.84
MR (kNm)	13.81	16.79	15.36	8.58	10.1	16.22	16.04
Tension (MPa)	76.71	86.41	81.76	59.67	64.62	84.54	83.96

Table 4.20: Maximum bending moment and axial force

Maximum moment in the piping system obtained from the Case Study	Maximum axial force in the piping system obtained from the Case Study
16.79 kNm	180.5 kN

It can be noted from Table 4.19 that these results are extremely conservative. The maximum of the values of moment and axial forces corresponding to the moments of Table 4.19 are collected in Table 4.20. As can be clearly seen from Table 4.20, these values were far from the values found from the experiments; see also Figure 4.38 and Figure 4.39 in this respect. It is, therefore, obvious that the proposed non-standard BFJs possessed a good capacity to operate safely under similar earthquakes considered in the Case Study.

4.10 Conclusions

An experimental test campaign carried out on non-standard BFJs was presented in this chapter. Favourable performance in bending and axial loading in terms of leakage, ductility and energy dissipation was displayed by both the joints. The joints exhibited high energy dissipation capacity and almost no degradation was observed under cyclic loading. High levels of leakage loads were found in all tests and no failure occurred in any of the flange joints.

During the bending tests, failure took place in the pipe near the joint where local buckling was observed. However, the level of maximum load was limited to 2000 kN in case of axial tests due to the capacity of the actuators. With this maximum load, no failure occurred in the BFJs or in the pipe. The cyclic tests carried out with the maximum possible displacement in axial tests showed favourable low cycle fatigue performance of the BFJs.

The experimental leakage and yielding loads were found considerably higher than the allowable seismic design loads suggested by Codes and Standards. Moreover, the Case Study carried out on a piping system showed that the seismic demands were significantly lower than the capacity of the BFJs which proved the suitability of the designed BFJs for seismic applications. Thus, the non-standard BFJs were found promising to be safely used in piping systems operating both under normal conditions and under regular earthquake events.

CHAPTER 5

CHARACTERIZATION OF ACTUATORS FOR PSEUDO-DYNAMIC AND REAL TIME TESTS

5.1 Introduction

As part of this thesis, a pseudo-dynamic and real time test campaign was carried out on a piping system which will be described in the next chapters. These dynamic tests were performed using two MOOG hydraulic actuators controlled by means of an MTS controller. The dynamics of the actuators with the control system is important as it may impair the reliability of an experiment in terms of amplitude error and phase delay (Jung et al., 2007). In particular, the time delay in the measured restoring forces can lead to instability of the system (Horiuchi et al., 1996). In this short chapter, the dynamic performance of the MOOG actuators used in the experiments is analysed. In addition, a characterization of the actuators based on a transfer function will be presented.

5.2 Hardware and software for hybrid tests

The pseudo-dynamic (PDDS) and real time (RTDS) tests -hybrid tests- were carried out using several hardware and software. The main hardware are listed below and shown in Figure 5.1.

Host PC

The Host PC is a computer where the algorithms of hybrid tests were developed in

a Simulink (Simulink, 2012) environment where it was compiled and then sent to an xPC target via a LAN connection.

xPC Target:

The xPC target is a real-time software environment from MathWorks which operated at the frequency of the controller (1024 Hz). It communicated with the MTS controller by means of a shared memory called 'SCRAMNET'.

MTS FT60 Controller

The MTS FT60 controller (MTS, 2008) controlled the hydraulic actuators. It received displacement commands for the test specimen from the xPC target and sent these commands to the MOOG actuators. Moreover, it read reaction forces from the actuators and returned this information to the xPC target.

MOOG Hydraulic Actuator

Two MOOG hydraulic actuators, MOOG1 and MOOG2, each with a capacity of +/- 1000 kN force were used to load the test specimen. The displacement range of the actuators was +/- 250 mm.

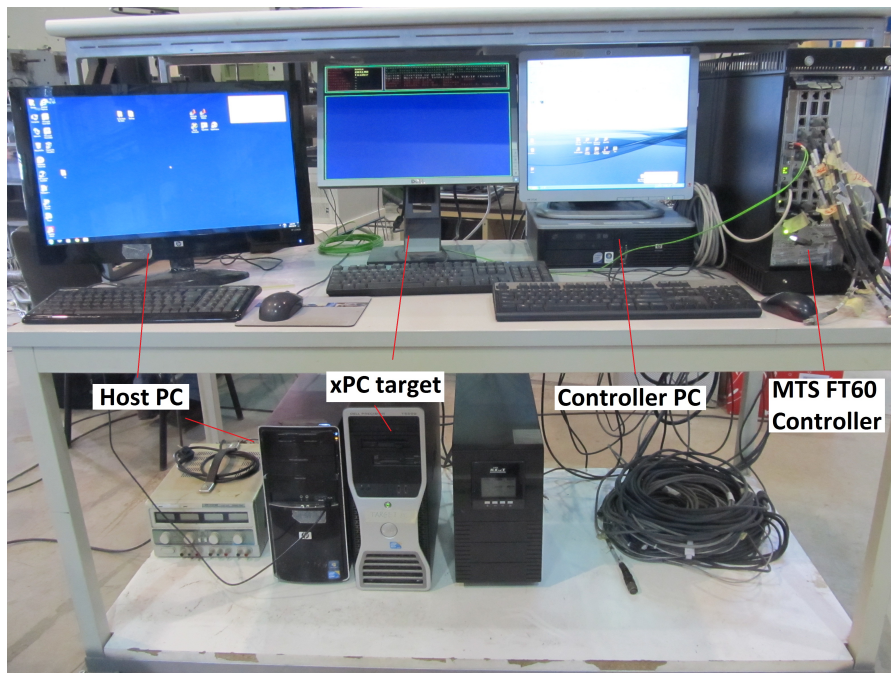


Figure 5.1: Hardware for hybrid tests.

5.3 Estimation of a transfer function of the actuator and control system

The MOOG actuators were controlled via an MTS FT60 controller. A PID controller along with a feed-forward gain was implemented in the control system in order to send a command to the servo-valve of the actuator as illustrated in Figure 5.2. By means of tuning the gains of the controller, i.e., proportional, P , derivative, D , integral, I , and feed-forward, F , an optimum response of the actuators could be achieved.

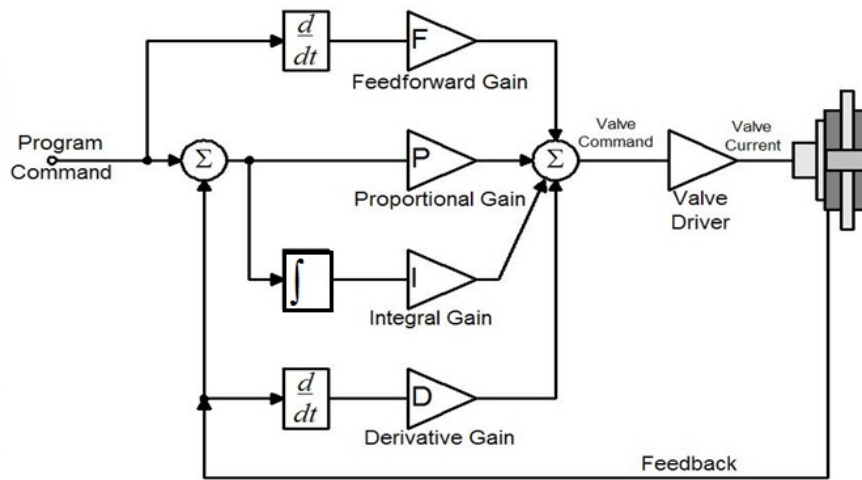


Figure 5.2: Controller configuration for a MOOG actuator.

In order to simulate the dynamic response of the transfer system, i.e., control loop together with the actuator, it was characterised in terms of a Transfer Function (TF), $G(s)$, defined as,

$$G(s) = \frac{y(s)}{u(s)} \tag{5.1}$$

where, s is a complex Laplace variable, $y(s)$ is the Laplace transformation of the actuator displacements and $u(s)$ is the Laplace transformation of the input signals.

Using the transfer function, $G(s)$, we can simplify Figure 5.2 to Figure 5.3.



Figure 5.3: Simplified representation of the TF of the transfer system.

In a first approximation, a 2nd order under-damped TF was considered as follows:

$$G(s) = \frac{1}{1+2\xi T_\omega s+(T_\omega s)^2} \quad (5.2)$$

where, T_ω and ξ are the natural frequency and damping ratio, respectively; s is called the poles of the system. The above equation shows that the system has two complex conjugate poles.

Identification of the TF was carried out by means of a time-domain system identification algorithm called AutoRegressive model with eXternal input (ARX) developed by Ljung (1986, 1987). We used a Matlab toolbox embedded with this algorithm to perform the identification.

Since the TF of an actuator could be sensitive to the level of load it operated, a linear TF was experimentally identified with different level of masses, i.e., 2500 kg and 5000 kg, attached to a MOOG actuator as shown in Figure 5.4. A sensitivity analysis of the TF with respect to increasing masses was then conducted using the following signals: (i) Band Limited White Noise (BLWN); (ii) Pseudo Random Binary Sequence (PRBS); and (iii) Sin Chirp (CHIRP). These signals contained a maximum frequency of 15 Hz with a displacement range of +/- 1 mm. Figure 5.5 shows a filtered sine chirp signal used during the identification. The identified values of T_ω and ξ with different signals are presented in Table 5.1.



Figure 5.4: A MOOG actuator attached with masses.

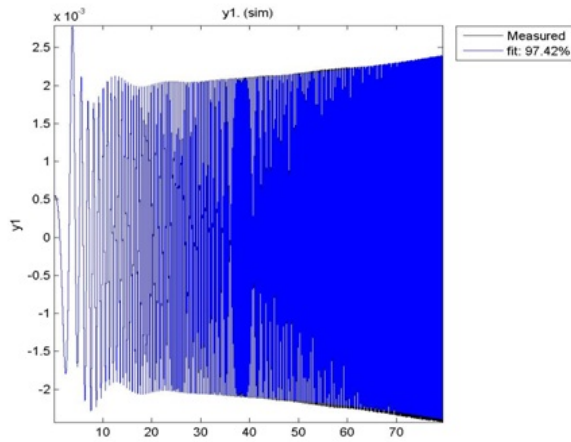


Figure 5.5: A sine chirp signal used for the estimation of actuator TF.

Table 5.1: Identified parameters of the actuator TF using the ARX algorithm

Signal	T_ω		ξ	
	1xMass (2500 kg)	2xMass (5000 kg)	1xMass (2500 kg)	2xMass (5000 kg)
BLWN 0-5 Hz	0,0088	0,0088	0,3142	0,2876
BLWN 0-10 Hz	0,0082	0,0081	0,3487	0,3302
BLWN 0-20 Hz	0,0073	0,0073	0,4011	0,3722
CHIRP 0-5 Hz	0,0092	0,0093	0,2791	0,2440
CHIRP 0-10 Hz	0,0091	0,0091	0,3536	0,3144
CHIRP 0-20 Hz	0,0088	0,0087	0,4333	0,4198
PRBS	0,0129	0,0128	0,6900	0,6823
Averaged values	0,0086	0,0085	0,3550	0,3280

It can be noted from Table 5.1 that, for the displacement range of interest, i.e., +/- 1 mm, the parameters identified by means of the ARX algorithm showed to be insensitive to the specimen mass. The average values of the identified parameters were used to develop the reference TF, $G(s)$, which reads,

$$G(s) = \frac{1}{1+2\cdot 0,3415\cdot 0,0085\cdot s+(0,0085\cdot s)^2} \quad (5.3)$$

The relevant bode diagram and step response of the MOOG actuator are presented in Figure 5.6 and Figure 5.7, respectively, while the original setting of controller gains are reported in Table 5.2. One may observe from Figure 5.7 that the step response showed an overshoot. In order to eliminate this overshoot and to achieve an optimized response of the MOOG actuator a derivative gain was added to the PID controller as reported in Table 5.3. Moreover, the total delays of the two actuators were also estimated as reported in Table 5.4.

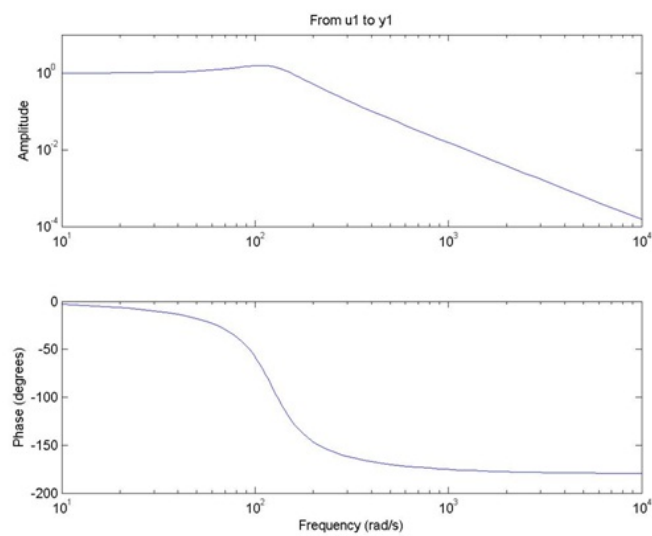


Figure 5.6: Bode diagram.

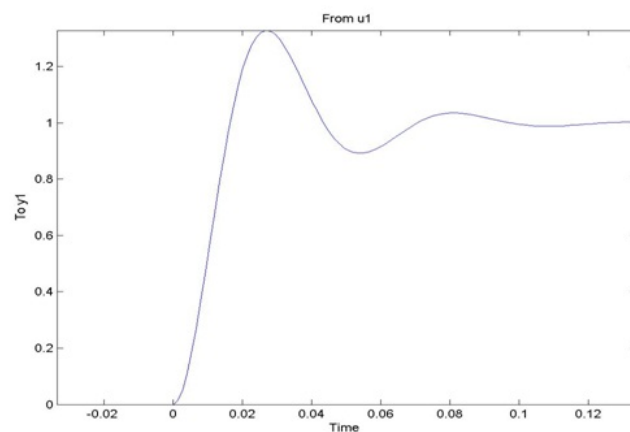


Figure 5.7: Step response.

Table 5.2: Original gains of the controller

Actuator	P	I	D	F
MOOG 1	15	1	0	0,05
MOOG 2	15	1	0	0,05

Table 5.3: Tuned gains of the controller

Actuator	P	I	D	F
MOOG 1	15	1	0.6	0,05
MOOG 2	15	1	0.6	0,05

Table 5.4: Estimation of total delay of MOOG actuators

Actuator	Delay
MOOG 1	11 ms
MOOG 2	11 ms

5.4 Performance of MOOG actuators coupled to the piping system

With the new setting of the transfer system, a performance assessment of the actuators coupled with the actual test specimen, as illustrated in Figure 5.8, was performed. The test specimen, i.e., the Physical Substructure (PS), was the part of a piping system; detail information on the piping system and the PS will be provided in next chapters. A pre-defined command displacement history -having a frequency content around 4 Hz- was given to the actuators and responses were compared with the input as illustrated in Figure 5.9. An amplitude lag for both the actuators was evident, which implied an incompatibility of the transfer system for an RTDS to be carried out on the piping system with a high level of PGA.

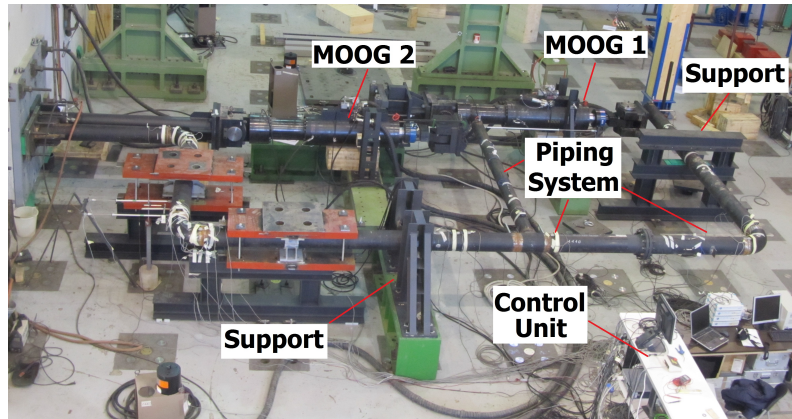
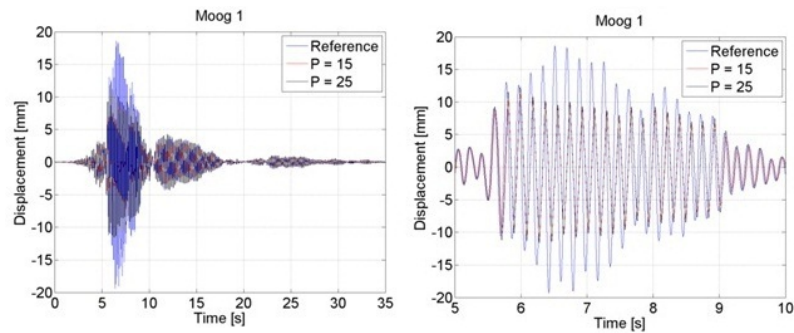
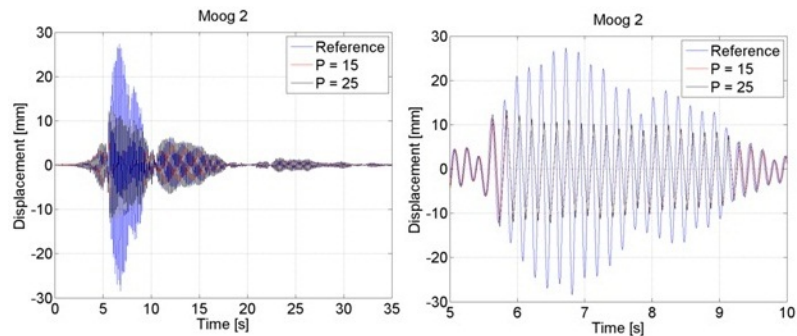


Figure 5.8: Experimental set-up for the hybrid tests.



(a)



(b)

Figure 5.9: Response of (a) MOOG 1 and (b) MOOG 2 actuator under an applied displacement history.

Hence, in order to estimate the maximum stroke of the MOOG actuators, X , that

could be achieved at a certain frequency, f , we used the following relationship,

$$X = \frac{5.3 Q_p}{A f} \quad (5.4)$$

where, X is the double amplitude displacement of the actuator for a sinusoidal motion shown in Figure 5.10, Q_p is the oil flow rate, A is the piston area and f is the frequency. Relevant values are: $Q_p = 800$ liters/minute; $A = 505 \text{ cm}^2$.

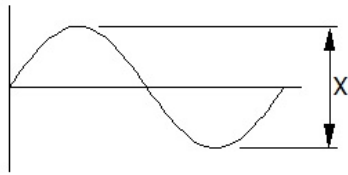


Figure 5.10: Double amplitude, X .

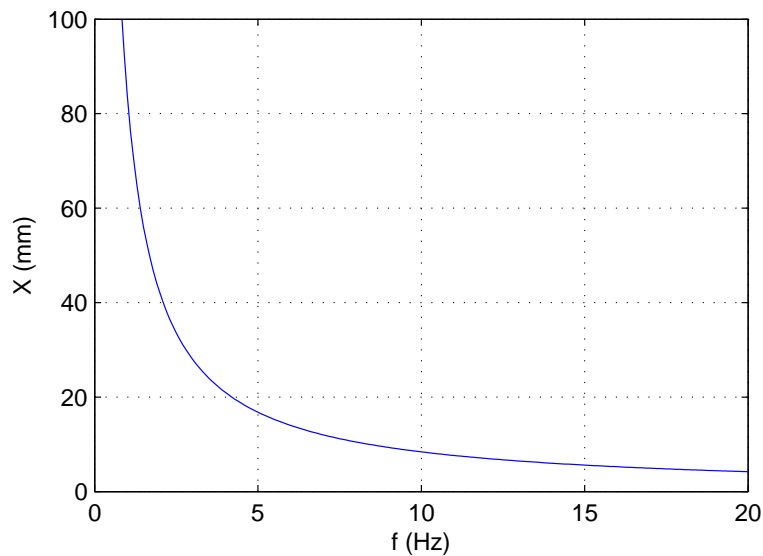


Figure 5.11: Frequency vs. displacements of MOOG actuators.

Equation (5.4) is presented graphically, in Figure 5.11 and one can note that an increase in the frequency considerably reduces the maximum displacement of the actuators. However, note that Equation (5.4) is based on only hydraulic power, Q_p , and does not consider control issues owing to, for example, delay, noise and leakage

of oil across the piston seal of the actuator. As a result, to run an RTDS, the maximum stroke has to be further reduced, and hence the corresponding input PGA as stated in Table 6.7 of Chapter 6.

5.5 Conclusions

A characterisation of the MOOG actuators to be used during hybrid tests has been presented in this chapter. A linear TF was experimentally identified for the transfer system by means of the ARX algorithm. The TF was found to be invariant of the quantity of masses attached to the actuators. An optimum response of the transfer system was adjusted by tuning the derivative gain of the PID controller through eliminating the overshoot.

Moreover, performance of the actuators coupled with the actual test specimen was evaluated by observing their responses under a command displacement history. Both the actuators exhibited an amplitude lag with respect to the command signal. It has been found that maximum displacements of the actuators depend on their operating frequencies; an increase in the frequency considerably reduces the maximum stroke. Hence, to carry out an RTDS on the piping system, the displacement range has to be reduced as well as the input PGA.

CHAPTER 6

NUMERICAL IMPLEMENTATIONS OF PSEUDO-DYNAMIC AND REAL TIME TESTING WITH DYNAMIC SUBSTRUCTURING ON A PIPING SYSTEM UNDER SEISMIC LOADING

6.1 Introduction

Pseudo-Dynamic and Real Time tests with Dynamic Substructuring -PDDS and RTDS, respectively- are novel hybrid experimental techniques and are applicable to testing several types of non-linear structures/systems. Their potential applications in seismic testing of piping systems were discussed in Chapter 2. In this chapter, implementations of these techniques to test a typical full-scale industrial piping system under seismic loading are presented. For brevity, the term "hybrid tests" is used herein to combinedly refer both the PDDS and RTDS.

In a hybrid test, the overall response of a structure is evaluated by combining the experimental response of the PS -which is generally the most critical part of the structure- with the numerical response of the NS. By the use of actuators, computers, finite element software and controllers, these tests can potentially reproduce shaking table tests. The main difference between a PDDS and an RTDS is the rate of execution of an experiment. An RTDS is carried out in the actual time scale of an earthquake, whereas a PDDS is carried out in an extended time scale. Because an RTDS is carried out in real time, it is capable of producing a more realistic response of a structure under dynamic loading. However, there are several reasons that may

restrict the implementation of an RTDS, e.g., limitations of actuator capacity, of hydraulic power etc.. In this case, as an alternative solution, a PDDS can be carried out which potentially approximates an RTDS because, for steel elements, rate dependent effects can be neglected. Nevertheless, efficient implementations of such techniques are challenging since they require overcoming certain problems, e. g., proper dynamic substructuring, reduction of external forces and actuator delay compensation.

6.2 Objectives of the hybrid tests

The objective of the PDDS and RTDS is to investigate the seismic performance of a piping system at full-scale and some of its components, e.g., elbow, Tee joint and bolted flange joint, under realistic earthquake loading. Until now, a few experiments - mainly through shaking table tests- have been performed on full-scale piping systems under realistic earthquake loading, e.g., DeGrassi et. al. (2008); Otani et al. (2011). In all seismic tests, piping systems and components exhibited good performance; they remained below yield limit under design level earthquake loading. Authors have confirmed that present seismic design criteria for such structures are highly conservative (Touboul et al., 2006; Otani et al., 2011). In this respect, we employed the aforementioned new hybrid testing techniques which potentially enables the seismic testing of a structure by using a limited number of actuators. However, implementations of hybrid tests on piping systems are challenging mainly because these are systems endowed with distributed masses that are subjected to distributed earthquake forces. Hence, the work presented in this study brings a novelty in the PDDS technique by enabling its applicability to structures having distributed masses. Moreover, the performance of a piping network under several levels of earthquake loading will be investigated in depth.

6.3 The piping system under investigation

The piping system to be experimentally tested is a typical industrial piping system placed on a support structure as shown in Figure 6.1. General dimensions and other

geometrical properties of the piping system are taken from (DeGrassi et. al., 2008). The piping system contains 8" and 6" straight pipes, several elbows, a T-joint and a Standard bolted flange joint. Material of all straight pipes and elbow elements is API 5L Gr. X52; see Table 6.2 for material properties. The pipes contain water with an internal pressure equal to 80% of the maximum allowable pressure of in the piping system. The bolted flange joint inserted in the piping system is an EN 1092-1 Standard PN40 weld-neck standard flange joint for which the maximum allowable pressure is 4.0 MPa, which governed the maximum allowable pressure of the system. Therefore we used an internal pressure of 3.2 MPa (80% of 4.0 MPa) for the experiments. Characteristics of the piping system are presented in Table 6.1, whereas specifications, dimensions and boundary conditions are illustrated in Figure 6.2 and Figure 6.3.

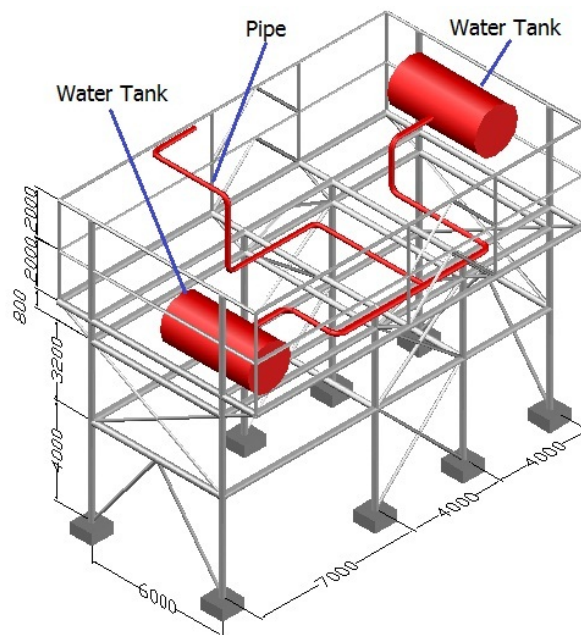


Figure 6.1: A 3D sketch of the reference piping system on a support structure (dimensions are in mm).

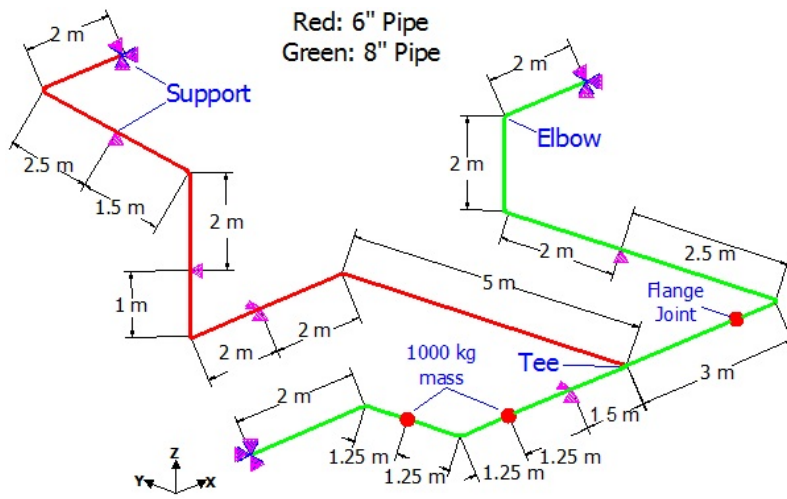


Figure 6.2: Specifications and dimensions of the piping system after DeGrassi et al. (2008).

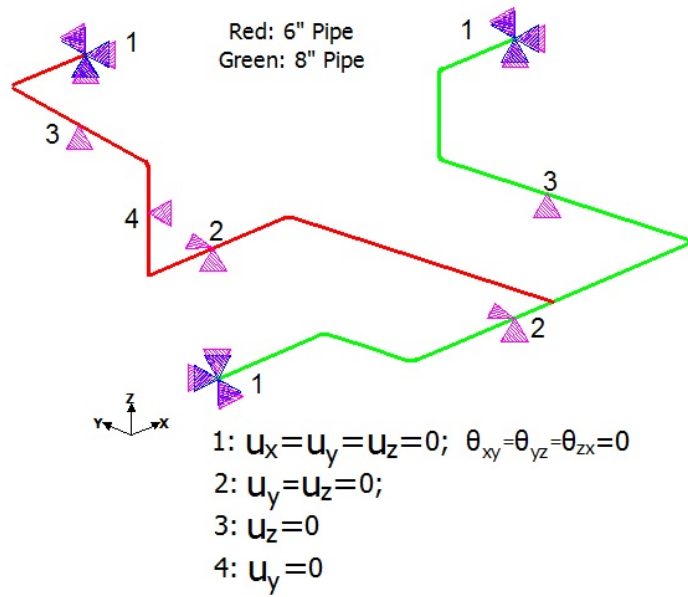


Figure 6.3: Boundary conditions present in the piping system (u = displacement; θ = rotation).

Table 6.1: Characteristics of the piping system

Pipe Size	Liquid	Internal Pressure
8" (NPS 8) and 6" (NPS 6) Schedule 40	Water	3.2 MPa

Table 6.2: Mechanical properties of the pipe material

Pipe Material	Yield Strength, f_y	Ultimate Strength, f_u	Max Elongation	KV min 27J at -50°
ASTM A 333Gr. 6 / API 5L Gr. X52	418 MPa	554 MPa	35.77%	244 for 8" Pipe 176 for 6" Pipe

6.4 FE modelling and modal analysis of the piping system

A 3D Finite Element (FE) model of the piping system was developed in SAP2000 (SAP, 2004) software in order to perform numerical analyses. All pipes including elbows were modelled using straight elements with pipe sections. Mass of the water present inside pipes was considered in the FE model by increasing the mass density of the pipe material. Two 1000 kg masses employed to take into account valves, etc., were applied in all the three principal axes in two relevant joints through joint masses. All boundary conditions were replicated through joint restraints.

Although elbows were modelled using straight elements in the FE model, flexibilities of these elbow elements were adjusted to have the equivalent flexibility properties found from an ABAQUS-based (Hibbit et al., 2003) FE analysis. Each elbow had a radius, R , equal to 1.5 times the outer diameter, d_{out} of the connecting pipe; moreover, we considered that the effect of flexibility of an elbow spreads across a distance, L equal to two times the mean diameter, d_m of the pipe as illustrated in Figure 6.4. Hence, an equivalent straight elbow of length, l as depicted in Figure 6.4 was obtained. The geometry of both 8" and 6" elbows are reported in Table 6.3.

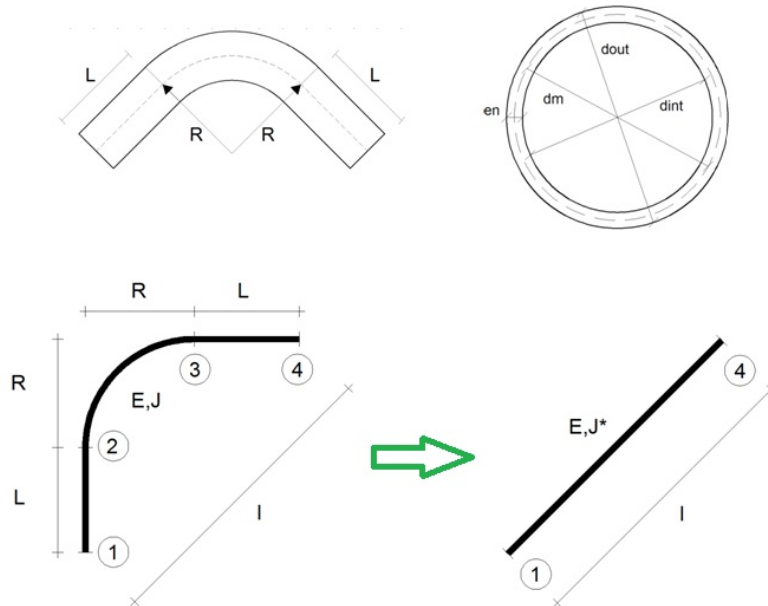


Figure 6.4: Geometry of the equivalent straight elbow element.

Table 6.3: Geometry of the original elbow elements (dimensions are in mm)

Elbow	d_{out}	d_m	d_{int}	e_n	R	L	I
8"	219.08	210.9	202.72	8.18	328.62	421.8	1060.38
6"	168.28	161.17	154.06	7.11	252.42	322.34	812.87

As depicted in Figure 6.4, the equivalent straight elbow element consisted of a curved and two straight parts. The flexibility of the actual system, F_{1234} (straight pipe + elbow) is the sum of the flexibilities of straight pipes and curved elbow, i.e.,

$$F_{1234} = \frac{1}{EJ} (4d_{out} + Rk_B) \quad (6.1)$$

where, J is the second moment of inertia and E is the elastic modulus. k_B is called the flexibility characteristics defined in Codes. EN 13480-3 (2002) defines k_B as,

$$k_B = \frac{1.65}{h} \quad (6.2)$$

in which, h is expressed as,

$$h = \frac{4Ren}{d_m^2} \quad (6.3)$$

The symbols used in (6.3) are defined in Figure 6.4. The values of k_B calculated for elbow elements are reported in Table 6.4. For straight pipes, $k_B = 1$.

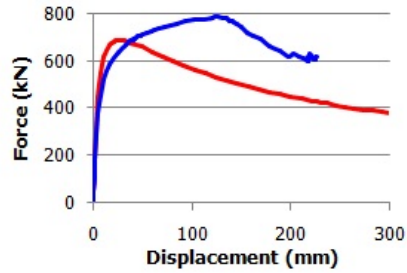
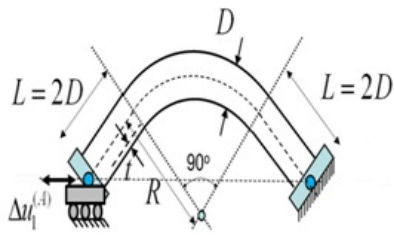
We assume J^* as the moment of inertia of the equivalent straight elbow and, therefore, its flexibility can be expressed as,

$$F_{14} = \frac{1}{EJ^*} \sqrt{2} (2d_{out} + R) \quad (6.4)$$

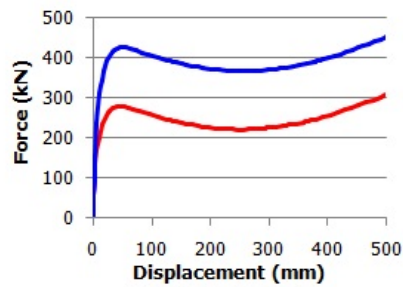
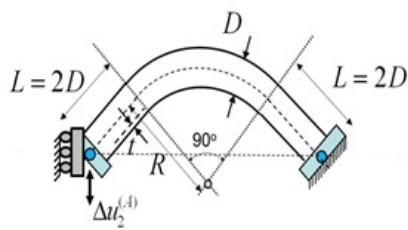
Then we equate the two stiffnesses expressed in (6.2) and (6.4); the equivalent moment of inertia of the straight elbow thus reads,

$$J^* = \frac{\sqrt{2}(2d_{out}+R)}{(4d_{out}+Rk_B)} J \quad (6.5)$$

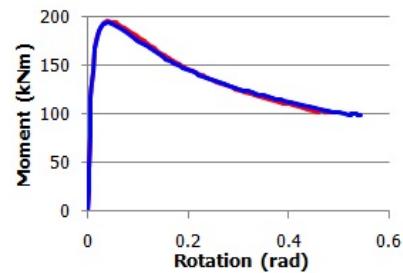
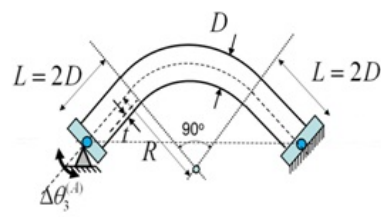
Due to the elbow complexity, an equivalence between the curved and straight elements presented in Figure 6.4, was further established. In this respect, results from an ABAQUS based FE analysis carried out on corresponding elbows within INDUSE project (Varelis et al., 2011) were utilised. The original curved elbow elements were modelled in ABAQUS and 2D FE analyses were performed under axial, shear and bending loading as illustrated in Figure 6.5. All analyses were performed assuming one end of the elbow to be fixed.



(a)



(b)



(c)

Figure 6.5: FE analysis on 8° elbow elements after Varelis et al. (2011): (a) force-displacement curve under axial loading; (b) force-displacement curve under shear loading; (c) moment-rotation curve under bending loading (Red- Closing; Blue- Opening).

Since, results of above FE analyses on elbow elements were more realistic than those found from analytical calculations, flexibilities/stiffnesses of straight elbow elements were adjusted according to these results. In this view, stiffness matrices of the equivalent straight elbows were developed according to the Euler-Bernoulli (EB) beam theory. The stiffness matrix of a straight elbow element constructed according

to the EB theory can be expressed in the form presented in the following equation,

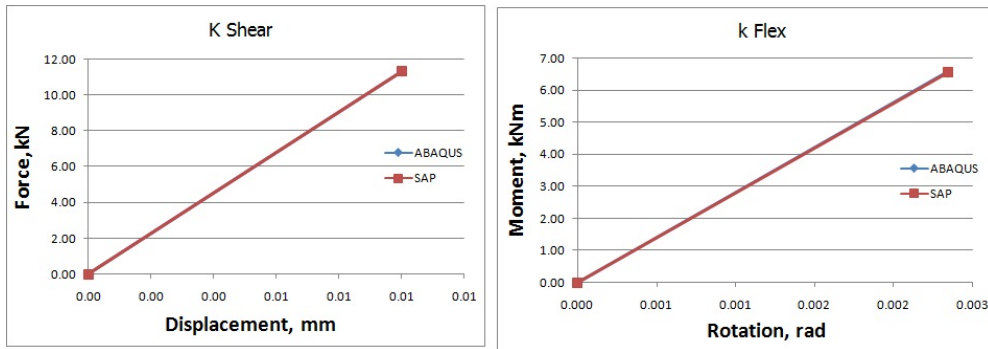
$$\begin{bmatrix} k_{11} & 0 & 0 & k_{14} & 0 & 0 \\ 0 & k_{22} & k_{23} & 0 & k_{25} & k_{26} \\ 0 & k_{32} & k_{33} & 0 & k_{35} & k_{36} \\ k_{41} & 0 & 0 & k_{44} & 0 & 0 \\ 0 & k_{52} & k_{53} & 0 & k_{55} & k_{56} \\ 0 & k_{62} & k_{63} & 0 & k_{65} & k_{66} \end{bmatrix} \begin{bmatrix} u_1 \\ v_1 \\ \phi_1 \\ u_4 \\ v_4 \\ \phi_4 \end{bmatrix} = \begin{bmatrix} H_1 \\ F_1 \\ M_1 \\ H_4 \\ F_4 \\ M_4 \end{bmatrix} \quad (6.6)$$

in which, u and v are displacements; ϕ is rotation; H and F are forces; M is moment, as seen in Figure 6.6.

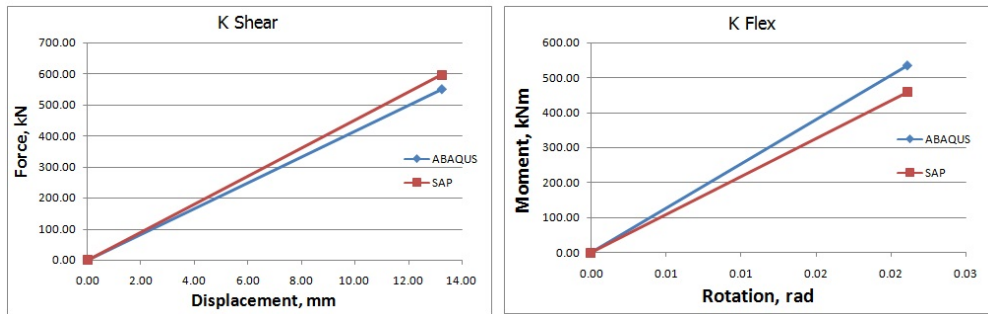


Figure 6.6: Displacement, rotation, force and moment in the EB Beam.

By varying the thicknesses, the elastic part of stiffnesses of the straight elbow elements -to be used in the SAP FE model- were fitted with those found from the ABAQUS analyses. For example, the shear and flexible stiffness, k_{22} and k_{33} , respectively, found from this optimisation are presented in Figure 6.7. The modified geometry and properties of straight elbow elements due to the changes in thicknesses considered in the FE model of the piping system are reported in Table 6.4. The FE model of the piping system is presented in Figure 6.8.



(a) Elastic stiffness comparison of 6" elbow



(b) Elastic stiffness comparison of 8" elbow

Figure 6.7: Comparison of elastic stiffness of 6" and 8" elbows.

Table 6.4: Modified properties of elbow elements considered in the piping system model

Property	8" Elbow		6" Elbow	
	Original	Modified	Original	Modified
e_n , mm	8.18	6.61	7.11	4.35
k_B	6.84	1.35	5.97	2.46
J^* mm ⁴	3.02×10^7	2.49×10^7	1.17×10^7	7.53×10^6

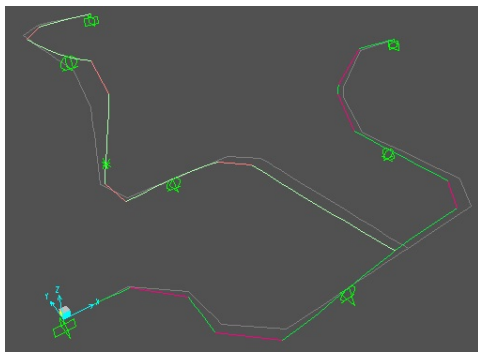


Figure 6.8: FE model of the piping system.

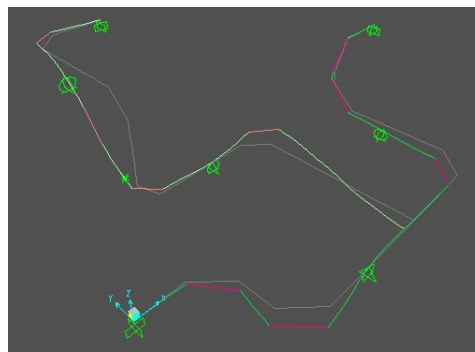
In order to find out eigenfrequencies, eigenmodes and modal participation masses, a modal analysis of the piping system was performed. The first 20 eigenfrequencies and corresponding mass participation in percentage (percentage of total mass excited by a mode) are reported in Table 6.5. A careful reader can observe that the first 20 modes are able to excite about 87% of the total mass of the piping system in the x direction ($\text{sumUX} = 87\%$). In detail, we were mainly interested in the response in x direction, see Figure 6.2, because, during the experiments reported by DeGrassi et. al. (2008), an elbow failed when the earthquake loading was applied to the piping system in that direction. Due to reduction requirements described in Subsection 6.9, the 1st and 2nd modes, shown in Figure 6.9, were the two main modes that we considered; they excited about 36% and 12% mass, respectively, in the x direction.

Table 6.5: First 20 eigenfrequencies and participation masses of the piping system model

Mode	Frequency Hz	% of mass participation								
		UX %	UY %	UZ %	SumUX %	SumUY %	SumUZ %	RX %	RY %	RZ %
1	5.18	36.00	8.64	1.47	36.00	8.64	1.47	1.62	0.12	1.32
2	6.32	12.00	0.01	1.09	48.00	8.66	2.55	1.73	0.02	5.56
3	6.69	0.29	0.42	28.00	48.00	9.08	30.00	8.99	4.36	0.44
4	7.44	0.97	0.41	0.16	49.00	9.49	30.00	5.19	0.41	0.55
5	7.87	2.44	13.00	1.20	52.00	22.00	32.00	0.52	0.00	38.00
6	9.22	8.33	21.00	0.01	60.00	43.00	32.00	0.68	0.10	12.00
7	10.84	1.44	0.01	5.11	62.00	43.00	37.00	10.00	4.62	8.25
8	11.35	8.13	3.07	1.90	70.00	46.00	39.00	2.82	4.03	0.84
9	11.98	0.64	23.00	3.38	70.00	69.00	42.00	3.76	2.40	4.32
10	14.33	0.26	1.42	25.00	71.00	70.00	67.00	7.90	18.00	1.55
11	16.19	0.79	4.48	0.26	71.00	75.00	68.00	7.85	2.08	3.29
12	17.59	9.56	2.01	0.19	81.00	77.00	68.00	0.07	1.37	1.09
13	18.52	0.38	0.15	5.34	81.00	77.00	73.00	3.31	8.62	1.05
14	23.50	1.11	0.02	2.25	82.00	77.00	75.00	0.00	7.41	0.10
15	27.22	1.64	3.42	2.05	84.00	80.00	77.00	0.00	6.85	0.68
16	28.23	0.43	0.20	5.33	84.00	81.00	83.00	16.00	3.06	0.51
17	28.78	1.01	3.43	0.03	85.00	84.00	83.00	0.01	0.73	0.84
18	29.46	0.14	0.01	0.50	86.00	84.00	83.00	8.79	0.36	0.04
19	33.75	1.59	7.77	1.04	87.00	92.00	84.00	0.00	5.62	5.65
20	37.19	0.26	1.60	1.93	87.00	93.00	86.00	6.71	1.45	0.78



(a)



(b)

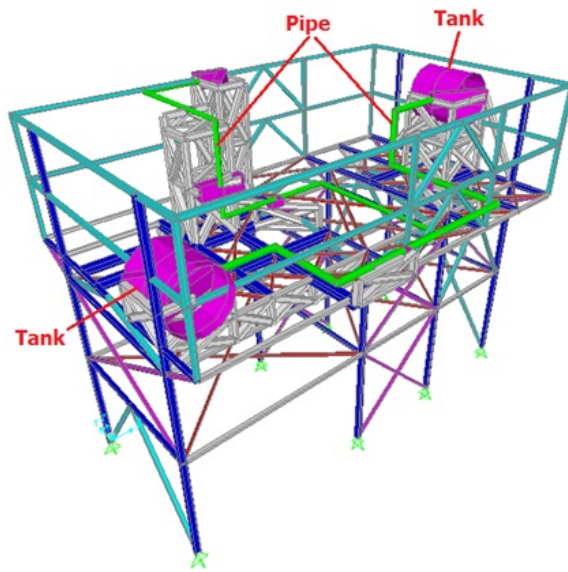
Figure 6.9: (a) Mode #1 and (b) Mode #2 of the piping system model.

6.5 Analyses of the piping system under seismic loading

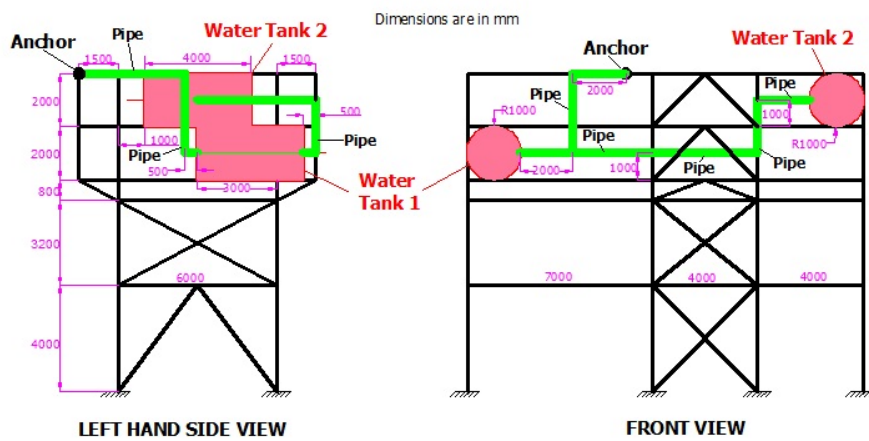
In order to perform a numerical investigation of the seismic response of the piping system, time history analyses on the piping system under earthquake loading were carried out using SAP2000 software. To carry out these analyses, it was necessary to define a realistic input seismic loading. The piping system considered was placed on a typical industrial steel support structure which worked as a dynamic filter and the earthquake to which the structure was subjected to was magnified at different structure levels.

6.5.1 Selection of input seismic loading

The support structure designed for generating the input earthquake acceleration was a 3D frame structure as illustrated in Figure 6.10. It was a steel frame structure; 12m high, mainly composed by steel HE and IPE profiles and some vertical and horizontal cross or K-steel bracings. Only a pipe ran on the frame supported by sub-frames placed at 3rd floor of the main frame. Two edges of the frame were connected to cylindrical storage tanks whereas the third one was connected to the frame by an anchor. Some design parameters considered for the structure are presented in Table 6.6.



(a)



(b)

Figure 6.10: Support structure of the piping system: (a) 3D FE model; (b) dimensions and lateral views.

Table 6.6: Some design parameters of the support structure

Location	High Seismic-prone region
PGA	0.33g
q factor	3.2
Ground type	C
Return Period	712 years
Importance Class	III*

* Industries with dangerous activities; Reference life, $V_r = 75$ years

By imposing an earthquake corresponding to the Safe Life Limit State (SLV) to the base of the structure, a set of earthquake accelerograms was generated in 7 different support points of the piping system as depicted in Figure 6.11. The accelerogram at point (1) of the first floor was chosen as the reference earthquake loading; in fact, this point belonged to the physical substructure and, the spectrum relevant to this earthquake, had a frequency content close to the natural frequency of the pipe. In this respect, the time history and response spectrum of the reference earthquake are shown in Figure 8. The Peak Floor Acceleration (PFA) of the accelerogram was about 4.13 m/s^2 and the period, T , at maximum amplification was around 0.2 sec which was close to the natural frequency of piping system.

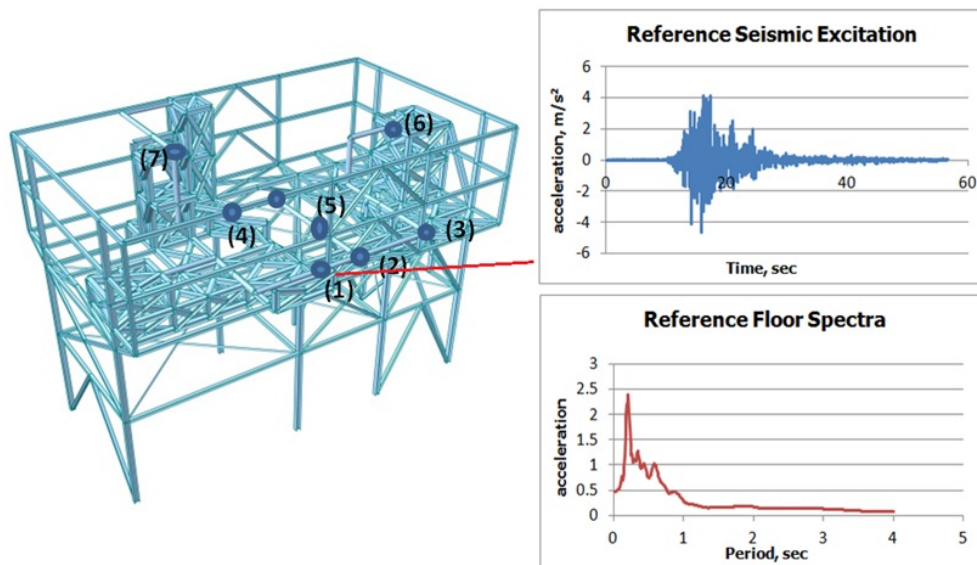


Figure 6.11: Support structure and filtered earthquake with relevant spectrum generated at point (1).

In order to comply with performance-based earthquake engineering, we chose the Italian Standard Norme Tecniche (2008). In fact and differently from Eurocode 8 Part 1, this Standard prescribes four limit states as listed in Table 6.7. PFA of the reference floor accelerogram was magnified corresponding to both serviceability (SLO, SLD) and ultimate limit states (SLV, SLC), as reported in Table 6.7 along with corresponding Peak Ground Accelerations (PGA).

Table 6.7: PGA corresponding to different limit states

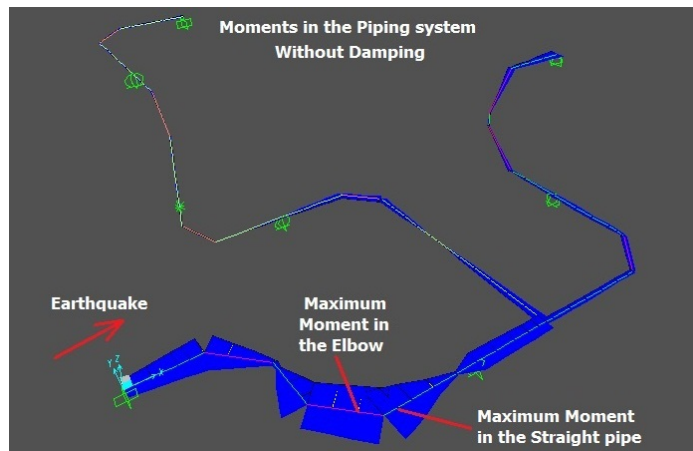
Limit States			PFA(g)	PGA(g)
Serviceability Limit States	SLO	Operational limit state	0.08	0.05
	SLD	Damage limit state	0.11	0.08
Ultimate Limit States	SLV	Safe life limit state	0.42	0.29
	SLC	Collapse limit state	0.60	0.41

6.5.2 Analyses of the piping system with selected seismic loading

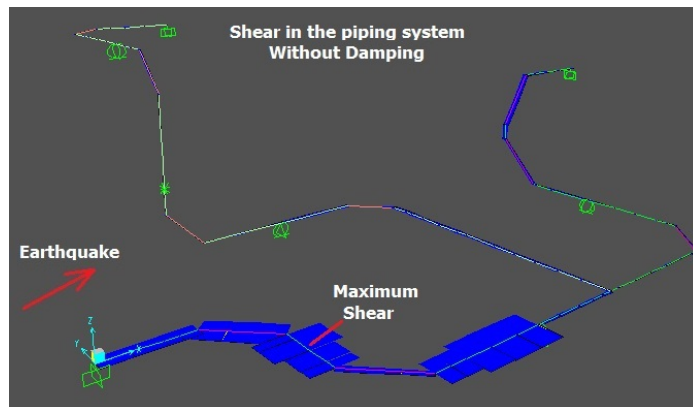
An elastic time history analysis on the piping system model was carried out by the SAP2000 software using the earthquake loading corresponding to SLV. The analysis was performed both with and without considering damping. The Rayleigh damping model was set according to Chopra (1995) assigning a 0.5% damping to both the 1st and 2nd eigenfrequency; it was computed through identification tests on the PS. The earthquake loading was applied to the piping system along the x axis horizontal direction. Locations of maximum bending moments and shears owing to the applied seismic loading without damping are presented in 6.12. Maximum values of moments, M_{max} and stresses, τ_{max} , σ_{max} are presented in Table 6.8.

Table 6.8: Maximum moment and stresses in the piping system under reference seismic loading

Maximum moment, M_{max} and stress, σ_{max} without damping			
Component	M_{max}	σ_{max}	Stress level
Elbow 2	69.15 kN	503.56 Mpa	Above yield strength
Straight pipe	81.56 kN	296.03 Mpa	Below yield strength
Maximum moment, M_{max} and stress, σ_{max} with damping			
Component	M_{max}	σ_{max}	Stress level
Elbow 2	43.63 kNm	317.74 Mpa	Below yield strength
Straight pipe	45.62 kNm	288.12 Mpa	Below yield strength
Maximum shear, τ_{max} in the straight pipe			
τ_{max} in the straight pipe without damping			95.48 kN
τ_{max} in the straight pipe with damping			59.71 kN



(a)



(b)

Figure 6.12: Actions of the piping system under reference earthquake loading without damping: (a) bending moment; (b) shear.

One can observe that although the maximum bending moment was in the straight pipe, the maximum normal stress was found in Elbow #2. This was due to the fact that the stress in an elbow is intensified owing to curved geometry and this value is calculated using a stress intensification factor, SIF of the elbow. The SIF , was calculated according to EN 13480-3 for the relevant elbow; its value was found to be 2.32. Stresses in both the pipe, σ_{pipe} and elbow, σ_{elbow} were calculated from the bending moment using the following formula:

$$\sigma_{elbow} = \frac{SIFMy}{I} \quad (6.7)$$

where M defines the moment, I is the second moment of inertia of the elbow and y represents the distance from the neutral axis to the outer diameter of the elbow. The value of SIF for a straight pipe is 1. SIF for an elbow can be calculated according to the formula given in EN 13480-3, which is expressed as follows:

$$SIF = \frac{0.9}{h^{2/3}} \quad (6.8)$$

in which h was defined in Equation (6.3).

The effect of damping in the seismic response of the piping system can also be noted from Table 6.8. The Rayleigh's damping considerably reduced normal and shear stresses in the piping system. Stresses in Elbow #2 exceeded its yield strength in the case without damping. Conversely, stresses in the piping system remained below yield limits of components in case of Rayleigh's damping.

6.6 Substructuring of the piping system

One of the unique features and main advantages of hybrid tests is dynamic substructuring. As mentioned earlier, during a hybrid test, a structure is divided into two parts: a PS which is physically built in the lab and loaded through actuators and a NS that describes the remainder of the system and is solved via software. The two substructures exchange information through coupling degrees of freedom they mutually share. In order to divide the piping system into two substructures, i.e., PS and NS, we needed to find proper coupling nodes and ensure the compatibility and equilibrium conditions at these nodes.

Number of coupling Degrees of Freedom (DoFs) during substructuring has to be chosen based on available resources, e.g., actuators and controllers available. Because in our laboratory, we have an MTS controller configured to control two actuators simultaneously, we, therefore, decided to choose two coupling nodes of the piping system for substructuring purposes. However, with these two actuators acting at those two coupling nodes, we only could impose one command, e.g., displacements or forces, to each of the coupling DoFs. Because, the earthquake loading were applied in the horizontal x direction, out-of-plane displacements and rotations of the coupling nodes could be neglected since these contributions were very small. In

fact measurements and reproduction of rotational contributions are very difficult to accomplish in practice (Duarte and Ewins, 1995; Gialamas et al., 1996; Liu and Ewins, 1999) and hence they could be neglected based on appropriate assumptions. The two coupling nodes were selected in the xy plane -most of the pipe runs in this plane- at the positions of bending moments closed to zero found from time history analyses. These analyses were performed with the reference seismic loading applied to the horizontal x direction. Maximum values of bending moments in the coupling nodes, M_{maxC} , relevant to the reference earthquake are reported in Table 6.9. The piping system with the two substructures and coupling nodes are presented in Figure 6.14, whereas specifications and dimensions of the PS are presented in Figure 6.15. The first 20 eigenfrequencies and relevant participation masses of the PS are reported in Table 6.10. One may note that about 96% of the total mass is excited by the first 20 modes in the x direction, among which Mode #1 and Mode #8 are the two main modes that excites about 76% and 8.50% mass, respectively.

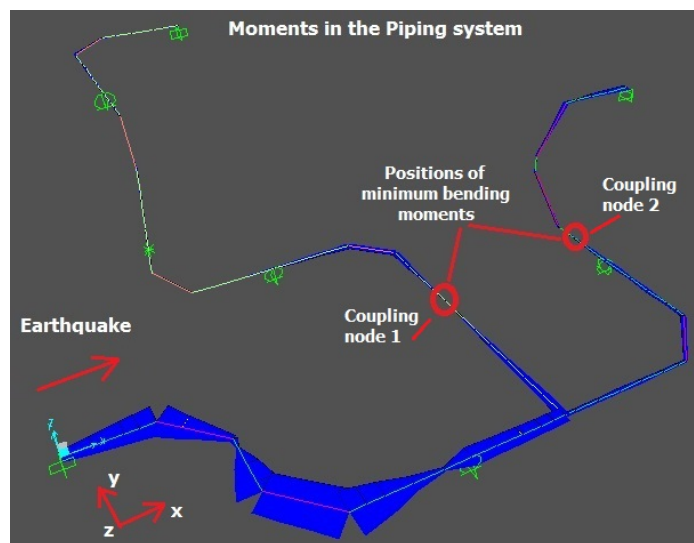


Figure 6.13: Bending moments close to zero in the piping system.

Table 6.9: Maximum values of bending moment in coupling nodes

Coupling Node	Maximum bending moment
Coupling Node #1	0.37 kNm
Coupling node #2	1.43 kNm

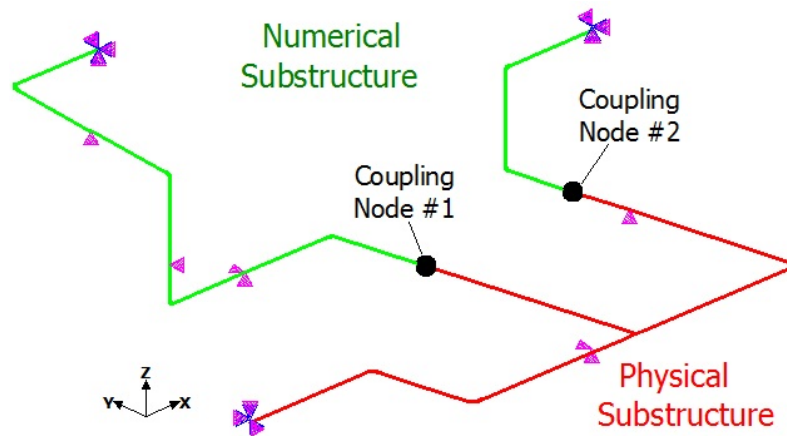


Figure 6.14: PS, NS and relevant coupling nodes.

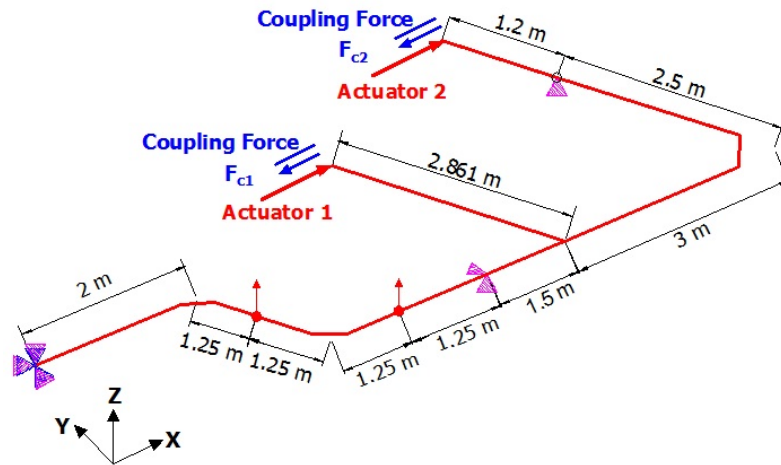


Figure 6.15: Dimensions, coupling forces and actuator positions in the PS.

Table 6.10: First 20 eigenfrequencies and participation masses of the PS

Mode	Frequency Hz	% of mass participation								
		UX %	UY %	UZ %	SumUX %	SumUY %	SumUZ %	RX %	RY %	RZ %
1	5.63	76.43	8.29	0.00	76.00	8.29	0.00	0.00	0.00	0.01
2	7.06	0.00	0.00	59.07	76.00	8.29	59.07	0.10	0.01	0.00
3	8.88	3.58	5.52	0.00	79.58	13.81	59.07	0.00	0.00	0.04
4	11.88	5.60	45.37	0.00	85.18	59.18	59.07	0.00	0.00	0.67
5	14.82	0.00	0.00	30.05	85.18	59.18	89.11	0.55	0.43	0.00
6	14.94	0.87	3.25	0.00	86.05	62.44	89.11	0.00	0.00	7.86
7	18.74	0.00	0.00	2.91	86.05	62.44	92.03	0.03	0.07	0.00
8	29.83	8.50	16.82	0.00	94.55	79.25	92.03	0.00	0.00	0.01
9	37.55	0.00	0.00	2.64	94.55	79.25	94.66	0.29	0.12	0.00
10	54.03	0.00	1.79	0.00	94.55	81.05	94.66	0.00	0.00	0.71
11	60.71	0.00	0.00	0.74	94.55	81.05	95.40	0.53	0.26	0.00
12	66.23	0.00	0.00	2.51	94.55	81.05	97.91	0.25	0.24	0.00
13	70.75	1.61	0.04	0.00	96.16	81.08	97.91	0.00	0.00	0.49
14	96.04	0.00	0.00	1.47	96.16	81.08	99.39	1.50	5.80	0.00
15	98.64	0.01	2.91	0.00	96.17	83.99	99.39	0.00	0.00	0.08
16	129.35	0.01	0.34	0.00	96.17	84.34	99.39	0.00	0.00	4.88
17	133.07	0.00	0.00	0.00	96.17	84.34	99.39	3.52	3.06	0.00
18	152.29	0.00	0.00	0.06	96.17	84.34	99.45	5.56	13.52	0.00
19	166.96	0.01	3.46	0.00	96.18	87.80	99.45	0.00	0.00	0.00
20	182.83	0.00	0.00	0.05	96.18	87.80	99.50	0.27	2.15	0.00

During the hybrid tests, we applied displacement commands to the two coupling nodes of the PS in the x direction. These displacements were equal to the relevant nodes of the NS. To better reflect this testing situation, we considered an FE model where the two coupling nodes were constrained to move together in the x direction thus satisfying the compatibility condition. Displacements in y and z were restrained (in fact, these displacements were found negligible from the above-mentioned time history analysis) while other movements were allowed. This model was considered as the Reference Model (RM) of the piping system.

A comparison between the RM and the Continuous Model (CM) of the piping system was made to understand how well the response of the CM was reproduced during experimental tests. For this purpose, the eigenfrequency, eigenmodes, and time history responses of the two models were compared. In this respect, the MAC matrix between eigenvectors of the CM and the RM is presented in Table 6.11; a good agree-

ment between the modal properties can be noted. In a greater detail, the MAC matrix shows a good agreement in the first 8 modes. Moreover, a time history analysis based on an earthquake with a PGA of 0.1g applied in the x direction, was performed between the two models and results were compared. In order to estimate the error between time history responses, a normalised Root Mean Square (RMS) error, e_{RMS} , defined as,

$$e_{RMS} = \frac{\sqrt{\frac{1}{N} \sum_{i=1}^N (x_{CM}^2)_i} - \sqrt{\frac{1}{N} \sum_{i=1}^N (x_{RM}^2)_i}}{\sqrt{\frac{1}{N} \sum_{i=1}^N (x_{CM}^2)_i}} \quad (6.9)$$

where, x_{CM} and x_{RM} are responses of the CM and RM, respectively, was calculated for each DoF of the two models. An average RMS error of all DoFs was then evaluated using individual values of e_{RMS} .

The time history responses of the two coupling nodes and of an end node of Elbow #2 (Node #5) of the RM and CM are presented in Figure 6.16 and Figure 6.17, respectively. A good agreement between responses can be observed. The normalised RMS errors, e_{RMS} , in some DoFs and its average value are presented in Table 6.12. All these comparisons indicated that, by satisfying the compatibility condition of the two coupling nodes in the x direction only, i.e., applying the same displacements in the x direction of the two coupling nodes of the PS and NS, we were potentially able to reproduce the seismic response of the piping system by means of experimental tests.

Table 6.11: MAC Matrix between eigenvectors of the RM and CM

Mode	1	2	3	4	5	6	7	8	9	10
1	0.94	0.26	0.00	0.01	0.00	0.00	0.02	0.00	0.05	0.00
2	0.10	0.92	0.00	0.01	0.00	0.02	0.01	0.00	0.02	0.02
3	0.00	0.00	0.92	0.01	0.00	0.00	0.00	0.06	0.00	0.00
4	0.03	0.03	0.07	0.86	0.10	0.00	0.02	0.00	0.02	0.01
5	0.00	0.00	0.00	0.00	0.93	0.00	0.00	0.00	0.02	0.00
6	0.00	0.03	0.00	0.02	0.01	0.88	0.14	0.00	0.00	0.03
7	0.02	0.02	0.00	0.08	0.04	0.00	0.88	0.00	0.00	0.01
8	0.00	0.00	0.05	0.00	0.00	0.00	0.00	0.97	0.00	0.03
9	0.00	0.01	0.00	0.00	0.00	0.02	0.00	0.00	0.01	0.66
10	0.04	0.02	0.00	0.01	0.00	0.00	0.02	0.00	0.86	0.02

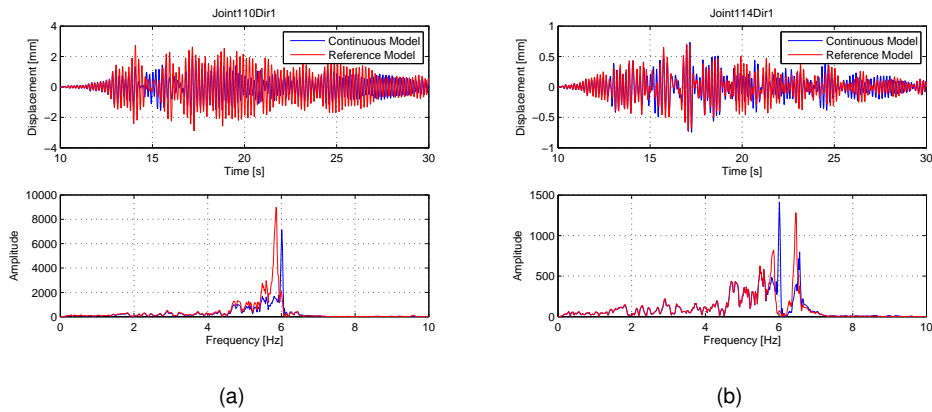


Figure 6.16: Displacement time histories (in x) and relevant Fourier spectra of (a) Coupling Node #1; (b) Coupling Node #2; (Blue CM; Red RM).

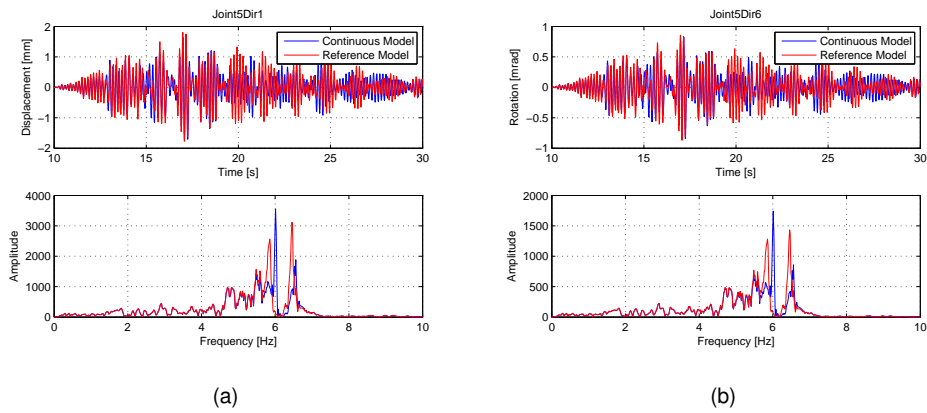


Figure 6.17: (a) Displacement (in x) and (b) rotation (along z) time histories and relevant Fourier spectra of Node #5 (Blue CM; Red RM).

Table 6.12: e_{RMS} between time history responses of the RM and CM

DoF	e_{RMS}
Displacement of Coupling Node #2 in x	0.04
Rotation of Node #5 along z	0.10
Average value	0.22

6.7 Equations of motion for hybrid tests

The pseudo-dynamic and real time testing of the piping system required the solutions of the equations of motion of the system through a suitable numerical integration method. In this section, we establish the system of equations of motion of the piping system under investigation, which is shown in Figure 6.18.

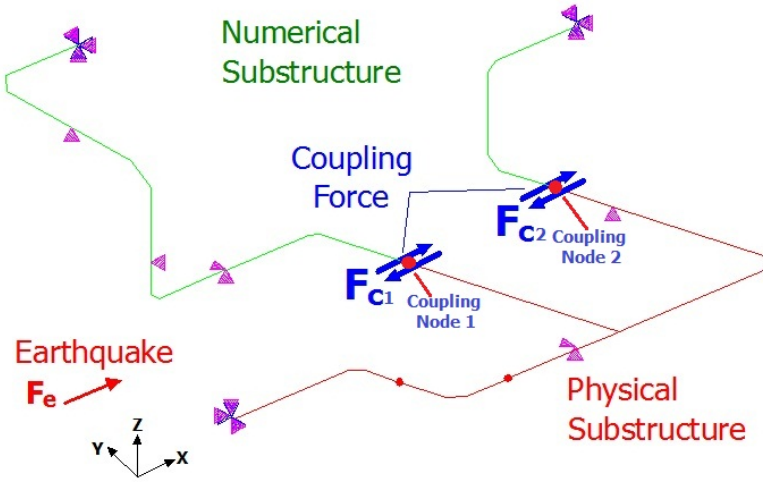


Figure 6.18: The two substructures of the piping system and forces acting on them.

The system of equations of motion of the piping system subjected to earthquake forces can be written as,

$$\mathbf{M}\ddot{\mathbf{u}} + \mathbf{C}\dot{\mathbf{u}} + \mathbf{K}\mathbf{u} = \mathbf{F}_e \quad (6.10)$$

where, $\ddot{\mathbf{u}}$, $\dot{\mathbf{u}}$ and \mathbf{u} are the acceleration, velocity and displacement vectors, respectively; \mathbf{M} , \mathbf{C} and \mathbf{K} are mass, damping and stiffness matrices of the piping system, respectively; \mathbf{F}_e is the earthquake force vector that can be expressed as follows:

$$\mathbf{F}_e = -\mathbf{M}\mathbf{I}\ddot{u}_g \quad (6.11)$$

in which, \ddot{u}_g is the PGA. \mathbf{I} is a vector full of 1 and 0 which projects earthquake forces to the required DoFs. Thus, the equation of motion of the system reads,

$$\mathbf{M}\ddot{\mathbf{u}} + \mathbf{C}\dot{\mathbf{u}} + \mathbf{K}\mathbf{u} = -\mathbf{M}\mathbf{I}\ddot{u}_g \quad (6.12)$$

Splitting the components into the PS and NS of (6.12), we obtain,

$$(\mathbf{M}^N\ddot{\mathbf{u}}^N + \mathbf{M}^P\ddot{\mathbf{u}}^P) + (\mathbf{C}^N\dot{\mathbf{u}}^N + \mathbf{C}^P\dot{\mathbf{u}}^P) + (\mathbf{K}^N\mathbf{u}^N + \mathbf{K}^P\mathbf{u}^P) = -(\mathbf{M}^N\mathbf{I}^N\ddot{u}_g + \mathbf{M}^P\mathbf{I}^P\ddot{u}_g) \quad (6.13)$$

where, superscripts N and P represents properties and forces of the NS and PS, respectively. Rearranging the components of the NS and PS, the equations of motions read,

$$\mathbf{M}^N\ddot{\mathbf{u}}^N + \mathbf{C}^N\dot{\mathbf{u}}^N + \mathbf{K}^N\mathbf{u}^N + \mathbf{M}^N\mathbf{I}^N\ddot{u}_g = -\mathbf{M}^P\mathbf{I}^P\ddot{u}_g - (\mathbf{M}^P\ddot{\mathbf{u}}^P + \mathbf{C}^P\dot{\mathbf{u}}^P + \mathbf{K}^P\mathbf{u}^P) \quad (6.14)$$

where, the terms,

$$-(M^P \ddot{u}^P + C^P \dot{u}^P + K^P u^P)$$

correspond to the PS and in case of an RTDS they are measured in the two coupling nodes during the experiment. Hence, (6.14) can be expressed as,

$$M^N \ddot{u}^N + C^N \dot{u}^N + K^N u^N + M^N I^N \ddot{u}_g + M^P I^P \ddot{u}_g = F_{CRT} \quad (6.15)$$

in which,

$$F_{CRT} = -(M^P \ddot{u}^P + C^P \dot{u}^P + K^P u^P) \quad (6.16)$$

In a PDDS, the inertia and damping forces are modelled numerically in the computer and, hence, these terms are no more inside the the coupling force. Equation (6.15) can be rewritten as,

$$M^N \ddot{u}^N + C^N \dot{u}^N + K^N u^N + M^P \ddot{u}^P + C^P \dot{u}^P + M^N I^N \ddot{u}_g + M^P I^P \ddot{u}_g = F_{CPD} \quad (6.17)$$

where, the term F_{CPD} depicts the coupling force and has the contribution only from the stiffness of the PS, i.e.,

$$F_{CPD} = -K^P u^P \quad (6.18)$$

A careful reader may note that in order to solve (6.15) or (6.17), the earthquake forces have to be applied to all nodes of the PS. This is not a feasible task during experiments since it requires an actuator per DoF of the PS. Therefore, we needed an earthquake force vector equivalent to $M^P I^P \ddot{u}_g$ having two elements corresponding to the two coupling nodes. Moreover, 2 by 2 mass and damping matrices equivalent to M^P and C^P , respectively, were also required to be numerically modelled. In order to overcome the above-mentioned problem, we adopted a strategy called substructure coupling or component mode synthesis, which allows for reducing the DoFs of a substructure system to a reduced number of DoFs retaining the properties of the original model. We will discuss about model reduction techniques in a later section.

Therefore, by means of model reduction techniques -suitable for the PDDS and RTDS - we reduced the PS to the two coupling degrees of freedom. This resulted in a 2 by 2 system of the PS, i.e., with reduced mass matrix M_{Red}^P , damping matrix C_{Red}^P , stiffness matrix, K_{Red}^P and an earthquake force vector having two components,

$-M_{Red}^P I_{Red}^P \ddot{u}_g$. For the case of PDDS, the inertial and damping terms, i.e., $M^P \ddot{u}$ and $C^P \dot{u}$, respectively, were also evaluated with the reduced 2 by 2 mass and stiffness matrices.

As a result, the system of equations of motion for the RTDS and PDDS can be expressed by,

$$M^N \ddot{u}^N + C^N \dot{u}^N + K^N u^N + M^N I^N \ddot{u}_g + M_{Red}^P I_{Red}^P \ddot{u}_g = F_{cRT} \quad (6.19)$$

$$M^N \ddot{u}^N + C^N \dot{u}^N + K^N u^N + M^N I^N \ddot{u}_g + M_{Red}^P \ddot{u}^P + C_{Red}^P \dot{u}^P + M_{Red}^P I_{Red}^P \ddot{u}_g = F_{cPD} \quad (6.20)$$

respectively. Note that in (6.19) and (6.20), only the coupling forces, i.e., F_{cRT} and F_{cPD} , were measured from the PS during experiments and were given as an input to the NS. The remaining terms were handled by the computer numerically.

To offer a better clarifications of the dimensions of different terms of Equation (6.19), and where the contributions of the PS are added, here we show the dimensions of the terms used in Equation (6.19). We define different terms as follows:

$$M^N \ddot{u}^N = \text{Inertia force of the NS} = I^N$$

$$C^N \dot{u}^N = \text{Damping force of the NS} = D^N$$

$$K^N u^N = \text{Restoring force of the NS} = R^N$$

$$M^N I^N \ddot{u}_g = \text{Earthquake force on the NS} = F_e^N$$

$$M_{Red}^P I_{Red}^P \ddot{u}_g = \text{Reduced earthquake force on the PS} = F_{eRed}^P$$

We can then rewrite Equation (6.17) as,

$$I^N + D^N + R^N + F_e^N + F_{eRed}^P = F_{cRT} \quad (6.21)$$

In vector forms, the equation of motion takes the following form:

$$\begin{pmatrix} I_1^N \\ I_2^N \\ \dots \\ I_{c1}^N \\ I_{c2}^N \end{pmatrix}_{nx1} + \begin{pmatrix} D_1^N \\ D_2^N \\ \dots \\ D_{c1}^N \\ D_{c2}^N \end{pmatrix}_{nx1} + \begin{pmatrix} R_1^N \\ R_2^N \\ \dots \\ R_{c1}^N \\ R_{c2}^N \end{pmatrix}_{nx1} + \begin{pmatrix} F_{e1}^N \\ F_{e2}^N \\ \dots \\ F_{ec1}^N \\ F_{ec2}^N \end{pmatrix}_{nx1} + \begin{pmatrix} 0 \\ 0 \\ \dots \\ F_{eRedc1}^P \\ F_{eRedc2}^P \end{pmatrix}_{nx1} = \begin{pmatrix} 0 \\ 0 \\ \dots \\ F_{RTc1} \\ F_{RTc2} \end{pmatrix}_{nx1} \quad (6.22)$$

where, n is the number of degrees of freedom of the NS. The two coupling nodes, represented by $c1$ and $c2$ were placed at the end of a vector. One may note that the

coupling forces, F_{RT} and reduced earthquake force of the PS, F_{eRed} were placed in the positions of coupling DoFs in the equation.

6.8 Time integration and delay compensation for hybrid tests

To carry out both RTDS and PDDS, we needed an appropriate time integration scheme which solved the system of equations of motion of the piping system in each time step and generated displacement commands to load the PS. Additionally, a delay compensation technique had to be implemented for the RTDS.

6.8.1 The LSRT2 integration algorithm

The L-stable real-time compatible integrator with two stages (LSRT2) developed by Bursi et al. (2008) was chosen for the hybrid tests. This integration algorithm results to be more competitive than popular Runge Kutta methods in terms of stability, accuracy and ease of implementation (Bursi et al., 2008). This method is unconditionally stable for uncoupled problems and entails a moderate computational cost for real-time performance. It can also effectively deal with stiff problems, i.e. complex emulated structures for which solutions can change on a time scale that is very short compared with the interval of time integration, but where the solution of interest changes on a much longer time scale. This algorithm becomes dissipative in high frequency range of the response via a proper choice of user-defined parameters. Other very important feature of this method is that it is L-stable and real time compatible, i.e., does not require the knowledge of the value of the function f or its derivatives at the end of the time step Δt , in order to obtain the solution of a differential equation of the form $\dot{y} = f(y, t)$.

Here, we recall the system of equations of motion developed in Section 6.7 which can be expressed as,

$$M^N \ddot{u}^N + C^N \dot{u}^N + K^N u^N + M^N J^N \ddot{u}_g + M_{Red}^P I_{Red}^P \ddot{u}_g = F_{cRT} \quad (6.23)$$

For brevity, here we denote the earthquake forces on both of the PS and NS as, \mathbf{F}_{eRT} ,

$$\mathbf{F}_{eRT} = -(\mathbf{M}^N \mathbf{I}^N \ddot{u}_g + \mathbf{M}_{Red}^P \mathbf{I}_{Red}^P \ddot{u}_g) \quad (6.24)$$

Note that the reduced earthquake force vector, $\mathbf{M}_{Red}^P \mathbf{I}_{Red}^P$ has only two non-zero elements which are placed at the end in order to add to the corresponding coupling DoFs of the earthquake force vector of the NS, $\mathbf{M}^N \mathbf{I}^N \ddot{u}_g$. The system of equations of motion hence takes the following form:

$$\mathbf{M}^N \ddot{\mathbf{u}}^N + \mathbf{C}^N \dot{\mathbf{u}}^N + \mathbf{K}^N \mathbf{u}^N = \mathbf{F}_{eRT} + \mathbf{F}_{cRT} \quad (6.25)$$

We can then write,

$$\ddot{\mathbf{u}}^N = \mathbf{M}^{N-1} [\mathbf{F}_{eRT} + \mathbf{F}_{cRT} - \mathbf{C}^N \dot{\mathbf{u}}^N - \mathbf{K}^N \mathbf{u}^N] \quad (6.26)$$

In order to apply the LSRT2 method, we write the equation of motion in a first-order form as,

$$\dot{\mathbf{y}} = \mathbf{f}(\mathbf{y}, t) = \left\{ \begin{array}{c} \mathbf{y}_2 \\ \mathbf{M}^{N-1} [\mathbf{F}_{eRT} + \mathbf{F}_{cRT} - \mathbf{C}^N \dot{\mathbf{u}}^N - \mathbf{K}^N \mathbf{u}^N] \end{array} \right\} \quad (6.27)$$

where \mathbf{y} is the state vectors, i.e.,

$$\mathbf{y} = \left\{ \begin{array}{c} \mathbf{u} \\ \dot{\mathbf{u}} \end{array} \right\} = \left\{ \begin{array}{c} \mathbf{y}_1 \\ \mathbf{y}_2 \end{array} \right\} \quad (6.28)$$

The solution of Equation 6.27 given by the LSRT2 method is as follows,

$$\mathbf{y}_{i+1} = \mathbf{y}_k + b_1 \mathbf{k}_1 + b_2 \mathbf{k}_2 \quad (6.29)$$

where, \mathbf{y}_{i+1} represents the estimate of the state vector at time step $i + 1$. Other parameters are defined below.

$$\mathbf{k}_1 = [\mathbf{I} - \gamma \Delta t \mathbf{J}]^{-1} \mathbf{f}(t_i, \mathbf{y}_i) \Delta t \quad (6.30)$$

$$\mathbf{k}_2 = [\mathbf{I} - \gamma \Delta t \mathbf{J}]^{-1} (\mathbf{f}(t_{i+\alpha_2}, \mathbf{y}_{i+\alpha_2}) + \mathbf{J} \gamma_{21} \mathbf{k}_1) \Delta t \quad (6.31)$$

where, $\mathbf{y}_{i+\alpha_2}$ represents the estimate of the state vector at the α_2 fraction of the time step, Δt ; the external force, $\mathbf{F}_{eRT, k+\alpha_2}$, is defined at time $t_{i+\alpha_2} = t_i + \alpha_2 \Delta t$ and the measured coupling force, $\mathbf{F}_{cRT, k+\alpha_2}$, is obtained by applying $\mathbf{y}_{i+\alpha_2}$ at the α_2 fraction of Δt . Thus,

$$\mathbf{y}_{i+\alpha_2} = \mathbf{y}_i + \alpha_{21} \mathbf{k}_1 \quad (6.32)$$

\mathbf{J} is the Jacobian operator and is defined as follows:

$$\mathbf{J} = \frac{\partial \mathbf{f}}{\partial \mathbf{y}} = \begin{bmatrix} \mathbf{0} & \mathbf{I} \\ -\mathbf{M}^{\mathbf{N}-1} \mathbf{K}^{\mathbf{N}} & -\mathbf{M}^{\mathbf{N}-1} \mathbf{C}^{\mathbf{N}} \end{bmatrix} \quad (6.33)$$

where, $\mathbf{M}^{\mathbf{N}}$, $\mathbf{C}^{\mathbf{N}}$ and $\mathbf{K}^{\mathbf{N}}$ are the mass, damping and stiffness matrix of the NS, respectively.

The following parameters are recommended for the LSRT2 method in order to achieve L stability second order accuracy and reduce the algorithmic damping in the low frequency range:

$$\begin{aligned} \gamma &= 1 - \frac{\sqrt{2}}{2} \\ \alpha_2 &= \alpha_{21} = \frac{1}{2} \\ \gamma_{21} &= -\gamma \\ b_1 &= 0 \\ b_2 &= 1 \end{aligned}$$

The LSRT2 method can be summarized in algorithmic form as follows:

- (1) Compute the Jacobian operator, \mathbf{J} from (6.33).
- (2) Compute \mathbf{k}_1 from (6.30) and evaluate $\mathbf{y}_{i+\alpha_2}$ from (6.32).
- (3) Impose $\mathbf{y}_{i+\alpha_2}$ to the PS, measure the coupling force, $\mathbf{F}_{\mathbf{SRT},i+\alpha_2}$, and evaluate \mathbf{y}_{i+1} from (6.29).
- (4) Impose \mathbf{y}_{i+1} to the PS and measure the coupling force, $\mathbf{F}_{\mathbf{SRT},i+\alpha_2}$.
- (5) Set $i = i + 1$ and go to step 2.

6.8.2 Delay compensation method for the RTDS

An inevitable problem during real time testing is the so called "time delay" which must be dealt with care to successfully carry out such a test. Time delay reduces the response accuracy and in the worst case causes instability of RTDS (Wu et al., 2012). In order to conduct the RTDS, we used the so called *Delay Overprediction method* developed by Wu et al. (2012). This is a new delay compensation scheme consisting of an upper bound delay and optimal feedback. This technique entails an

equivalent positive damping on the whole emulated structure, ensures dynamic stability and achieves a nearly exact compensation for delay (Wu et al., 2012).

The idea behind this overprediction technique is to assume an upper bound delay, τ_C , not less than the possible maximum delay, τ , present in the RTDS, and use it for prediction; then the actual delay will be compensated. The maximum delay of the transfer system can be measured through an experimental test, e.g., a dynamic cyclic test, and comparing the input-output signals. The schematic of the Overprediction technique is illustrated in Figure 6.19 and the procedure can be described as follows.

1. Estimate structural response, x_{i+1} , at time, t_{i+1} ;
2. Predict $x(t_{i+1} + \tau_C)$, i.e. the displacement at $t_{i+1} + \tau_C$, where, τ_C is an upper bound system delay;
3. Send out the predicted displacement at t_{i+1} ;
4. Search for the measured feedback force, $r_m(t)$, corresponding to the closest measured displacement $x_m(t)$ to x_{i+1} , and feedback the force to the NS.

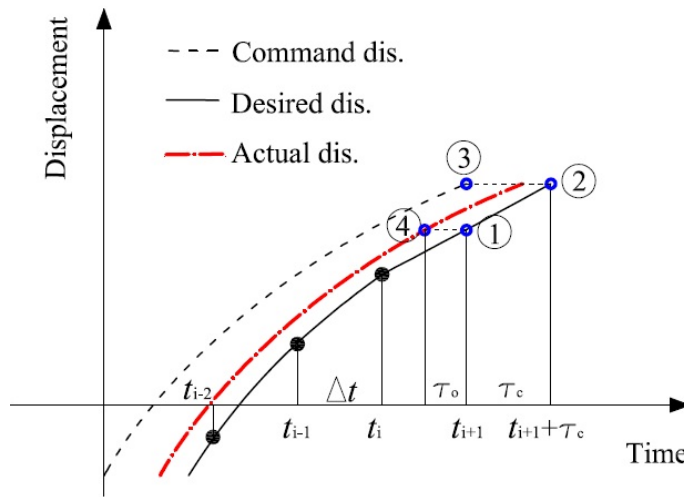


Figure 6.19: Schematics of the delay overprediction scheme.

An exact delay compensation is achieved if the chosen displacement in step 4 matches x_{i+1} , which means that the measured force $r_m(t)$ corresponds to the desired displacement, x_{i+1} without errors owing to prediction methods and actuator control.

Compared to conventional delay compensation methods, no matter how error exists in the predicted displacement, the error is minimized by choosing, from among recent data, the displacement $x_m(t)$ nearest to the desired one x_{i+1} . As a result, satisfactory properties such as error reduction and stability improvement can be expected.

The delay overcompensation method was implemented and incorporated with the Simulink model of the RTDS. A maximum total delay of about 11 ms was found for the MOOG actuators as reported in Table 5.4 of Chapter 5. Moreover, a low pass filter which was implemented to read reaction forces from actuator load cells contributed some additional delay. Hence, a value of $\tau_c=22$ ms was considered.

6.9 Model reduction of the Physical Substructure

In this Section, a detailed discussion on Model Reduction techniques and the use of some of these methods for the reduction of the Physical Substructure (PS) are provided. All analyses were performed in Matlab using matrices of the piping system and of the substructures extracted from FE models.

Let us consider a system with n DoF. Our aim is to reduce it to a f DoF system -which we call master DoF- while deleting d DoF from the system ($d = n - f$). The relationship between master and deleted DoF is,

$$\mathbf{u}_n = \begin{Bmatrix} \mathbf{u}_f \\ \mathbf{u}_d \end{Bmatrix} = \mathbf{T} \mathbf{u}_f \quad (6.34)$$

where \mathbf{u} is the coordinate vector of a system and \mathbf{T} is a transformation matrix.

A reduced matrix, \mathbf{A}_f of a system can then be written using this transformation matrix, \mathbf{T} , as follows,

$$\mathbf{A}_f = \mathbf{T}^T \mathbf{A}_n \mathbf{T} \quad (6.35)$$

where \mathbf{A} can be any matrix, e.g., mass, damping or stiffness, of the system.

While using a model reduction method, one has to find the transformation matrix, \mathbf{T} , which takes different forms depending on the reduction technique used. Note that (6.34) also provides a possibility to perform a model expansion, i.e., to return back to the original system from the master DoF using the transformation matrix.

A number of model reduction techniques are available in literature, e.g., Guyan method (Guyan, 1965), dynamic IRS method (Zhang, 1995; O'Callahan, 1989a), SEREP method (O'Callahan, 1989b), Craig Bampton method (Craig and Bampton, 1968). Herein we discuss some of these methods which will be used in our analysis.

Guyan reduction method

One of the oldest and most popular reduction methods is static or Guyan reduction (Guyan, 1965). The so-called static reduction or Guyan's reduction allows for a transformation matrix to be calculated which reduces mass and stiffness matrices to the terms related to the useful DoFs. However, in this reduction method, the inertia terms associated with the discarded degrees of freedom are neglected. While exact for a static model, when applied to a dynamic model the reduced model generated by this technique is not exact and often lacks the required accuracy (Friswell et al., 1995).

Let us consider the system of equations of motion of the PS of the piping system defined in Section 6.7,

$$\mathbf{M}_n^P \ddot{\mathbf{u}}_n^P + \mathbf{C}_n^P \dot{\mathbf{u}}_n^P + \mathbf{K}_n^P \mathbf{u}_n^P = \mathbf{F}_{en}^P \quad (6.36)$$

where, \mathbf{M}^P , \mathbf{C}^P and \mathbf{K}^P are the mass, damping and stiffness matrices of the PS; $\ddot{\mathbf{u}}_n^P$, $\dot{\mathbf{u}}_n^P$ and \mathbf{u}_n^P are the acceleration, velocity and displacement; \mathbf{F}_e^P is the earthquake force and n refers to the number of DoFs of the PS. Our aim is to reduce the size of the system to a smaller number so that the model includes only 2 DoFs that are necessary for our purposes.

We now partition the coordinate vector, \mathbf{u}_n into two parts: the coordinates to retain, \mathbf{u}_f and the coordinates to delete, \mathbf{u}_d , and write (6.36) -neglecting the damping for now- in the following form,

$$\begin{bmatrix} \mathbf{M}_{ff}^P & \mathbf{M}_{fd}^P \\ \mathbf{M}_{df}^P & \mathbf{M}_{dd}^P \end{bmatrix} \begin{Bmatrix} \ddot{\mathbf{u}}_f^P \\ \ddot{\mathbf{u}}_d^P \end{Bmatrix} + \begin{bmatrix} \mathbf{K}_{ff}^P & \mathbf{K}_{fd}^P \\ \mathbf{K}_{df}^P & \mathbf{K}_{dd}^P \end{bmatrix} \begin{Bmatrix} \mathbf{u}_f^P \\ \mathbf{u}_d^P \end{Bmatrix} = \begin{bmatrix} \mathbf{F}_{ef}^P \\ \mathbf{F}_{ed}^P \end{bmatrix} \quad (6.37)$$

where, f and d refer to the number of DoF to be retained and deleted, respectively, with $n = f + d$.

Now, assuming inertia terms and earthquake forces to be zero, Equation (6.37) can

be reduced to be the following form:

$$K_{df}^P u_f^P + K_{dd}^P u_d^P = 0 \quad (6.38)$$

which may be used to eliminate u_d^P , so that,

$$u_n^P = \begin{Bmatrix} u_f^P \\ u_d^P \end{Bmatrix} = \begin{bmatrix} I \\ [-K_{dd}^P]^{-1} K_{df}^P \end{bmatrix} \begin{Bmatrix} u_f^P \end{Bmatrix} = T_G u_f^P \quad (6.39)$$

where T_G is the Guyan transformation matrix. It is used to obtain the reduced matrices and force vector, i.e.,

$$\hat{M}_G^P = T_G^T M^P T_G; \hat{C}_G^P = T_G^T C^P T_G; \hat{K}_G^P = T_G^T K^P T_G; F_{eG}^P = T_G^T F_e^P$$

where, \hat{M}_G^P , \hat{C}_G^P and \hat{K}_G^P are the reduced mass, damping and stiffness matrices; F_{eG}^P is the reduced force vector.

SEREP reduction method

A very effective reduction techniques was developed by O'Callahan and others called the System Equivalent Reduction Expansion Process (SEREP) that utilizes computation of eigenvectors to produce the transformation between master and slave coordinates (O'Callahan, 1989b). This technique offers the following advantages:

- i) The eigenvalues of the reduced system are always equal to the eigenvalues of the full system for the modes of interest retained in the model.
- ii) The modes that are preserved in the reduced model may be arbitrarily selected from those modes of interest in the original model.
- iii) The eigensolution of the reduced system is exact and does not depend on the location or number of points preserved in the reduced model.

Let us recall Equation (6.37) of the PS assuming earthquake force on the deleted DoFs to be zero.

$$\begin{bmatrix} M_{ff}^P & M_{fd}^P \\ M_{df}^P & M_{dd}^P \end{bmatrix} \begin{Bmatrix} \ddot{u}_f^P \\ \ddot{u}_d^P \end{Bmatrix} + \begin{bmatrix} K_{ff}^P & K_{fd}^P \\ K_{df}^P & K_{dd}^P \end{bmatrix} \begin{Bmatrix} u_f^P \\ u_d^P \end{Bmatrix} = \begin{Bmatrix} F_{ef}^P \\ 0 \end{Bmatrix} \quad (6.40)$$

Next, we split the mass normalized eigenvector of the system, ϕ as follows,

$$\phi = [\phi_{af} \quad \phi_{ad}] \quad (6.41)$$

where, ϕ_{af} are the modes to be retained and ϕ_{ad} are the modes to be deleted. ϕ_{af} and ϕ_{ad} are matrices of dimensions $n \times f$ and $n \times (n - f)$, respectively. We now define a modal coordinate for the equation as, $\mathbf{u} = \phi \mathbf{r}$, where, \mathbf{r} is the modal coordinate vector. Substituting,

$$\mathbf{u}_n^P = \begin{bmatrix} \mathbf{u}_f^P \\ \mathbf{u}_d^P \end{bmatrix} = \phi \mathbf{r} = \begin{bmatrix} \phi_{af} & \phi_{ad} \end{bmatrix} \begin{bmatrix} \mathbf{r}_f^P \\ \mathbf{r}_d^P \end{bmatrix} = \begin{bmatrix} \phi_{ff} & \phi_{fd} \\ \phi_{df} & \phi_{dd} \end{bmatrix} \begin{bmatrix} \mathbf{r}_f^P \\ \mathbf{r}_d^P \end{bmatrix} \quad (6.42)$$

Now, if we pre-multiply the equation of motion by ϕ^T , i.e.,

$$\phi^T \mathbf{M}_n^P \phi \ddot{\mathbf{r}}_n + \phi^T \mathbf{K}_n^P \phi \mathbf{r}_n = \phi^T \mathbf{F}_{en}^P \quad (6.43)$$

the equation takes the following form,

$$\mathbf{I}_n \ddot{\mathbf{r}}_n + \lambda \mathbf{r}_n = \phi^T \mathbf{F}_{en}^P \quad (6.44)$$

where, \mathbf{I}_n is an identity matrix and is expressed as follows,

$$\mathbf{I}_n = \begin{bmatrix} \mathbf{I}_f & \mathbf{0} \\ \mathbf{0} & \mathbf{I}_d \end{bmatrix} \quad (6.45)$$

$$\begin{bmatrix} \phi_{af}^T \\ \phi_{ad}^T \end{bmatrix} \begin{bmatrix} \mathbf{M}_{ff}^P & \mathbf{M}_{fd}^P \\ \mathbf{M}_{df}^P & \mathbf{M}_{dd}^P \end{bmatrix} \begin{bmatrix} \phi_{af} & \phi_{ad} \end{bmatrix} = \begin{bmatrix} \phi_{af}^T \mathbf{M}^P \phi_{af} & \phi_{af}^T \mathbf{M}^P \phi_{ad} \\ \phi_{ad}^T \mathbf{M}^P \phi_{af} & \phi_{ad}^T \mathbf{M}^P \phi_{ad} \end{bmatrix} = \begin{bmatrix} \mathbf{I}_f & \mathbf{0} \\ \mathbf{0} & \mathbf{I}_d \end{bmatrix} \quad (6.46)$$

λ is a matrix that contains the natural frequencies of the PS.

$$\lambda_n = \begin{bmatrix} \lambda_f & \mathbf{0} \\ \mathbf{0} & \lambda_d \end{bmatrix} \quad (6.47)$$

$$\begin{bmatrix} \phi_{af}^T \\ \phi_{ad}^T \end{bmatrix} \begin{bmatrix} \mathbf{K}_{ff}^P & \mathbf{K}_{fd}^P \\ \mathbf{K}_{df}^P & \mathbf{K}_{dd}^P \end{bmatrix} \begin{bmatrix} \phi_{af} & \phi_{ad} \end{bmatrix} = \begin{bmatrix} \phi_{af}^T \mathbf{K}^P \phi_{af} & \phi_{af}^T \mathbf{K}^P \phi_{ad} \\ \phi_{ad}^T \mathbf{K}^P \phi_{af} & \phi_{ad}^T \mathbf{K}^P \phi_{ad} \end{bmatrix} = \begin{bmatrix} \lambda_f & \mathbf{0} \\ \mathbf{0} & \lambda_d \end{bmatrix} \quad (6.48)$$

Now, we truncate the modal vector, $\mathbf{r}_n = [\mathbf{r}_f \quad \mathbf{r}_d]^T$ by assuming $\mathbf{r}_d = \mathbf{0}$. Equation (6.44) then reduces to

$$\mathbf{I}_f \ddot{\mathbf{r}}_f + \lambda_f \mathbf{r}_f = \phi_{af}^T \mathbf{F}_{ef}^P \quad (6.49)$$

Substituting, $\mathbf{r}_f = \phi_{ff}^{-1} \mathbf{u}_f$ in (6.49), we can write,

$$\phi_{ff}^{-1T} \phi_{af}^T \mathbf{M}^P \phi_{af} \phi_{ff}^{-1} \ddot{\mathbf{u}}_f + \phi_{ff}^{-1T} \phi_{af}^T \mathbf{K}^P \phi_{af} \phi_{ff}^{-1} \mathbf{x}_r = \phi_{ff}^{-1T} \phi_{af}^T \mathbf{F}_e^P \quad (6.50)$$

We can now define a Transformation matrix, \mathbf{T}_S as follows:

$$\mathbf{T}_S = \phi_{af} \phi_{ff}^{-1} = \begin{bmatrix} \phi_{ff} \\ \phi_{df} \end{bmatrix} \phi_{ff}^{-1} = \begin{bmatrix} I \\ \phi_{df} \phi_{ff}^{-1} \end{bmatrix} \quad (6.51)$$

so that the solution of equations of motion of the reduced system can be written as,

$$\hat{\mathbf{M}}_S^P \ddot{\mathbf{u}}_f + \hat{\mathbf{C}}_S^P \dot{\mathbf{u}}_f + \hat{\mathbf{K}}_S^P \mathbf{u}_f = \hat{\mathbf{F}}_e^P \quad (6.52)$$

in which, $\hat{\mathbf{M}}_S^P$, $\hat{\mathbf{C}}_S^P$ and $\hat{\mathbf{K}}_S^P$ are the reduced mass, damping and stiffness matrices of the PS having a dimensions of 2 by 2 matrix; $\hat{\mathbf{F}}_e^P$ is the reduced earthquake force vector of the PS with two elements. These terms are defined as follows:

$$\hat{\mathbf{M}}_S^P = \mathbf{T}_S^T \mathbf{M}^P \mathbf{T}_S; \hat{\mathbf{C}}_S^P = \mathbf{T}_S^T \mathbf{C}^P \mathbf{T}_S; \hat{\mathbf{K}}_S^P = \mathbf{T}_S^T \mathbf{K}^P \mathbf{T}_S; \hat{\mathbf{F}}_e^P = \mathbf{T}_S^T \mathbf{F}_e^P$$

Equation (6.51) shows that in order to find the transformation matrix, \mathbf{T} , one has to find the eigensolution of a system and choose the modes to be retained. The modes can be chosen based on their importance evaluated from different criteria, e.g., modes that excite most participation masses. In order to reduce the PS, we used two approaches namely, SEREP1 and SEREP2.

The *SEREP1* reduction was performed by considering the eigenvectors and the most important modes of the PS on the basis of modal mass participation. In this case we preserved modal behaviour of the PS in the reduced model. Mode #1 and Mode #8 of the PS were considered for this reduction since they had the highest mass participations in the x direction, i.e., in the direction of earthquake, see Table 6.10.

In the *SEREP2* method, reduction of the PS was performed by considering eigenvectors and important modes of the total piping system. In this way, modal properties of the original system could be preserved in the reduced system. In particular, Mode #1 and Mode #2 of the total piping system, which had the highest two mass participations in the x direction, see Table 6.5, were chosen for this reduction purpose.

Craig-Bampton method

The Craig-Bampton (CB) reduction technique, originally developed by Craig and Bampton (1968), is a particularly useful technique for the reduction of a substructure. This technique produces a reduced model of the substructure that captures its fundamental low frequency response modes (Young, 2000). The mode shape information consists of all free modes expressed in physical coordinates and a deleted set of elastic modes expressed in modal coordinates.

The following formulation of the CB technique is based on (Gordon, 1999). Let us recall Equation (6.36), without considering damping for simplicity,

$$M_n^P \ddot{u}_n^P + K_n^P u_n^P = F_{en}^P \quad (6.53)$$

In the CB reduction, the co-ordinate vector of the PS, u_n^P is divided into two parts: one containing the coupling DoFs, u_C and the other containing the internal DoFs (rest of the DoFs), u_L , i.e.,

$$u_n^P = \begin{Bmatrix} u_C \\ u_L \end{Bmatrix} \quad (6.54)$$

The CB reduction is defined as,

$$u_n^P = \begin{Bmatrix} u_C \\ u_L \end{Bmatrix} = \begin{bmatrix} I & 0 \\ \phi_R & \phi_L \end{bmatrix} \begin{Bmatrix} u_C \\ q \end{Bmatrix} \quad (6.55)$$

where,

$$\begin{bmatrix} I & 0 \\ \phi_R & \phi_L \end{bmatrix} = \phi_{CB} = CB \text{ Transformation matrix}$$

u_C = Coupling DoF

u_L = Internal DoF

ϕ_R = Rigid body vector

ϕ_L = Fixed based mode shapes

q = modal coordinates

Combining (6.55) and (6.53) and pre-multiplying by ϕ_{CB}^T , we have,

$$\phi_{CB}^T M_n^P \phi_{CB} \begin{Bmatrix} \ddot{u}_C \\ \ddot{q} \end{Bmatrix} + \phi_{CB}^T K_n^P \phi_{CB} \begin{Bmatrix} u_C \\ q \end{Bmatrix} = \phi_{CB}^T \begin{Bmatrix} F_{eC} \\ F_{eL} \end{Bmatrix} \quad (6.56)$$

The CB mass and stiffness matrices are defined as,

$$M_{CB} = \phi_{CB}^T M_n \phi_{CB} = \begin{bmatrix} M_{CC} & M_{Cq} \\ M_{qC} & M_{qq} \end{bmatrix} \quad (6.57)$$

$$K_{CB} = \phi_{CB}^T K_n \phi_{CB} = \begin{bmatrix} K_{CC} & 0 \\ 0 & K_{qq} \end{bmatrix} \quad (6.58)$$

Using the CB mass and stiffness matrices, (6.56) can be re-written as,

$$\begin{bmatrix} M_{CC} & M_{Cq} \\ M_{qC} & M_{qq} \end{bmatrix} \begin{Bmatrix} \ddot{u}_C \\ \ddot{q} \end{Bmatrix} + \begin{bmatrix} K_{CC} & 0 \\ 0 & K_{qq} \end{bmatrix} \begin{Bmatrix} u_C \\ q \end{Bmatrix} = \begin{Bmatrix} F_{eC} \\ 0 \end{Bmatrix} \quad (6.59)$$

where input forces are only applied at the boundary, $F_{eL} = 0$.

Note that M_{CC} is the total mass matrix of the PS translated to the coupling points, whereas, K_{CC} is the stiffness matrix at the coupling points which is equivalent to the Guyan stiffness matrix. Now, if we consider mass normalized eigenvectors,

$$K_{qq} = \begin{bmatrix} \backslash & 0 \\ & \lambda \\ 0 & \backslash \end{bmatrix} \quad (6.60)$$

$$M_{qq} = \begin{bmatrix} \backslash & 0 \\ & I \\ 0 & \backslash \end{bmatrix} \quad (6.61)$$

where λ_i are the eigenfrequencies of the system defined as,

$$\lambda_i = k_i/m_i = \omega_i^2 \quad (6.62)$$

the dynamic system of equations of motion of the reduced PS can finally be written as,

$$\begin{bmatrix} M_{CC} & M_{Cq} \\ M_{qC} & I \end{bmatrix} \begin{Bmatrix} \ddot{u}_C \\ \ddot{q} \end{Bmatrix} + \begin{bmatrix} 0 & 0 \\ 0 & 2\zeta\omega \end{bmatrix} \begin{Bmatrix} \dot{u}_C \\ \dot{q} \end{Bmatrix} + \begin{bmatrix} K_{CC} & 0 \\ 0 & \omega^2 \end{bmatrix} \begin{Bmatrix} u_C \\ q \end{Bmatrix} = \begin{Bmatrix} F_{eC} \\ 0 \end{Bmatrix} \quad (6.63)$$

where, ζ is the damping ratio and $2\zeta\omega$ is called modal damping.

Using the CB transformation matrix shown in (6.55), we could perform a reduction of the PS. An advantage of the CB technique over the SEREP2 method was that, in the CB reduction, contributions of any number of dynamic modes of the PS could be considered in the reduced model. We chose to retain two dynamic modes on the basis of mass participation factor of the PS. In particular, like in SEREP1 reduction, Mode #1 and Mode #8 of the PS -which had the highest mass participations in the x direction, see Table 6.10- were chosen for this reduction purpose.

6.9.1 Effectiveness of different reduction techniques

As discussed earlier, because a PDDS was carried out at a slower rate than the actual time scale of the earthquake, it could not experimentally measure the inertia and damping forces of the PS. Hence, we needed to numerically model these contributions, whereas, the restoring force was measured during the experiment. However, due to the slow-rate execution of the PDDS, the two actuators could excite only the static modes of the PS and the measured restoring force was the contribution of these modes. A good approximation of this restoring force could be produced by the Guyan stiffness, \hat{K}_G^P . However, since the Guyan reduction is inaccurate for a dynamic model, it would not reproduce the actual response of the piping system during the experiment.

The CB technique offered a suitable solution for the PDDS. In this reduction, the overall response of the PS was given by the combination of two contributions: (1) response of the internal nodes owing to the static movements of the two coupling nodes and (2) response of the internal nodes owing to the local dynamic modes of interest of the PS. Note that the measured restoring force during an experiment was the contribution of (1), whereas, the contribution of (2) was considered numerically. As a result, the overall interaction between the PS and NS could be taken into account and behaviour of the emulated system could potentially be reproduced.

With regard to RTDS, all the contributions of the coupling force, i.e., inertia, damping and restoring force, were experimentally measured. In this case, both the SEREP1

and SEREP2 techniques could be used because they were based on a dynamic reduction: the SEREP1 method preserved the dynamic modes of the PS, while the SEREP2 method retained the dynamic modes of the piping (emulated) system. Since an RTDS aimed at the reproduction of the overall dynamics of a system, the SEREP2 method could potentially better approximate the actual response of the piping system.

In order to assess the effectiveness of the reduction techniques discussed above, several time history simulations were carried out on the Reduced Model of the piping system (NS + reduced PS) and results were compared with those of the Reference Model by means of a normalized root mean square (RMS) error, e_{RMS} , defined in Equation (6.9). All reduction methods were validated through numerical simulations implemented with the LSRT2 algorithms presented in Subsection 6.8.1 and analyses were performed in Matlab using the matrices and force vectors of the piping system and substructures. Relevant matrices were extracted from an FE model of the piping system developed by means of ANSYS (2007), as depicted in Figure 6.20. The design accelerogram was scaled to 0.1g PGA and a 0.5% damping was considered.

The e_{RMS} between simulations results of the Reduced and Reference Models in the two coupling nodes are reported in Table 6.13; see Figure 6.21 for relevant displacement histories in Coupling Node #2. A keen reader may note that the minimum errors were found with the CB and the SEREP2 reductions. This trend justifies previous considerations made about the limitations of the SEREP1 technique. The considerations made above about the proper use of the CB and SEREP2 methods will be corroborated in Chapter 7, where actual tests will be commented.

Table 6.13: e_{RMS} for different reduction methods

Reduction	e_{RMS}	
	Coupling Node #1	Coupling Node #2
CB	0.30	0.02
SEREP1	0.48	0.13
SEREP2	0.31	0.17

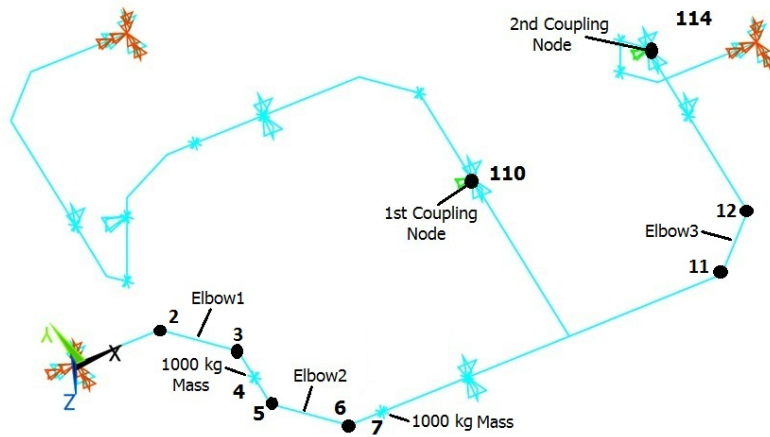


Figure 6.20: FE model of the piping system developed in ANSYS.

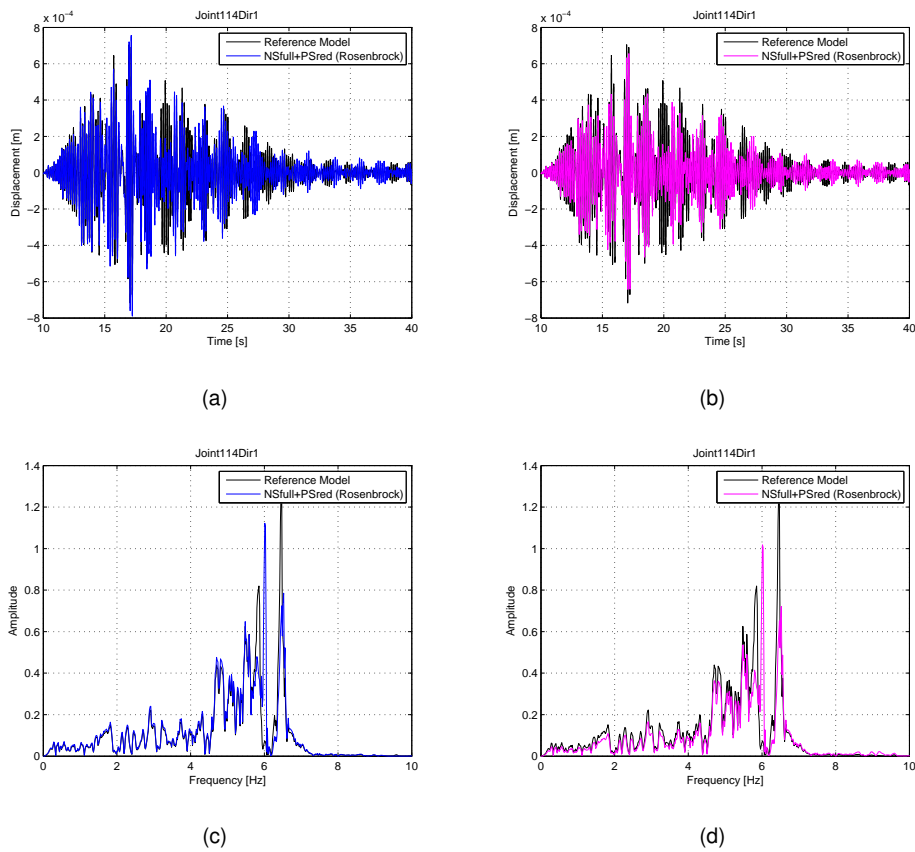


Figure 6.21: Displacement histories and relevant Fourier spectra of Coupling Node #2: (a) and (b) are relevant to the CB reduction; (b) and (d) are relevant to SEREP2 reduction.

6.10 Modification of the piping system model for the RTDS

With regard to the RTDS, a critical limitation was found on the capacity of the MOOG actuators. As discussed in Chapter 5, maximum displacements of the MOOG actuators depended on the frequency to which they operated. Moreover, during an RTDS, control issues owing to several factors, such as delay and noise, further narrowed the effective frequency and displacement ranges of the actuators. It was not, therefore, possible to carry out an RTDS on the piping system. Hence, in order to obtain a real time compatible structure, the NS was modified by adding masses to several nodes, thus reducing the eigenfrequencies of the piping system as shown in Figure 6.22 and Table 6.14. The first 10 eigenfrequencies of the modified system are presented in Table 6.15. Thus, we were able to carry out the RTDS on this modified piping system with small levels of PGA.

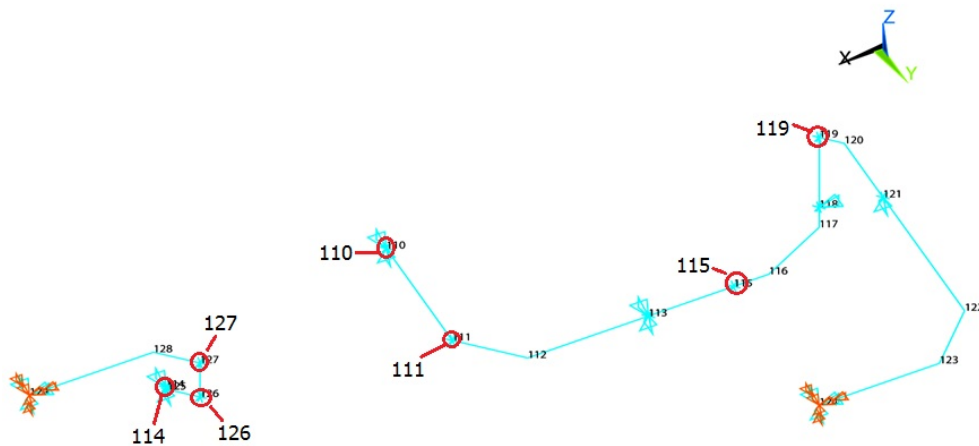


Figure 6.22: Added masses in the NS.

Table 6.14: Added masses in the nodes of the NS model

Node	110	111	114	115	119	126	127
Mass (kg)	22000	20000	26000	18000	18000	22000	22000

Table 6.15: 1st ten eigenfrequencies of the modified FE model of the piping system

Mode	1	2	3	4	5	6	7	8	9	10
Frequency (Hz)	0.78	1.10	1.11	1.39	1.60	1.79	2.60	3.41	5.00	6.58

The RTDS simulations were performed using the properties of the modified systems. The reference earthquake accelerogram was scaled to a 0.02g PGA and a 0.5% damping was used. The reduced earthquake force vector was obtained by the SEREP2 reduction method. Displacement histories and relevant Fourier spectra in the two coupling nodes are presented in Figure 6.23. A good agreement between the simulation results of the Reference Model (RM with added masses in relevant nodes) and Reduced Model can be noted; the value of e_{RMS} between the responses being close to zero. This also proves the effectiveness of the SEREP2 reduction method.

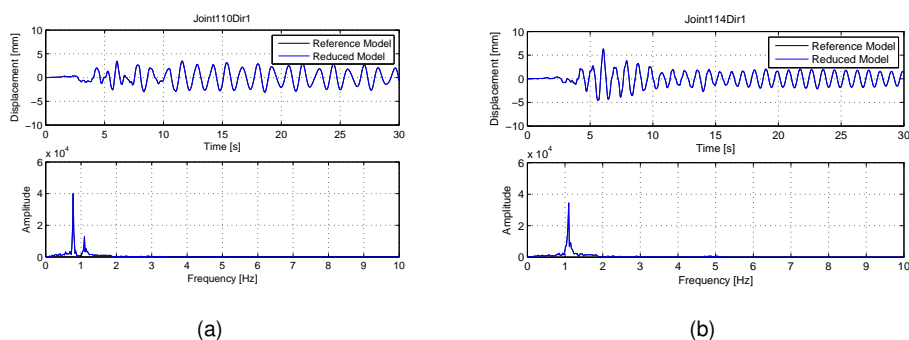


Figure 6.23: Displacement histories and relevant Fourier spectra of (a) Coupling Node #1 and (b) Coupling Node #2 (Blue- Reduced Model; Black- Reference Model).

6.11 Hardware-Software architecture for hybrid tests

The hybrid tests were conducted using the hardware and software presented in Chapter 5. The LSRT2 algorithms were developed in Matlab/Simulink environment in a Host PC where it was compiled and then sent to an xPC target via a LAN connection. During the experimental tests, the LSRT2 integration algorithm solved the system of equations of motion in the xPC target and estimated displacement commands for the PS. These displacement commands were written locally to the xPC target

which instantaneously copied these signals to the MTS controller through SCRAMNET. The controller then commanded the actuators to move the coupling DoFs to the desired positions and read back reaction forces from the actuators. The measured reaction forces were instantaneously copied to the xPC target via SCRAMNET. The hardware-software scheme for the hybrid tests is presented in Figure 6.24.

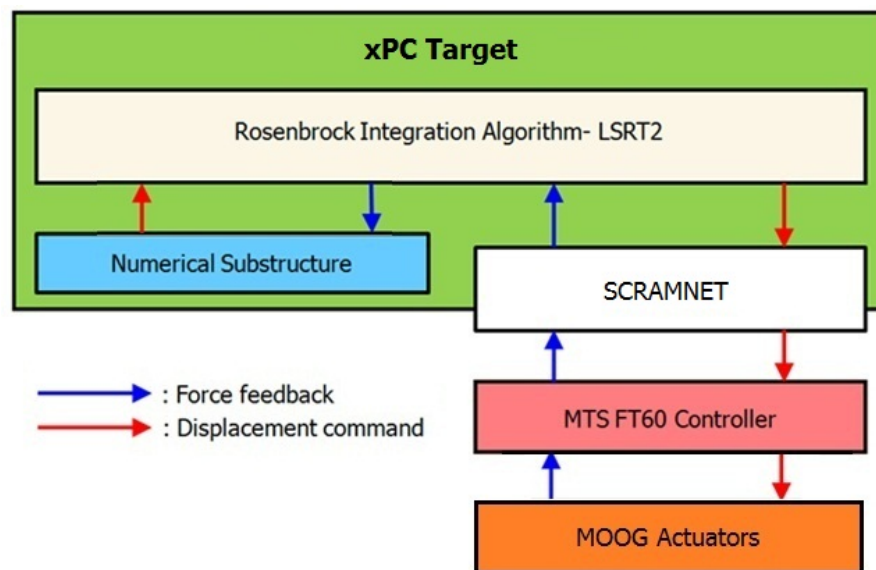


Figure 6.24: Hardware-Software configuration for the hybrid tests.

6.12 Conclusions

This chapter described the implementations of PDDS and RTDS schemes for seismic testing of a piping system at full-scale. Seismic performance assessment of the piping system through FE analyses was presented and discussed. The selection procedure of realistic input earthquake loading for analyses and experiments according to a performance-based earthquake engineering Italian Standard was presented.

Implementations of PDDS and RTDS were challenging mainly because the piping system was a structure characterised by distributed masses and subjected to distributed earthquake forces. During substructuring, the coupling nodes were found based on the minimum bending moments in the piping system found through time history analyses. Applications and effectiveness of a number of model reduction

techniques were presented in order to reduce the PS and earthquake forces on the two coupling nodes. Among different model reduction techniques, the Craig-Bampton method was found to be the most suitable method for the PDDS. By considering both static and dynamic parts of a structure this method allowed us to take into account also the dynamic part of the restoring forces coming from the reduced system. In case of an RTDS, the SEREP2 reduction was found to be suitable, in which only the earthquake forces needed to be condensed. Thus, these two reduction methods were selected to carry out the experimental tests.

With regard to RTDS, the eigenfrequencies of the piping system model were reduced. This enabled us to develop an RTDS scheme for the modified piping system to be tested with small level of earthquake loading. Numerical validations of both PDDS and RTDS algorithms were shown by means of the LSRT2 integration scheme using relevant reduction methods. Moreover, a hardware-software configuration to be used in the hybrid tests were presented.

CHAPTER 7

EXPERIMENTAL TESTS ON THE PIPING SYSTEM: PSEUDO-DYNAMIC AND REAL TIME TESTS

7.1 Introduction

In order to investigate the performance of the piping system and its components, presented in Chapter 6, under realistic seismic loading, a number of PDDS and RTDS were carried out under several levels of earthquake loading corresponding to serviceability and ultimate limit states suggested by performance-based earthquake engineering Standards. The experimental activities carried out on the piping system are described in this chapter. Experimental results are analysed and commented in detail; the seismic performance of the piping system and its components are discussed. Finally, a comparison between numerical and experimental results is made.

7.2 Test program

A number of experimental tests were carried out in order to investigate the seismic performance of the piping system and its components under different levels of earthquake loading relevant to serviceability and ultimate limit states. The experimental test program is presented in Table 7.1.

Table 7.1: Experimental test program on the piping system

Test Case			Excitation Wave	Excitation Direction	PFA* (g)	PGA (g)
Identification tests of the PS	IDT	Hammer Test	Hammer Impact	-	-	-
Real time tests	RT1	RTDS	Seismic	Horizontal	0.02	-
	RT2	RTDS	Seismic	Horizontal	0.02	-
Elastic test	ET	PDDS	Seismic	Horizontal	0.042	-
Serviceability limit state tests	Operational limit state test, SLOT	PDDS	Seismic	Horizontal	0.08	0.05
	Damage limit state test, SLDT	PDDS	Seismic	Horizontal	0.11	0.08
Ultimate limit state tests	Safe life limit state test, SLVT	PDDS	Seismic	Horizontal	0.42	0.29
	Collapse limit state test, SLCT	PDDS	Seismic	Horizontal	0.60	0.41

* PFA refers to Peak Floor Accelerations applied during experiments.

As can be noted from Table 7.1, several PDDS and RTDS were carried out on the piping system. However, the RTDS were conducted with a low PFA and considering a similar structure owing to the limitations commented in Section 6.10 of Chapter 6. Based on the discussion presented in Subsection 6.9.1 of Chapter 6, the PDDS were carried out with the CB reduction, while both the CB and SEREP2 reduction techniques were adopted to perform the RTDS.

In addition to the hybrid tests, some identification tests were also performed on the PS in order to characterize the dynamic properties of the PS and to have an estima-

tion of actual damping to be used in the NS. An elastic test, ET, was carried out to observe elastic responses of the piping system with a low PFA. These tests provided an opportunity to check the hybrid test algorithms safely without damaging the test specimen. In all tests, the earthquake loading was applied in the horizontal x direction, and an internal pressure of 3.2 MPa was used.

7.3 Test Specimen and experimental set-up

The test specimen corresponds to the PS of the piping system identified through substructuring techniques described in Subsection 6.6. Specifications and components of the test specimen are shown in Figure 7.1. In detail, it consisted of 8" and 6" pipes, three 8" elbows, one Tee joint and one bolted flange joint. The experimental set-up was placed on the reaction floor of the Materials and Structural Testing laboratory of the University of Trento. All pipes were filled with water at an internal pressure of 3.2 MPa. A schematic of the test set-up is presented in Figure 7.2, while the actual set-up and some components are shown in Figure 7.3 and Figure 7.4, respectively.

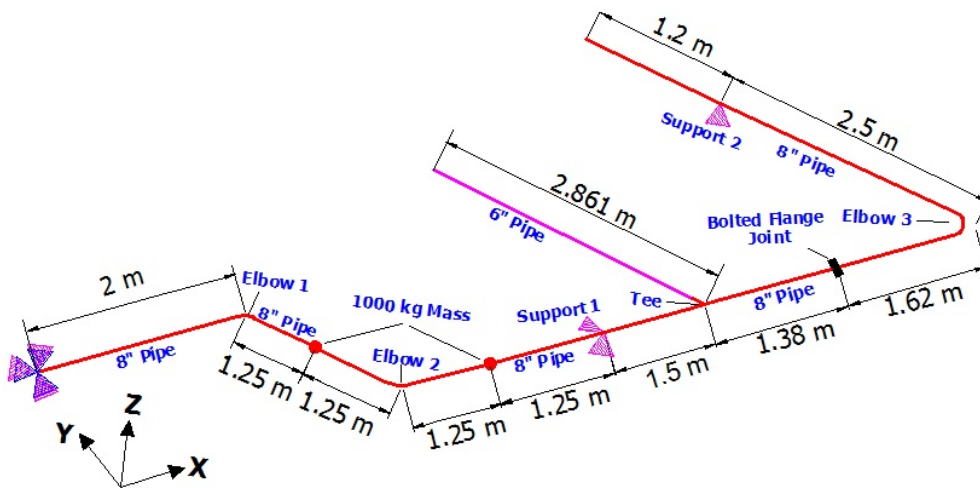


Figure 7.1: Specifications and components of the test specimen.

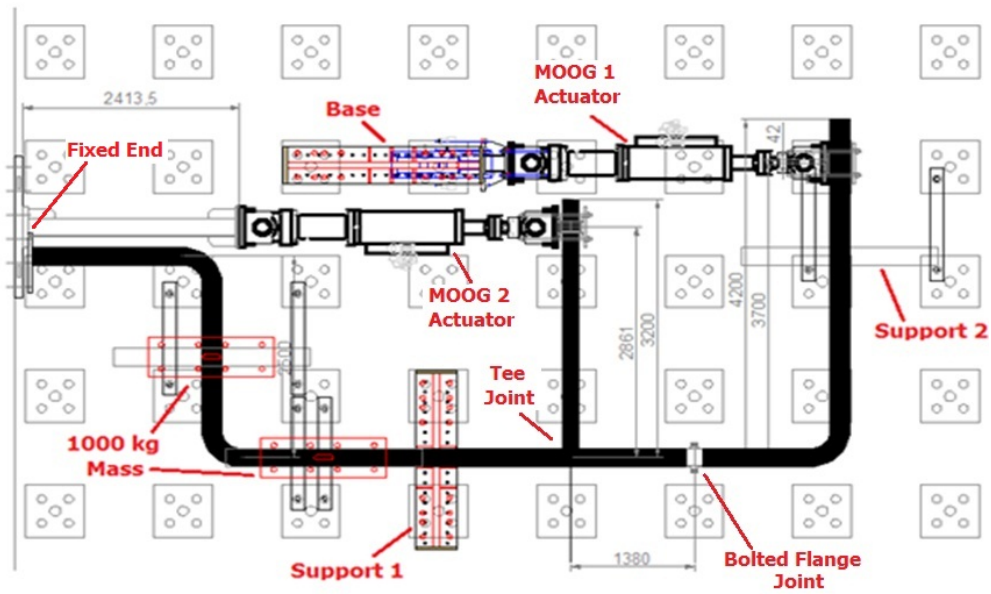


Figure 7.2: Schematic of the experimental set-up for the hybrid tests.

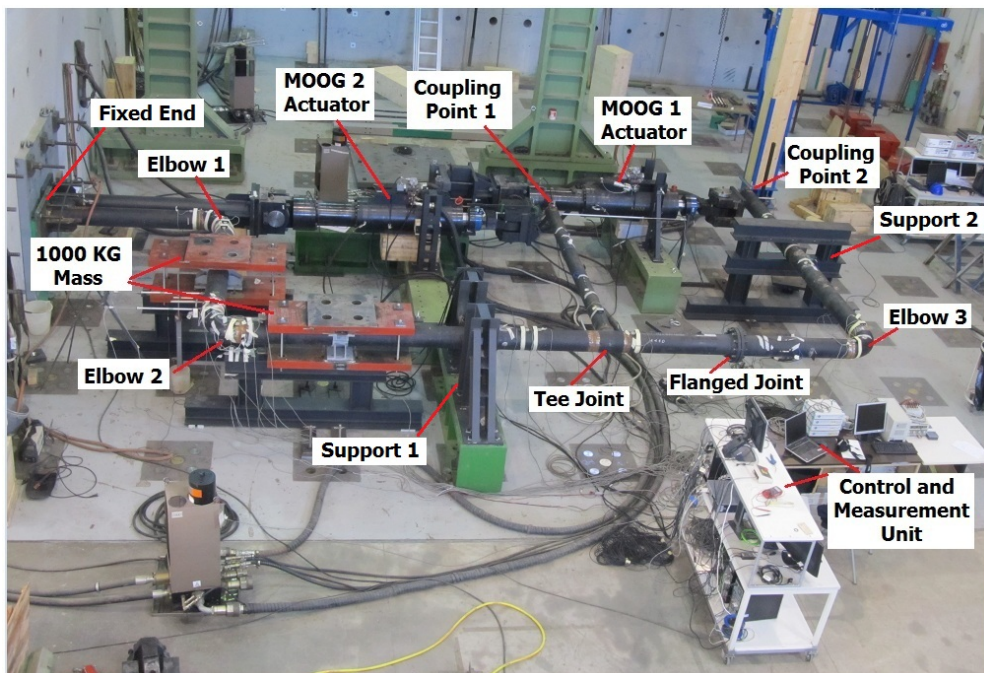


Figure 7.3: Actual test set-up for the hybrid tests.

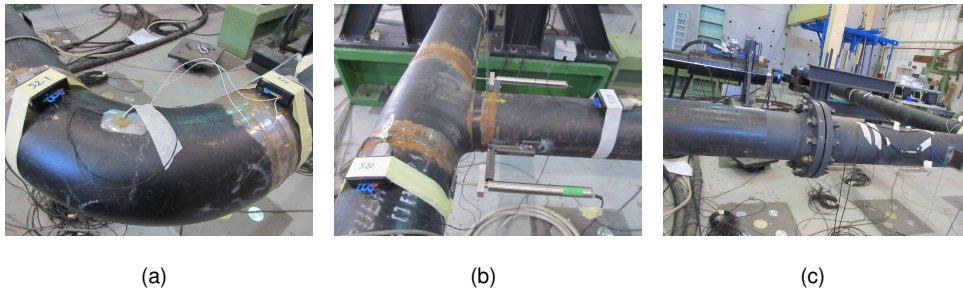


Figure 7.4: Some components of the test specimen: (a) Elbow #1; (b) Tee joint; (c) bolted flange joint.

The two supports were built on two heavy iron blocks connected to the reaction floor by means of bolted connections. Support #1 restricted movements of the pipe in the y and z directions, whereas Support #2 restricted pipe movements in the z direction. In order to reduce friction, both Support #1 and support #2 were endowed with four roller bearings and four ball bearings, respectively, as illustrated in Figure 7.5. The two 1000 kg masses were realized by two iron plates as shown in Figure 7.7.

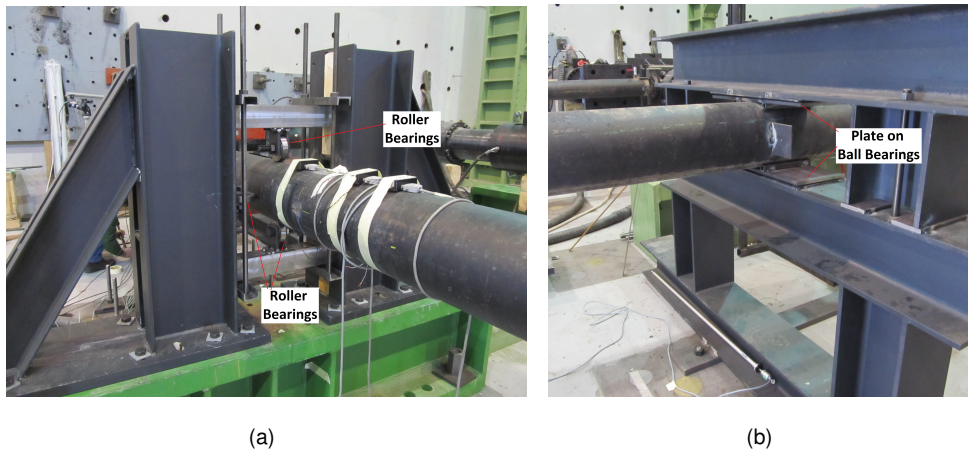


Figure 7.5: (a) Support #1; (b) Support #2.

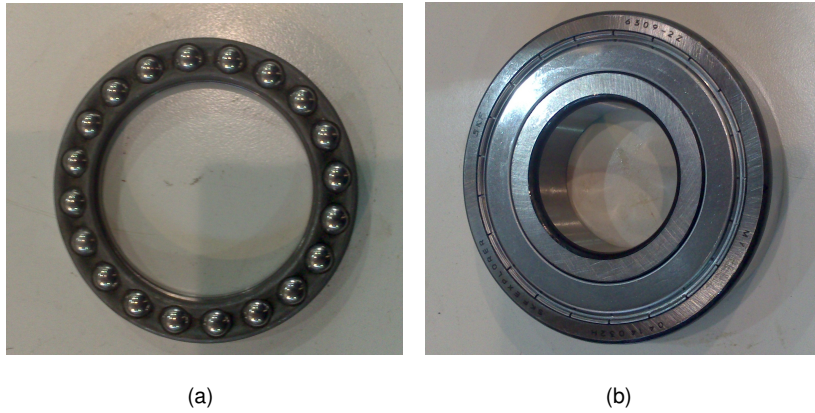


Figure 7.6: (a) A ball bearing; (b) a roller bearing.

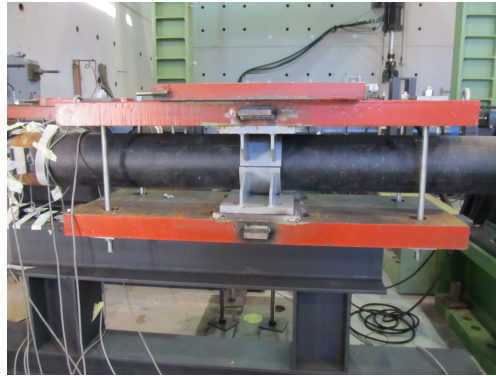


Figure 7.7: A 1000 kg mass attached to the pipe.

7.4 Instrumentation and measurements

The test specimen was instrumented with several strain gauges and displacement transducers. In detail, 21 strain gauges were mounted on the test specimen in order to measure strains at its different locations. Moreover, in order to measure displacements and rotations of different components of the PS, 7 displacement transducers as listed in Table 7.2 were used. The experimental data were acquired by 4 Spider8 data acquisition systems (DAQs).

Table 7.2: No of strain gauges and displacement transducers used during hybrid tests

Strain gauges		
Instrument	Total no	Acquisition device
Strain gauges	21	Spider8

Displacement Transducers		
Instrument	Total no	Acquisition device
Gefran 1000mm	1	Spider8
Gefran 500mm	2	Spider8
AEP 100mm	4	Spider8

Strain gauges were placed in the most stressed zones of the PS as depicted in Figure 7.8. In addition to Elbow #2, which was found to be the most critical one, we also placed strain gauges in the other two elbows and in straight pipes both in longitudinal and circumferential direction. In the elbows, strain gauges were mounted in different positions of the crown and the flank, see Figure 2.10 for definition, as illustrated in Figure 7.9, Figure 7.10 and Figure 7.11.

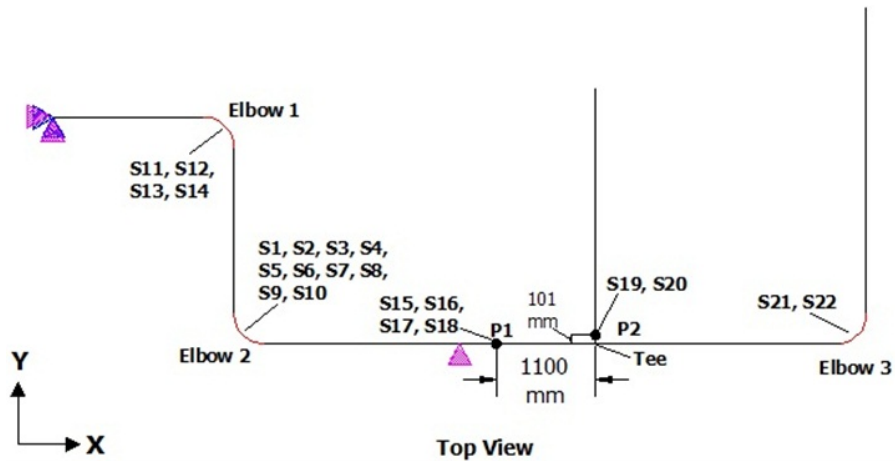


Figure 7.8: Locations of strain gauges.

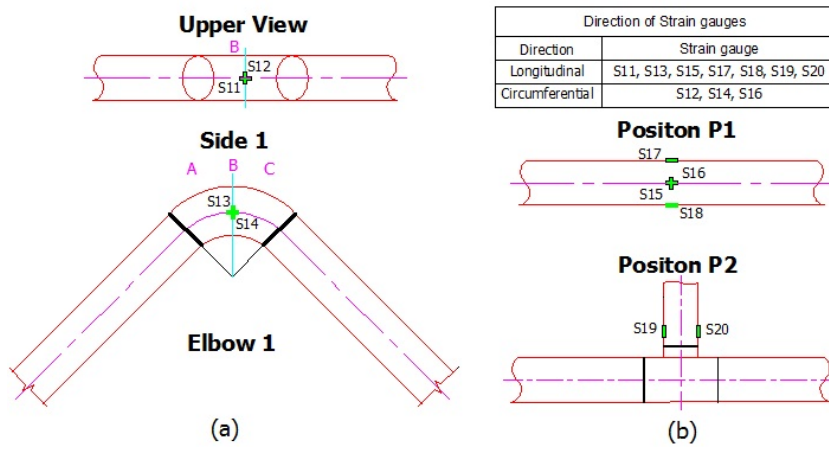


Figure 7.9: Positions of strain gauges in (a) Elbow #1 and (b) straight pipe.

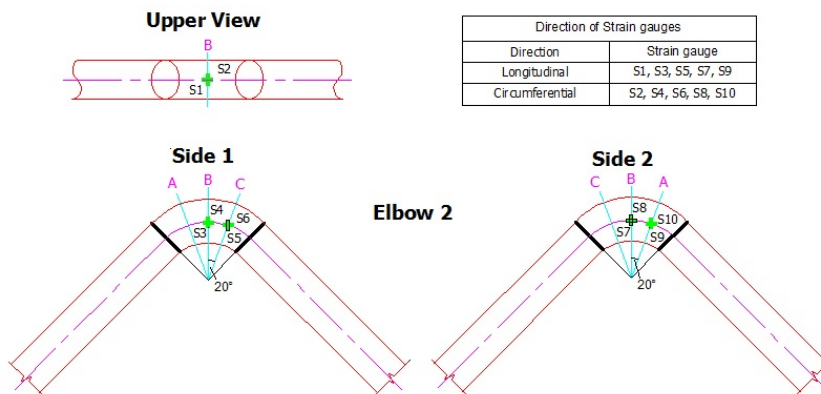


Figure 7.10: Positions of strain gauges in Elbow #2.

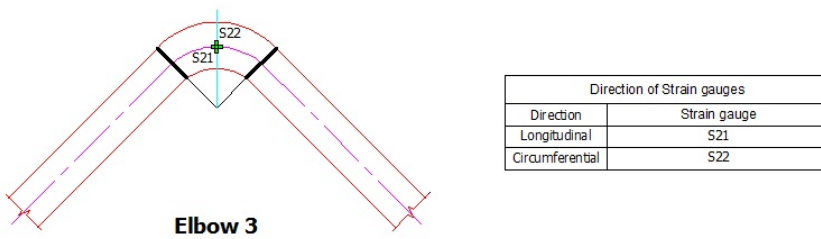


Figure 7.11: Positions of strain gauges in Elbow #3.

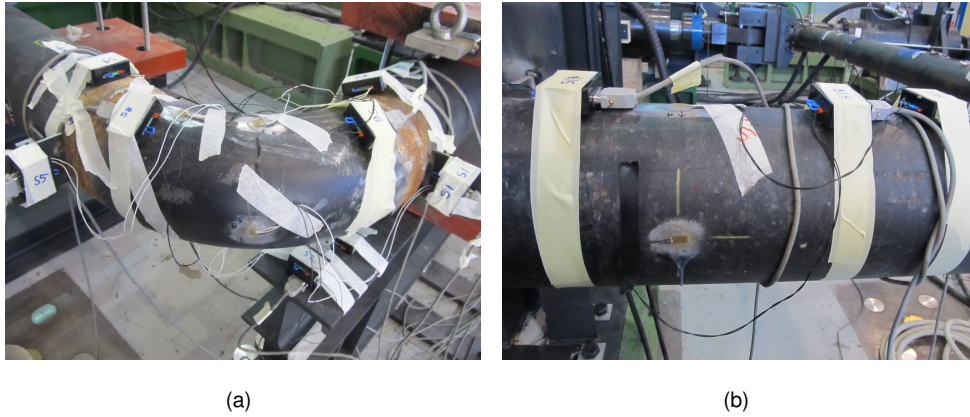


Figure 7.12: Strain gauges mounted in (a) Elbow #2; (b) straight pipe.

Measurements of displacements and rotations of different parts of the test specimen were carried out by 7 displacement transducers as shown in Figure 7.13. The types of displacement sensors used in the experimental tests are listed in Table 7.3. Displacement transducers, G1 and T4 were used to measure displacements of the two coupling nodes, externally.

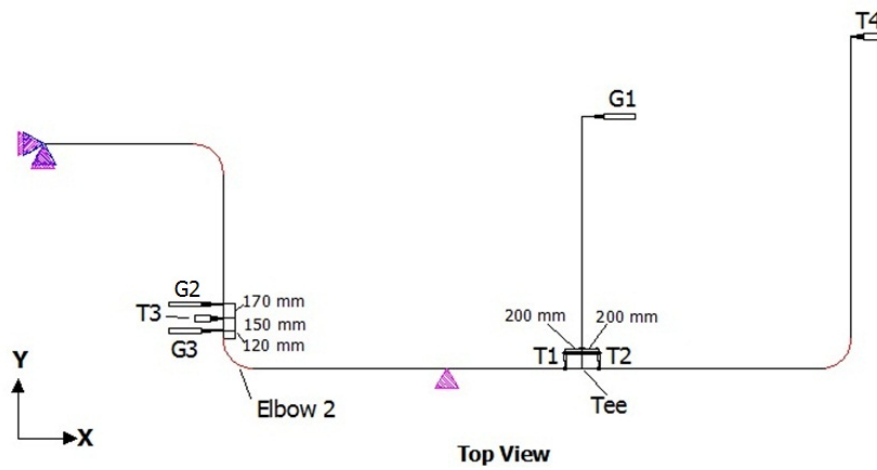


Figure 7.13: Locations of displacement transducers.

Table 7.3: Types and number of displacement transducers

Displacement Transducers	Label	No
AEP	T1, T2, T3, T4	4
Gefran	G1, G2, G3	3

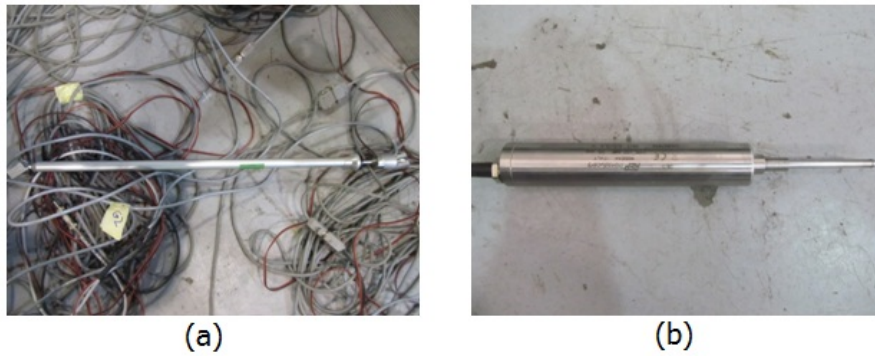


Figure 7.14: Displacement transducers: (a) Gefran 500 mm, G2; (b) AEP, T2.

In order to measure rotations of the Tee joint, two AEP displacement transducers T1 and T2 were used as illustrated in Figure 7.15. We defined two rotations of the Tee joint: (i) one corresponding to the rotation, θ_L in the left; (ii) the other corresponding to the rotations, θ_R , in the right, as shown in Figure 7.15.

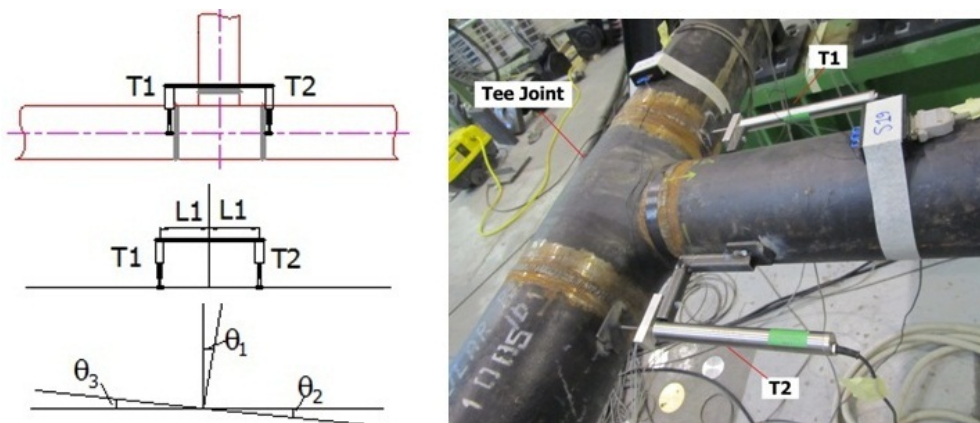


Figure 7.15: Measurement of rotations of the Tee joint.

θ_L and θ_R are defined as,

$$\theta_L = \theta_1 - \theta_3 \quad (7.1)$$

$$\theta_R = \theta_1 - \theta_2 \quad (7.2)$$

where, θ_1 , θ_2 and θ_3 are the clockwise rotations of the three branches of the Tee joint shown in Figure 7.15.

We could then define rotations of the Tee joint as,

$$\tan\theta_L = \frac{T1}{L1} \quad (7.3)$$

$$\tan\theta_R = \frac{T2}{L1} \quad (7.4)$$

where, L_1 is the distance equal to 200 mm as shown in Figure 7.15.

Rotations of the most critical elbow, i.e., Elbow #2 were measured using three displacement transducers, T3, G2 and G3 as illustrated in Figure 7.16. The relative rotations of an end point of Elbow #2 were measured and defined as the rotations of this elbow, θ .

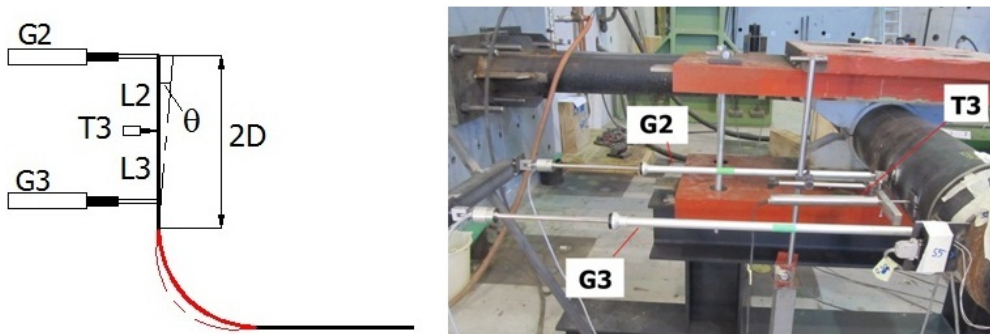


Figure 7.16: Measurement of rotations of Elbow #2.

The relative rotations, θ can be measured in different ways using these three displacement transducers which are defined as follows:

$$\tan\theta = \frac{G2-T3}{L2} \quad (7.5)$$

$$\tan\theta = \frac{T3-G3}{L3} \quad (7.6)$$

$$\tan\theta = \frac{G2-G3}{(L2+L3)} \quad (7.7)$$

where $G2$, $G3$ and $T3$ are the measurements of displacements by transducers, $G2$, $G3$ and $T3$, respectively; distances, $L2$ and $L3$ are 170 mm and 150 mm, respectively.

Note that displacement transducer, $G2$, was placed at a distance equal to twice the outer diameter of the corresponding pipe from the end point of the elbow. This was done in order to be consistent with the FE model of the piping system where the end point of an elbow was placed at a distance twice the mean diameter of the pipe from the end point of the elbow. As a result, a comparison of the movements on this point could be made between numerical and experimental results.

7.5 Identification tests on the PS

Before carrying out the hybrid tests, we performed some Identification Tests (IDTs) on the PS in order to estimate some dynamic properties, e.g., eigenfrequencies, and to have an estimation of the actual damping to be used in the NS during the hybrid tests. The Eigensystem Realization Algorithm (ERA) developed by Juang and Pappa (1984) was used to identify dynamic properties of the specimen, using data obtained during identification tests. The ERA algorithm is a system identification technique used for system identification of many types of systems (William et al., 2003; Caicedo et al., 2004). ERA can be used as a modal analysis technique and generates a system realization using the time domain response multi-input and multi-output data. In order to carry out IDTs, we used a Matlab toolbox called Structural Dynamic Identification Toolbox (SDIT) (Ceravolo and Abbiati, 2009). Four IDTs as listed in Table 7.4 were carried out.

Table 7.4: Identification tests carried out on the physical substructure

Identification Tests	Description
IDT 1	Without water
IDT 2	With water and low pressure (0.1 MPa)
IDT 3	With water and pressure (3.2 MPa)
IDT 4	Long signal with water and low pressure (0.1 MPa)

As can be noted from Table 7.4, IDTs were performed both with and without the presence of water and pressure. In the second case, a low pressure was applied to avoid any movement of water inside pipes which might affect the identification results. A long IDT was carried out in the fourth case to identify the damping of the PS.

The test specimen was excited through hammer impacts on several positions. Locations of accelerometers and hammer impacts were decided based on a modal analysis of the PS. A total of 8 accelerometers were used in IDT 1 and 10 accelerometers were used in the other IDTs, as schematically depicted in Figure 7.17 and reported in Table 7.5. Locations of hammer impacts are shown in Figure 7.18 and potential excited modes due to these impacts are reported in Table 7.6. An accelerometer placed in the test specimen is shown in Figure 7.19(a). A National Instrumentation data acquisition system (DAQ) was used to carry out the IDTs.

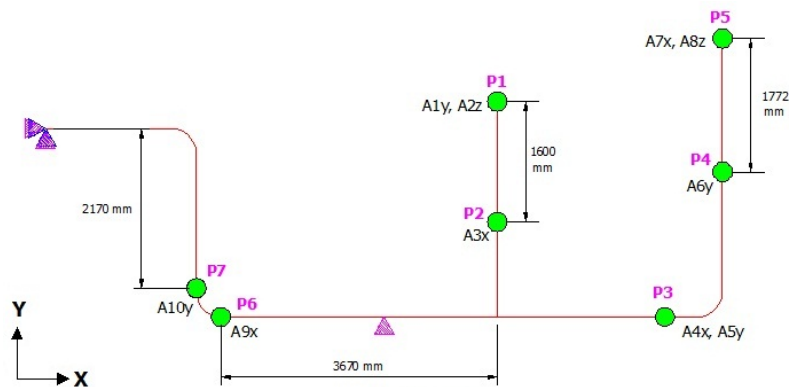


Figure 7.17: Positions of accelerometers in the test specimen.

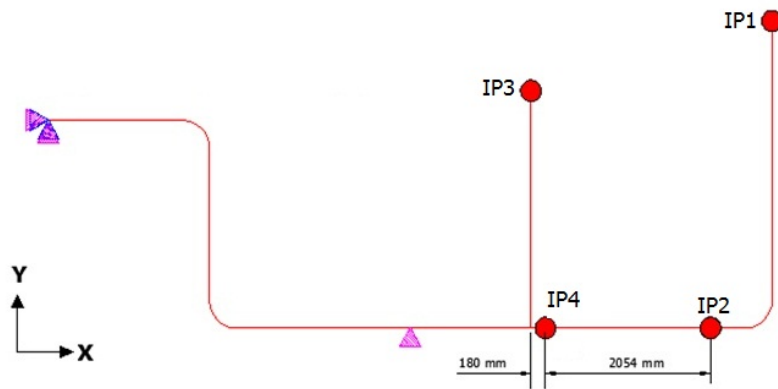


Figure 7.18: Points of hammer impacts.

Table 7.5: Positions and directions of accelerometers used in the identification tests

No	Positions	Accelerometer	Direction
1	P1	A1y	Y
2	P2	A2z	Z
3	P2	A3x	X
4	P3	A4x	X
5	P3	A5y	Y
6	P4	A6y	Y
7	P5	A7x	X
8	P5	A8z	Z
9	P6	A9x	X
10	P7	A10y	Y

Table 7.6: Points of hammer impact and relevant excited modes

Position	Impact Directions	Excited Modes
IP1	x	1,3,4
IP2	z	2
IP3	y	5,6
IP3	x	7,8
IP3	z	9
IP4	y	10



Figure 7.19: (a) Accelerometer, A4x; (b) hammer.

The first 10 modes (first 8 modes in case of IDT1) of the PS were confirmed through the IDTs. The eigenfrequencies and damping were estimated by the SDIT software utilizing the identification data acquired through the National Instrument DAQ. The estimated damping and frequencies from IDT1, IDT2 and IDT3 are summarized in Table 7.7, while the stabilization and cluster diagram from SDIT relevant to IDT3 are presented in Figure 7.20. One may note from Table 7.7 that, frequencies and damping ratios change, though not significantly, from the case without water to the case with water inside pipes. We see that introduction of water in the pipe reduced the frequencies to some extent. However, the internal pressure corresponding to 3.2 MPa did not considerably affect frequencies and damping values identified from IDT2 and IDT3.

Table 7.7: Summary of results of identification tests

Identified Mode	Frequency (Hz)			Damping		
	IDT1	IDT2	IDT3	IDT1	IDT2	IDT3
1	4	3.41	3.46	0.0048	0.0059	0.003
2	7.01	5.55	5.54	0.0032	0.012	0.0016
3	7.98	7.17	7.23	0.0151	0.0018	0.002
4	8.74	8.94	7.54	0.0033	0.0193	0.006
5	9.28	10.14	9.15	0.0124	0.012	0.0234
6	11,85	12.47	10.17	0.0022	0.0149	0.0125
7	12,21	14.38	12.58	0.002	0.0058	0.0051
8	14,15	16.68	14.46	0.0056	0.0024	0.0042
9	-	17.32	16.72	-	0.0145	0.001
10	-	-	18.19	-	-	0.0183

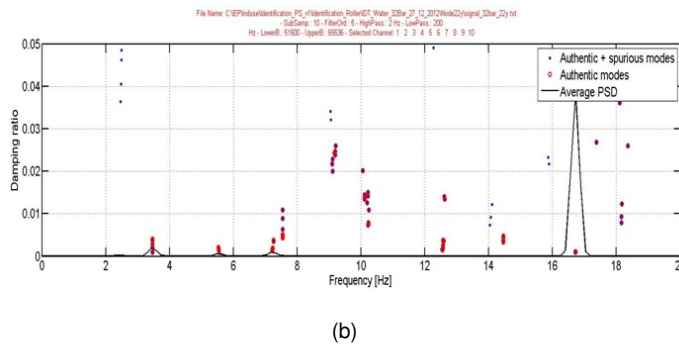
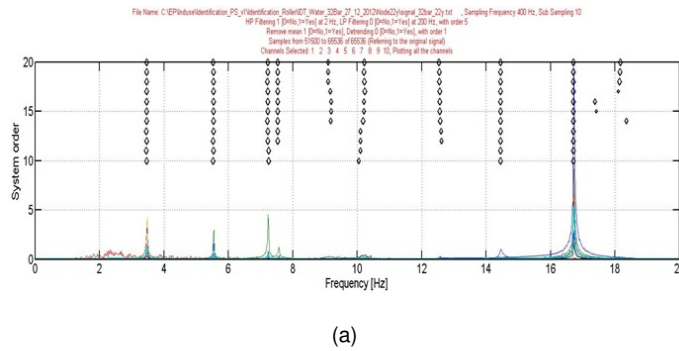


Figure 7.20: IDT3: (a) Stabilization diagram for frequency estimation; (b) Cluster diagram for damping estimation.

In case of IDT4 and in order to estimate the damping ratio of the PS through the Wigner-Ville time frequency transform (Classen and Mecklenbrauker, 1980), a 400s length signal was acquired at 400 Hz. Several hammer impacts were given to the specimen to acquire the long signal. The instantaneous damping of the PS estimated through the Matlab toolbox is presented in Figure 7.21. As can be noted from Figure 7.21, IDT4 confirmed an average damping ratio of about 0.5% of the test specimen which was in agreement with the outcome of ERA damping from the other IDTs. Hence, we decided to use this value of damping ratio to carry out experimental tests.

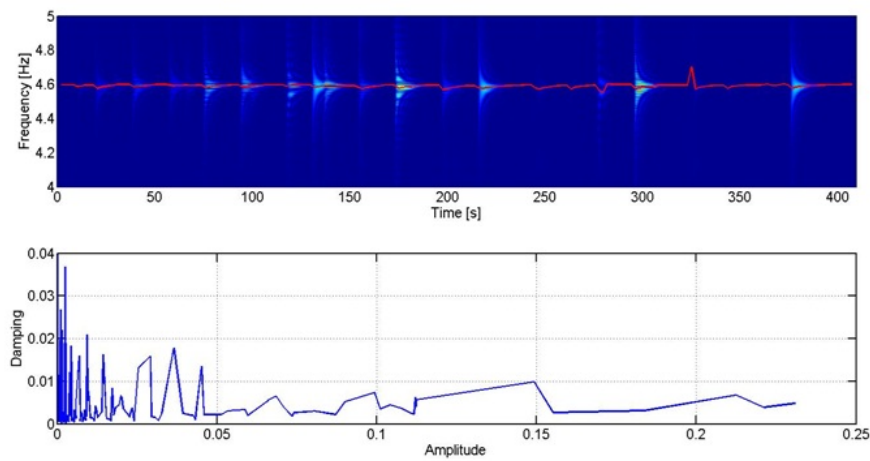


Figure 7.21: Estimation of damping using long signal acquired during IDT4.

7.6 Main observations and results from experimental tests

Experimental tests were carried out according to the test program presented in Table 7.1. All tests were performed in the horizontal x direction with an internal pressure of 3.2 MPa and considering a 0.5% damping identified through IDTs described in Section 7.5.

7.6.1 Results of PDDS

As can be noted from Table 7.1, all experiments relevant to limit state earthquakes were performed by means of PDDS. A total of 5 PDDS were carried out using a time scale factor, $\lambda = 50$; λ is defined in Equation (2.13) of Chapter 2.

The piping system and its components exhibited a favourable performance under all limit state earthquakes. In fact, it was observed that, even under the Collapse Limit State (SLCT) earthquake, the piping system remained below its yield limits and no leakage occurred in any of the components. Elbow #2 was found to be the most stressed component in all tests. In this respect, strain histories of Elbow #2 at SLVT and SLCT are presented in Figure 7.22. One may note that the maximum strain at SLCT was about $950 \mu\text{m/m}$ which was well below the yield strain, i.e., $2019 \mu\text{m/m}$, of the corresponding elbow. Note that the same elbow was found to be the most stressed component from relevant numerical simulations as discussed in Subsection 6.5.2 of Chapter 6.

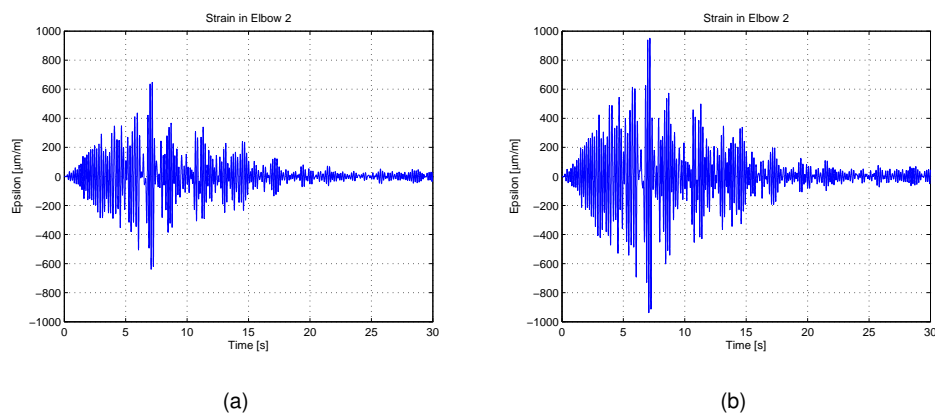


Figure 7.22: Strain histories in the flank of Elbow #2 at: (a) SLVT; (b) SLCT.

With regard to kinematic variables, limited rotations were observed in the elbows during the tests; the maximum being in Elbow #1 shown in Figure 7.3. A maximum rotation of about 7 millirad at SLCT was found in Elbow #1, as it can be noted from Figure 7.23. This level of rotation confirmed the elastic behaviour of the elbow as illustrated in Figure 7.24, in which a moment-rotation curve of the relevant elbow

found from an FE analysis -discussed in Section 6.4 of Chapter 6- is presented.

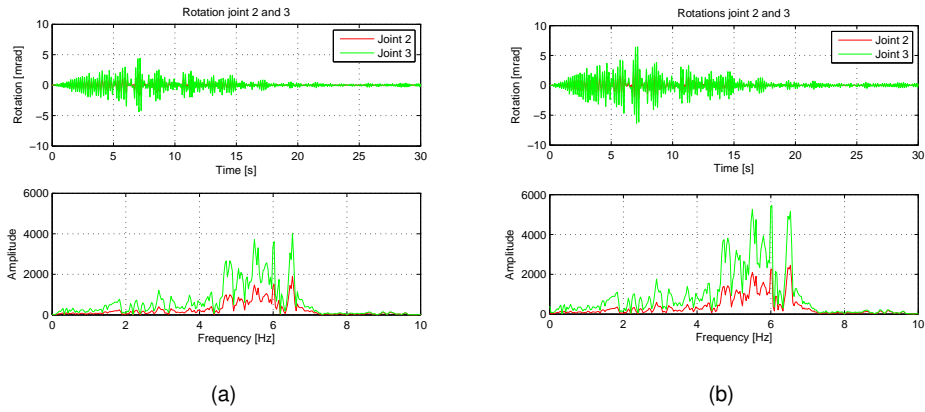


Figure 7.23: End node rotation histories and relevant Fourier spectra for Elbow #1 at: (a) SLVT; (b) SLCT.

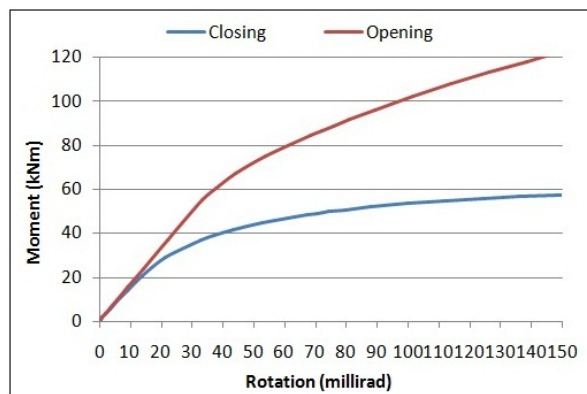


Figure 7.24: Moment-Rotation curve relevant to Elbow #1 obtained from an FE analysis.

With reference to the Tee joint, a small level of rotation was observed in all tests as depicted in Figure 7.25, where the right rotation of Tee joint, θ_R , defined in Equation (7.4), both at SLVT and SLCT are presented. A maximum rotation of about 1.6 millirad at SLCT can be noted. Similar left rotations, θ_L , defined in Equation (7.3) were observed. This level of rotation indicated that the Tee joint remained within its elastic range. In fact, in the 6" branch pipe of the Tee joint, the maximum strain obtained at SLCT, shown in Figure 7.26(b), was about $150 \mu\text{m}/\text{m}$ which is well below its yield strain, i.e., $2019 \mu\text{m}/\text{m}$.

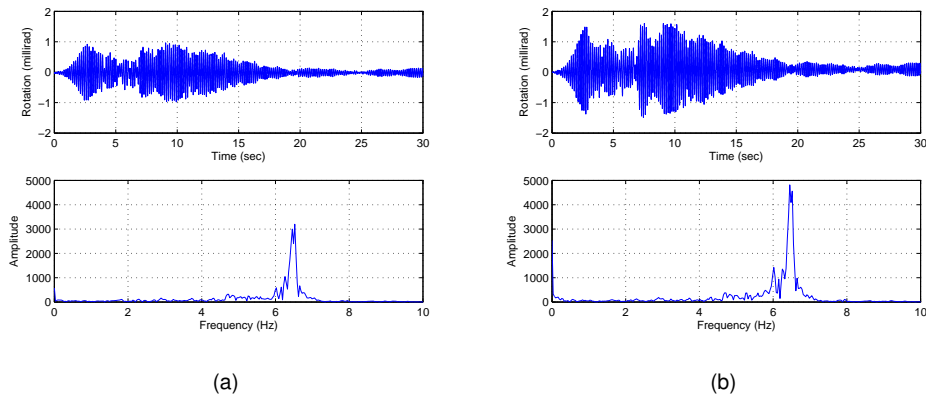


Figure 7.25: Rotation histories and relevant Fourier spectra of the Tee joint at: (a) SLVT; (b) SLCT.

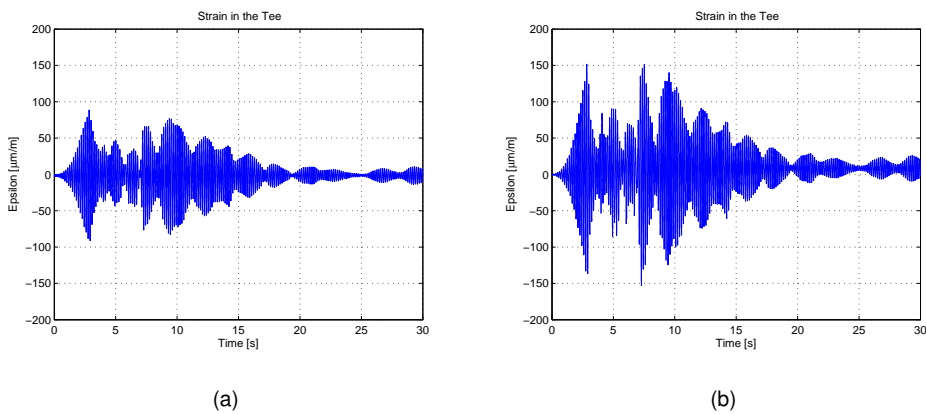


Figure 7.26: Strain histories in the 6" branch pipe of the Tee joint at: (a) SLVT; (b) SLCT.

During experimental tests, significant amplifications of input earthquake accelerations were found in the piping system as can be observed from Figure 7.28, where accelerations of Coupling Node #1 at SLVT and SLCT are presented. One may note that the maximum acceleration at SLCT was about twice of the corresponding input PFA.

The horizontal displacements of the piping system can be observed from Figure 7.27, in which displacement histories of Coupling Node #1 at SLVT and SLCT are illustrated; a maximum displacement of about 11 mm at SLCT can be noted. Moreover, Fourier spectra of the aforementioned figures illustrate that dynamic responses

of the piping system were dominated by its lower modes corresponding to frequencies of 5.87 Hz and 6.54 Hz.

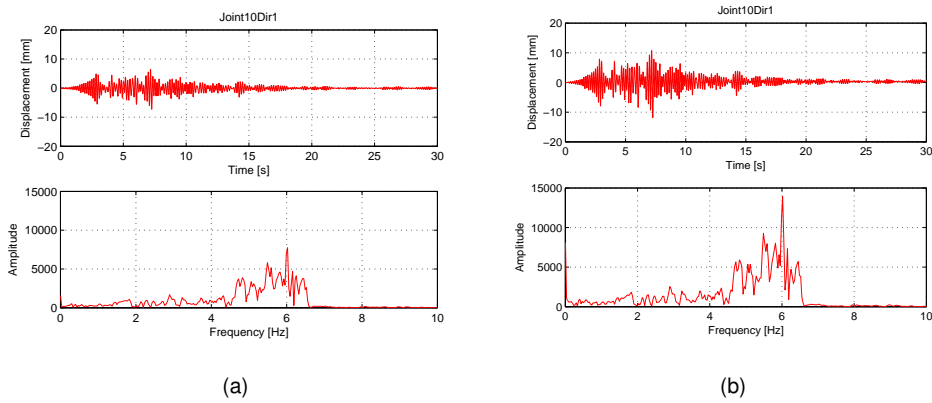


Figure 7.27: Displacement histories and relevant Fourier spectra of Coupling Node #1 at: (a) SLVT; (b) SLCT.

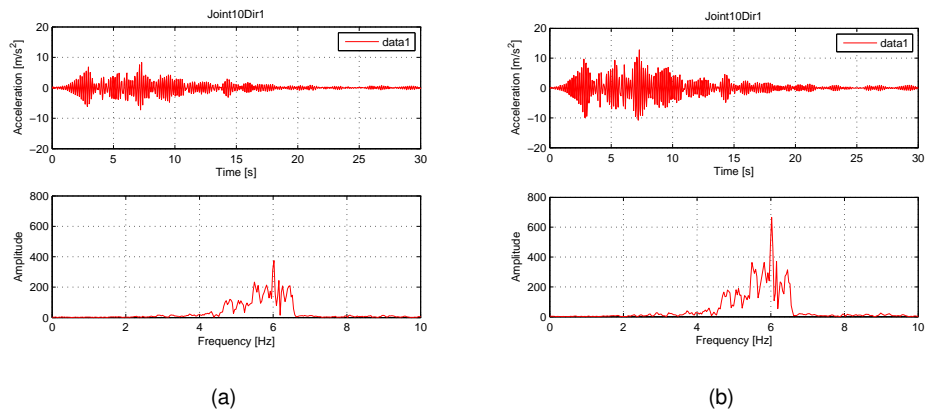


Figure 7.28: Acceleration histories and relevant Fourier spectra of Coupling Node #1 at: (a) SLVT; (b) SLCT.

Maximum absolute responses of the piping system and components in the PDDS are collected in Table 7.8. The increase of responses with respect to the increase of input PFAs is evident.

Table 7.8: Maximum responses of the piping system and components from PDDS

Maximum absolute response	Test				
	ET	SLOT	SLDT	SLVT	SLCT
PFA (m/s^2)	0.41	0.77	1.09	4.12	5.88
Strain in Elbow #2 (flank) ($\mu m/m$)	60	110	170	650	950
Rotation of Elbow #1 (millirad)	0.45	0.70	1.10	5.00	7.00
Rotation of the Tee joint (millirad)	0.11	0.18	0.26	0.98	1.60
Displacement of Coupling Node #1 (mm)	0.50	1.00	1.50	7.00	11.00
Acceleration of Coupling Node #1 (m/s^2)	0.60	1.10	1.80	8.00	12.00

A comparison between numerical and experimental results was made for all tests. This is depicted in Figure 7.29, where experimental displacements of Coupling Node #2 at SLVT and SLCT are compared with relevant simulation results; a good agreement can be noted for both time histories and relevant Fourier spectra. In particular, a value of normalised RMS error, e_{RMS} -calculated according to Equation (6.9) defined in Chapter 6- between these numerical and experimental results was found to be about 2% and 11%, at SLVT and SLCT, respectively. However, a small difference between the two responses can be observed from Figure 7.29; the numerical displacements were found to be a little higher than those found from experiments. This happened owing to the presence of the supports and 1000 kg masses which, due to friction, dissipated some energy; the effect of friction was neglected in the numerical model. Nevertheless, the above-mentioned agreement between numerical and experimental results justified the effectiveness of the CB reduction technique for the PDDS, as analytically predicted in Subsection 6.9.1.

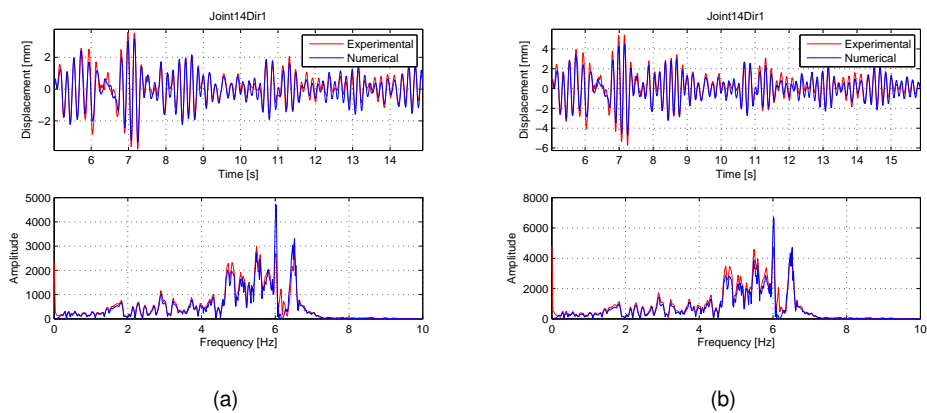


Figure 7.29: Displacement histories and relevant Fourier spectra of Coupling Node #2 at (a) SLVT; (b) SLCT (Red- Experimental; Blue- Numerical).

7.6.2 Results of RTDS

As discussed in Section 6.10 of Chapter 6, in order to obtain a real time compatible system, the FE model of the piping network was modified. Two RTDS -namely RT1 and RT2- were carried out on this modified structure with a low PFA earthquake level, i.e., 0.02g, as reported in Table 7.1. In particular, RT1 and RT2 were conducted using the SEREP2 and CB reduction techniques, respectively. The aim of these tests was to experimentally validate the RTDS test algorithm and to test the effectiveness of the SEREP2 and CB reduction techniques.

Displacement, velocity and acceleration histories and relevant Fourier spectra of the two coupling joints corresponding to test RT1 are presented in Figure 7.30, Figure 7.31 and Figure 7.32, respectively. A maximum displacement of about 3.4 mm and 5.3 mm were observed in Coupling Node #1 and Coupling Node #2, respectively. It can be noted from Figure 7.32, that the input PFA was amplified about three times in Coupling Node #2. Moreover, one may observe from relevant Fourier spectra that the system's responses were dominated by the lower modes corresponding to frequencies 0.78 Hz and 1.10 Hz.

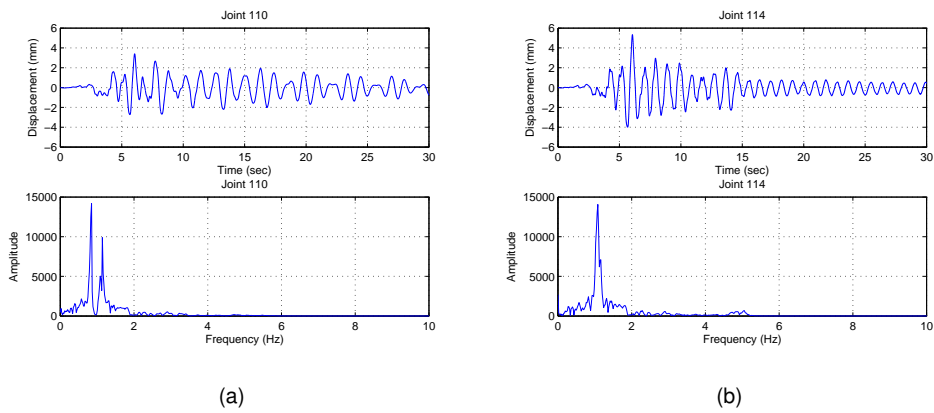


Figure 7.30: Displacement histories and relevant Fourier spectra of (a) Coupling Node #1; (b) Coupling Node #2 at RT1.

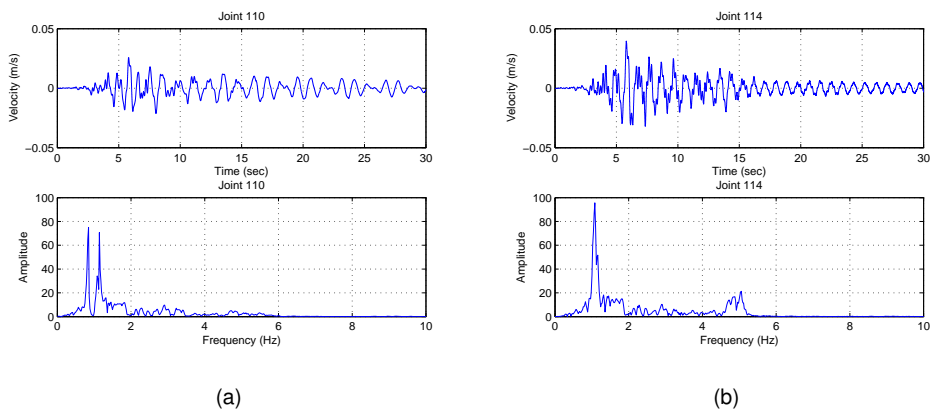


Figure 7.31: Velocity histories and relevant Fourier spectra of (a) Coupling Node #1; (b) Coupling Node #2 at RT1.

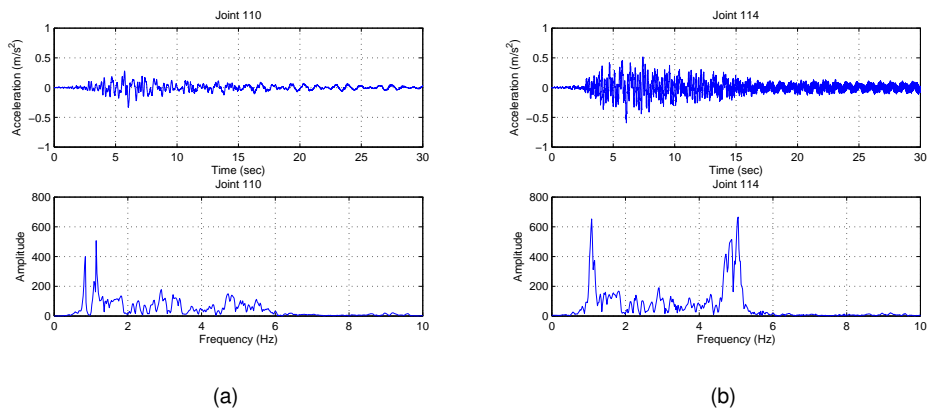


Figure 7.32: Acceleration histories and relevant Fourier spectra of (a) Coupling Node #1; (b) Coupling Node #2 at RT1.

A similar response of the system was found from RT2 as can be noted from Figure 7.33 - Figure 7.35, in which displacement, velocity and acceleration histories and relevant Fourier spectra of the two coupling joints are presented. A maximum displacement of about 3.4 mm and 5.3 mm were observed in Coupling Node #1 and Coupling Node #2, respectively. The input PFA was amplified about three times in Coupling Node #1 as illustrated in Figure 7.35. Moreover, relevant Fourier spectra depict that the lower modes corresponding to frequencies 0.78 Hz and 1.10 Hz governed the system's responses.

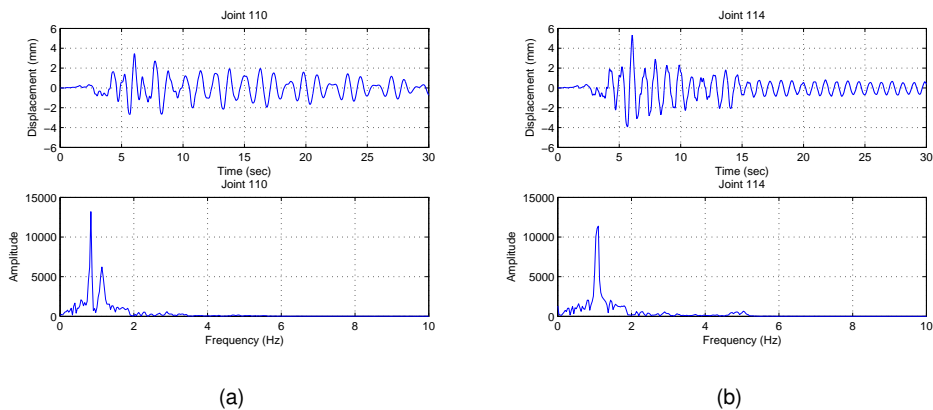


Figure 7.33: Displacement histories and relevant Fourier spectra of (a) Coupling Node #1; (b) Coupling Node #2 at RT2.

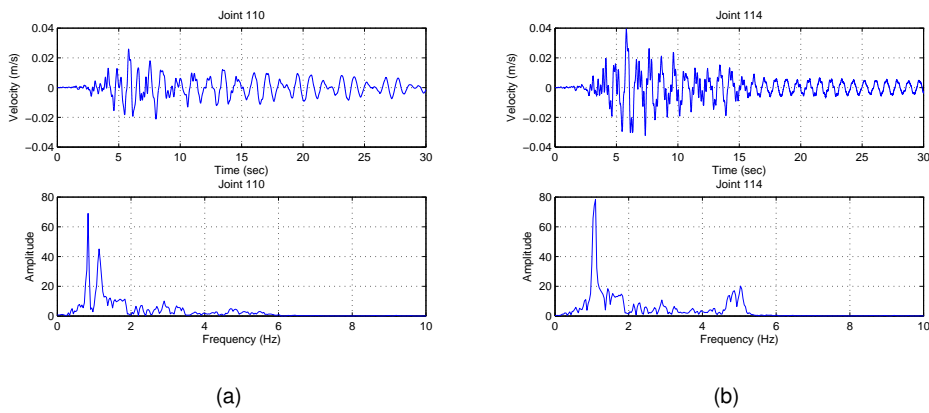


Figure 7.34: Velocity histories and relevant Fourier spectra of (a) Coupling Node #1; (b) Coupling Node #2 at RT2.

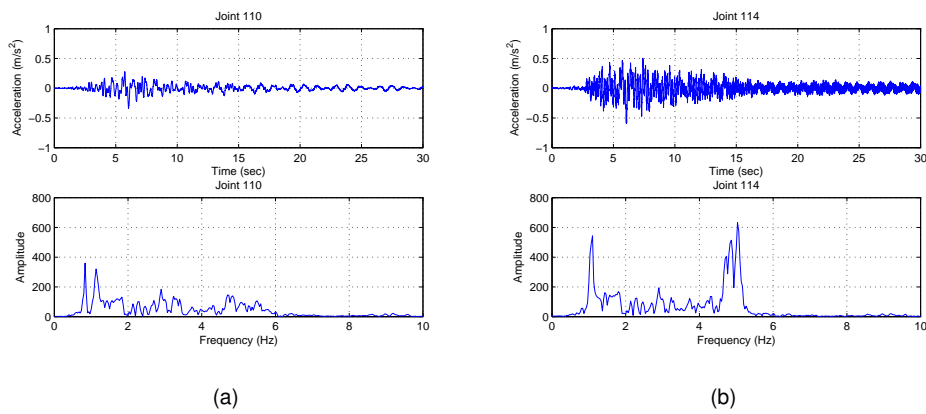


Figure 7.35: Acceleration histories and relevant Fourier spectra of (a) Coupling Node #1; (b) Coupling Node #2 at RT2.

The effect of delay present in the transfer system, as discussed in Section 5.3 of Chapter 5, was compensated through the delay overprediction method presented in Subsection 6.8.2 of Chapter 6. This is illustrated in Figure 7.36 where displacement time history of Coupling Node #1 at RT1 is presented with the desired, command, feedback and optimum signals. A careful reader may note that the optimum and desired signals overlap indicating a nearly perfect compensation of the delay.

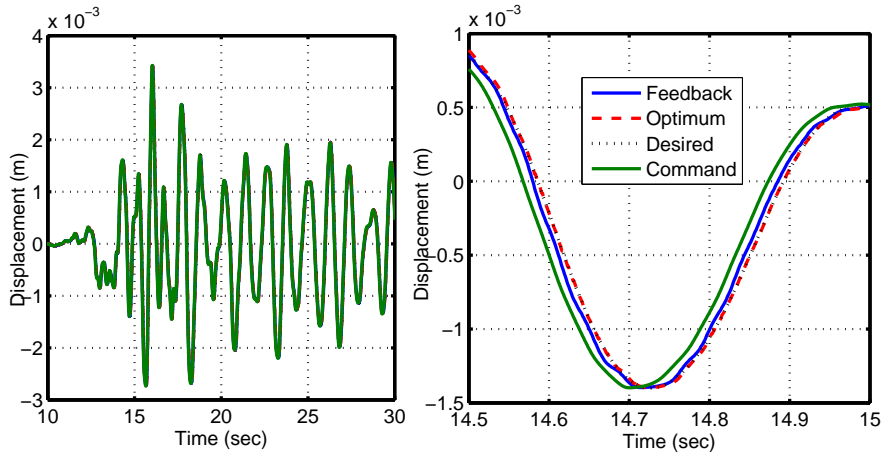


Figure 7.36: Experimental delay compensation.

In order to appreciate the effectiveness of the SEREP2 and CB reduction techniques, a comparison between numerical and experimental responses was made. It entailed a favourable agreement as depicted in Figure 7.37 and Figure 7.38, in which displacement time histories and relevant Fourier spectra of the two coupling nodes obtained from RT1 and RT2, respectively, are presented. A value of e_{RMS} , defined in Equation (6.9), between time histories of the two responses was found to be about 38% and 28% in Coupling Node #1 and Coupling Node #2, respectively in RT1. In case of RT2, the value of e_{RMS} was about 38% and 31% in Coupling Node #1 and Coupling Node #2, respectively. No significant frequency shift between the responses are observed from relevant Fourier spectra. However, like in PDDS, one may observe that numerical responses were a bit higher than experimental ones. This happened owing to the energy dissipation by support friction during experimental tests. As a result, the experimental test specimen exhibited the presence of a higher damping than that considered in the numerical model. Thus, effectiveness of the SEREP2 and CB reduction technique for the RTDS was experimentally justified.

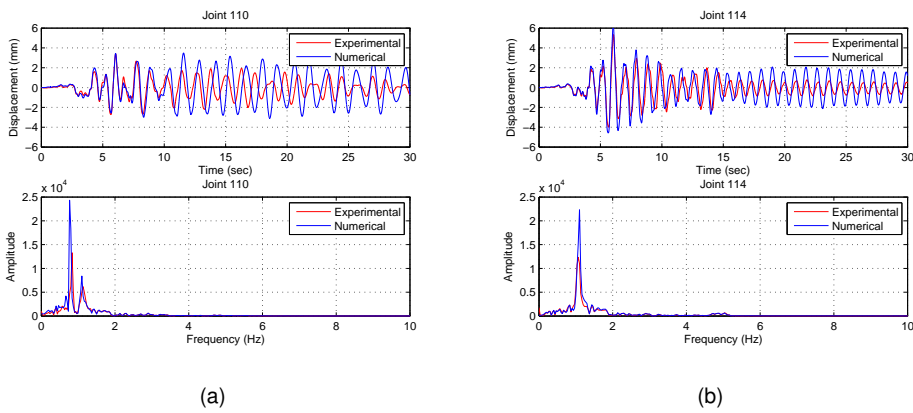


Figure 7.37: Displacement histories and relevant Fourier spectra of (a) Coupling Node #1; (b) Coupling Node #2 at RT1 (Red- Experimental; Blue- Numerical).

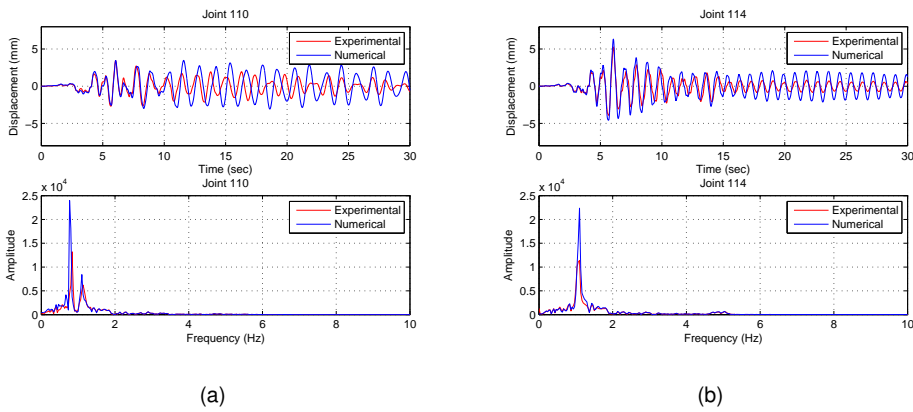


Figure 7.38: Displacement histories and relevant Fourier spectra of (a) Coupling Node #1; (b) Coupling Node #2 at RT2 (Red- Experimental; Blue- Numerical).

7.7 Conclusions

A pseudo-dynamic and real time test campaign carried out on a full-scale piping system was presented in this chapter. A number of identification tests were also carried out in order to identify some dynamic properties of the PS. A 0.5% damping ratio found through the identification tests was used during the experimental tests.

In detail, several PDDS and RTDS on the piping system were performed under different levels of earthquake PGAs corresponding to serviceability and ultimate limit

states suggested by performance-based Italian Standards. Experimental and numerical results showed a good agreement in all tests. The experimental test specimen was found to be a bit stiffer than numerical model mainly due to the presence of friction in the supports and masses which was difficult to take into account in the numerical model. Nevertheless, successful executions of these tests justified the effectiveness of the CB and SEREP2 reduction techniques for the PDDS and RTDS. In addition, effectiveness of the delay overprediction method was also proved during the RTDS.

A favourable seismic performance of the piping system was observed during the experiments. It was found that, even under the Collapse Limit State level earthquake, both the piping system and its critical components did not fail or yield while no leakage was observed in any of the components. Note that such behaviour of piping system is desirable under strong earthquakes. We, therefore, conclude that present seismic design rules for piping systems and components are conservative and proper and justified amendments would overcome some degree of conservatism.

CHAPTER 8

SUMMARY, CONCLUSIONS AND FUTURE PERSPECTIVES

8.1 Summary

This thesis has dealt with the seismic safety assessment of an industrial piping system and some of its components through numerical and experimental activities. In particular, it pursued the following issues: (i) design of two non-standard bolted flange joints suitable for seismic applications; (ii) experimental testing of the designed flange joints under monotonic and cyclic loading, in order to check their leakage, bending and axial capacities; (iii) finite element analysis of a piping system containing several critical components under seismic loading; (iv) implementation of a pseudo-dynamic and real time testing schemes to test the piping system under seismic loading; and (v) pseudo-dynamic and real time tests on the piping system under several levels of earthquake loading corresponding to serviceability and ultimate limit states.

In order to achieve a better performance under seismic loading, two non-standard bolted flange joints comparatively thinner than the standard ones were designed. Initial dimensions of the flanges were taken from Eurocode EN 1092-1 to be used with an 8" connecting pipe under regular operating conditions of a petrochemical industry. The thickness of this standard flange was then reduced based on Mode 1 and Mode 2 failures according to structural Eurocode EN 1993-1-8. Dimensions of other components of the BFJs were selected from relevant European standards. Materials compatible with design operating conditions were chosen for different components of the flange joints. A calculation on the designed BFJs according to the new European standard EN 1591-1 was then performed to check their mechanical integrity

and leak-tightness performance.

A number of experimental tests were carried out on the designed non-standard BFJs under monotonic and cyclic loading in order to investigate their bending and axial capacity and performance. A moderate internal pressure of 1.5 MPa -which was 50% of a regular operating pressure used in a typical petrochemical industry- was used in all the tests. A total of eight experiments including four bending and four axial tests were performed. The monotonic tests were mainly performed to estimate the maximum capacity and to find required parameters to build ECCS45 loading protocols to be used for cyclic tests. Test specimens were constructed by placing the flange joints in the middle of two connecting pipes. Loading were applied to the test specimens by means of MOOG actuators with the capacity of 1000 kN. During the bending tests, loading were applied till the failure of the test specimens; whereas, the maximum level of loading during axial tests was limited by the capacity of actuators. A detail analysis on the experimental results was conducted and performance of the designed BFJs was discussed. Experimental results were compared with the allowable, yield and ultimate loads suggested by Codes. A comparison was also made between the capacity of the designed joints and the seismic demands on such joints coming from a Case Study performed on a petrochemical piping system.

A numerical and experimental investigation was undertaken on a typical industrial piping system at full scale in order to assess its performance under realistic seismic loading. The piping system contained several critical elements including some elbows, a bolted flange joint and a Tee joint. It was filled with water with an internal pressure of 3.2 MPa corresponding to 80% of the maximum allowable pressure of the piping system. An FE model of the piping system was developed in SAP2000 software to carry out numerical analyses. Elbow elements were modelled as equivalent straight elements having the flexibility properties found from an ABAQUS-based FE analysis. To define a realistic input earthquake loading for the analyses and experimental tests, a typical steel support structure for the piping system was designed to generate filtered earthquake accelerogram on its elevated floors. The structure was considered to be placed in a highly seismic-prone area. By imposing an earthquake - to the base of the structure- corresponding to the Safe Life Limit State, an appropriate input earthquake was evaluated on the elevated floor where the piping system rested.

In order to comply with performance-based earthquake engineering Standards, PGA of the reference earthquake was magnified corresponding to both serviceability and ultimate limit states. Time history analyses were carried out in SAP2000 using the input accelerograms and results were discussed.

The techniques of pseudo-dynamic and real time testing with dynamic substructuring were adopted to carry out experimental activities on the piping system under seismic loading. The challenging implementations of these techniques on the piping system were presented step-by-step. In particular, the substructuring technique and strategies to minimize the error due to substructuring were shown. During substructuring of the piping system, the two coupling nodes were chosen based on the values of minimum bending moment in the pipes in the direction of the input earthquake loading. The LSRT2 integration scheme and delay overprediction method were presented. A number of model reduction techniques and their uses in the reduction of the PS and earthquake forces were described. Effectiveness of different reduction methods for the PDDS and RTDS were analysed and validation of test algorithms using the reduction methods were illustrated. A characterization of the MOOG actuators based on a transfer function to be used for the PDDS and RTDS was performed and shown. Identification of the actuator transfer function was performed using a Matlab toolbox embedded with the ARX algorithm.

Experimental tests on the piping system under several levels of earthquake loading corresponding to serviceability and ultimate limit states were conducted through PDDS and RTDS. Experimental results for each test were reported and compared with simulation results. A detail discussion was offered on the performance of the piping system under different limit state earthquake loading suggested by Standards.

8.2 Conclusions

An appraisal of seismic performance of a typical full-scale industrial piping system and some of its critical components was carried out in this thesis. Both numerical and experimental activities were performed in order to conduct this evaluation.

The non-standard BFJs that were designed in Chapter 3 based on structural Eu-

rocode were comparatively thinner than standard joints. A design check according to EN 1591-1 was made and found that these BFJs did not satisfy the mechanical integrity and leak-tightness criteria according to this Standard under design operating conditions. The experimental program on non-standard BFJs was described in Chapter 4. It was found during the experimental tests that both the designed BFJs exhibited favourable performance when subjected to bending and axial loading under moderate pressure. Experimental results proved that the joints possessed good capacity in terms of strength, ductility and energy dissipation. Almost no degradation of the joints in cyclic loading was observed and no failure occurred in any of the joints. In all tests, leakage was observed for a high level of loading.

During cyclic bending tests, failure took place in the pipe wall, where local buckling was observed. The axial resistance of the BFJs was very high and axial loading were applied by means of two MOOG actuators, with a capacity of 1000 kN each. Nevertheless, due to the capacity of the actuators, we were limited to a maximum axial load of 2000 kN. With this level of maximum axial load, test specimens remained within its elastic limit while very small levels of flange displacement were found. To assess a low cycle fatigue behaviour of the BFJs in axial loading, once the limit load of the actuators was reached, we continued several cycles of loading with the maximum displacement attained. Nevertheless, no failure or yielding occurred in the flanges or in any part of the joints.

The comparison between experimental results and Coded loads displayed a good performance of non-standard BFJs with moderate internal pressure. Allowable seismic design loads calculated according to design Codes were considerably lower than experimental leakage and yielding loads. The levels of earthquake demands on a piping system found from a realistic Case Study where non-linearities were considered was significantly lower than the capacity of the designed joints. Thus, the non-standard BFJs were considered suitable for regular seismic applications. Hence, they could be used in piping systems operating both under normal conditions and under seismic events.

In Chapter 5, a characterization of the MOOG actuators used in the PDDS and RTDS was shown based on its transfer function. The transfer function was found to

be invariant with the level of mass attached to it. By means of tuning the gains of the PID controller, an optimum response of the actuators was adjusted. It was found that, owing to several factors such as the capacity of hydraulic power and actuator size, the maximum achievable strokes of the actuators depended on the frequency at which they operated; an increase in the frequency significantly reduced the maximum displacements of the actuators.

Implementations of the PDDS and RTDS on the piping system were presented in Chapter 6. These implementations were challenging mainly because the piping system was a structure with distributed masses and it was subjected to distributed earthquake forces. Until now, the pseudo-dynamic technique has been considered inadequate to test systems with distributed masses. In this respect, this work brought a novelty in the pseudo-dynamic testing technique by enabling its applications to structures having distributed masses. Application and effectiveness of a number of model reduction techniques were presented in order to reduce the PS in the two coupling nodes. The Craig-Bampton reduction method was found to be suitable for the PDDS. This method allowed to consider both the static and dynamic properties of the PS to be retained in the reduced model. The SEREP2 reduction technique was considered suitable for real time tests in which only the earthquake forces needed to be condensed.

Due to the incompatibility of MOOG actuators in real time testing of the piping system with high level of amplitudes, the FE model of the piping system was modified by adding masses in the nodes of the NS thus reducing the eigenfrequencies of the piping system. In this way, we were capable of conducting RTDS with small level of earthquake PGAs considering a different system. Both PDDS and RTDS algorithms were validated through numerical simulations using relevant reduction methods.

The experimental program on the piping system was detailed in Chapter 7. Several PDDS and RTDS were successfully carried out on the piping system under different limit state earthquake loading. A good agreement between experimental and numerical results was found in all tests. Effectiveness of the CB and SEREP2 reduction techniques were experimentally justified both for the PDDS and RTDS. Moreover, experimental results exhibited a good seismic capacity of the piping system and its

components. It was found that, even with the earthquake corresponding to the Collapse Limit State, the piping system remained in the elastic region while no leakage was observed in any of the components. Small levels of rotations and strains were observed both in the elbows and in the Tee joint.

A favourable seismic capacity of the piping system was thus evident. Similar results were also reported in several past researches conducted on these types of structures. It was, therefore, concluded that the piping system and its components under investigation remained safe under limit state earthquake levels suggested by Standards. Thus, we concluded that seismic design rules provided by available Codes and Standards for piping systems and components were over-conservative and proper amendments could overcome some degree of conservatism.

8.3 Future perspectives

The following future developments are envisioned relevant to the investigated issues.

Although the designed non-standard BFJs showed favourable performances during the experimental tests, note that the experiments were carried out only in one operating condition. In particular, a moderate internal pressure of 1.5 MPa was considered for the experiments. To complete the investigation, performance of the BFJs under different operating conditions, e.g., at the actual operating pressure, should also be investigated. In addition, other combination of loading, e.g., bending and axial, can also be used to assess the performance of the flange joints. Moreover, in axial tests, the maximum level of applied load was incapable of producing a failure or yielding in the test specimens. In order to observe the failure and/or yielding behaviour of the BFJs under axial loading, experiments should be carry out with higher levels of loading. This ought to be done by increasing the number of actuators or by using actuators with higher capacities.

As mentioned earlier, during pseudo-dynamic and real-time tests, the numerical model of the piping system was considered elastic during the experimental tests. The CB and SEREP2 reductions of the Physical Substructure were performed in the

linear range and the reduced model of the PS was not updated during experimental tests. However, if the experimental structure entered into the non-linear region, this assumption would not hold. Nonetheless, assuming no mass changes, both stiffness and eignemodes can be updated between two successive tests. As a result, a more complete investigation of the piping system under seismic loading could be performed by updating the linear reduced model of the PS.

Differently from the reduction methods used during experimental tests which preserved modal properties of the original system, there exist reduction techniques which were developed from a perspective of control engineering. An example of such a model reduction technique is the so called "gramian based approach" developed by Hahn and Edgar (2002) for the reduction of linear/non-linear control systems. This technique reduces non-linear systems while retaining most of the input-output properties of the original system. It is based on empirical gramians that capture the non-linear behaviour of the system near an operating point. The resulting reduced-order model is non-linear, and has input and output suitable for control. This kind of reduction method could be employed for the PDDS and RTDS for a better control of desired output, e.g., elbow rotations, using input forces. As a result, a more reliable response of the piping system could be attained.

Regarding the RTDS, due to actuator limitations previously discussed, the piping system model was modified in order to obtain a real time compatible structure. Thus, RTDS were carried out considering a structure partly different from the original piping system and under small level of earthquake PGA. By overcoming this limitation, e.g., by increasing hydraulic power or by using smaller actuators, the proposed numerical techniques would allow for carrying out the RTDS on the original piping system even for severe limit state earthquake loading.

BIBLIOGRAPHY

- Abid M. and Nash D. H., 2006. Joint relaxation behaviour of gasketed bolted flanged pipe joint during assembly. Proceedings of the 2nd WSEAS Int. Conference on Applied and Theoretical Mechanics, Venice, Italy, November 20-22, 2006.
- Abid M. and Nash D. H., 2003. Comparative study of the behaviour of conventional gasketed and compact non-gasketed flanged pipe joints under bolt up and operating conditions. International Journal of Pressure Vessels and Piping 80 (2003) 831841.
- Abid M., Khan K. A., Chattha J. A. and Nash D. H., 2011a. Leakage analysis of gasketed flanged joints under combined internal pressure and thermal loading. Proceedings of the ASME 2011 Pressure Vessels & Piping Division Conference PVP2011, July 17-21, 2011, Baltimore, Maryland, USA.
- Abid M., Khan K. A. and Chattha J. A., 2011b. Performance testing of a gasketed bolted flange Pipe joint under combined pressure and thermal loading. November/December 2011, Experimental Techniques.
- Ahmadizadeh M., Mosqueda G. and Reinhorn A. M., 2008. Compensation of actuator delay and dynamics for real-time hybrid structural simulation. Earthquake Engineering and Structural Dynamics 2008; 37(1):2142.
- American Lifelines Alliance, 2002. Seismic Design and Retrofit of Piping Systems, 2002.
- ANSYS, 2007. Release 11.0 documentation for ANSYS. Online Manual, ANSYS, Inc.
- ANSI/ASME B16.1, 2005. Gray Iron Pipe Flanges and Flanged Fittings: Classes 25, 125, and 250.

ANSI/ASME B16.20, 2007. Metallic Gaskets for Pipe Flanges: Ring-Joint, Spiral-Wound, and Jacketed.

ANSI/ASME B16.21, 2005. Nonmetallic Flat Gaskets for Pipe Flanges.

ANSI/ASME B16.24, 2006. Cast Copper Alloy Pipe Flanges and Flanged Fittings: Classes 150, 300, 600, 900, 1500 and 2500.

ANSI/ASME B16.34, 2009. Valves Flanged, Threaded and Welding End.

ANSI/ASME B16.48, 2009. Valves Flanged, Threaded and Welding End.

ASCE 7-02, 2002. Minimum Design Loads for Buildings and Other Structures, American Society of Civil Engineers / 01-Dec-2002 / 352 pages.

ASCE7-05, 2006. Minimum Design Loads for Buildings and Other Structures, American Society of Civil Engineers.

ASCE, Committee on Gas and Liquid Fuel Lifelines, 1984. Guidelines for the seismic design of oil and gas pipeline systems. American Society of Civil Engineers, New York, N.Y.

Asfura A. and Kiureghian, A. D., 1986. Floor response spectrum method for seismic analysis of multiply supported secondary systems. Earthquake Engineering and Structural Dynamics, 14: 245265. doi: 10.1002/eqe.4290140206.

ASME B16.42, 1998. Ductile Iron Pipe Flange and Flanged fittings- class 150 and 300.

ASME B16.47, 2006. Large Diameter Steel Flanges, NPS 26 through NPS 60.

ASME B16.5, 2009. Pipe Flanges and Flanged Fittings.

ASME B18.2.1, 2010. Square, Hex, Heavy Hex and Askew Head Bolts and Hex, Heavy Hex, Hex Flange, Lobed Head, and Lag Screws (Inch Series).

ASME B18.2.2, 2010. Nuts for General Applications: Machine Screw Nuts, Hex, Square, Hex Flange and Coupling Nuts(Inch Series).

ASME B18.2.5M, 2009 Metric 12-Point Flange Screws.

ASME B31.1, 2001. Power Piping.

ASME B31.3, 2006. Process Piping.

ASME B31.4, 2002. Pipeline Transportation Systems for Liquid Hydrocarbons and Other Liquids.

ASME B31.8, 2003. Gas Transmission and Distribution Piping Systems.

ASME Boiler and Pressure Vessel Code, Code Case N-411-1, 1986. Alternative Damping Values for Response Spectra Analysis of Class 1, 2 and 3 Piping. Section III, Division 1, American Society of Mechanical Engineers, New York, February 20, 1986.

ASME PCC-1, 2010. Guidelines for pressure boundary bolted flange joint assembly.

ASME Section I, 2010. Rules for Construction of Power Boilers.

ASME Section III, 2007. Components Rules for Construction of Nuclear Facility Components.

ASME Section III Division 1, 2002. Rules for Construction of Nuclear Facility Components, NB 3600 Edition 2002.

ASME Section V, 2001. ASME Boiler and Pressure Vessel Code, NY, USA.

ASME Section VIII Division 1, 2007. Rules for Construction of Pressure Vessels.

ASME Section VIII Division 2, 2007. Alternative Rules - Rules for Construction of Pressure Vessels.

ASME Section VIII Division 3, 2010. Alternative Rules for Construction of High Pressure Vessels.

Azizpour O., Hosseisni M., 2009. A verification of ASCE Recommended Guidelines for seismic evaluation and design of combination structures in petrochemical facilities. Journal of Applied Sciences.

Blach A. E., and Bazergui A. B., 1981. Methods of Analysis of Bolted Flanged Connections-A Review. Welding Research Council, Bulletin 271, New York.

- Blakeborough A., Williams M. S., Darby A. P., and Williams, D. M., 2001. The development of real-time substructure testing. *Philosophical Transaction of the Royal Society: Theme Issue on Dynamic Testing of Structures*, A 359: 1869-1891.
- Blay N., Touboul F., Blanchard M. T., Breton L., 1997. Piping seismic design criteria: experimental evaluation. *Transactions of the 14th International Conference on Structural Mechanics in Reactor Technology (SMiRT 14)*, Lyon, France, August 17-22, 1997.
- Bonelli A. and Bursi O.S., 2004. Generalized- α methods for seismic structural testing. *Earthquake Engineering & Structural Dynamics*, 2004, Vol. 33, Issue 10, pp. 1067-1102.
- Buonopane S., 1997. Seismic Evaluation of a Masonry In-filled Reinforced Concrete Frame by Pseudo Dynamic Technique. M.S. Thesis, School of Civil and Environmental Engineering, Cornell University, Ithaca, New York, 1997.
- Bursi O. S., Jia C., Vulcan L., Neild S. A., Wagg D. J., 2011. Rosenbrock-based algorithms and subcycling strategies for real-time nonlinear substructure testing. *Earthquake Engineering and Structural Dynamics*, 40, 1, 2011, 1-19.
- Bursi O. S., Buelga A. G., Vulcan L., Neild S. A., Wagg D. J., 2008. Novel coupling Rosenbrock-based algorithms for real-time dynamic substructure testing. *Earthquake Engineering and Structural Dynamics*, 2008; 37:339360.
- Bursi O.S., Aribert J.M., Lachal A., 2002. Energy-based Damage Models in Seismic Analysis of Steel-Concrete Composite Members. 12th European Conference on Earthquake Engineering, London, September, 2002.
- Bursi O.S. and Jaspart J.P., 1997. Benchmark for Finite Element Modelling of Bolted Steel Connections. *Journal of Constructional Steel Research*, Voi. 43, n. 1-3, 1997, 17-42.
- Bursi O. S., Shing P. B., 1996. Evaluation of some implicit time-stepping algorithms for pseudo dynamic tests. *Earthquake Engineering and Structural Dynamics*, 25(1996) 333-55.

- Caicedo J. M., Dyke S. J. and Johnson E. A., 2004. Natural Excitation Technique and Eigensystem Realization Algorithm for Phase I of the IASC-ASCE Benchmark Problem: Simulated Data. *Journal of Engineering Mechanics* 130 (1).
- Cardone D., Cesare A. D., Ponzo F. C. and Blonna C., 2008. Evaluation of Behaviour Factor for Flag-Shaped Hysteretic Models. *EngOpt 2008 - International Conference on Engineering Optimization Rio de Janeiro, Brazil, 01 - 05 June 2008*.
- Carrion J. E. and Spencer B. F. Jr., 2007 Model-based Strategies for Real-time Hybrid Testing. NSEL Report Series Report No. NSEL-006, December 2007
- Carrion J. E. and Spencer B. F. Jr., 2006 Real Time Hybrid Testing Using Model-Based Delay. 4th International Conference on Earthquake Engineering Taipei, Taiwan October 12-13, 2006
- Ceravolo R. and Abbiati G., 2009. SDIT Release 3.1 User's Manual. Structural Identification Toolbox for Matlab Politecnico di Torino, Turin (Italy).
- Chang S. Y., 1997. Improved numerical dissipation for explicit techniques in pseudo dynamic tests. *Journal Earthquake Engineering and Structural Dynamics*, 26(1997) 917-29.
- Chattopadhyay J., Kushwaha H.S., Roos E., 2006. Some recent developments on integrity assessment of pipes and elbows. Part I: Theoretical investigations. *International Journal of Solids and Structures* 43 (2006) 29042931.
- Chen C. and Ricles J., 2010. Tracking error-based servohydraulic actuator adaptive compensation for real-time hybrid simulation. *Journal of Structural Engineering* 2010; 136(4):432440.
- Chen C. and Ricles J., 2009. Improving the inverse compensation method for real-time hybrid simulation through a dual compensation scheme. *Earthquake Engineering and Structural Dynamics* 2009; 38(10):12371255.
- Chen C. and Ricles J. M., 2008. A General Approach for Analysis of Actuator Delay Compensation Methods for Real-Time Testing. *The 14th World Conference on Earthquake Engineering October 12-17, 2008, Beijing, China*.

- Chopra A. K., 1995. Dynamics of Structures. Publisher: Prentice Hall, ISBN 0-13-855214-2.
- Classen T. A. C. M., Mecklenbrauker W. F. G., 1980. The Wigner distribution - a tool for time-frequency signal analysis. Part I. Continuous-time signals. Philips J. Res. 35 (1980), 217-250.
- Combescure D, Pegon P., 1997. Operating splitting time integration technique for pseudo dynamic technique; error propagation analysis. Soil Dynamics and Earthquake Engineering, 16(1997) 427-43.
- Costa J. L. D., 2003. Standard Methods for Seismic Analyses. Report BYGDTU R-064, 2003, ISSN 1601-2917, ISBN 87-7877-126-9.
- Craig R. and Bampton M., 1968. Coupling of Substructures for Dynamic Analysis. AIAA Journal, Vo1.6, (7), 1968.
- CSA-Z662, 2007. Canadian standards association. Oil and gas pipeline systems. exdale, Ontario, Canada.
- Darby A. P., Williams M. S. and Blakeborough A., 2002. Stability and delay compensation for real-time substructure testing. Journal of Engineering Mechanics 2002; 128(12):12761284.
- Darby A. P., Blakeborough A. and Williams M. S., 2001. Improved control algorithm for real-time substructure testing. Earthquake Engineering and Structural Dynamics, 30(3):431448.
- Darby A. P., Williams M. S. and Blakeborough A., 1999. Stability and delay compensation for real-time substructure testing. Journal of Engineering Mechanics, ASCE, 128(12): 1276-1284.
- Darby A. P., Blakeborough A. and Williams M. S., 1999b. Real-time substructure tests using hydraulic actuator. Journal of Engineering Mechanics, ASCE, 125(10):1133-1139.
- DeGrassi G., Hofmayer C., Murphy A., Suzuki K. and Namita, Y., 2003. BNL nonlinear pre-test seismic analysis for the NUPEC ultimate strength piping test program. Transaction of SMiRT 17 Conference.

- DeGrassi G., Nie J., Hofmayer C., 2008. Seismic Analysis of Large-Scale Piping Systems for the JNES-NUPEC Ultimate Strength Piping Test Program U.S. NRC. NUREG/CR-6983, BNL-NUREG-81548-2008.
- Dermitzakis S. N. and Mahin S. A., 1985. Development of substructuring techniques for on-line computer controlled seismic performance testing. Earthquake Engineering Research Center, University of California, Berkeley.
- Duarte M. and Ewins D., 1995. Some Insights into the Importance of Rotational Degrees of Freedom and Residual Terms in Coupled Structure Analysis Proceedings of the Thirteenth International Modal Analysis Conference, Society for Experimental Mechanics, Bethel, CT, Feb. 1995, pp. 164170.
- ECCS TC1 TWG 1.3, 1986. Recommended testing procedure for assessing the behaviour of structural steel elements under cyclic loading. European convention for constructional steelwork, Brussels. 1986, 45, Technical Committee 13.
- EN 1092-1, 2007. Flanges and their joints - Circular flanges for pipes, valves, fittings and accessories, PN designated - Part 1: Steel flanges.
- EN 1092-2, 1997. Flanges and their joints - Circular flanges for pipes, valves, fittings and accessories, PN designated. Part 2. Cast iron flanges.
- EN 1092-3, 2003. Flanges and their joints - Circular flanges for pipes, valves, fittings and accessories, PN designated - Part 3: Copper alloy flanges.
- EN 1092-4, 2004. Flanges and Their Joints - Circular Flanges for Pipes, Valves, Fittings and Accessories, PN Designated - Part 4: Aluminium Alloy Flanges.
- EN 12560-1, 2001. Flanges and their joints. Gaskets for Class-designated flanges. Non-metallic flat gaskets with or without inserts.
- EN 12560-2, 2001. Flanges and their joints. Gaskets for Class-designated flanges. Spiral wound gaskets for use with steel flanges.
- EN 12560-3, 2001. Flanges and their joints. Gaskets for Class-designated flanges. Non-metallic PTFE envelope gaskets.

- EN 12560-4, 2001. Flanges and their joints. Gaskets for Class-designated flanges. Corrugated, flat or grooved metallic and filled metallic gaskets for use with steel flanges.
- EN 12560-5, 2001. Flanges and their joints. Gaskets for Class-designated flanges. Metallic ring-joint gaskets for use with steel flanges.
- EN 12560-6, 2003. Flanges and their joints. Gaskets for Class-designated flanges. Kammprofile gaskets for use with steel flanges.
- EN 12560-7, 2004. Flanges and their joints. Gaskets for Class-designated flanges. Covered metal jacketed gaskets for use with steel flanges
- EN 13445-3, 2002. Unfired pressure vessels Part 3: Design.
- EN 13480-3, 2002. Metallic industrial piping - Part 3: Design and calculation.
- EN 1514-1, 1998. Flanges and their joints - Gaskets for PN-designated flanges - Part 1: Non-metallic flat gaskets with or without inserts.
- EN 1514-2, 2005. Flanges and their joints - Gaskets for PN-designated flanges - Part 2: Spiral wound gaskets for use with steel flanges.
- EN 1514-3, 1998. Flanges and their joints - Gaskets for PN-designated flanges - Part 3: Non-metallic PTFE envelope gaskets.
- EN 1514-4, 1998. Flanges and their joints - Gaskets for PN-designated flanges - Part 4: Corrugated, flat or grooved metallic and filled metallic gaskets for use with steel flanges.
- EN 1514-5, 1998. Flanges and their joints - Gaskets for PN-designated flanges - Part 5: Metallic ring-joint gaskets for use with steel flanges.
- EN 1514-6, 2004. Flanges and their joints - Gaskets for PN-designated flanges - Part 6: Kammprofile gaskets for use with steel flanges.
- EN 1514-7, 2005. Flanges and their joints - Gaskets for PN-designated flanges - Part 7: Covered metal jacketed gaskets for use with steel flanges.
- EN 1515-1, 2002. Flanges and their joints - Bolting - Part-1: Selection of bolting

- EN 1515-2, 2004. Flanges and their joints - Bolting - Part-2: Classification of bolt materials for steel flanges, PN designated.
- EN 1515-3, 2004. Flanges and their joints - Bolting - Part-3: Classification of bolt materials for steel flanges, Class designated.
- EN 1591-1, 2009. Flanges and their joints - Design rules for gasketed circular flange connections - Part 1: Calculation method.
- EN 1591-2, 2009. Flanges And Their Joints Design Rules For Gasketed Circular Flange Connections - Part 2: Gasket Parameters.
- EN 1759-1, 2004. Flanges and their joints. Circular flanges for pipes, valves, fittings and accessories, class-designated. Steel flanges, NPS 1/2 to 24.
- EN 1759-2, 2002. Flanges and Their Joints - Circular Flanges for Pipes, Valves, Fittings and Accessories, PN Designated - Part 2: Cast Iron Flanges
- EN 1759-3, 2003. Flanges and their joints - Circular flanges for pipes, valves, fittings and accessories, Class designated - Part 3: Copper alloy flanges.
- EN 1759-4, 2004. Flanges and their joints - Circular flanges for pipes, valves, fittings and accessories, Class designated - Part 4: Aluminium alloy flanges.
- EN 1993-1-8, 2005. Eurocode 3: Design of steel structures - Part 1-8: Design of joints.
- EN 1993-4-3, 2006. Eurocode 3 - Design of steel structures - Part 4-3: Pipelines.
- EN 1998-1, 2005. Eurocode 8: Design of structures for earthquake resistance - Part 1: General rules, seismic actions and rules for buildings.
- EN 1998-2, 2005. Eurocode 8 - Design of structures for earthquake resistance - Part 2 - Bridges.
- EN 1998-3, 2005. Eurocode 8 - Design of structures for earthquake resistance - Part 3 - Assessment and retrofitting of buildings.
- EN 1998-4, 2006 Eurocode 8 - Design of structures for earthquake resistance - Part 4: Silos, tanks and pipelines.

- EPRI TR-102792-V1, 1994. Piping and Fitting Dynamic Reliability Program, Volume 1: Project Summary, Oct. 1994.
- Eshghi S., Razzaghi M. S., 2003. The Behavior of Special Structures During the Bam Earthquake of 26 December 2003. JSEE: Special Issue on Bam Earthquake, 197-207.
- FEMA 450, 2003. NEHRP Recommended Provisions for seismic regulations for new buildings and other structures.
- Ferdinando A. D. and Lopez J. D., 2001. General design rule for bolt tightening. Document code: JSD 0400, Serial No: 03.
- Friswell M. I., Garvey S. D., Penny J. E. T., 1995. Model reduction using dynamic and iterated IRS techniques. Journal of Sound and Vibration (1995)186(2), 311-323.
- Gialamas T., Tsahalis D., Bregant L., Otte D., and van der Auweraer H., 1996. Substructuring by Means of FRFs: Some Investigations on the Significance of Rotational DOFs. Proceedings of the Fourteenth International Modal Analysis Conference, Society for Experimental Mechanics, Bethel, CT, Feb. 1996, pp. 619625.
- Giannini R. and Paolacci F., 2006. Performance of oil refineries in past earthquakes. Progetto ISPESL, Dipartimento Insediamenti Produttivi ed Interazione con Ambiente.
- Global Risk Miyamoto., 2007. 2007 Niigata Chuetsu-Oki Japan Earthquake, Reconnaissance Report. <http://www.grmcat.com/images/Niigata-Chuetsu-Oki-Japan-Report.pdf>.
- Gordon S., 1999. The Craig-Bampton Method. FEMCI Presentation, <http://femci.gsfc.nasa.gov/>
- Karamanos S. A., Varelis G. E. and Gresnigt A. M., 2013. Pipe elbows under strong cyclic loading. Journal of Pressure Vessel Technology, 2013, Vol. 135/011207-1.
- Varelis G. E., Karamanos S. A. and Gresnigt A. M., 2012. Pipe elbows under strong cyclic loading. Proceedings of the ASME 2012 Pressure Vessels & Piping Division Conference PVP2012, July 15-19, 2012, Toronto, Ontario, CANADA.

- Varelis G. E., Pappa P., Karamanos S. A., 2011. Finite element analysis of industrial steel elbows under strong cyclic loading. Proceedings of the ASME 2011 Pressure Vessels & Piping Division Conference PVP2011, July 17-21, 2011, Baltimore, Maryland, USA.
- Guizzo A. C., 1998. Experimental behavior of bolted joints. 1998 fluid sealing association technical symposium, Global Sealing Challenges of the 21st Century, Nashville, TN, April, 1998.
- Guyan R.J., 1965. Reduction of stiffness and mass matrices. American Institute of Aeronautics and Astronautics Journal 3(2), 380.
- Hahn J., Edgar T. F., 2002. An improved method for nonlinear model reduction using balancing of empirical gramians. Computers and Chemical Engineering 26 (2002) 1379-1397.
- Hibbit H. D., Karlsson B. I., and Sorensen, 2003. Theory Manual, ABAQUS version 6.3. Providence, RI. USA.
- Hobbacher A., 2008. Recommendations for fatigue design of welded joints and components. XIII-2151r4-07/XV-1254r4-07, Paris, France.
- Horiuchi K., Takagi Y., Sawa T., 2011. FEM Stress Analysis and the Sealing Performance Evaluation of Pipe Flange Connections Subjected to External Bending Moments and Internal Pressure. Proceedings of the ASME 2011 Pressure Vessels & Piping Division Conference PVP2011, July 17-21, 2011, Baltimore, Maryland, USA.
- Horiuchi T. and Konno T., 2001. A new method for compensating actuator delay in real-time hybrid experiment. Philosophical Transactions of the Royal Society of London A 359, 1893-1909.
- Horiuchi T., Inoue M., Konno, T. and Namita Y., 1999. Real-time hybrid experimental system with actuator delay compensation and its application to a piping system with energy absorber. Earthquake Engineering and Structural Dynamics, 28(10): 1121-1141.

- Horiuchi T., Nakagawa M., Sugano M. and Konno T., 1996. Development of a real-time hybrid experimental system with actuator delay compensation. In Proc. 11th World Conf. Earthquake Engineering, Paper No. 660.
- Huang, Y. N., Whittaker A. S., Constantinou M. C. and Malushte S., 2007. Seismic demands on secondary systems in base-isolated nuclear power plants. *Earthquake Engineering and Structural Dynamics* 36,1741-1761.
- IBC, 2000. International Building Code (IBC). International Code Council, Inc. (ICC).
- Iervolino I., Galasso C. and Cosenza E., 2009. REXEL: computer aided record selection for code-based seismic structural analysis. *Bulletin of Earthquake Engineering*, 8:339-362. DOI 10.1007/s10518-009-9146-1.
- INDUSE, 2009. Structural safety of industrial steel tanks, pressure vessels and piping systems under seismic loading. INDUSE Project, Contr. No: RFSR-CT-2009-00022, Research Fund for Coal and Steel.
- Juang, J. N. and Pappa, R. S., 1984. An eigensystem realisation algorithm (ERA) for modal parameter identification and modal reduction. NASA/JPL Workshop on Identification and Control of Flexible Space Structures.
- Jung R. Y., Shing P. B., Stauffer E. and Thoen B., 2007. Performance of a real-time pseudodynamic test system considering nonlinear structural response. *Earthquake Engineering and Structural Dynamics* 2007; 36(12):1785-1809.
- Klerk D. D., Rixen D. J., and Voormeeren S. N., 2008. General Framework for Dynamic Substructuring: History, Review, and Classification of Techniques. *AIAA JOURNAL* Vol. 46, No. 5, May 2008.
- Krausmann E., Cruz A. M., Affeltranger B., 2010. The impact of the 12 May 2008 Wenchuan earthquake on industrial facilities. European Commission, Joint Research Centre, Institute for the Protection and Security of the Citizen. Accident Risks Division, B.P. 2 ALATA, F-60550 Verneuil en Halatte, France. 2010.
- Kumar K., Muthumani K., Jeyasehar C. A. and Iyer N. R., 2012. Newmark implicit time integral for application in pseudo-dynamic testing experimental verification. *Asian*

- journal of civil engineering (building and housing) Vol. 13, No. 6 (2012) Pages 805-820.
- Liu B., Liu X.J. and Zhang H., 2009. Strain-based design criteria of pipelines. *Journal of Loss Prevention in the Process Industries* 22 (2009) 884-888.
- Liu W., and Ewins D., 1999. Importance of Assessment of RDOF in FRF Coupling Analysis Proceedings of the Seventeenth International Modal Analysis Conference, Society for Experimental Mechanics, Bethel, CT, Feb. 1999, pp. 1481-1487.
- Ljung L., 1987. *System Identification - Theory for the User*. Prentice Hall, Englewood Cliffs, NJ, 1987.
- Ljung L., 1986. *The System Identification Toolbox: The Manual*. The MathWorks Inc. 1st ed., (4th ed. 1994), Natick, MA, 1986.
- Magonette G., 2001. Development and application of large-scale continuous pseudodynamic testing techniques. *Philosophical Transactions of The Royal Society of London*, 359(1786):1771-1799, 2001.
- Mahin S. A., and Shing P. B. 1985. Pseudodynamic method for seismic testing. *Journal of Structural Engineering*, 111(7): 1482-1503.
- Mahin S. A., Shing P. B., Thewalt C. R., and Hanson R. D., 1989. Pseudodynamic test method. Current status and future directions. *Journal of Structural Engineering*, ASCE, 115(8): 2113-2128.
- Mahin S. A. and Shing P. B., 1985. Extension of pseudodynamic methods for seismic performance evaluation. Proc., Joint Tech. Meeting, U.S.-Japan Cooperative Earthquake Res. Program, Maui, Hawaii.
- Mair D., 2011. Demonstrating leak tight joints during piping design. Proceedings of the ASME 2011 Pressure Vessels & Piping Division Conference, PVP 2011, July 17-21, 2011, Baltimore, Maryland, USA.
- Martinez G. E. S., 2007. A comparative study of piping system subjected to earthquake loads using finite element modeling and analysis. Network for Earthquake Engineering Simulation (NEES), 13 September 2007.

- Melo F. J. M. Q. de, Carneiro J. A. O., Lopes H. R., Rodrigues J. F. D. and Gomes J. F. S., 2001. The dynamic analysis of piping systems using pseudo-dynamic techniques. *Journal of Strain Analysis*, Vol 36 NO 5.
- Mikitka R. W., 2002. The why and how of proposed ASME rules for bolted flanged joints based on tightness. *PVRC Workshop on Tightness Based Bolted Flange Gasket Constants and Design Rules*, Safety Harbor, FL; 2002.
- Molina F. G., Verzeletti G., Magonette G., Buchet P. H. and Geradin M., 1998. Bidirectional pseudodynamic test of a full-size three-story building. *Earthquake Engineering and Structural Dynamics*, 28(12):1541-1566, 1998.
- Mourad H. M. and Younan M. Y. A., 2001. Nonlinear analysis of pipe bends subjected to out-of-plane moment loading and internal pressure. *Journal of Pressure Vessel Technology*, ASME, 123, No. 2, pp. 253-258.
- MTS Models FlexTest 40/60/100/200 Controller Hardware, 2008. MTS Systems Corporation.
- Nagata S., Sawa T., Kobayashi T., Tsuji H., 2011. Finite element stress analysis for leak tests of pipe flange connections subject to internal pressure and bending moment. *Proceedings of the ASME 2011 Pressure Vessels & Piping Division Conference PVP2011*, July 17-21, 2011, Baltimore, Maryland, USA.
- Nakamura I., Otani A., Sato Y., Takada H., Takahashi K. and Shibutani T., 2011. Investigation of the seismic safety capacity of aged piping system - shake table test on piping systems with wall thinning by E-Defense. *Proceedings of the ASME 2011 Pressure Vessels & Piping Division Conference PVP2011*, July 17-21, 2011, Baltimore, Maryland, USA.
- Nakamura I., Otani A. and Shiratori M., 2010a. Comparison of Failure Modes of Piping Systems With Wall Thinning Subjected to In-Plane, Out-of-Plane and Mixed Mode Bending Under Seismic Load: An Experimental Approach. *Journal of Pressure Vessel Technology*, 132, pp. 031001-1 031001-8.
- Nakamura I, Otani, A., Sato Y. Takada, H. and Takahashi, K. 2010b. Tri-Axial Shake Table Test On The Thinned Wall Piping Model and Damage Detection before Failure. *Proceedings of the ASME PVP2010*, PVP2010-25839.

- Nakamura I., Otani A. and Shiratori M., 2004. Failure behavior of piping systems with wall thinning under seismic loading. Transactions of the ASME, Journal of Pressure Vessel Technology, 126, pp.85-90.
- Nakashima M., 2001. Development, potential, and limitations of real-time online (pseudodynamic) test. Philosophical Transactions of the Royal Society, (359):1851-1867, 2001.
- Nakashima M., and Masaoka, N., 1999. Real time on-line test for MDOF systems. Earthquake Engineering and Structural Dynamics, 28(4):393-420.
- Nakashima M., Kato H., and Takaoka E., 1992. Development of real-time pseudo dynamic testing. Earthquake Engineering and Structural Dynamics, (21):79-92, 1992.
- Namita Y., Suzuki K., Abe H., Ichihashi I., Shiratori M., Tai K., Iwata K. and Nebu A., 2003. Seismic proving test of eroded piping (status of eroded piping component and system test) pp15-21, PVP Vol.466, 2003, PVP2003-2097.
- Nash D. H. and Abid M., 2000. Combined external load tests for standard and compact flanges. International Journal of Pressure Vessels and Piping 77,799-806.
- Nash D. H. and Abid M., 1998. Experimental and analytical study of compact flange joints subjected to combined loading. Private Report to Shell UK, August 1998.
- Nayyar M. L., 2007. Piping Handbook. McGraw Hill, New York.
- Neild S. A., Stoten D. P., Drury D. and Wagg D. J., 2005. Control issues relating to real-time substructuring experiments using a shaking table. Earthquake Engineering and Structural Dynamics 2005; 34(9):1171-1192.
- Norme Techniche, 2008. Norme Techniche per le costruzioni. DM Infrastrutture, 14 gennaio 2008.
- O'Callahan J.C., Avitabile P. and Riemer R., 1989b. System equivalent reduction expansion process (SEREP). Proceedings of the 6th International Modal Analysis Conference, Las Vegas, January 1989, 29-37.

- O'Callahan J., 1989a. A new procedure for and improved reduced system IRS. In IMAC VII, Las Vegas, 1989.
- Otani A., Nakamura I., Takada H., Shiratori M., 2011. Consideration on seismic design margin of elbow in piping. Proceedings of the ASME 2011 Pressure Vessels and Piping Division Conference PVP2011 July 17-21, 2011, Baltimore, Maryland, USA.
- Pan P, Tada M., and Nakashima M., 2005. Online hybrid test by internet linkage of distributed test-analysis domains. *Earthquake Engineering and Structural Dynamics*, 34(1407-1425), 2005.
- Paolacci F., Reza M. S., Bursi O. S., 2011. Seismic design criteria of refinery piping systems. COMPDYN 2011 -III ECCOMAS Thematic Conference on Computational Methods in Structural Dynamics and Earthquake Engineering, Corfu, Greece, 2628 May 2011.
- Payne J. R., 2002. Understanding the ROTT test and the PVRC/ASME constants G_b , a and G_s . PVRC Workshop on Tightness Based Bolted Flange Gasket Constants and Design Rules, Safety Harbor, FL; 2002.
- Pegon P., 2008. New Approaches to Analysis and Testing of Mechanical and Structural Systems Modern Testing Techniques for Structural Systems, 2008, CISM Courses and Lectures, Volume 502, Editor- Oreste S. Bursi, David Wagg.
- Pegon P. and Pinto A. V., 2000. Pseudo-dynamic testing with substructuring applications at the elsa laboratory. *Earthquake Engineering and Structural Dynamics*, 29(7):905-925, 2000.
- Pinto A. V., Pegon P., Magonette G. and Tsionis G., 2004. Pseudo-dynamic testing of bridges using non-linear substructuring. *Earthquake Engineering and Structural Dynamics*, 33:1125-1146, 2004.
- Power D. J., 1997. A study of conventional and unconventional flanged pipe joint styles using nonlinear finite element analysis techniques. MPhil thesis, University of Strathclyde, Glasgow, August 1997.
- RCC-MR Code, 2002. B3600 and C3600, Tuyauteries classe 1, Edition 2000.

- RCCM Code, 2000. B3600 and C3600, Tuyauteries classe 1, Edition 2002.
- Reinhorn A. M., Sivaselvan M. V., Liang Z. and Shao X., 2004. Real-time dynamic hybrid testing of structural systems. Proceeding of the 13th World Conference on Earthquake Engineering, Vancouver, Canada, 2004.
- Rodabaugh E. C., George H. H., 1957. Effect of Internal Pressure on Flexibility and Stress-Intensification Factors of Curved Pipe or Welding Elbows. pp939-948, TRANSACTION OF THE ASME, MAY, 1957.
- SAP2000, 2004 Linear and Nonlinear Static and Dynamic Analysis and Design of Three-Dimensional Structures. v9, Computers and Structures, Inc., Berkeley, California, USA.
- Schellenberg A., Kim H., Mahin S.A. and Fenves G.L., 2005. Environment independent implementation of a software framework for fast local and geographically distributed hybrid simulations. The 14th World Conference on Earthquake Engineering October 12-17, 2008, Beijing, China.
- Semke W. H., Bibel G. D., Jerath S., Gurav S. B. and Webster A. L., 2006. Efficient dynamic structural response modelling of bolted flange piping systems. International Journal of Pressure Vessels and Piping 83 (2006) 767776.
- Sezen H. and Whittaker A. S., 2006. Seismic Performance of Industrial Facilities Affected by the 1999 Turkey Earthquake. Journal of Performance of Constructed Facilities, Vol. 20, No. 1, February 1, 2006.
- Shengzhi S. and Yongbo S., 2011. Static Strength of Tubular T-joint with Reinforced Chord Under In-plane Bending Load The Open Ocean Engineering Journal, 2011, 4, 65-70.
- Shibutani T., Nakamura I and Otani A., 2011. Fracture Analysis of piping systems with thinned elbows on tri-axial shake table tests. Proceedings of the ASME 2011 Pressure Vessels & Piping Division Conference PVP2011, July 17-21, 2011, Baltimore, Maryland, USA.

- Shing P. B., 2008. Real Time Hybrid Testing Techniques. Modern Testing Techniques for Structural Systems, 2008, CISM Courses and Lectures, Volume 502, Editor-Oreste S. Bursi, David Wagg.
- Shing P. B., Wei Z., Jung R. Y. and Stauffer E., 2004. NEES fast hybrid test system at the University of Colorado. Proceedings of the 13th World Conference on Earthquake Engineering, Vancouver, Canada, Paper No. 3497.
- Shing P. B., Nakashima M., and Bursi O. S., 1996. Application of pseudodynamic test method to structural research. Earthquake Spectra, EERI, 12(1):29-54.
- Shing P. B. and Mahin S. A., 1990. Experimental error effects in pseudodynamic testing. Journal of Engineering Mechanics 116(4): 805-821, 1990.
- Shing P. B. and Mahin S. A., 1987. Cumulative experimental errors in pseudodynamic tests. Earthquake Engineering and Structural Dynamics 15: 409-424, 1987.
- Simulink v 8.0, 2012. The MathWorks, Inc.
- Slagis G. C., 1997. Experimental data on seismic response of piping, Part 3. pp163-167, PVP Vol. 345, 1997.
- Suzuki K., 2006. 2006 Earthquake Damage to Industrial Facilities and Development of Seismic and Vibration Control Technology Based on Experience from the 1995 Kobe (Hanshin-Awaji) Earthquake. Journal of Disaster Research, Vol.1 No.2.
- Suzuki K. and Abe H., 2005. Seismic Proving Test of Ultimate Piping Strength. PVP2005- 71005, ASME PVP Conference, Denver, CO.
- Suzuki K., Namita Y., Abe H., Ichisashi I., Suzuki K., Ishiwata M., Fujiwaka T., and Tai K., 2003. Seismic Proving Test of Ultimate Piping Strength (Simulation analysis of simplified piping test). pp23-30, PVP Vol.466, 2003, PVP2003-2098.
- Suzuki N. and Nasu M., 1989. Non-Linear Analysis of Welded Elbows Subjected to In-Plane bending. Computers and Structures, 32, No.3/4, pp.871-881.
- Takanashi, K., and Nakashima, M. 1987. Japanese activities on on-line testing. Journal of Engineering Mechanics, ASCE, 113(7): 1014-1032.

- Takanashi K., Udagawa K., Seki K., Okada T. and Tanaka H., 1975. Nonlinear earthquake response analysis of structures by a computer-actuator on-line system. Bull. of earthquake resistant structure research center, no. 8, Institute of Industrial Science, University of Tokyo, Japan, 1975.
- Taucer F. (ed.), 2004. Recent advances and future needs in experimental earthquake engineering. CASCADE Project Report 7, 2004.
- Tenma K., Kikuchi T., Sawa T., Horiuchi K., 2011. Evaluation of sealing performance and fem calculations in bolted flange connections with ring joint gasket subjected to internal pressure Proceedings of the ASME 2011 Pressure Vessels & Piping Division Conference PVP2011, July 17-21, 2011, Baltimore, Maryland, USA.
- Touboul F., Blay N., Sollogoub P., Chapuliot S., 2006. Enhanced seismic criteria for piping. Nuclear Engineering and Design 236, 1-9.
- Touboul F., Sollogoub P. Blay N., 1999. Seismic behaviour of piping systems with and without defects: experimental and numerical evaluations. Nuclear Engineering and Design, 192, 243-260.
- Wagg D., Neild S. and Gawthrop P., 2008. Real time testing with dynamic substructuring. Modern Testing Techniques for Structural Systems, 2008, CISM Courses and Lectures, Volume 502, Editor- Oreste S. Bursi, David Wagg.
- Wallace M. I., Wagg D. J. and Neild S. A., 2005. An adaptive polynomial based forward prediction algorithm for multi-actuator real-time dynamic substructuring. Proceedings of the Royal SocietyA 2005; 461(2064):38073826.
- Wallace M. I., Sieber J., Neild S. A., Wagg D. J. and Krasukopf B., 2004. Stability analysis of real-time dynamic substructuring using delay differential equation models. Earthquake Engineering and Structural Dynamics 2004; 34(15): 18171832.
- Waters E. O., Rossheim D. B., Wesstrom D. B. and Williams F. S. G., 1937. Development of General Formulas for Bolted Flanges. Chicago, IL: Taylor-Forge and Pipe Works; 1937.
- William B. J. M., Pilate M., Piotr O., Yong L., 2003. Assessment of Highway Bridge Upgrading by Dynamic Testing and Finite-Element Model Updating. Journal of

Bridge Engineering 8 (3): 162172. doi:10.1061/(ASCE)1084-0702 (2003)8:3(162).
ISSN 1084-0702.

William J. K., 2006. Bolted flange joints and connections. ASME Companion Guide to the ASME Boiler & Pressure Vessel Code, Second Volume, Second Edition: Criteria and Commentary on Select Aspects of the Boiler & Pressure Vessel and Piping Codes. Editor: Rao K. R.

Wu B., Wang Z. and Bursi O. S., 2012. Actuator dynamics compensation based on upper bound delay for real-time hybrid simulation. Earthquake Engineering and Structural Dynamics, 2012 (In press).

Wu B., Wang Q. Shing P. B. and Ou J., 2007. Equivalent force control method for generalized real-time substructure testing with implicit integration. Earthquake Engineering and Structural Dynamics 35(9): 1127-1149, 2007.

Wu B., Wang Q-Y., Shi P-F., Ou J-P. and Guan, X-C., 2006. Real-time substructure test of JZ20-2NW offshore platform with semi-active MR dampers. Proceedings of the 4th International Conference on Earthquake Engineering, Taipei, Taiwan, Paper No. 185.

Wu B., Wang Q. and Willams M. S., 2006b. Operator-splitting method for real-time substructure testing. Earthquake Engineering and Structural Dynamics 35(3): 293-314, 2006.

Yahiaoui K., Moffat D. G. and Moreton D.N., 2002. Evaluation of limit load data for cracked pipe bends under opening bending and comparisons with existing solutions. International Journal of Pressure Vessels and Piping, Vol. 79, 2002, pp. 27-36.

Yahiaoui K., Moffat D. G. and Moreton D.N., 2000. Plastic loads of cracked forged piping branch junctions: experimental results and comparison with numerical data. International Journal of Pressure Vessels and Piping 77 (2000) 249-260. pp. 27-36.

Young J. T., 2000. Primer on the Craig-Bampton method (Based on input from William B. Haile).

- Zare M. R. and Wilkson S., 2010. Resilience of wastewater pipelines in earthquakes. Proceedings of the 9th U.S. National and 10th Canadian Conference on Earthquake Engineering, Toronto, Ontario, Canada, 25-29 July 2010.
- Zerres H. and Guerout Y., 2004. Present calculation methods dedicated to bolted flange connections. International Journal of Pressure Vessels and Piping 81 (2004) 211216.
- Zhang N., 1995. Dynamic condensation of mass and stiffness matrices. Journal of Sound and Vibration, 188(4):601615, 1995.
- Zhao X. L., Herion S., Packer J.A., Puhtli R. S., Sedlacek G., Wardenier J., Weynand K., Wingerde A. M. van and Yeomans, N. F., 2001. Design guide for circular and rectangular hollow section welded joints under fatigue loading, construction with hollow steel sections. 8, TUV-Verlag GmbH, Unternehmensgruppe TV Rheinland/Berlin-Brandenburg, Koln.